Knee

14

Carlo Martinoli and Stefano Bianchi

CONTENTS

14.1 **Introduction** *637*
14.2 **Clinical Anatomy** *638*
14.2.1 Osseous and Articular Anatomy *638*
14.2.2 Joint and Ligamentous Complexes *639*
14.2.2.1 Femorotibial Joint *639*
14.2.2.2 Patellofemoral Joint *641*
14.2.2.3 Superior Tibiofibular Joint *641*
14.2.3 Tendons *642*
14.2.3.1 Extensor Mechanism *642*
14.2.3.2 Posterior Tendons *642*
14.2.4 Popliteal Fossa *644*
14.2.4.1 Popliteal Vessels *644*
14.2.4.2 Tibial and Peroneal Nerves *646*
14.2.5 Bursae *646*
14.3 **Essentials of Clinical History and Physical Examination** *648*
14.3.1 Knee Joint Effusions *649*
14.4 **Normal US Findings and Scanning Technique** *650*
14.4.1 Anterior Knee *650*
14.4.2 Medial Knee *662*
14.4.3 Lateral Knee *664*
14.4.4 Posterior Knee *665*
14.5 **Knee Pathology** *671*
14.5.1 Anterior Knee Pathology *671*
14.5.1.1 Quadriceps Tendinopathy *671*
14.5.1.2 Quadriceps Tendon Tear *672*
14.5.1.3 Medial Plica Syndrome *676*
14.5.1.4 Prepatellar Bursitis *677*
14.5.1.5 Abnormalities of the Patella *678*
14.5.1.6 Patellar Tendinopathy *679*
14.5.1.7 Deep and Superficial Infrapatellar Bursitis *683*
14.5.2 Medial Knee Pathology *684*
14.5.2.1 Medial Collateral Ligament Injury *685*
14.5.2.2 Pes Anserinus Bursitis *690*
14.5.3 Lateral Knee Pathology *690*
14.5.3.1 Lateral Collateral Ligament Injury *692*
14.5.3.2 Iliotibial Band Friction Syndrome *692*
14.5.3.3 Distal Iliotibial Band Tendinopathy *693*
14.5.3.4 Superior Tibiofibular Joint Ganglia *694*
14.5.3.5 Peroneal Neuropathy *696*
14.5.4 Posterior Knee Pathology *700*
14.5.4.1 Baker Cyst *700*
14.5.4.2 Extra-articular Ganglia *711*
14.5.4.3 Semimembranosus Bursitis *711*
14.5.4.4 Cruciate Ligament Ganglia *713*
14.5.5.5 Cruciate Ligament Tears *716*
14.5.4.6 Popliteal Aneurysms *717*
14.5.4.7 Popliteal Artery Entrapment Syndrome *717*
14.5.5 Joint and Bone Disorders *720*
14.5.5.1 Knee Synovitis *721*
14.5.5.2 Lipohemarthrosis *723*
14.5.5.3 Intra-articular Loose Bodies *725*
14.5.5.4 Cartilage Abnormalities and Osteoarthritis *727*
14.5.5.5 Meniscal Cysts *729*
14.5.5.6 Meniscal Degeneration and Tears *732*
14.5.5.7 Meniscal Calcifications *732*
14.5.5.8 Meniscal Ossicles *733*
14.5.5.9 Total Knee Replacement *736*
14.5.6 Knee Masses *736*
14.5.6.1 Lipoma Arborescens *736*
14.5.6.2 Pigmented Villonodular Synovitis *738*
14.5.6.3 Tensor Fasciae Suralis Muscle *739*
References *740*

C. Martinoli, MD
Associate Professor of Radiology, Cattedra "R" di Radiologia – DICMI – Università di Genova, Largo Rosanna Benzi 8, 16132 Genova, Italy
S. Bianchi, MD
Privat-docent, Université de Genève, Consultant Radiologist, Fondation et Clinique des Grangettes, 7, ch. des Grangettes, 1224 Genève, Switzerland

14.1 Introduction

A variety of disorders involving tendons, vessels, nerves, joints and para-articular structures of the knee can be accurately assessed with US (Grobbelaar and Bouffard 2000; Friedman et al. 2001). On the other hand, this technique has specific limitations in the assessment of knee disorders affecting the menisci and the cruciate ligaments. Since the referring clinician may ignore these limitations, knowledge of the presumptive clinical diagnosis is important for the examiner in order to avoid inappropriate studies. US examination of the knee is performed using a broadband linear array transducer working at a frequency band range of 5–10 MHz. For evaluation of the popliteal fossa, a probe with a center frequency of 5 MHz can help

to image the deepest structures, whereas US frequencies in the 10–15 MHz band range may improve the assessment of the most superficial structures, such as the patellar tendon and the peroneal nerve around the fibular head. The use of extended-field-of-view technology may be useful to obtain a panoramic view of the knee region and to allow a more accurate measurement and follow-up comparison of space-occupying masses. In addition, it makes the interpretation of the US images easier and more acceptable for the clinician.

14.2 Clinical Anatomy

A basic description of the complex anatomy of the knee with emphasis on the anatomic structures amenable to US examination, such as joint and ligamentous complexes, tendons, neurovascular structures and bursae, is included here.

14.2.1 Osseous and Articular Anatomy

In the knee, the medial and lateral condyles of the femur articulate with tibial plateau (Fig. 14.1). The femoral condyles project posteriorly and are separated by a deep U-shaped intercondylar notch. The superior surface of the tibia is flat and consists of the medial and lateral tibial plateaux which are separated by the intercondylar eminence. The medial and lateral articular surfaces of the femur and tibia are incongruent and, therefore, are more firmly fitted by triangular-shaped fibrocartilaginous structures, the knee menisci (Fig. 14.1b). Anterior to the femorotibial joint, the patella, the largest sesamoid bone in the body, appears as an inverted triangle with the apex directed caudally. The patella has a slightly convex anterior surface and a posterior surface covered by hyaline cartilage. A vertical ridge divides its posterior surface into lateral and medial facets, the lateral one being larger and more concave (Figs. 14.1, 14.2a). The articular surfaces of the patella are in front of the corresponding facets of the femoral trochlea, while its vertical ridge is apposed to the trochlea groove. At birth, the patella is entirely cartilaginous (Fig. 14.2b). Multiple ossification centers appear in the first years of life to complete the ossification process at puberty. Caudal to its lateral condyle, the tibia articulates with the fibula through a small facet (Fig. 14.1). A prominent anterior apophysis, the tibial tuberosity, exists on the proximal metaphysis of the tibia to give insertion to the patellar tendon: it is found approximately 5 cm distal to the apex of the patella (Fig. 14.1). From the functional stand-

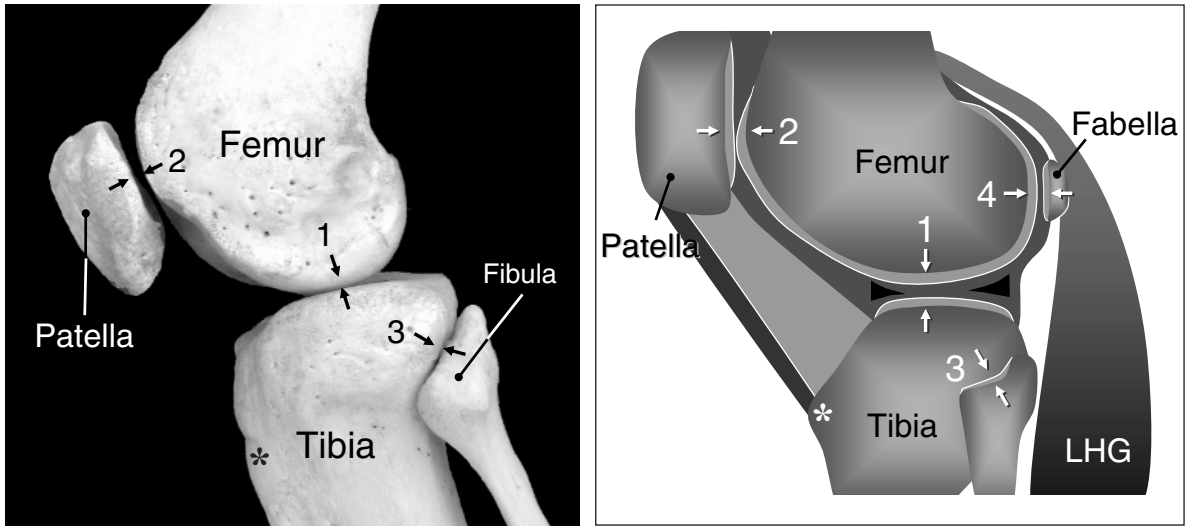

a b

Fig. 14.1a,b. Knee joint. Articular anatomy. **a** Lateral view of the knee bones with **b** schematic drawing correlation illustrates the articular relationships among femur, tibia, patella and fibula. Four synovial joints are found in this region: the femorotibial joint (*1*), the patellofemoral joint (*2*), the superior tibiofibular joint (*3*) and the fabellofemoral joint. The femorotibial, femoropatellar and fabellofemoral joints communicate with each other and share a common synovial cavity. The superior tibiofibular joint communicates with the main knee cavity in approximately 10% of subjects. Observe the position of the fabella, included in the proximal tendon of the lateral head of gastrocnemius (*LHG*), and the anterior tibial tuberosity (*asterisk*), which gives insertion to the patellar tendon

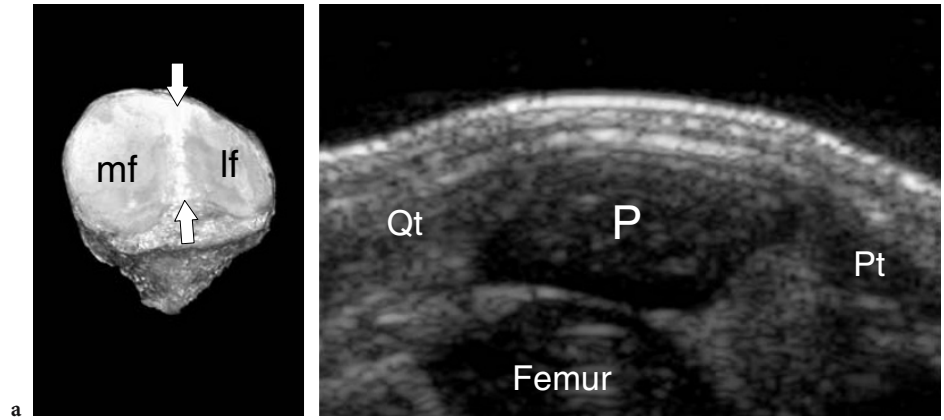

a b

Fig. 14.2a,b. Patella. **a** Posterior view of the patella reveals its posterior surface divided into medial (*mf*) and lateral (*lf*) articular facets by a vertical ridge (*arrows*). **b** Longitudinal 12–5MHz US image over the patella (*P*) in a newborn. The immature bone is entirely cartilaginous and appears homogeneously hypoechoic at US. For that reason, its overall shape and the appearance of the underlying femoral trochlea can be nicely depicted. Note the attachments of the quadriceps (*Qt*) and the patellar (*Pt*) tendons

point, the knee is an intrinsically unstable joint, the main stabilizers being represented by powerful ligaments and muscles that bind the femur and the tibia together. Its movements include flexion and extension, but also mild degrees of internal and external rotation, abduction and adduction.

14.2.2 Joint and Ligamentous Complexes

The knee consists of three separate synovial joints which can be assessed with variable accuracy with US. These are the femorotibial, patellofemoral and superior tibiofibular joint (Fig. 14.1). In some patients, a fourth articulation can exist between the lateral condyle and the fabella, an accessory bone enclosed in the proximal tendon of the lateral head of the gastrocnemius (Fig. 14.1b).

14.2.2.1 Femorotibial Joint

The femorotibial joint consists of two compartments: medial and lateral. The medial compartment is composed of the larger medial condyle and the concave superior aspect of the medial tibial plateau and has a wider anteroposterior diameter compared with the lateral one. The lateral compartment is formed by the smaller lateral condyle and the flat or convex articular surface of the lateral tibial plateau. The medial compartment gives stability to the joint, whereas the lateral one allows mobility. The lateral and medial fibrocartilaginous menisci help to increase the congruity between the convex femoral condyles and the relatively flat tibial surfaces. In addition, they greatly enhance joint stability, transmitting nearly 60% of the forces applied during axial loading to the bones. Stability of the femorotibial joint is essentially maintained by the articular capsule, a thick fibrous structure inserting into the bones and periosteum at the edges of the articular cartilages, by several powerful ligaments and by the action of para-articular muscles. The most important ligaments of the knee are the collaterals and the cruciate ligaments.

The supporting structures on the medial knee are organized in three main layers (Irizarry and Recht 1997). The most superficial is composed of the crural fascia, which blends with the intermediate layer to form the medial patellar retinaculum. The intermediate layer contains the superficial portion of the medial collateral ligament, which is a strong fibrous band with a straight vertical course arising proximally from the medial femoral epicondyle about 5 cm above the joint line and inserting at the medial aspect of the tibia approximately 6–7 cm below the joint and posterior to the pes anserinus complex (Fig. 14.3). At gross examination, the superficial portion of the medial collateral ligament appears as a flattened band approximately 15 mm in width and 10–11 cm in length. The deep layer consists of the joint capsule, which becomes thickened just deep to the superficial portion of the medial collateral ligament to form the deep portion of this

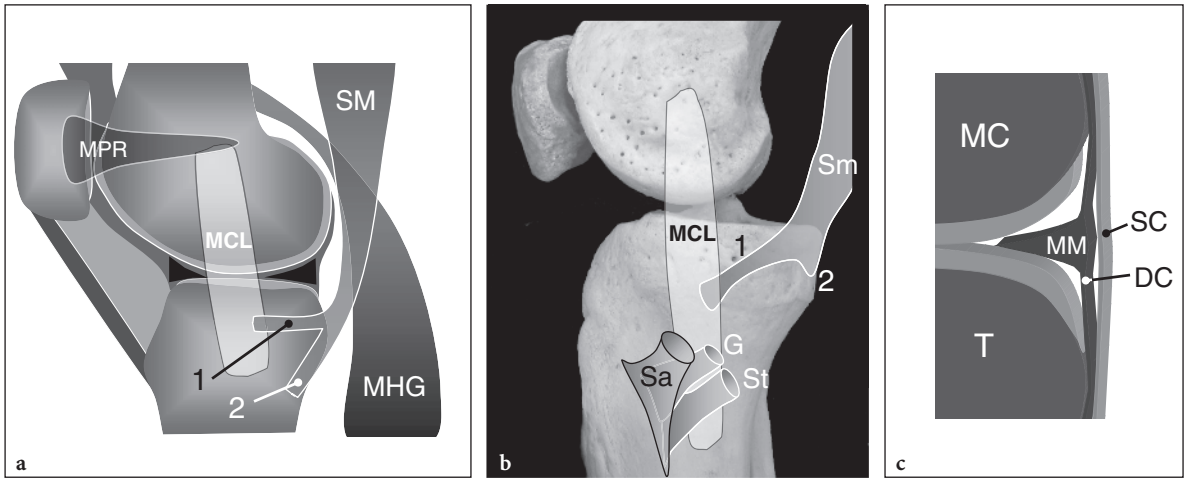

Fig. 14.3a–c. Anatomy of the medial knee. **a** Schematic drawing and **b** corresponding medial view through the knee illustrate the medial collateral ligament (*MCL*) as a wide band joining the medial femoral epicondyle with the medial aspect of the tibial epiphysis. Note that the medial patellar retinaculum (*MPR*) has a common femoral origin with the medial collateral ligament and inserts anteriorly into the medial edge of the patella. The indirect tendon (*1*) of the semimembranosus muscle (*SM* in **a**, *Sm* in **b**) lies in a bone groove at the medial aspect of the tibial epiphysis covered by the distal part of the medial collateral ligament. The stronger direct tendon (*2*) attaches into the posterior aspect of the tibia. The medial head of the gastrocnemius (*MHG*) crosses the distal myotendinous junction of the semimembranosus muscle to insert into the posterior aspect of the supracondylar region. More caudally, the tendons of the sartorius (*Sa*), gracilis (*G*) and semitendinosus (*St*) inserts on the tibial shaft superficial to the attachment of the medial collateral ligament to form the so-called pes anserinus. **c** Schematic drawing of a coronal view through the medial femorotibial joint demonstrates the medial collateral ligament composed of a superficial (*SC*) and a deep (*DC*) component. The latter is formed by the meniscofemoral ligament which joins the medial meniscus (*MM*) to the medial condyle (*MC*) and by the meniscotibial ligament which joins the meniscus to the tibia (*T*). A synovial bursa lies between the two ligament components; in normal conditions, it cannot be visualized at US

ligament. This layer is intimately interlaced with the medial meniscus and attaches to each articular margin of the joint forming the meniscofemoral and meniscotibial ligaments (Fig. 14.3b). The superficial portion of the medial collateral ligament remains taut during flexion and extension movements of the knee and plays an essential role as a restraint against valgus stress, abnormal external rotation and anterior tibial translation.

The lateral supporting structures of the knee are less commonly injured than the medial ones. They also include three layers (Irizarry and Recht 1997). The most superficial layer houses the iliotibial band anteriorly and the biceps tendon posteriorly including their fascial expansions in the thigh and calf. The intermediate layer includes the lateral patellar retinaculum and the patellofemoral ligaments anteriorly and the lateral collateral ligament posteriorly. The lateral collateral ligament is a cord-like structure which arises proximally from the lateral femoral epicondyle and ends with a conjoined insertion at the fibular head together with the biceps femoris tendon (Fig. 14.4a,b). The deep layer is represented by the lateral joint capsule, which attaches on the femoral and tibial articular boundaries. More posteriorly, the deep layer includes the fabellofibular and arcuate ligaments, that cannot be imaged with US. The capsule and the lateral meniscus are pierced by the popliteus tendon which enters the joint through a hiatus (Fig. 14.4). In coordination with the other lateral supporting structures, the lateral collateral ligament slackens with increased flexion of the knee and offers the main restraint to varus stress and knee hyperextension.

The anterior cruciate ligament is an intracapsular extrasynovial structure which originates on the posterior and medial aspect of the lateral femoral condyle and inserts anterior to the tibial spines. It fans out distally and is composed of three separate fascicles with fat interspersed among them. The ligament has an outward spiral course and an overall configuration resembling a ribbon-like cord. The anterior cruciate ligament is the main restraint to tibial rotation, especially internal rotation of the knee. Similar to the anterior cruciate ligament, the posterior cruciate ligament is an intracapsular and extrasynovial structure. It is stronger and thicker than the anterior ligament and ruptures less frequently. The posterior

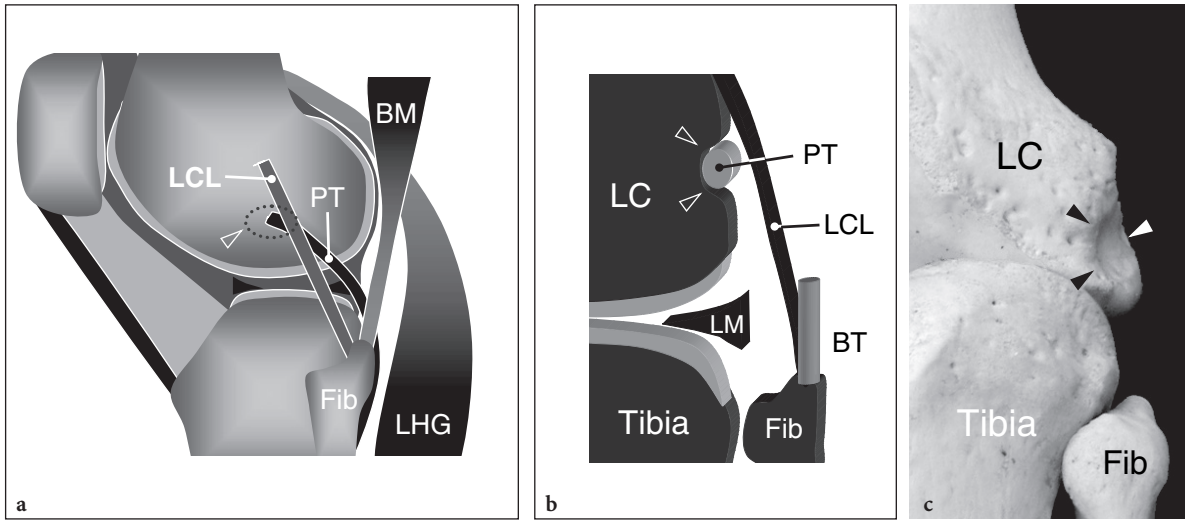

Fig. 14.4a–c. Anatomy of the lateral knee. **a,b** Schematic drawings of a lateral (**a**) and coronal (**b**) view through the knee illustrate the lateral collateral ligament (*LCL*) as a cord-like structure joining the lateral femoral epicondyle with the apex of the fibula (*Fib*). Note that the tendon (*BT*) of the biceps muscle (*BM*) has a conjoined insertion with the lateral collateral ligament on the fibular head. The popliteus tendon (*PT*) inserts into a small bone fossa (*arrowheads*) located on the lateral aspect of the lateral condyle (*LC*). It is covered by the proximal part of the lateral collateral ligament. *LHG*, lateral head of gastrocnemius. *LM*, lateral meniscus. **c** Lateral view of the knee bones reveals the groove (*arrowheads*) on the external aspect of the femur into which the popliteus tendon inserts. *LC*, lateral condyle

cruciate ligament has a posteriorly convex course and joins the posterolateral surface of the medial femoral condyle with a depression in the posterior tibia approximately 1 cm below the articular surface. Its main function is to counteract posterior translational movements of the tibia.

The main recesses of the femorotibial joint are the suprapatellar recess, which is also referred to as the subquadriceps recess, the lateral or parapatellar recesses, located medial and lateral to the patella, and the medial and lateral posterior femoral recesses, which are small recesses that have a close relationship with the internal aspect of the femoral condyles. The suprapatellar recess is the widest recess of the knee joint. It derives from the fusion of the subquadriceps bursa with the joint cavity, a process which occurs during intrauterine life. In normal states, this recess contains a small amount of fluid.

14.2.2.2 Patellofemoral Joint

The patellofemoral joint is formed by the groove of the femoral trochlea and the V-shaped articular facet of the patella (Fig. 14.2a). The orientation of the articular surfaces of these bones varies from cranial to caudal. In fact, the groove of the trochlea is less pronounced in the upper portion and becomes deeper inferiorly. At least in part, this may explain why patellar dislocations are almost always observed during the first degrees of knee flexion, when the patella is not yet well stabilized within the trochlea. During flexion and extension movements of the femorotibial joint, the patella is stabilized by its convex shape that matches the corresponding concave trochlea. Additional stabilizers are the lateral and medial patellar retinacula, fibrous bands which arise from the lateral and medial edges of the patella and insert into the femoral epicondyles. From the biomechanical point of view, the patella lessens the stress on the quadriceps and patellar tendons during contraction of the quadriceps muscle and increases the efficacy of muscle contraction by displacing the vector forces transmitted by these tendons more anteriorly.

14.2.2.3 Superior Tibiofibular Joint

The superior tibiofibular joint consists of the articulation between the medial articular facet of the fibular head and the corresponding facet of the tibia. It is a small joint located inferolateral to the femorotibial

joint (Fig. 14.1). Like the other joints of the knee, the superior tibiofibular joint is lined by a synovial membrane and a layer of hyaline cartilage covers its bony ends. In most cases, the superior tibiofibular joint is completely separated from the larger femorotibial joint, although a communication between them has been described in approximately 10% of normal subjects (Resnick et al. 1978).

14.2.3 Tendons

Based on their different location and function, the para-articular tendons of the knee can be divided into an anterior (extensors) and posterior (flexors) group.

14.2.3.1 Extensor Mechanism

The anterior tendons consist of the quadriceps and patellar tendons which house the patella as a sesamoid. On the whole, these structures form the extensor mechanism of the knee (Fig. 14.5). The quadriceps tendon is a flat trilaminar complex derived from the confluence of the individual tendons of the four muscle bellies of the quadriceps femoris. In detail, it is composed of distinct superficial (from the rectus femoris), intermediate (from blending of the vastus medialis and lateralis in the midline) and deep (from the vastus intermedius) layers which fuse in a common tendon approximately 1 cm from the patellar insertion (Fig. 14.6). The superficial layer is the longest because it arises at the distal third of the thigh from the rectus femoris muscle. Thin bands of fibrofatty tissue intervene among the tendon layers to allow some gliding movements during quadriceps muscle activation. The quadriceps tendon inserts into the upper pole (base) of the patella. Then, the most superficial fibers of the rectus femoris layer overlie the patella to continue down in the patellar tendon. From the anatomic standpoint, the patellar tendon should be considered a ligament (ligamentum patellae) rather than a tendon because it joins two bones, the patella and the tibia. It appears as a broad fibrous band 3–5 mm thick which arises from the lower pole (apex) and the lateral and medial edges of the patella to insert into the anterior tibial tuberosity (Fig. 14.5). The patellar tendon is a very strong structure capable of transmitting very high tensile forces. On each side, the patellar tendon is in continuity with the medial and lateral patellar retinacula which are composed of fibers from the vastus medialis and lateralis respectively (Fig. 14.5b,c). Posterolateral to it, the distal part of the fascia lata can be followed down to its insertion into a small tubercle, Gerdy's tubercle, located at the anterolateral aspect of the tibial epiphysis.

14.2.3.2 Posterior Tendons

The posterior tendons of the knee can be divided in lateral and medial (Fig. 14.7). The lateral tendons are: the distal tendon of the biceps femoris which originates from the union of the long and short head of the biceps muscle, the origin of the lateral head of the gastrocnemius and the popliteus tendon. The biceps tendon is a strong cord-like structure which attaches onto the tip and the lateral aspect of the fibular head in close relationship with the lateral collateral and the arcuate ligaments. The insertion of these structures is, in part, conjoined. The biceps also sends aome fibers to the distal iliotibial band and the lateral tibial condyle. A bursa may be present between the lateral collateral ligament and the biceps femoris tendon. On the lateral side of the popliteal fossa, the biceps tendon courses in close proximity to the peroneal nerve that runs just posterior and medial to it (Fig. 14.7). In common with the other hamstring muscles, the main action of the biceps femoris is to flex the knee joint and to assist in extending the hip joint. The peroneus longus tendon arises from the anterior aspect of the fibular head, whereas the soleus muscle takes its origin from the posterior aspect of the fibular head and, more distally, from the tibial shaft. Anterior to the origin of the peroneus longus, the extensor digitorum and the tibialis anterior arise from the inferior aspect of the lateral tibial condyle (see also Chapter 15). The popliteus tendon inserts onto a depression on the lateral surface of the lateral femoral condyle, just distal to the lateral femoral epicondyle, in close relationship with the posterior edge of the lateral meniscus (Fig. 14.4c). It traverses the capsule and continues downward in an obliquely oriented muscle which arises above the soleus attachment on the posterior aspect of the tibia. An accessory popliteus muscle has recently been described in the literature (Duc et al. 2004).

The medial tendons of the knee include the distal attachments of the semimembranosus, semitendinosus, gracilis, sartorius and the medial head of the gastrocnemius (Figs. 14.7, 14.8). The semimembran-

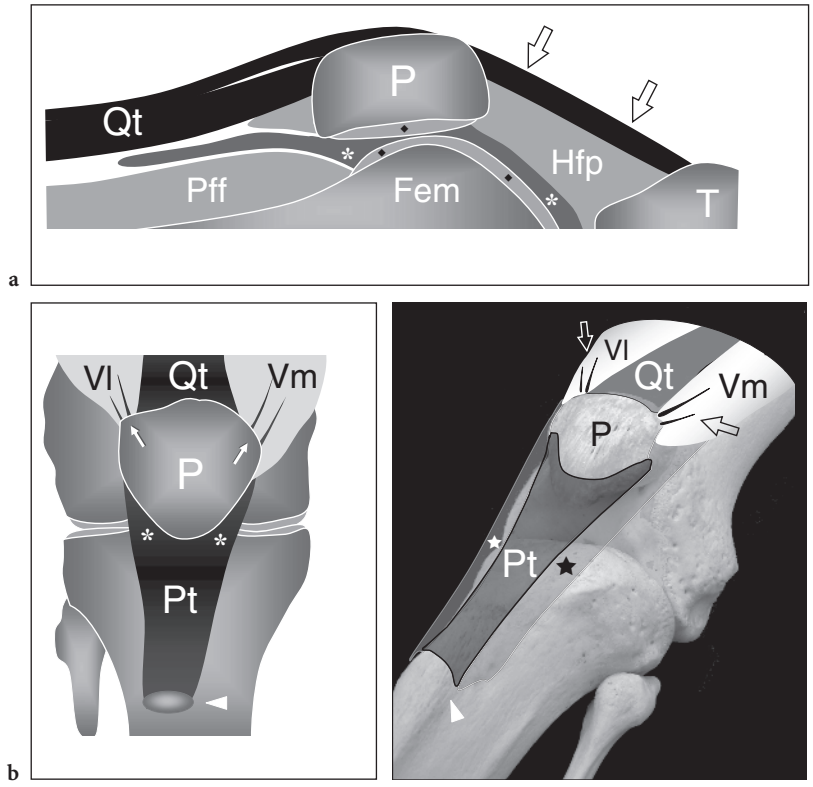

Fig. 14.5a–c. Anatomy of the extensor mechanism of the knee. **a** Schematic drawing of a sagittal view through the knee demonstrates the quadriceps tendon (*Qt*), the patella (*P*) and the patellar tendon (*arrows*). The prefemoral fat (*Pff*) is located anterior to the distal metaphysis of the femur (*Fem*), whereas the Hoffa fat pad (*Hfp*) is between the patellar tendon and the trochlea. Note the articular surfaces of the patellofemoral joint covered by cartilage (*rhombi*) and the joint space (*asterisks*). *T*, tibia. **b,c** Schematic drawings of an **b** anterior and **c** lateral oblique views of the knee illustrate the extensor mechanism of the knee. On each side of the quadriceps tendon (*Qt*), contributes of fibers from the vastus lateralis (*Vl*) and medialis (*Vm*) insert directly into the lateral and medial edges of the patella (*P*, *arrows*). The patellar tendon (*Pt*) is wider proximally as it inserts into the lateral and medial edges of the lower half of the patella (*asterisks*). Note that it has an oblique course because the anterior tibial tuberosity (*arrowhead*) is placed more laterally relative to the apex of the patella. *Stars*, patellar retinacula

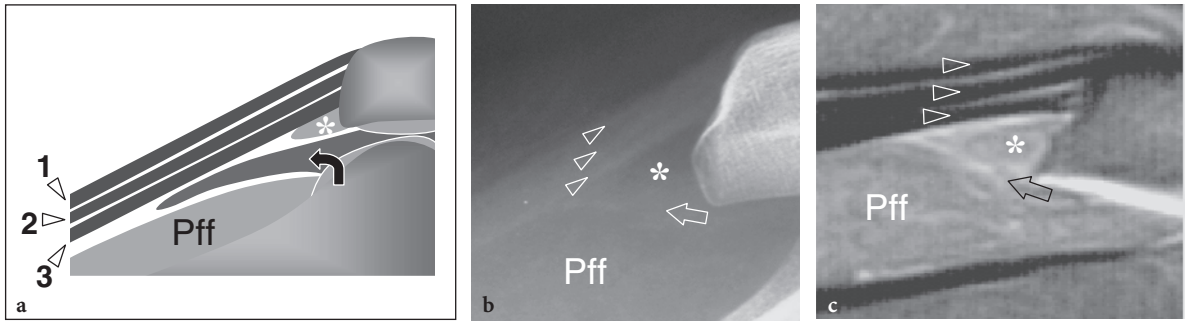

Fig. 14.6a–c. Anatomy of the quadriceps tendon. **a** Schematic drawing with **b** lateral radiographic and **c** sagittal fat-suppressed T2-weighted MR imaging correlation demonstrates the multilayered appearance (*arrowheads*) of the quadriceps tendon, formed by three layers: the most superficial layer (*1*) is formed by the rectus femoris; the middle layer (*2*) is formed by the vastus lateralis and medialis; and the deep layer (*3*) is formed by the vastus intermedius. The suprapatellar synovial recess (*arrow*) lies between the triangular suprapatellar fat pad (*asterisk*) and the large prefemoral fat pad (*Pff*)

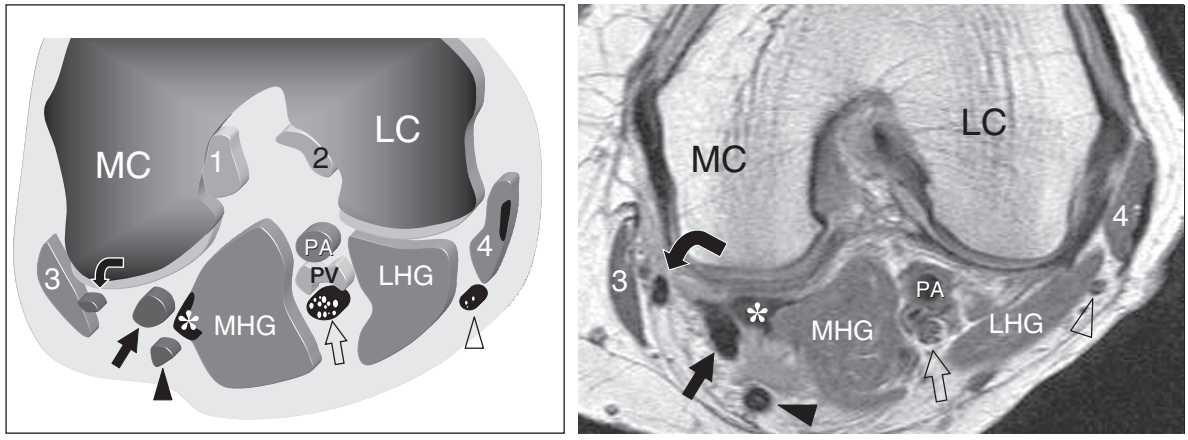

Fig. 14.7a,b. Anatomy of the posterior tendons. **a** Transverse schematic drawing through the middle third of the popliteal space with **b** MR imaging correlation illustrates the anatomic arrangement of the medial tendons, including the semimembranosus (*black straight arrow*), semitendinosus (*black arrowhead*), gracilis (*curved arrow*), sartorius (*3*) and the comma-shaped tendon (*asterisk*) of the medial head of the gastrocnemius (*MHG*). Lateral tendons include the biceps femoris (*4*) and the lateral head of the gastrocnemius (*LHG*). The popliteal artery (*PA*) and vein (*PV*) and the tibial nerve (*open arrow*) are located between the two heads of the gastrocnemius muscle. The common peroneal nerve (*open arrowhead*) courses just posterior to the biceps muscle. Note the relationship of the posterior (*1*) and anterior (*2*) cruciate ligaments with the medial (*MC*) and lateral (*LC*) femoral condyles

osus is the deepest and strongest. It has two main distal tendons which insert into the posteromedial (direct tendon) and medial (indirect tendon) aspect of the tibial epiphysis (Fig. 14.3a,b). In addition, a third, weak expansion of this tendon blends with the posterior capsule of the knee joint. The semitendinosus has a long, thin tendon which arises at the junction of the middle and distal thirds of the thigh and descends superficial to the posterior aspect of the semimembranosus muscle and, more distally, to the semimembranosus tendon. The gracilis and sartorius lie in a more medial position. The sartorius muscle has a very short flat tendon, which inserts on the anteromedial aspect of the tibia together with the semitendinosus and gracilis to make up the so-called pes anserinus complex, whose name derives from the flattened appearance of these tendons which resembles a goose's foot (Fig. 14.3b). A bursa is often present deep to the pes anserinus.

14.2.4 Popliteal Fossa

The popliteal space is a rhombic space bounded proximally by the semimembranosus and semitendinosus (medially) and the biceps femoris (laterally) muscles and distally by the medial and lateral heads of the gastrocnemius (Fig. 14.8a). The fossa appears as a hollow space when the knee joint is flexed and, in general, is smaller than expected because the muscular boundaries are packed closely together. The muscles and tendons delimiting the fossa can easily be seen on the skin and felt by palpation (Fig. 14.8b). The popliteal fossa contains important neurovascular structures, including the popliteal artery and vein, the small saphenous vein, the tibial and common peroneal nerves, and a small muscle, the plantaris, which can be found in approximately 90% of individuals (Fig. 14.9). This latter muscle takes its origin from the lower part of the lateral supracondylar line and the adjacent popliteal surface of the femur and continues downward in a slim tendon which crosses the entire calf between the medial head of the gastrocnemius and the soleus to insert into the calcaneus on the medial side of the Achilles tendon. Loose connective and fatty tissue fill the space among vessels and nerves.

14.2.4.1 Popliteal Vessels

The popliteal artery is the direct continuation of the femoral artery. It begins at the adductor hiatus and ends at the inferior edge of the popliteus muscle where it divides into the anterior and posterior tibial arteries. In the popliteal fossa,

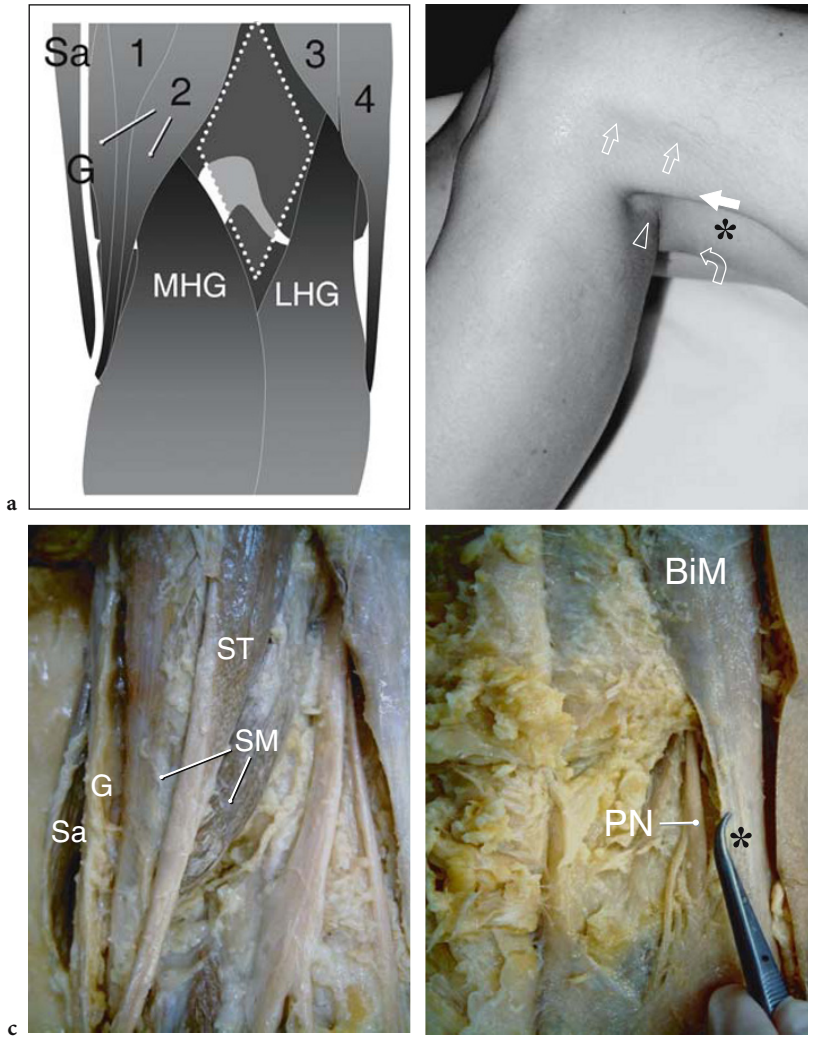

Fig. 14.8a–d. Anatomy of the popliteal space: tendons. **a** Schematic drawing of a posterior view of the knee reveals the popliteal space as a rhombus-shaped area (*dotted light-gray rhombus*) delimited by medial and lateral tendons. Medial tendons include the semitendinosus (*1*), semimembranosus (*2*), gracilis (*G*) and sartorius (*Sa*) and the medial head of the gastrocnemius (*MHG*). Lateral tendons include the short (*3*) and long (*4*) heads of the biceps muscle cranially and the caudal lateral head of the gastrocnemius (*LHG*) caudally. **b** Photograph of the posterolateral aspect of a flexed knee reveals the main surface features of the popliteal fossa (*asterisk*), bounded superolaterally by the biceps femoris tendon (*straight white arrow*) and superomedially by the semitendinosus tendon (*curved arrow*). Note the prominence of the tendon of the medial head of the gastrocnemius (*arrowhead*) and the iliotibial band (*open straight arrows*). **c** Gross cadaveric view of the medial popliteal fossa demonstrates the thin tendon of the semitendinosus (*ST*) which lies on the posterior aspect of the semimembranosus (*SM*) muscle. The tendons of the gracilis (*G*) and sartorius (*Sa*) are located more medially. **d** Gross cadaveric view of the lateral popliteal fossa reveals the relationship of the biceps muscle (*BiM*) and tendon (*asterisk*) with the common peroneal nerve (*PN*)

the popliteal artery gives off a series of geniculate branches to supply the joint capsule and the ligaments. They are the lateral superior and inferior, the medial superior and inferior and the middle genicular arteries. These vessels anastomose with each other to form a superficial and deep arterial network. The inferior medial genicular artery passes deep to the pes anserinus complex and can be appreciated with US. The popliteal vein is located superficial to the artery and deep to the tibial nerve (Fig. 14.7a). In the popliteal fossa, the popliteal vein may be single (56%) or double (44%) and receives the small saphenous vein, the genicular veins and the gemellary veins (Quinlan et al. 2003). The tibial nerve is posterior relative to the popliteal vessels.

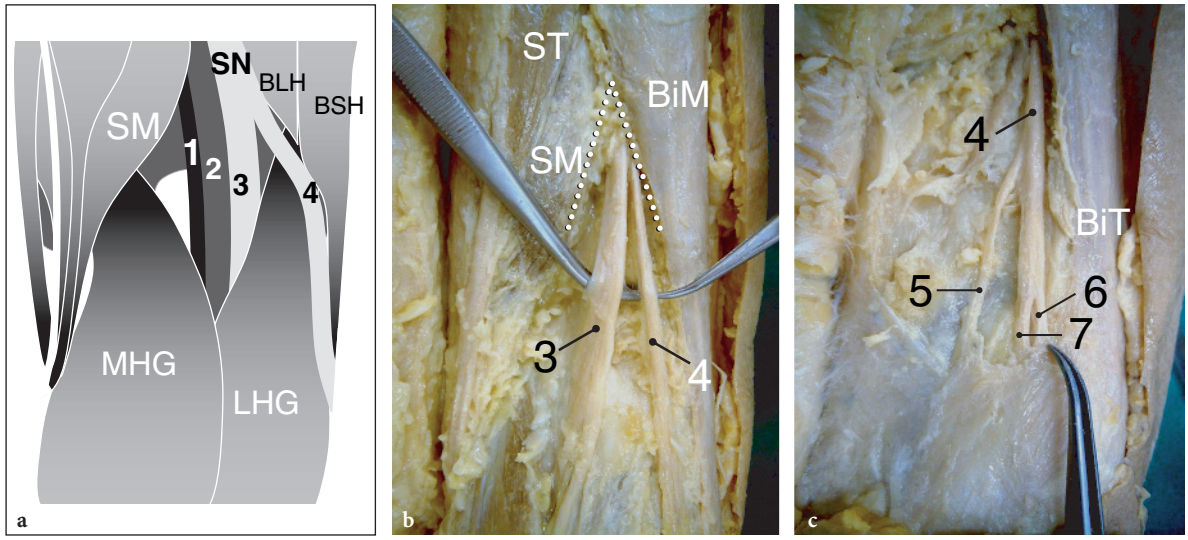

Fig. 14.9a–c. Anatomy of the popliteal space: nerves. **a** Schematic drawing of a posterior view of the knee illustrates the vertical course of the popliteal artery (*1*) and vein (*2*) though the popliteal fossa. The tibial (*3*) and common peroneal (*4*) nerves arise from the sciatic nerve (*SN*) at the superior apex of the popliteal space. *BLH* and *BSH*, long and short heads of the biceps femoris; *LHG* and *MHG*, medial and lateral heads of the gastrocnemius; *SM*, semimembranosus. **b,c** Corresponding gross cadaveric view of the popliteal fossa shows **b** the apex of the popliteal space (*dotted line*) delimited by the medial edge of the biceps (*BiM*) and the lateral edge of the semimembranosus (*SM*). *ST*, semitendinosus. The larger tibial nerve (*3*) and the smaller peroneal nerve (*4*) are also demonstrated. **c** More caudally, the common peroneal nerve (*4*) is seen dividing into its terminal branches: the lateral sural cutaneous nerve (*5*); the deep peroneal (*6*) and the superficial peroneal (*7*) nerves. Note the close relationship between these nerves and the biceps femoris tendon (*BiT*)

14.2.4.2 Tibial and Peroneal Nerves

The sciatic nerve descends the thigh with two series of fascicles grouped independently in a medial and lateral trunk which split at the apex of the popliteal fossa to proceed down as the tibial and the common peroneal nerves (Fig. 14.9a,b). Posterior to the popliteal vessels, the tibial nerve continues the straight direction of the sciatic nerve to enter the leg beneath the soleus arcade. It gives off the sural nerve in the popliteal fossa and, more distally, sends out motor branches for the posteromedial compartment of the leg. On the lateral side of the tibial nerve, the common peroneal nerve descends obliquely through the lateral portion of the popliteal fossa along the posteromedial aspect of the biceps femoris muscle and tendon and external to the lateral head of gastrocnemius (Figs. 14.8c, 14.9, 14.10a,b). More distally, this nerve curves anteriorly to pass in a restricted space under the fascia and then deep to the attachment of the peroneus longus muscle to the fibula, the so-called fibular tunnel (Fig. 14.10a,c). Exiting this tunnel, the nerve winds around the fibular neck to enter the anterolateral compartment of the leg where it divides into its two terminal branches, the superficial and deep peroneal nerves. The first supplies the peroneal muscles, the second the tibialis anterior, the extensor hallucis longus and the extensor digitorum longus and brevis of the fingers (Fig. 14.10a,d). A recurrent articular branch arises from the proximal segment of the deep peroneal nerve, just distal to the division of the common peroneal nerve into the deep and superficial nerves, so one could consider the peroneal bifurcation to be in fact a trifurcation (Fig. 14.10a) (Spinner et al. 2003a,b). This recurrent branch courses around the fibula to supply the superior tibiofibular joint and is implicated in the pathogenesis of the intraneural peroneal ganglia (Spinner et al. 2003a,b).

14.2.5 Bursae

There are several bursae around the knee. These may be either subcutaneous in location (such as the prepatellar bursa and the superficial infrapatellar bursa), between tendons and bone (such as the deep infrapatellar bursa) or between tendons and ligaments (such as the anserine bursa, the semimembranosus-medial collateral ligament bursa and

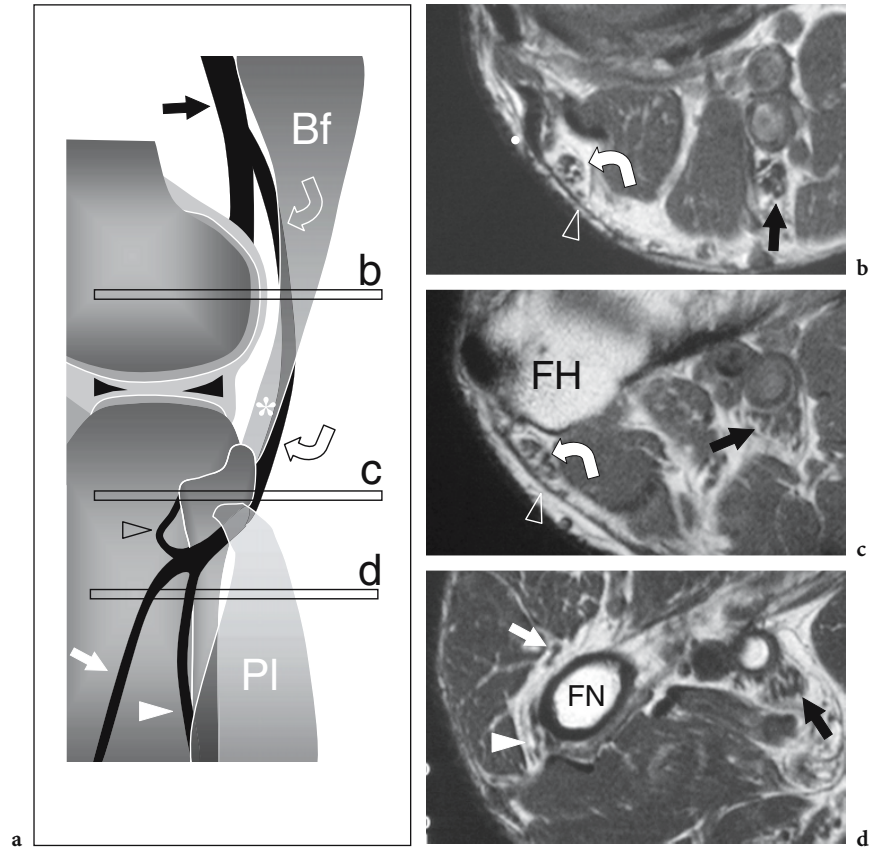

Fig. 14.10a–d. Anatomy of the peroneal nerve. **a** Schematic drawing of a lateral view of the knee illustrates the course of the common peroneal nerve (*curved arrows*) which branches from the sciatic nerve (*black arrow*) at the apex of the popliteal fossa and descends posterior to the biceps femoris muscle (*Bf*) and tendon (*asterisk*) to turn anteriorly around the fibular head. The nerve then continues down between the lateral side of the neck of the fibula and the peroneus longus muscle (*Pl*). Here the peroneal nerve divides into its two terminal branches, the superficial peroneal nerve (*white arrowhead*) and the deep peroneal nerve (*white arrow*), and sends a recurrent articular branch (*open arrowhead*). **b-d** Transverse T1-weighted MR images obtained at the levels indicated in **a** (*horizontal bars*) reveal the normal position of the common peroneal nerve (*curved arrow*) relative to the biceps tendon, the crural fascia (*open arrowhead*) fibular head (*FH*). Note the relationships of the main trunk and the superficial (*white arrowhead*) and deep (*white arrow*) peroneal nerves with the fibular and neck (*FN*). *Black arrow*, tibial nerve

the biceps femoris-lateral collateral ligament bursa). These bursae reduce friction and allow a smooth and autonomous gliding of these structures during joint movements (McCarthy and McNally 2004). The semimembranosus-gastrocnemius bursa and the semimembranosus-medial collateral ligament bursa may communicate with the femorotibial joint.

From the anatomic point of view, the subcutaneous prepatellar bursa is located anterior to the lower half of the patella and the proximal patellar tendon, just deep to the skin. More caudally, the superficial infrapatellar bursa is located between the tibial tuberosity and the skin. The deep infrapatellar bursa lies between the deep boundary of the distal patellar tendon and the anterior aspect of the tibia. The anserine bursa intervenes between the superficial pes anserinus complex and the deep tibial insertion of the medial collateral ligament and medial tibial condyle, slightly distal to the insertion of the semimembranosus. The semimembranosus-tibial collateral ligament bursa lies between the semimembranosus tendon and the medial collateral ligament, and has a deeper extension between the semimembranosus tendon and the medial tibial condyle. The biceps femoris-lateral collateral ligament bursa has an inverted-J shape and lies superficial to the lateral collateral ligament and deep to the anterior aspect of the long head of the biceps femoris.

The semimembranosus-gastrocnemius bursa is located at the medial aspect of the popliteal space, between the semimembranosus tendon and the medial head of the gastrocnemius (Guerra et al.

1981) (Fig. 14.11). This bursa is lined with synovium and derives from the fusion of the superficial semimembranosus bursa, which is interposed between the tendon of the semimembranosus and the medial head of gastrocnemius, and the deep medial head bursa, which separates the tendon of the medial head of the gastrocnemius from the joint capsule. In some instances these two bursae do not communicate, leading to the presence of two separate synovial cavities that can undergo independent distension by fluid. The communication between the semimembranosus-gastrocnemius bursa and the knee joint is increasingly observed with aging (Fig. 14.11). In children, the bursa is completely separated from the posterior joint space, whereas in adults the bursa is in communication in approximately 35–55% of cases through a thin transverse opening located at the superomedial aspect of the femoral condyle. It has been postulated that chronic friction generated by the two tendons over the condyle and between themselves can result in degeneration, thinning of the posterior capsule and perforation, thus allowing communication between the articular cavity and the semimembranosus-gastrocnemius bursa (Lindgern and Willen 1977). From the anatomic standpoint, the semimembranosus-gastrocnemius bursa consists of three main portions: the base, the neck and the body (Fig. 14.11b,d). The base is small, anteriorly located and communicates with the femorotibial joint; the neck is a narrow tract between the semimembranosus tendon and the medial head of the gastrocnemius; the body is the largest posterior portion of the bursa and lies dorsal to the gastrocnemius.

14.3 Essentials of Clinical History and Physical Examination

The first question to ask to the patient with knee complaints is whether the symptoms are chronic or acute. In chronic abnormalities, the possible occurrence of systemic articular disorders such as rheumatoid and psoriatic arthritis, seronegative spondyloarthropathy, and degenerative and metabolic disorders should be considered. Close coop-

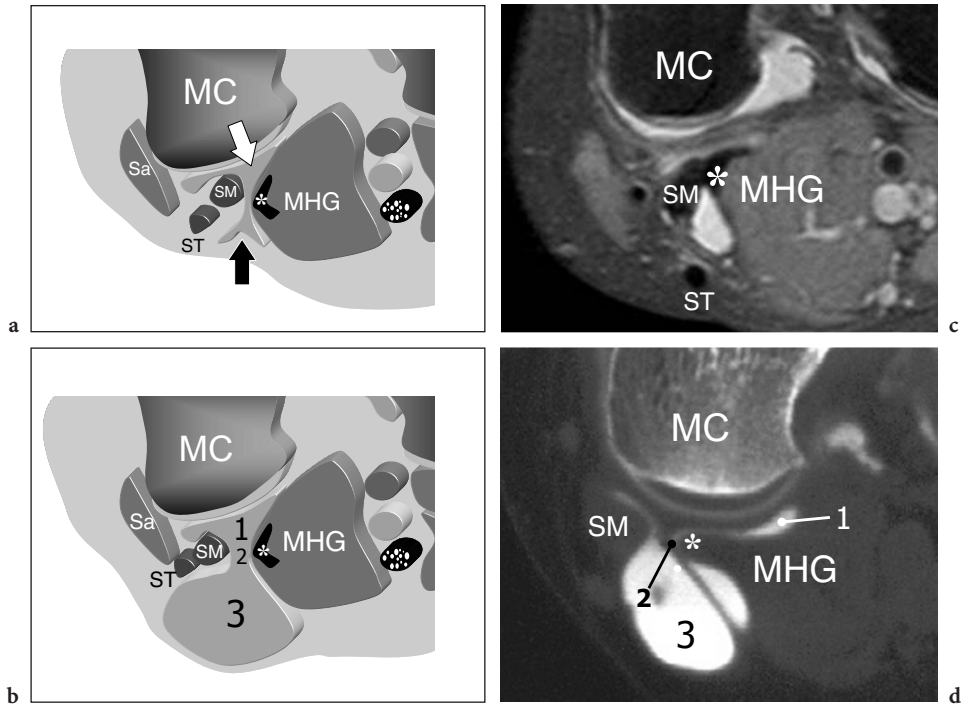

Fig. 14.11a–d. Anatomy of the semimembranous-gastrocnemius bursa. **a,b** Schematic drawings of a transverse view through the popliteal fossa show the normal position of the bursa located between the tendon of the semimembranosus (*SM*), the tendon (*asterisk*) of the medial head of the gastrocnemius (*MHG*) and the posterior aspect of the medial femoral condyle (*MC*). *Sa*, sartorius; *ST*, semitendinosus. **b** When the bursa is distended by effusion, its three components are better identified: the deep base (*1*), a narrow neck (*2*) and the large superficial body (*3*). Note that the semitendinosus tendon (*ST*) lies more remotely from the bursa than the semimembranosus. **c,d** Correlative axial **c** fat-suppressed T2-weighted MR and **d** CT-arthographic images

eration with the referring clinician is of the utmost importance in evaluating patients with knee complaints. Chronic knee symptoms may also derive from local repetitive microtrauma related to sporting or professional activities. In these patients, the type of occupation and sport practiced by the patient must be considered, as some sporting activities are commonly associated with specific pathologic conditions affecting the knee. Volleyball players, for instance, are prone to Osgood-Schlatter disease and patellar tendinitis due to repetitive shocks on the anterior aspect of the knee and sudden intense contractions of the extensor mechanism during jumping. On the other hand, acute knee symptoms are related, in most cases, to trauma. The circumstances in which the traumatic event has occurred (e.g., traffic accident, sporting accident), the magnitude and direction of the traumatic force and the behavior after trauma (feeling of instability, preserved ability to walk and run, knee swelling, etc.) should be clarified because these data may help to focus the US examination on specific anatomic structures. For instance, trauma occurring in valgus stress usually leads to strain and tearing of the medial collateral ligament, whereas excessive hyperextension of the knee may cause damage to the anterior cruciate ligament or the hamstring muscles. In a definite traumatic setting, however, the possibility that knee arthritis may be a coexisting condition must always be considered. Following a direct blow on the knee, for example, patients affected by gout can present with acute microcrystalline synovitis. Septic arthritis may develop from even a small penetrating soft-tissue injury. On the other hand, knee locking should recall meniscal lesions and patients with intra-articular loose bodies.

Next, every effort should be made to localize the pain as precisely as possible because this can provide useful information to target the US examination. As a general rule, diffuse knee pain derives from joint lesions, whereas more localized pain is more commonly related to tendon involvement and local disorders. Information on the character, duration and location of pain is extremely helpful in the evaluation of tendinitis. In "jumper's knee", for instance, the patient typically reports pain over the most proximal portion of the patellar tendon, just behind the tip of the patella. Runners complaining of lateral knee pain and tenderness should be questioned for signs of tendinitis affecting the distal insertion of the biceps femoris and the iliotibial band, so-called "runner's knee". In the event of soft-tissue lumps or indeterminate swelling around the knee, the patient should be asked about the onset of the finding, whether immediate or delayed, because rapidly growing masses are most often associated with benign conditions (e.g., synovitis). On the anterior aspect of the knee, joint synovitis is usually revealed by a diffuse soft-tissue swelling around the superior and lateral aspects of the patella. When a large Baker cyst is present, a mass is palpated at the medial aspect of the popliteal space. Typically, a Baker cyst is tense in extension and compressible in knee flexion. One should be aware, however, that other painful masses in the posterior fossa may mimic a Baker cyst, including posterior ganglia.

A basic inspection of both knees for comparison and palpation with the patient standing can be easily performed while taking the patient's history. Any detection of asymmetry in the soft tissues around the abnormal knee compared with the joint contour of the unaffected side and local areas of increased temperature should be noted. The range of knee joint movements can be rapidly investigated by asking the patient to perform flexion/extension movements. Impaired knee extension may suggest meniscal lesions with impingement. Several other specific maneuvers to detect meniscal lesions and assess collateral and cruciate ligaments (varus-valgus tests, anterior and posterior drawer signs, pivot shift test) are beyond the knowledge required for carrying out a complete US examination.

Similar to other joints, viewing of recent standard radiographs is an essential step before starting the US examination of the knee. The availability of knee radiographs may occasionally be helpful for a correct interpretation of troublesome US images. The US appearance of bone exostoses can be misleading, for instance, and their diagnosis time-consuming, while they are readily evident on standard radiographs. On the other hand, given the diagnosis on plain films, US can assess the thickness and regularity of the cartilaginous cap of the exostosis and can be useful to follow up the lesion (Malghem et al. 1992).

14.3.1 Knee Joint Effusions

Clinical demonstration of a knee effusion depends on the amount of intra-articular fluid. Abundant joint effusions can be detected by the "patellar tap" test in which the examiner first compresses the suprapatellar recess with one hand to squeeze the fluid under the patella and then pushes the patella

against the trochlea with the other hand. In large effusions, a shock wave can be felt with the hand when the patella impacts on the anterior aspect of the trochlea. Smaller effusions can be demonstrated by the "bulging" sign. First, the examiner squeezes the fluid away from the medial aspect of the joint by applying pressure with one hand over it. Then, he or she looks at the medial parapatellar region while squeezing the lateral aspect of the knee. When small effusions exist, a local wave or bulging can be appreciated on the skin corresponding to the fluid displaced from lateral to medial.

14.4 Normal US Findings and Scanning Technique

The anterior aspect of the knee is basically examined with the patient supine on the examination table. Only in selected cases changes in the patient's position may be helpful. If intra-articular loose bodies are suspected, correlative images obtained by alternating supine and standing position may be helpful to produce displacement of the fragments (Bianchi and Martinoli 1999). In case of small cysts arising from the anterior horn of the lateral meniscus, the knee joint should be examined with the patient squatting to induce changes in the size and location of the cyst, making it more prominent and, therefore, more visible with US. With the patient supine, different degrees of knee flexion and extension can be obtained to facilitate the evaluation of normal and pathologic structures. In knee extension, the cartilage of the femoral trochlea cannot be seen with US because it is masked by the patella, whereas during progressive flexion the superior, intermediate and inferior portions of this cartilage become gradually uncovered by the patella and can reliably be assessed. Routine assessment of the trochlear cartilage is obtained on anterior transverse US images obtained with the knee forcefully flexed (Martino et al. 1998). On the other hand, US examination of the medial patellar cartilage must be performed while keeping the knee extended because this position allows the patella to be less firmly adherent to the trochlea. During full extension, the patella is subluxed medially to reposition its medial cartilage and the medial plica for an adequate examination.

In most cases, US examination of the posterior aspect of the joint is carried out with the patient prone keeping the knee extended. However, imaging the posterior structures in slight flexion can reduce tension on the posterior tendons and may reveal a communication of some Baker cysts with the knee joint. In addition, knee flexion allows an increase in the internal pressure of the posterior veins to obtain their full distension. The ability to perform a dynamic study is a specific advantage of US over other imaging modalities. A variety of structures, such as paraarticular ligaments and tendons, can be examined at rest, with stress maneuvers or during active muscle contraction. In many cases, dynamic scanning may add supplementary information to the morphologic findings. Snapping syndromes, for instance, can be assessed while the patient reproduces the exact movement for clicking. In these circumstances, care should be taken to avoid excessive pressure with the probe on the skin so as not to hinder the motion of the structures which cause the snapping sensation.

In most cases, the evaluation of the contralateral unaffected knee is not essential and, therefore, we do not perform it routinely. It may become helpful while evaluating small intra-articular effusions. Because small quantities of intra-articular fluid can be present in normal states, mild joint fluid must be compared with the findings in the contralateral knee before considering it abnormal.

The routine US examination of the knee starts with its anterior aspect, followed by the medial, lateral and posterior aspects.

14.4.1 Anterior Knee

As already stated, the anterior aspect of the knee is best examined with the patient supine. A knee flexion of approximately 20°–30° obtained by placing a small pillow beneath the popliteal space stretches the extensor mechanism and avoids possible artifacts related to anisotropy which are secondary to the concave profile these tendons assume in full extension (Bianchi et al. 1994). In this position, the anterior aspect of the knee is examined starting from cranial to caudal. The suprapatellar, juxtapatellar and infrapatellar regions are imaged in succession (Fig. 14.12).

Relevant anatomic structures in the suprapatellar region that are amenable to US examination are: the quadriceps tendon, the suprapatellar synovial recess, the suprapatellar fat pad, the prefemoral fat, the distal femoral metaphysis and the trochlea. Longitudinal US images obtained in the midline with the probe placed with its distal edge on the patella are

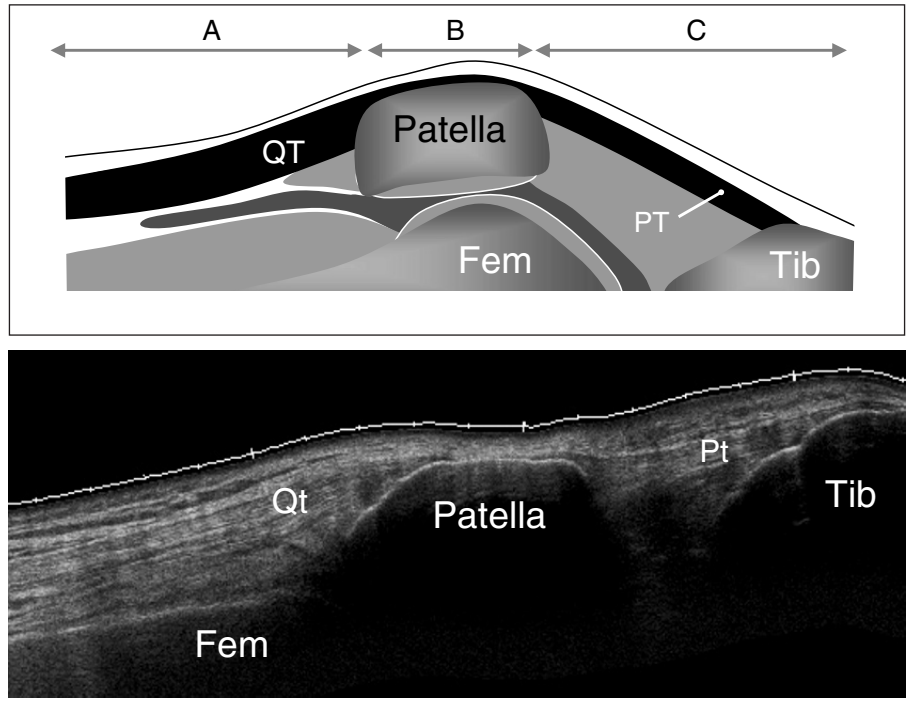

Fig. 14.12a,b. Anterior aspect of the knee. **a** Schematic drawing with **b** corresponding extended-field-of-view longitudinal 12–5 MHz US image over the anterior aspect of the knee demonstrates the extent of the suprapatellar (*A*), iuxtapatellar (*B*) and infrapatellar (*C*) regions. Due to their superficial location, the main structures of the extensor mechanism of the knee, the quadriceps tendon (*Qt*), the patella and the patellar tendon (*Pt*) are well depicted with US. *Fem*, femur; *Tib*, tibia

able to display the quadriceps tendon. If the quadriceps tendon is stretched and the US beam is perpendicular to its long axis, it shows a hyperechoic fibrillar appearance (Fig. 14.13a,b). On the contrary, when the knee is extended, the quadriceps becomes loose and assumes a concave appearance (Fig. 14.13c,d). In this case, a wavy, hypoechoic preinsertional portion can be appreciated, possibly mimicking pathologic changes (Fornage 1987). During full knee flexion, the quadriceps tendon is pushed anteriorly by the femoral trochlea and assumes a curved appearance over it (Fig. 14.14). Using high-frequency probes, the quadriceps tendon exhibits a multilayered appearance on both long- and short-axis planes due to the close apposition and distal union of the three tendon layers arising from the four bellies of the quadriceps femoris muscle (Fig. 14.15). While the superficial layer is always evident, differentiation between the intermediate and deep layers may not be so straightforward (Bianchi et al. 1994). Thin hyperechoic nonfibrillar bands reflecting fibrofatty planes are visible among the fibrillar layers. The ability to evaluate the intratendinous structure and to discriminate among the individual tendon components has a practical value as it allows differentiation between full- (involvement of all three layers) and partial-thickness (selective involvement of one or two layers) tears. In these cases, transverse US images must always be obtained to assess the width of the tear in the coronal plane and to identify more lateral lesions that can go unnoticed on longitudinal planes obtained in the midline. Shifting the probe cranially, the myotendinous junctions of the quadriceps muscle bellies can be appreciated: that of the rectus femoris is located at a more proximal level compared with the others (Fig. 14.15c).

Just deep to the quadriceps tendon and superficial to the metaphysis of the femur, two fat pads (suprapatellar and prefemoral) and the suprapatellar recess can be identified with US (Fig. 14.16). The small suprapatellar fat pad is located cranial to the patella and posterior to the distal third of the quadriceps tendon. On longitudinal images, it appears as a well-defined hyperechoic triangle with its base located distally and the apex pointing cranially. Immediately superficial to the femur, the prefemoral fat pad appears as a large hyperechoic space. The suprapatellar synovial recess lies deep to the quadriceps tendon and the suprapatellar fat pad and superficial to the prefemoral fat. In normal conditions, mid-longitudinal US images

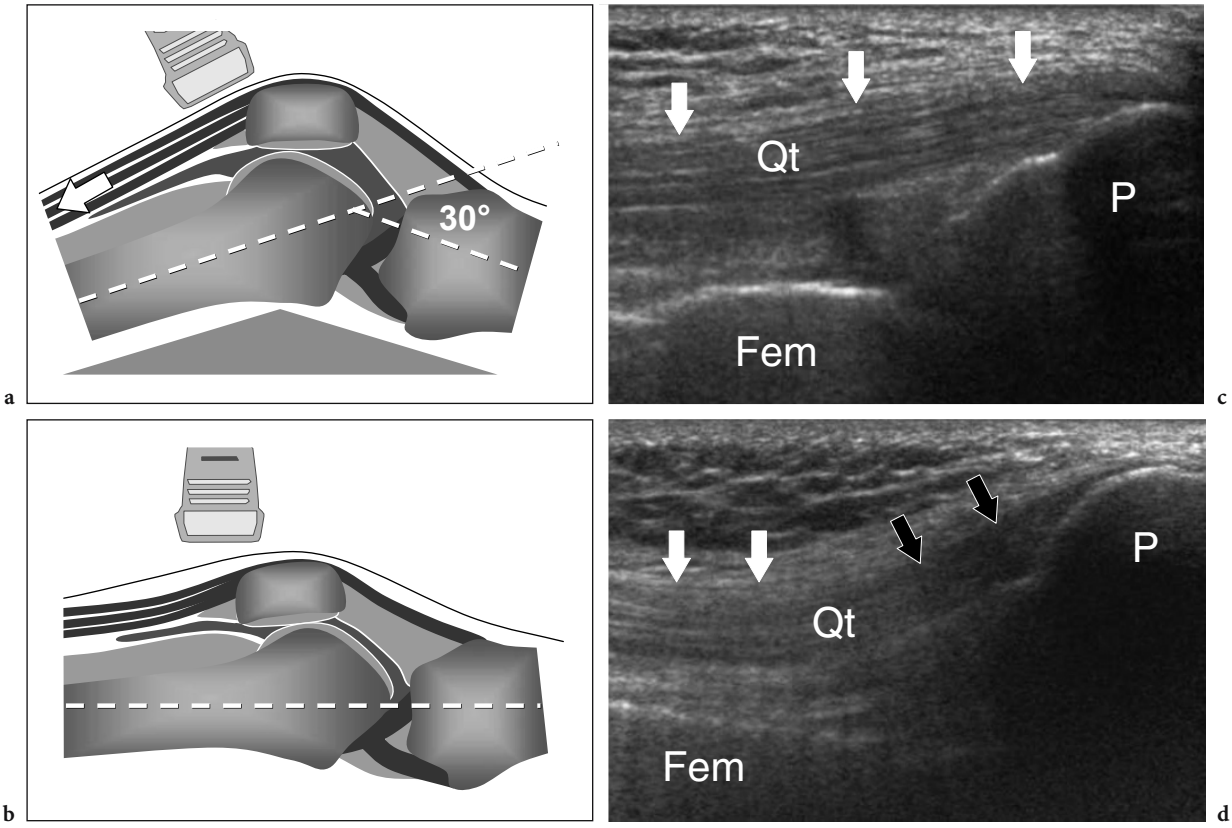

Fig. 14.13a–d. Quadriceps tendon: scanning technique. **a,b** Schematic drawings show the US study of the quadriceps tendon **a** with the knee flexed at approximately 30° and **b** extended. Both the quadriceps and the patellar tendons are stretched (*arrow*) and assume a straight course when the knee is flexed by placing a pillow under the popliteal space. **c,d** Corresponding long-axis 12–5 MHz US images of the quadriceps tendon (*Qt*) obtained with flexed (**c**) and extended knee (**d**). In **c**, the tendon tends to assume a perpendicular course relative to the US beam and, therefore, is characterized by a hyperechoic structure with a discrete fibrillar echotexture (*white arrows*). Note that the distal tendinous portion can be accurately evaluated until its insertion into the upper pole of the patella. **d** With full knee extension, the distal portion (*black arrows*) of the quadriceps tendon (*white arrows*, *Qt*) assumes a falsely hypoechoic appearance as a result of anisotropy because the tendon is loose. *Fem*, femur; *P*, patella

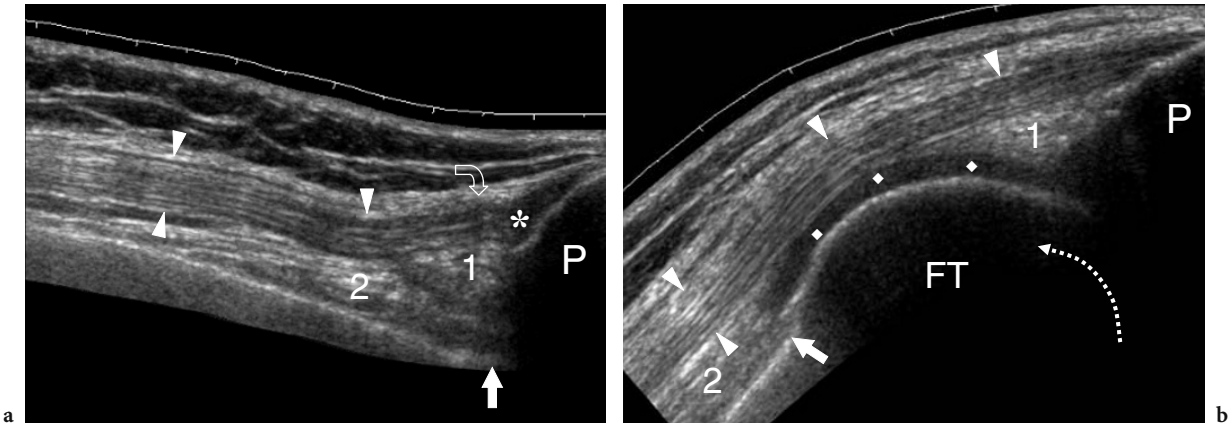

Fig. 14.14a,b. Quadriceps tendon. **a,b** Long-axis extended-field-of-view 12–5 MHz US images over the quadriceps tendon obtained **a** with the knee extended and **b** with the knee maximally flexed. **a** With extended knee, the quadriceps tendon (*arrowheads*) is loose and wavy and exhibits a hypoechoic preinsertional portion (*asterisk*) which could mimic a pathologic condition. **b** When the knee is maximally flexed, the tendon is pushed anteriorly, over the cartilage (*rhombi*) of the femoral trochlea (*FT*) and assumes a curved appearance over it. Note the suprapatellar (*1*) and prefemoral (*2*) fat pads which lie adjacent during extension and separate during flexion. Also, observe the metaphysis of the femur (*arrow*) which moves away from the patella during knee flexion

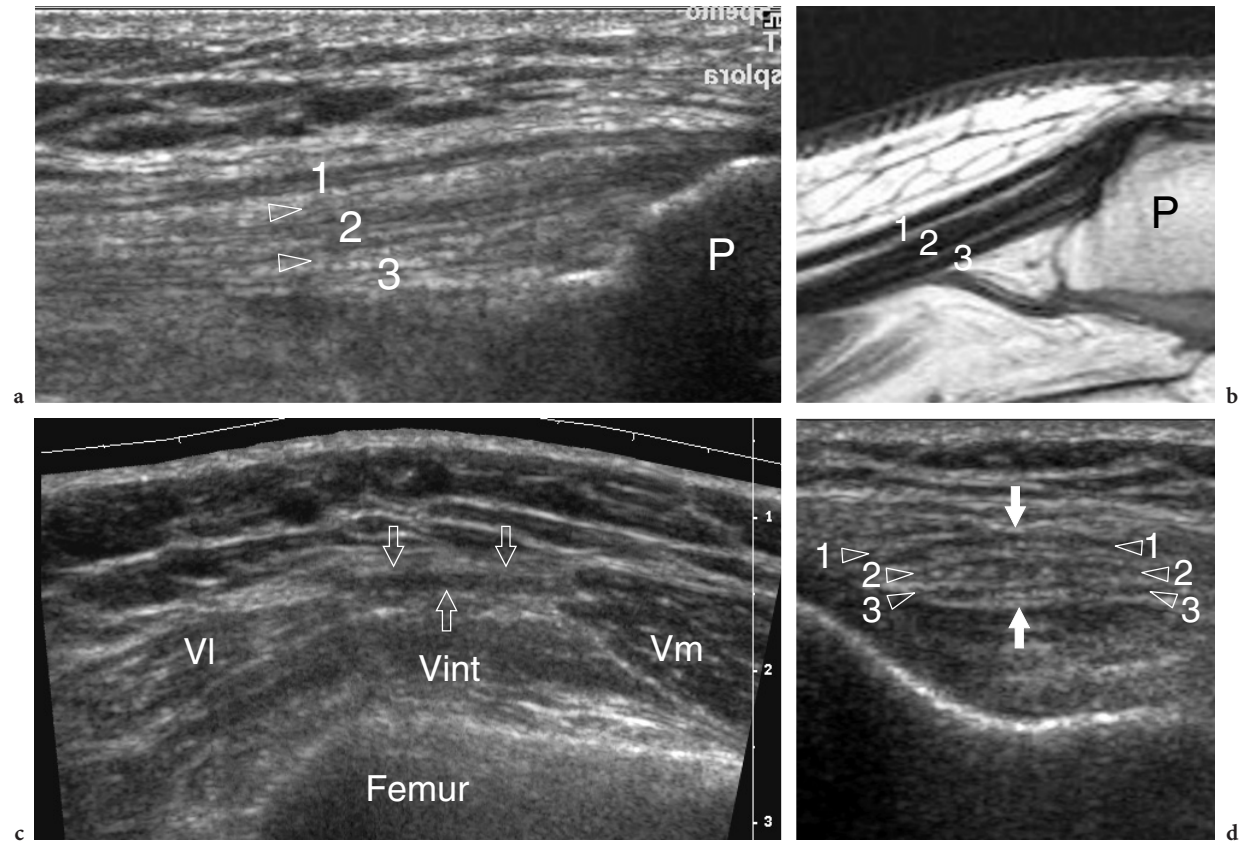

Fig. 14.15a–d. Quadriceps tendon. **a** Longitudinal 12–5 MHz US image over the suprapatellar region with **b** sagittal T1-weighted MR imaging correlation demonstrates the multilayered appearance of the quadriceps tendon consisting of the superficial layer of the rectus femoris (*1*), the intermediate layer of the vastus medialis and lateralis (*2*) and the deep layer of the vastus intermedius (*3*). These layers exhibit a well-defined fibrillar echotexture. Intervening bands of fibrofatty tissue (*arrowheads*) can be demonstrated among them. *P*, patella. **c,d** Transverse 12–5 MHz US images obtained **c** at the anterior distal thigh and **d** just above the patella. **c** The myotendinous junctions of the quadriceps muscle can be appreciated with the bellies of the vastus lateralis (*Vl*), vastus medialis (*Vm*) and vastus intermedius (*Vint*) converging toward the flattened tendon of the rectus femoris (*arrows*). **d** The three layers (*1, 2, 3*) of the quadriceps tendon (*arrows*) are also appreciated on the short-axis plane

demonstrate the suprapatellar recess as a thin hypoechoic space which results from a collapsed anterior and posterior synovial membrane (Fig. 14.16b). Intra-articular fluid can be seen with US as an anechoic collection located inside the recess. Although joint effusion can be manifest at physical examination, detection of small amounts of fluid is more accurate and reliable using US (Hauzeur et al. 1999). Dynamic examination obtained during isometric contraction of the quadriceps muscle or forced dorsiflexion of the foot with the knee extended may be helpful to detect small effusions within the suprapatellar recess. Quadriceps activation and hyperextension induce cranial shifting of fluid displacing the Hoffa fat pad against the femoral condyles and tightening the posterior fascia. However, small amounts of synovial fluid tend to accumulate in the lateral and medial parts of the recess (which are dependent with the patient supine) and within the parapatellar recesses, rather than in the midline. This would suggest obtaining scanning not only in the midline but also along the lateral and medial sides of the quadriceps tendon. A mild amount of intra-articular fluid is normal in asymptomatic subjects and correlation with clinical data and with the findings observed in the contralateral knee is mandatory. When the analysis of synovial fluid is essential to plan the diagnostic investigation (suspected septic or gout arthritis), US can help in identifying the puncture site and guiding the aspiration when the fluid is not abundant. A focal bulging of the hyperechoic prefemoral fat within the inferolateral aspect of the suprapatellar recess is a common finding at US and can occasionally mimic a synovial mass (Fig. 14.17). This image should not

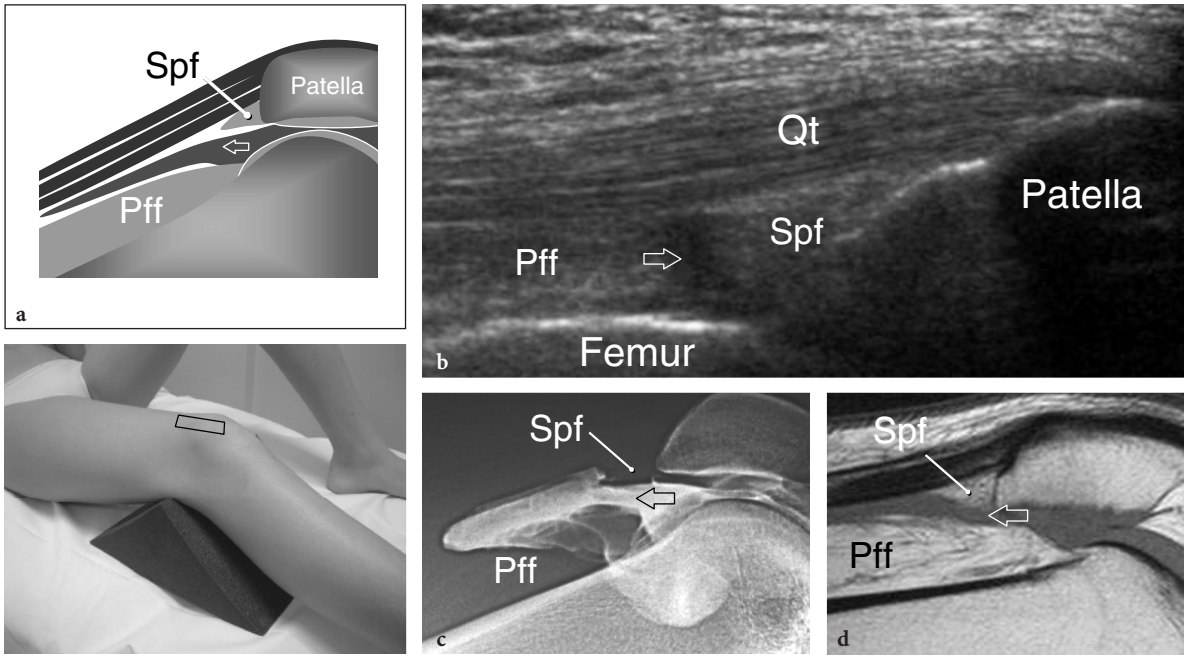

Fig. 14.16a–d. Suprapatellar region. **a** Schematic drawing and **b** corresponding long-axis 12–5 MHz US image over the quadriceps tendon (*Qt*) with **c** lateral arthrographic and **d** longitudinal T1-weighted MR imaging correlation demonstrate the relationship of the suprapatellar synovial recess (*arrow*) with the suprapatellar (*Spf*) and prefemoral (*Pff*) fat pads. The photograph at the bottom left indicates probe positioning

be confused with hypertrophied synovium or lipoma arborescens. Typically, the pseudomass has clear-cut margins and a nodular appearance. Gradual compression with the probe reveals a soft compressible nature (Fig. 14.18).

Remnants of embryonic life, such as the suprapatellar plica, can be identified with US. In intrauterine life the cranial limit of the joint cavity is at the level of the patella. More proximally, a synovial bursa lies deep to the quadriceps tendon. The two synovial cavities – the bursa and the joint – are separated by a thin transversely oriented septum formed by the apposition of the two synovial membranes (Fig. 14.19a). Perforation and resorption of the septum normally occurs at the end of the fifth fetal month and allows free communication between the

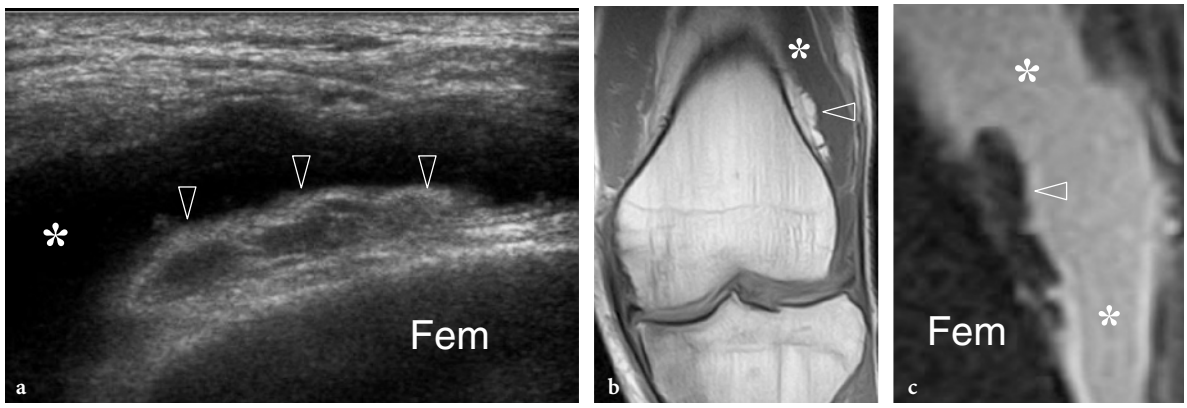

Fig. 14.17a–c. Prefemoral fat pad. **a** Coronal 12–5 MHz US image over the suprapatellar recess shows a pseudomass appearance of the prefemoral fat pad (*arrowheads*) which may become manifest when it is surrounded by an anechoic intra-articular effusion (*asterisk*). **b** Coronal T1-weighted and **c** fast STIR MR imaging correlation demonstrates a well-defined lobulated mass (*arrowheads*) which has the same signal as fat surrounded by joint effusion (*asterisks*). *Fem*, femur

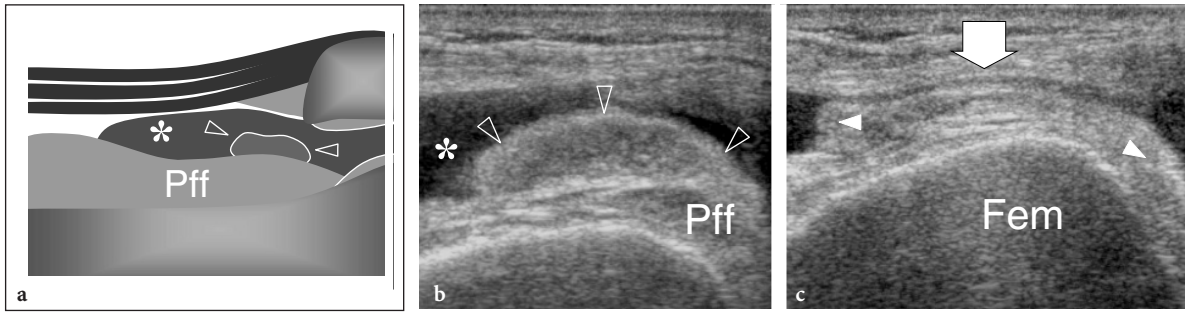

Fig. 14.18a–c. Prefemoral fat pad. **a** Schematic drawing of a midsagittal plane over the suprapatellar region and **b,c** transverse 12–5 MHz US images obtained without **b** and with **c** compression applied with the probe on the skin. The prefemoral fat (*arrowheads*) forms a well-circumscribed mass arising from the anterior aspect of the prefemoral fat and projecting inside the suprapatellar recess (*asterisk*). **b** At US, it appears as a slightly hypoechoic well-defined structure (*arrowheads*) surrounded by an anechoic effusion (*asterisk*) and blending with the deep layers of the prefemoral fat pad (*Pff*). *Fem*, femur. In **c,** note the collapse of the pseudomass (*arrowheads*) while applying pressure with the probe over it (*arrow*)

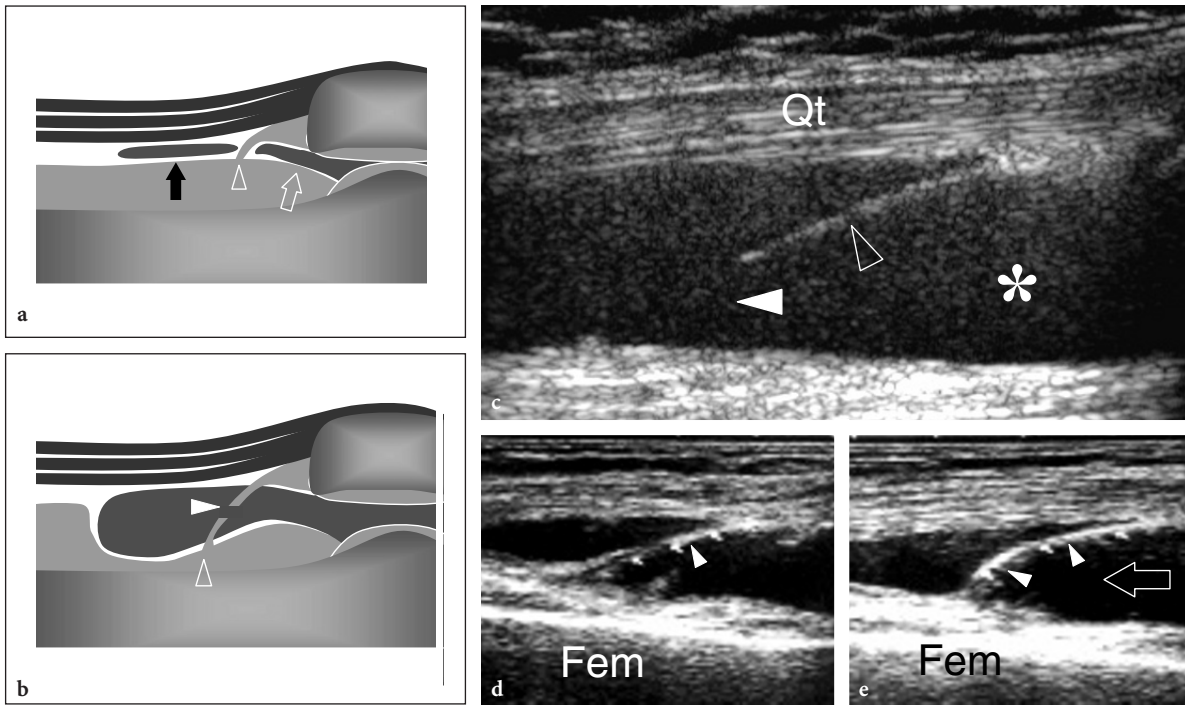

Fig. 14.19a–e. Suprapatellar plica. **a,b** Schematic drawing of a complete (**a**) and incomplete (**b**) suprapatellar plica. **a** The complete plica (*open arrowhead*) separates the suprapatellar recess (*open arrow*) from the suprapatellar bursa (*black arrow*), thus preventing communication between the two synovial cavities. **b** When the plica (*open arrowhead*) is incomplete, the suprapatellar recess communicates with the knee cavity through a small opening (*white arrowhead*). **c** Longitudinal 12–5 MHz US appearance of the suprapatellar region in a patient with an incomplete plica. Deep to the quadriceps tendon (*Qt*), the plica appears as a thin incomplete hyperechoic septum (*open arrowhead*) which projects inside a distended suprapatellar recess (*asterisk*). The opening is well depicted (*white arrowhead*). **d,e** Longitudinal 10–5 MHz US images obtained **d** at rest and **e** during manual squeezing of the infrapatellar region in a patient with an incomplete plica. During squeezing, proximal bulging of the plica can be appreciated with US as induced by cranial fluid displacement (*arrow*). *Fem*, femur

two synovial spaces, thus transforming the suprapatellar bursa in the suprapatellar recess. Incomplete resorption of the septum leads to the formation of the suprapatellar synovial plica (Fig. 14.19b). This happens commonly, with a complete septum found in 12% and an opening in 20% of normal subjects (Boles and Martin 2001). The suprapatellar plica can be identified with US as a small crescent-shaped fold located 2 cm above the patella, particularly when an abundant intra-articular effusion distends the recess (Fig. 14.19c). In the absence of significant joint effusion, the plica is barely visible with US because it tends to collapse over the synovium. During squeezing of the distal joint cavity by pressing over the parapatellar recesses, dynamic US examination may show an increased concavity of the plica secondary to the cranial displacement of internal fluid, the so-called "sail sign" (Fig. 14.19d,e). In most cases, the plica is asymptomatic. However, the examiner must be familiar with its appearance because the plica might be confused with a postinflammatory fibrous septum or hypertrophied synovium (Wang et al. 1999a). Also, the suprapatellar plica should not be confused with the medial plica, which is less common but more frequently symptomatic. The presence of a suprapatellar plica can impede the intra-articular diffusion of steroids injected into the suprapatellar recess for treatment of rheumatoid arthritis, thus minimizing their therapeutic efficacy (Hertzbergerten Cate et al. 1992).

During full flexion of the knee, the femoral trochlea and the overlying cartilage can be evaluated on transverse planes. The trochlear cartilage appears as a hypoanechoic band which covers the continuous hyperechoic line of the subchondral bone (Grassi et al. 1999). In normal conditions, the cartilage of the trochlea is thicker in its central portion, has regular margins and a homogeneous appearance (Fig. 14.20). Its mean thickness ranges between 1.8 and 2.5 mm depending on the site of measurement

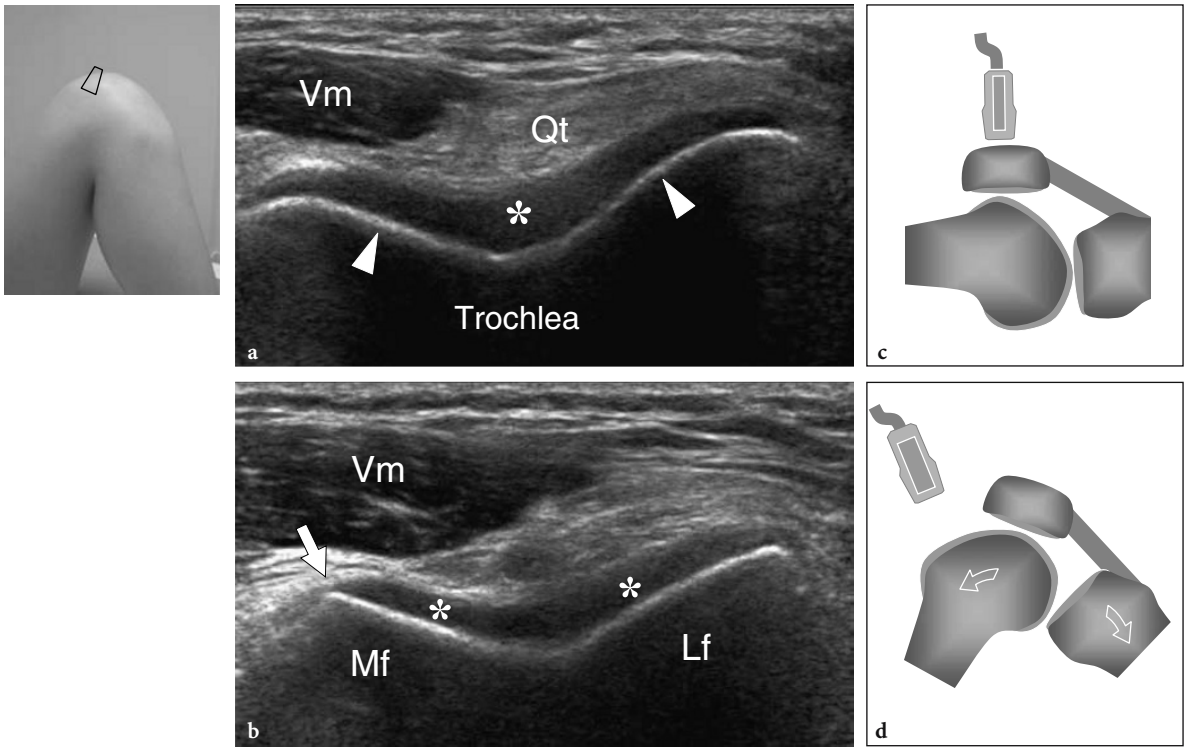

Fig. 14.20a–d. Normal trochlear cartilage. **a,b** Transverse 12–5 MHz US images obtained over the middle (**a**) and cranial (**b**) portion of the trochlea. US demonstrates the trochlear cartilage (*asterisks*) as a homogeneous hypoanechoic band overlying the bright hyperechoic line of the subchondral bone plate (*arrowheads*). In **b** observe the typical pointed appearance (*arrow*) of the edge of the medial facet (*Mf*) of the trochlea. Superficial to it, the vastus medialis muscle (*Vm*) can be seen converging toward the quadriceps tendon (*Qt*). *Lf*, lateral facet of the trachlea. **c,d** Schematic drawings illustrate the US examination technique for the trochlear cartilage. **c** When the patient is examined with the knee extended or slightly flexed, the posterior acoustic shadowing of the patella does not permit visualization of the trochlear cartilage. **d** With maximal flexion of the knee, the trochlear cartilage is repositioned (*arrows*) from underneath the patella and can be clearly appreciated. The photograph at the upper left of the figure indicates probe positioning

(Iagnocco et al. 1992). The sulcus angle and the trochlear depth can be assessed with US and correlate well with the CT findings (Martino et al. 1998). In addition, US is able to evaluate the cartilaginous sulcus angle (Fig. 14.21).

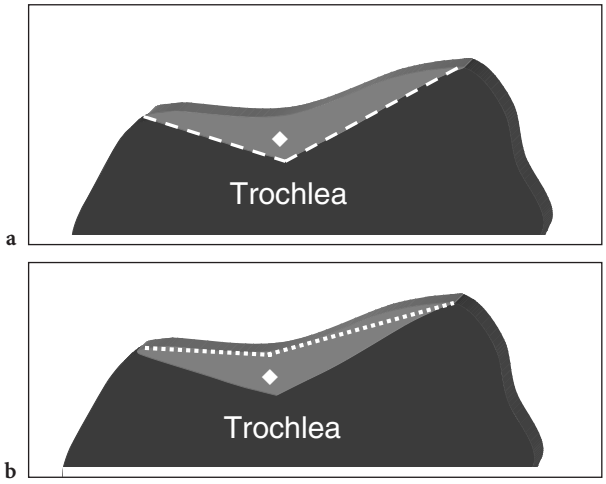

a
b

Fig. 14.21a,b. Normal trochlear cartilage. **a,b** Schematic drawings of the trochlear cartilage (*rhombus*). *Dashed line* indicates the bone sulcus in **a**. *Dotted line* indicates the cartilage sulcus in **b**. Differences in the cartilage thickness can explain why the trochlear angle measured on the bone boundaries may not correspond to the cartilage sulcus angle

Over the anterior aspect of the patella, the medial and lateral patellar retinacula can be imaged with US. Transverse planes are the best to examine these structures. The anterior aspect of the patella appears as a slightly convex bright line due to the cortical surface of bone. In asymptomatic aged patients, small calcific deposits at the proximal pole of the patella are often observed as a result of enthesopathy of the quadriceps tendon. Just over the bone, a thin fibrillar layer formed by the most superficial fibers of the rectus femoris tendon and the patellar periosteum can be seen (Fig. 14.22). More distally, these superficial fibers gradually blend with the patellar tendon. Arising from the internal and external edges of the patella, the patellar retinacula direct posteriorly to insert into the femur. They act as stabilizing structures limiting the mobility of the patella in the transverse plane (Fig. 14.23). Transverse US images demonstrate the retinacula as bilaminar structures characterized by discrete superficial and deep layers which cannot be discriminated from the underlying joint capsule (Starok et al. 1997; O'Reilly et al. 2003). An attempt to evaluate the medial articular facet of the patella with US can be made by tilting and pushing it internally while keeping the knee extended (Fig. 14.24). The lateral facet cannot be imaged with US.

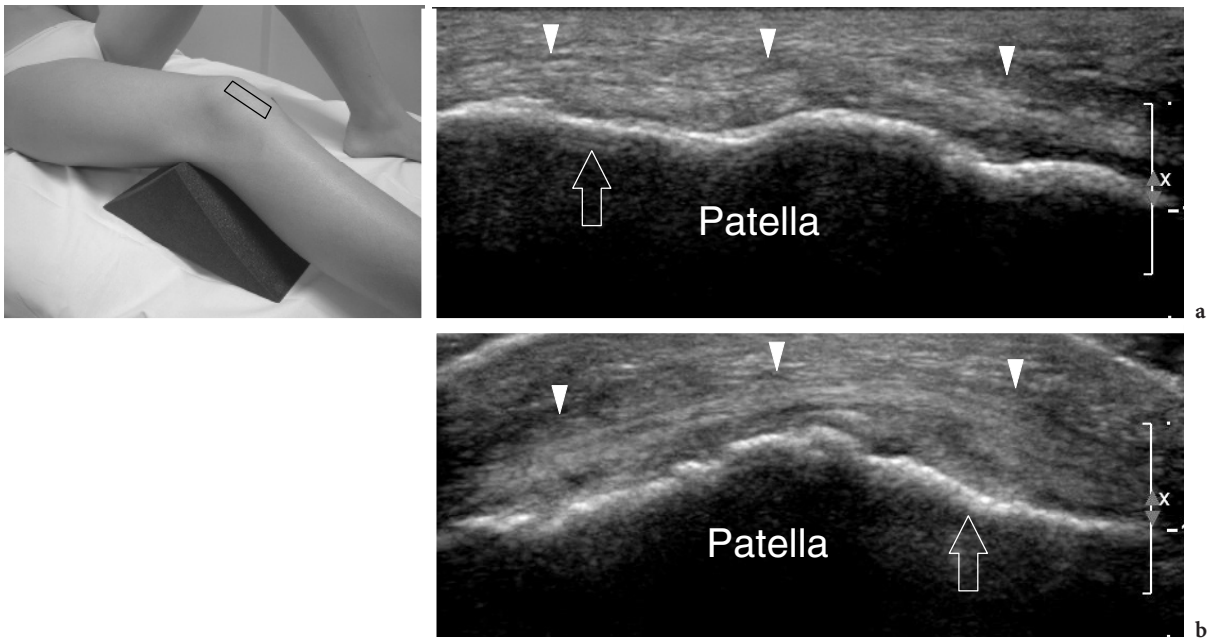

a
b

Fig. 14.22a,b. Patellar surface. **a** Longitudinal and **b** transverse 12–5 MHz US images obtained over the anterior aspect of the patella show the patellar periosteum and the most anterior fibers of the rectus femoris which combine to form a hyperechoic fibrillar band (*arrowheads*) overlying the ripple hyperechoic profile (*arrow*) of the bone. This band continues downward into the patellar tendon. The photograph at the upper left of the figure indicates probe positioning

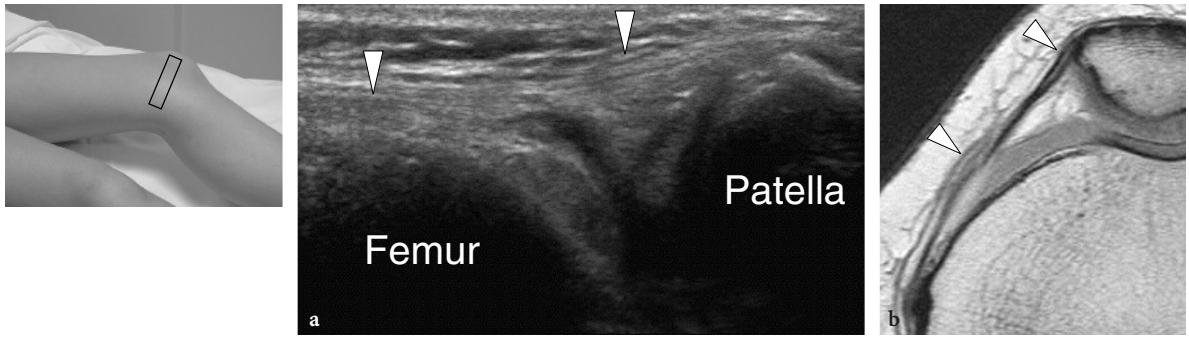

Fig. 14.23a,b. Patellar retinacula. **a** Transverse 12–5 MHz US image over the medial aspect of the patellofemoral joint with **b** corresponding proton density MR imaging correlation displays the medial retinaculum as a hyperechoic fibrillar structure (*arrowheads*) joining the internal edge of the patella and the medial condyle. The photograph at the upper left of the figure indicates probe positioning

Bipartite patella is a common anatomic variant caused by the nonunion of an accessory ossification center of the bone. Three types of anomaly have been described (Fig. 14.25): the type 1 anomaly is characterized by a separate nucleus at the lower pole of the patella; type 2 describes a more elongated fragment on the lateral side of the bone; type 3 is typified by a separate nucleus at its superolateral aspect. Types 1 and 2 are rarely encountered in clinical practice, whereas type 3 is common and can mimic a patellar fracture. US is able to identify type 1 anomaly as a discontinuity on the anterior cortical bone of the patella and type 3 anomaly by detecting the accessory superolateral fragment (Fig. 14.26). Differentiation of this variant from a fracture can be obtained with US by showing the regular rounded borders of the bone and the absence of pain on local pressure with the probe (Blankstein et al. 2001). From the

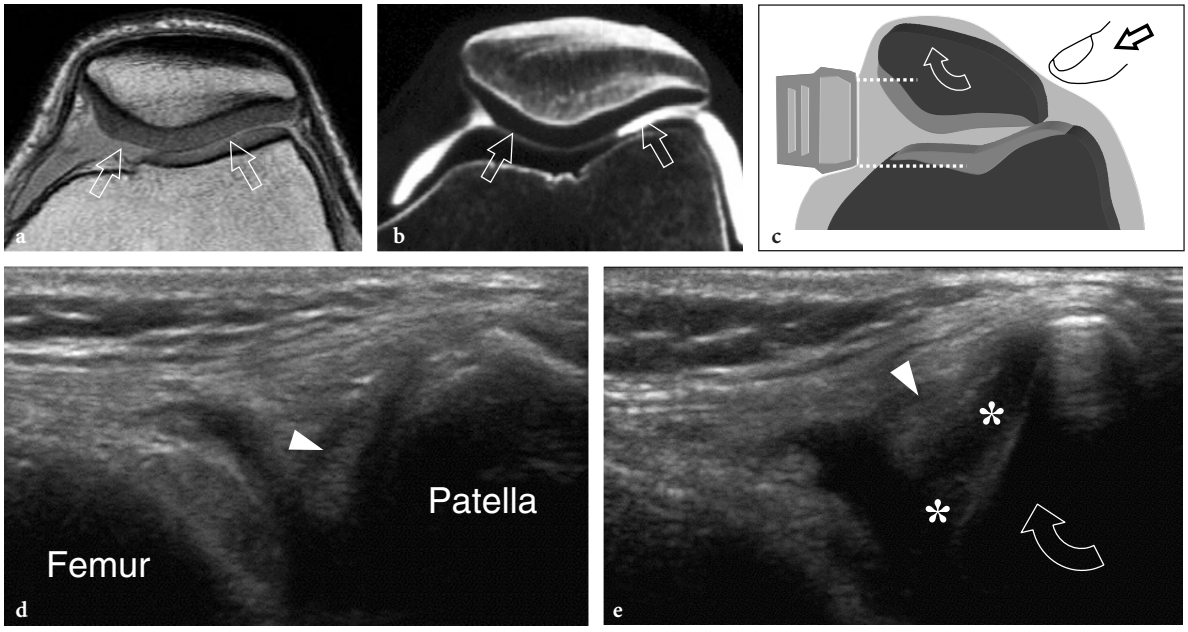

Fig. 14.24a–e. Retropatellar cartilage. **a** Transverse proton density MR and **b** CT-arthrographic images illustrate the normal cross-sectional appearance of the retropatellar cartilage (*arrows*). **c** Schematic drawing describes the US technique for examination of the cartilage of the medial patellar facet: it includes transverse scanning while inducing medial patellar subluxation (*curved arrow*) by pressure (*straight arrow*) applied over the lateral side of the patella (*straight arrow*). **d,e** Transverse 12–5 MHz US images over the medial patella obtained **d** without acting on the patella and **e** during its medial tilting. Medial patellar tilt (*curved arrow*) increases visibility of the medial facet cartilage (*asterisks*). *Arrowheads*, parapatellar fat

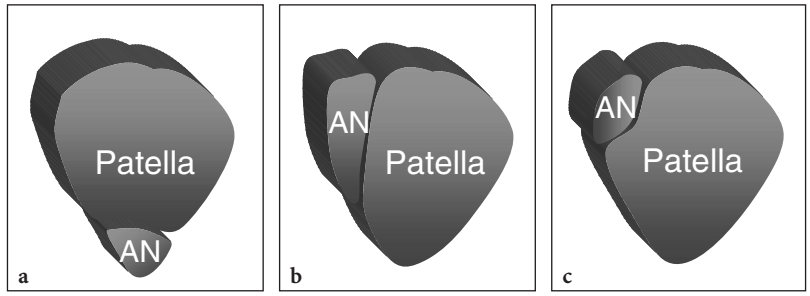

Fig. 14.25a–c. Patella bipartita. Schematic drawings show the three main types of patella bipartita. **a**, In type 1, the accessory nucleus (*AN*) is located on the lower patellar tip; **b**, in type 2, it lies on the lateral edge of the bone; **c**, in type 3, the most common type, the accessory nucleus affects the superolateral aspect of the patella

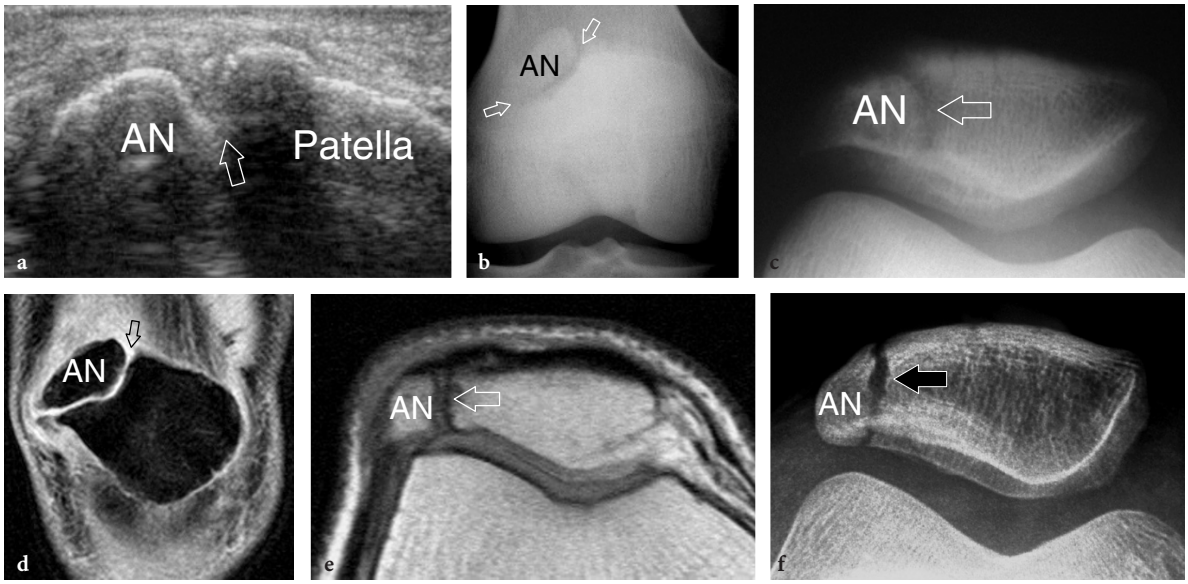

Fig. 14.26a–f. Patella bipartita. **a** Sagittal oblique 10–5 MHz US image demonstrates the accessory nucleus (*AN*) as an individual bone with rounded margins located at the superolateral aspect of the patella. The nucleus is separated from the rest of the bone by a fibrocartilaginous space (*open arrow*). Anteroposterior and **c** femoropatellar views show the typical radiographic appearance of type 3 patella bipartita. The accessory nucleus appears as a rounded calcified structure that articulates with the superolateral corner of the patella. **d** Coronal STIR and **e** transverse proton density sequences demonstrate the MR appearance of type 3 patella bipartita. **f** Patellar fracture. Unlike patella bipartita, a patellar fracture presents with sharp margins of the fragments (*black arrow*) and absence of sclerotic boundaries

clinical standpoint, the assessment of the position of the patella relative to the femoral trochlea is important, because a high position predisposes to lateral instability. Although easily assessed radiographically, the so-called "patella alta" can also be recognized with US in children and adults. In children, the main advantage of US is that the interpretation of findings is independent on the degree of patellar ossification (Jozwiak and Pietrzak 1998).

The infrapatellar area includes the patellar tendon, the prepatellar and infrapatellar bursae and the Hoffa fat pad. Both longitudinal and transverse US images are necessary to accurately assess this area. The patellar tendon must be systematically examined from its cranial origin down to its distal insertion on long- and short-axis planes. As for the quadriceps tendon, a careful scanning technique is needed to examine this tendon. In fact, with the knee extended it appears wavy with alternating hypoechoic and hyperechoic segments (Fig. 14.27). At appropriate degrees of knee flexion, this tendon appears taut and exhibits a flattened homogeneous structure with well-defined margins and a fibrillar echotexture (Fig. 14.28). The normal tendon meas-

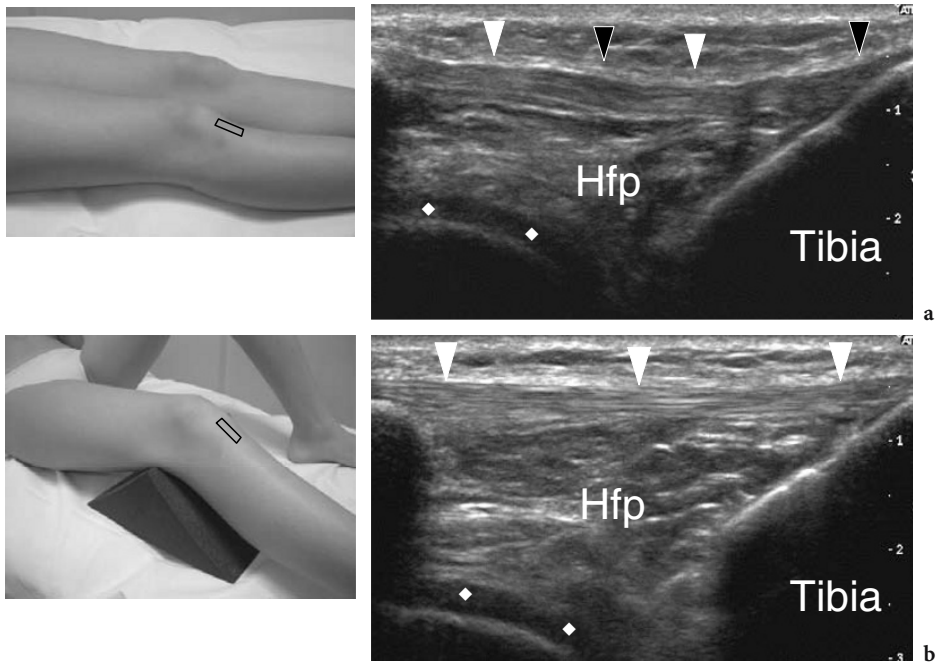

Fig. 14.27a,b. Patellar tendon. **a,b** Longitudinal 12–5 MHz US images over the patellar tendon obtained with **a** the knee extended and **b** the knee flexed. In **a**, the patellar tendon is characterized by a wavy appearance with alternating hypoechoic (*black arrowheads*) and hyperechoic (*white arrowheads*) segments as a result of a different orientation of the tendinous fibers with respect to the incidence of the US beam. In **b**, the tendon (*white arrowheads*) is taut and assumes a homogeneously hyperechoic appearance. Deep to the patellar tendon, the Hoffa fat pad (*Hfp*) and the inferior aspect of the femoral trochlea covered by a hypoechoic layer of articular cartilage (*rhombi*), are visualized. The photographs at the left of the figure indicate respective probe positioning

ures 4–5 mm in anteroposterior thickness (Carr et al. 2001). Because the tendon is formed by a single bundle of fibers, no multilayered arrangement is recognized within it at US. In asymptomatic athletes, the intratendinous structure may occasionally reveal fine textural abnormalities with internal hypoechoic areas (Cook et al. 1998). Knowledge of this finding has implications for clinicians who manage athletes with anterior knee pain. Because the lower pole of the patella has a V-shaped appearance, one should be aware that the tendon inserts not only on the apex but also along the inferior lateral and medial edges of the bone (Fig. 14.29). In addition, some of its proximal fibers attach to the anterior aspect of the patella (Basso et al. 2001). A slight increase in thickness of the proximal and distal third of the patellar tendon is normal and should not be misinterpreted as a sign of focal tendinopathy. This finding can be explained by the fact that the tendon is thin and wide proximally and thick and narrow distally, due to the converging arrangement of fibers toward the tibial tuberosity. The distal portion of the patellar tendon lies in close apposition with the tibial epiphysis before inserting on the tuberosity (Fig. 14.28). Somewhat similar to the situation with the supraspinatus tendon, the examiner should be aware that the actual site of insertion is indicated by the prominence of the tuberosity and not by the anterior aspect of the tibial epiphysis. Short-axis US images of the patellar tendon are essential because the involvement by tendinopathy may occur out of the midline and possibly limited to the external borders of the tendon (Fig. 14.30). These planes depict a flattened tendon, shaped like a rectangle. In addition, they allow assessment of the medial and lateral patellar retinacula as sheet-like fibrous expansions attached on each side of the tendon (Fig. 14.30). Calcifications and ossification of the distal portion of the tendon can be encountered in asymptomatic subjects and are usually related to consequences of Osgood-Schlatter disease.

Deep to the patellar tendon and superficial to the anterior aspect of the condyles, the intracapsular Hoffa pad appears as a fatty tissue space containing hyperechoic septations (Fig. 14.28). The deep infrapatellar bursa is a small synovial cavity located between the distal portion of the patellar tendon and the anterior aspect of the tibial epiphysis. Occasion-

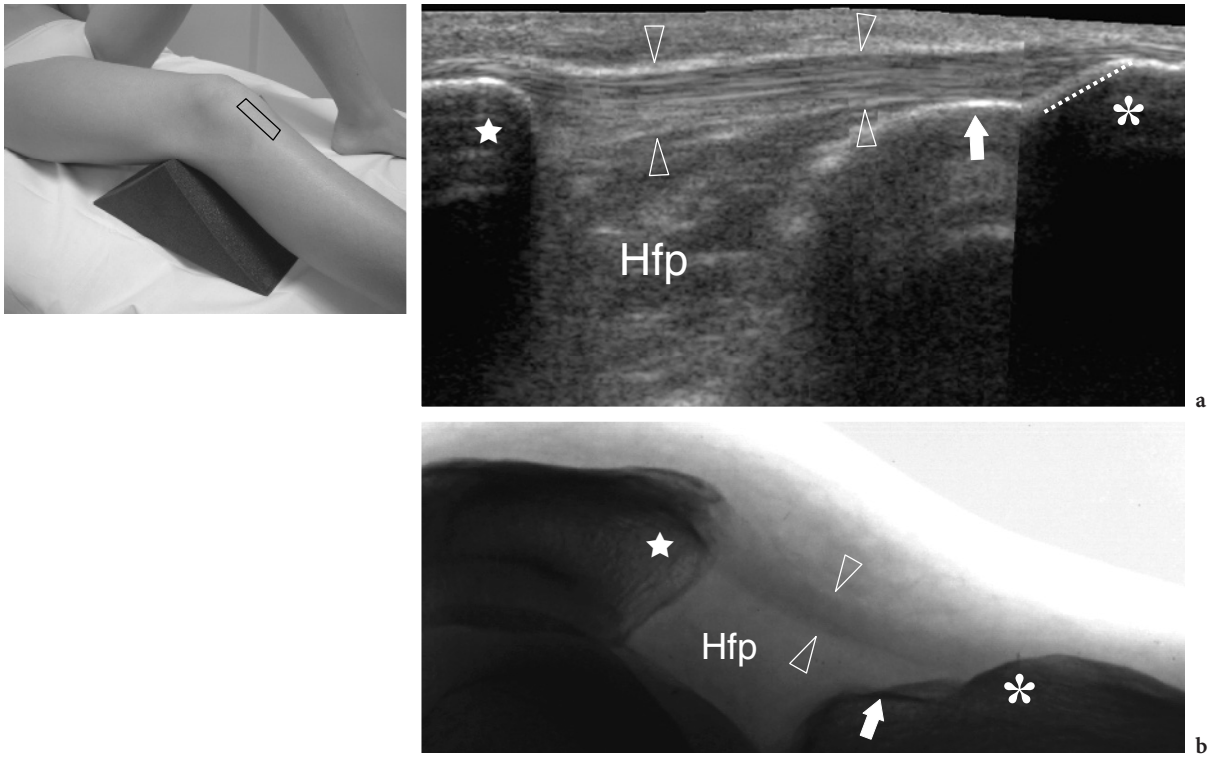

Fig. 14.28a,b. Patellar tendon. **a** Long-axis extended field-of-view 12–5 MHz US image of the patellar tendon (*arrowheads*). The tendon is depicted from its proximal insertion into the patella (*star*) through its distal attachment on the anterior tibial tuberosity (*asterisk*), superficial to the Hoffa fat pad (*Hfp*). The normal tendon demonstrates a homogeneous fibrillar echotexture and well-defined margins. Note that the actual site of its distal insertion (*dotted line*) is restricted to the prominence of the tuberosity and does not extend more proximally on the anterior aspect of the tibial epiphysis (*arrow*). **b** Lateral radiographic correlation obtained with extended knee gives an additional demonstration that the patellar tendon (*arrowheads*) is only inserted on the tuberosity (*asterisk*), being able to lift up from the anterior tibial epiphysis (*arrow*). *Star*, patella. The photograph at the upper left of the figure indicates probe positioning

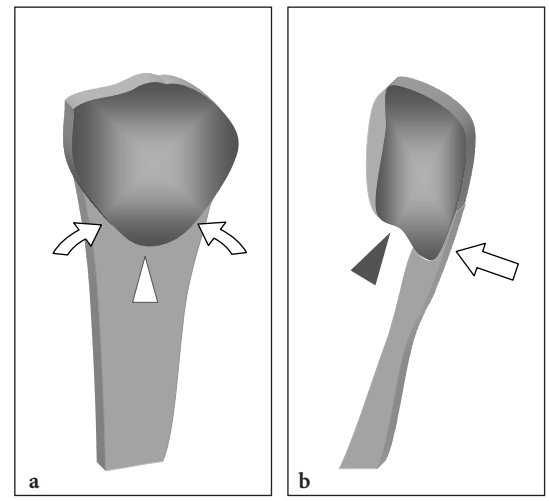

Fig. 14.29a,b. Patellar tendon. Schematic drawings illustrate the insertion of the patellar tendon into the lower pole of the patella. **a** Anterior view of the patella shows that the patellar tendon inserts not only into the apex of the patella (*arrowhead*) but also along its lateral and medial edges (*curved arrows*). **b** Lateral view of the patella reveals that some anterior fibers (*arrow*) of the patellar tendon overlie the anterior surface of the patella. In contrast, the posterior aspect of the patella (*arrowhead*) does not give any attachment to the tendon

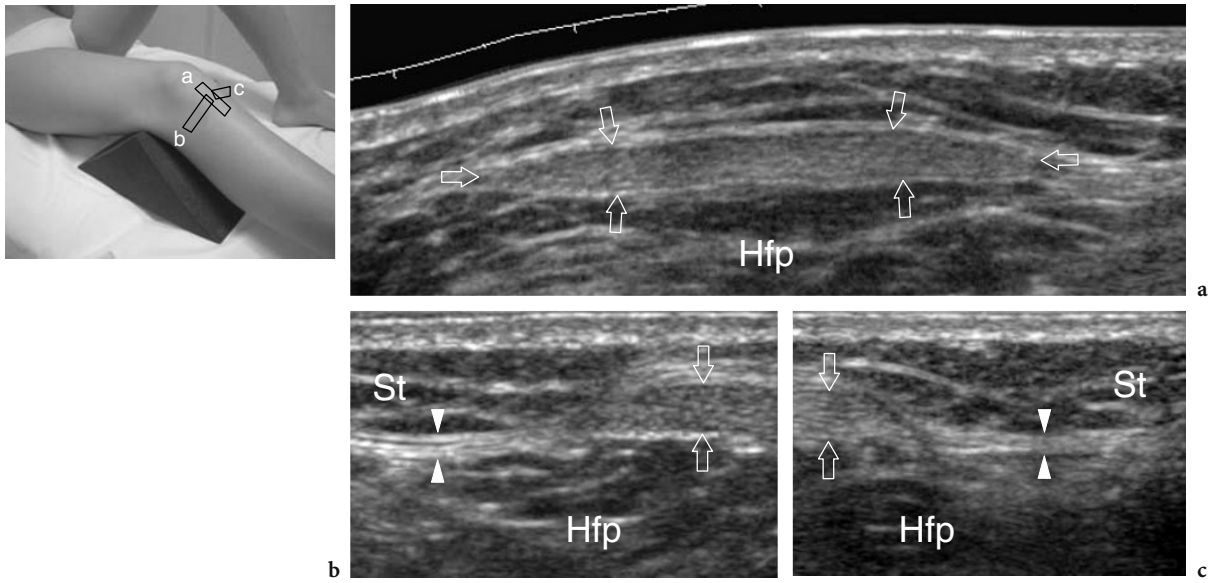

Fig. 14.30a–c. Patellar tendon. **a** Short-axis extended field-of-view 12–5 MHz US image of the patellar tendon (*arrows*) demonstrates a hyperechoic flattened rectangular-shaped tendon, lying superficial to the Hoffa fat pad (*Hfp*). **b,c** Attached to its **b** right and **c** left sides, the medial and lateral patellar retinacula appear as sheet-like fibrous expansions (*arrowheads*) located between the Hoffa fat pad (*Hfp*) and the subcutaneous tissue (*St*). The photograph at the upper left of the figure indicates probe positioning

ally, US can demonstrate a small amount of fluid within the bursa: this sign should be regarded as a normal finding. A diagnosis of bursitis can be made in cases of large effusions or when local pain is generated by pressure with the probe over the inflamed bursa. The prepatellar bursa is located in the subcutaneous tissue which overlies the lower pole of the patella and the proximal patellar tendon. In normal conditions, the bursa cannot be demonstrated with US because of its thin walls and absence of internal fluid. Detection of even a minimal amount of fluid within the bursa should be regarded as a sign of local inflammation (prepatellar bursitis). During US examination, care should be taken not to apply excessive pressure with the probe on the skin to avoid the inadvertent squeezing of the fluid away from the field-of-view of the US image. This could result in a false negative examination. Large amounts of gel may help to avoid excessive pressure on the bursa with the probe.

14.4.2 Medial Knee

The medial aspect of the knee joint is best examined with the leg externally rotated. Relevant anatomic structures in this area that are amenable to US examination are: the medial collateral ligament, the medial femorotibial joint space, the medial meniscus and the pes anserinus complex. US assessment of the medial aspect of the knee begins with coronal images obtained over the medial collateral ligament. This ligament appears as an elongated band 1–3 mm thick formed by two definite hyperechoic layers reflecting the superficial part and the deep meniscofemoral and meniscotibial components of the ligament separated by a slight hypoechoic line related to fatty tissue (Fig. 14.31) (De Maeseneer et al. 1998). On transverse planes, the ligament reveals its superficial component as a small, crescentic-shaped hyperechoic structure located just over the femoral and tibial cortex. Care should be taken to examine the entire length of the ligament. In particular, the most proximal portion of its superficial component should be carefully evaluated so as not to miss a Pellegrini-Stieda lesion. Between the two components of the medial collateral ligament, a synovial bursa (medial collateral ligament bursa) creates a gliding plane with knee flexion. Although this bursa is described in more than 90% of knees on cadaveric studies (Lee and Yao 1991), it cannot be demonstrated at US because of its thin walls and absence of sufficient internal fluid. Dynamic US images obtained during valgus stress can improve the assessment of integrity of

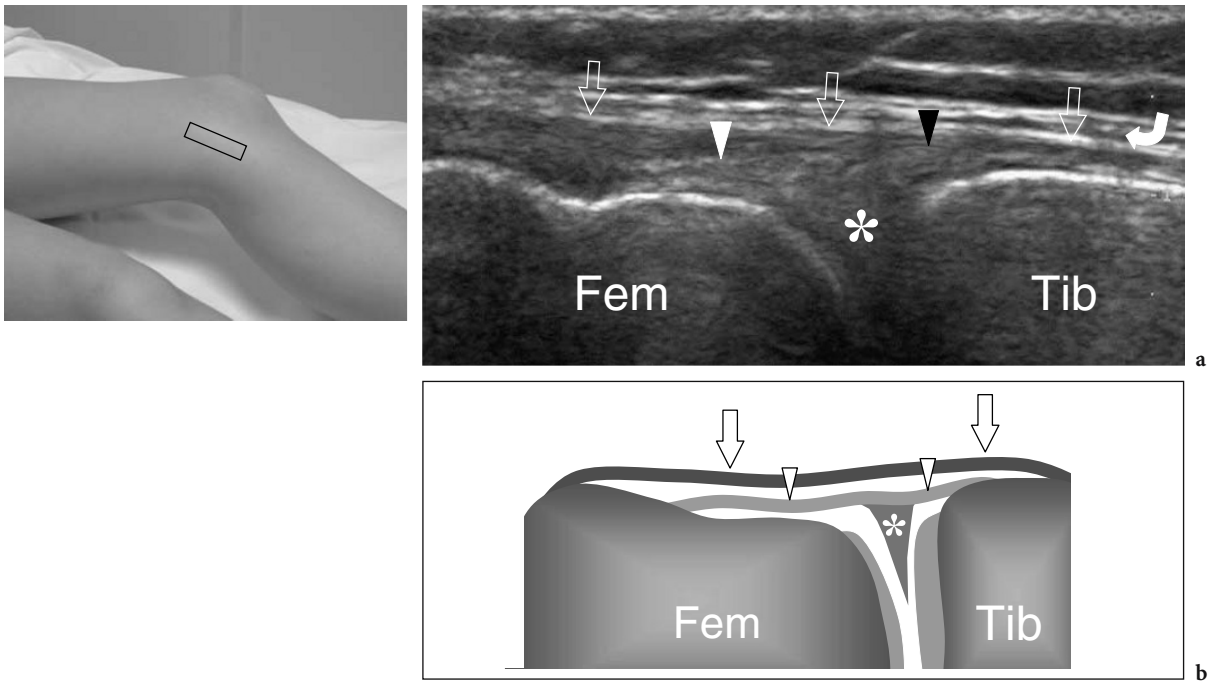

Fig. 14.31a,b. Medial collateral ligament. **a** Coronal 12–5 MHz US image over the medial collateral ligament with **b** schematic drawing correlation demonstrates this ligament is composed of two definite superficial (*straight arrows*) and deep (*arrowheads*) layers. The superficial layer appears as a thick, straight fibrillar band located just deep to the superficial fascia (*curved arrow*). The deep layer is formed by the meniscofemoral (*white arrowhead*) and the meniscotibial (*black arrowhead*) ligaments which are depicted as hyperechoic thin bands connecting the meniscus (*asterisk*) with the femur (*Fem*) and the tibia (*Tib*) respectively. The photograph at the upper left of the figure indicates probe positioning

this ligament (De Flaviis et al. 1988). For this purpose, the patient is asked to lean on the same side of the examined knee maintained in a slight flexion (10–20° approximately). First, coronal US images are obtained over the ligament at rest. Then, a small stiff pillow is placed under the lateral aspect of the knee to produce a valgus stress due to the weight of the leg. The same coronal images are also obtained in this latter position. The distance between tibia and femur is then measured and compared between the two positions. In doubtful cases, a bilateral examination should be performed and the measured distance compared with that of the unaffected knee. As an alternative, the examiner can study the internal joint space while an assistant induces a valgus stress on the joint with the patient supine.

The medial meniscus is imaged on coronal and coronal oblique US images obtained by placing the probe perpendicular to its base. Transverse US images are difficult to obtain in the plane of the meniscus and do not add significant information. The meniscus appears as a triangular hyperechoic structure located between the femur and the tibia (Fig. 14.31). Its base is located superficially, whereas its apex points toward depth. Due to the attenuation of the US beam and its small size, the apex of the meniscus is difficult to examine with US. Widening of the medial joint space by valgus stress has been suggested to increase the overall visibility of the medial meniscus.

The pes anserinus complex, which is referred to the intermingling tendons of the sartorius, gracilis and semitendinosus, inserts into the anteromedial aspect of the tibial metaphysis, 5–6 cm below the joint line. At a more proximal level (i.e., where the hamstrings still course along the posteromedial knee), the individual tendons of the pes anserinus can be distinguished with US based on their different shapes and anatomic locations. On the contrary, when these tendons approach their distal insertion they blend together and cannot be differentiated from one another (Fig. 14.32). The indirect insertion of the semimembranosus is located in a sulcus on the posteromedial aspect of the tibia that can be visualized on coronal planes with the transducer placed along the posterior third of the medial side of the knee as a shallow groove of the cortical line (De Maeseneer et al. 2002). Several synovial bursae

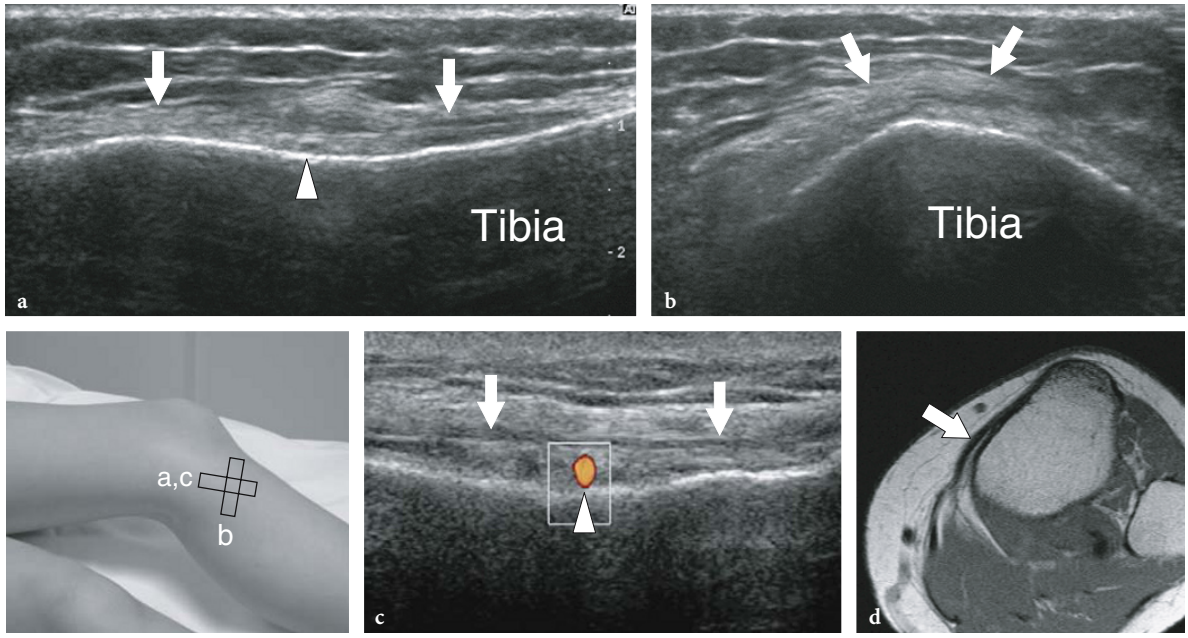

Fig. 14.32a–d. Pes anserinus complex. **a** Long-axis and **b** short-axis 12–5 MHz US images over the pes anserinus complex demonstrate a hyperechoic band (*arrows*) inserting into the anterolateral aspect of the proximal tibial metaphysis. Discrimination among the different tendons cannot be obtained with US. In **a** the inferior medial genicular artery (*arrowhead*) is seen as a hypoechoic dot lying between the pes anserinus complex and the cortical bone of the tibia. **c** Color Doppler imaging gives a better depiction of this artery (*arrowhead*). **d** Transverse proton density MR image shows the pes anserinus complex with precise correspondence with the US image shown in **b**. The photograph at the bottom left indicates probe positioning

located among these tendons and between them and the tibial cortex attenuate local frictional stresses. In normal states, these bursae are not visible with US. They may become apparent only when distended by effusion. Between the straight tendons and the concave medial cortex of the tibial metaphysis, some vessels, such as the inferior medial genicular artery, can be depicted with US (Fig. 14.32).

14.4.3 Lateral Knee

The lateral aspect of the knee joint is examined by asking the patient to rotate the leg internally. From anterior to posterior, the structures to be evaluated are: the distal aspect of the iliotibial band, the external femorotibial joint space with the lateral meniscus, the lateral collateral ligament, the popliteus tendon and the superior tibiofibular joint.

The distal segment of the iliotibial band is best imaged on long-axis scans. If doubts exist as to whether the probe is correctly oriented, one should consider that the iliotibial band is located between the anterior and middle third of the lateral aspect of the knee and oriented along the major axis of the thigh. The iliotibial band can be appreciated as a thin fibrillar structure which inserts onto a tibial tubercle located at the anterolateral aspect of the tibial epiphysis, the Gerdy's tubercle (Bonaldi et al. 1998; De Maeseneer et al. 2002). Its two anatomic layers cannot be demonstrated at US (De Maeseneer et al. 2002). As the iliotibial band normally fans out just before its insertion into the tibia, this appearance should not be misinterpreted as a sign of focal tendinopathy (Fig. 14.33). In doubtful cases, it should be considered that local compression with the probe is typically painful in tendinitis.

US evaluation of the lateral meniscus shares the same intrinsic limitations already described for the medial meniscus (Fig. 14.34). In addition, the lateral meniscus is smaller than the medial one. When a meniscal cyst is suspected on clinical grounds, examining the knee in forceful flexion may be useful as it causes bulging of the cyst outside the joint space and improves its detection.

The lateral collateral ligament appears as a cord-like fibrillar structure located at the posterolateral aspect of the joint, which inserts into the lateral femoral condyle and the peroneal head (Fig. 14.34).

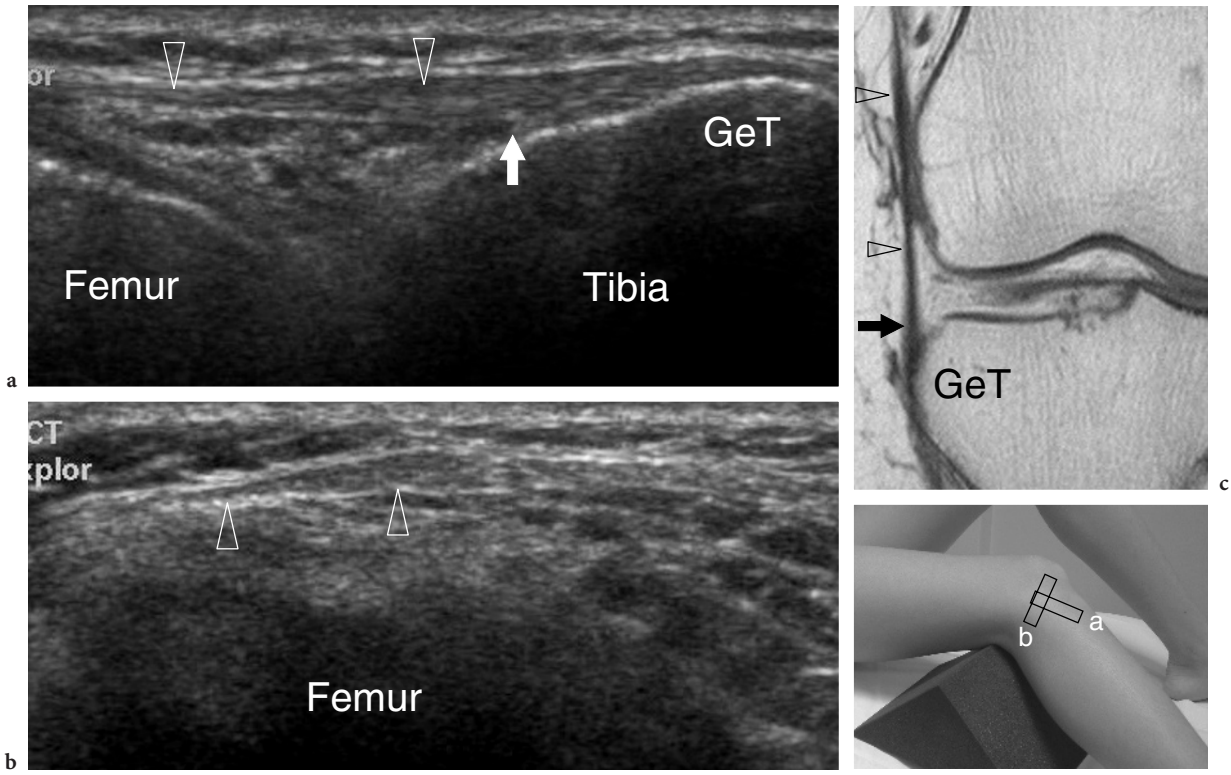

Fig. 14.33a–c. Iliotibial band. **a** Coronal oblique and **b** transverse 12–5 MHz US images over the iliotibial band demonstrate it as a hyperechoic band (*arrowheads*) inserting into Gerdy's tubercle (*GeT*). Observe the normal preinsertional widening of the band (*arrow*). **c** Corresponding coronal proton density MR image shows an excellent correlation with the US appearance. The photograph at the bottom right of the figure indicates probe positioning

It is 3–4 mm thick and lies in a more anterior plane than the biceps tendon (De Maeseneer et al. 2002). When imaged with 20°–30° of knee flexion, this ligament assumes a vertical oblique orientation, quite different from that of the iliotibial band. The lateral collateral ligament is best evaluated on oblique coronal US images by placing the lower edge of the probe on the peroneal head and then rotating the transducer until the ligament becomes as elongated as possible in the US image. One should consider this ligament to be taut with the knee extended. This latter position may be helpful to exclude a ligament injury, when the ligament assumes an artifactually hypoechoic pattern related to its wavy course. Due to the small field-of-view of small-parts probes, which is often inadequate to depict the long axis of the ligament on a single image, imaging of the lateral collateral ligament would benefit from the extended field-of-view technique. Transverse US planes may be helpful to assess the relationship of the ligament with the more posterior biceps tendon. Dynamic examination during varus stress has not yet been described for examining the lateral collateral ligament and actually seems to add little to the findings already observed on static scans.

Just deep to the proximal part of the lateral collateral ligament, the popliteus tendon can be imaged on coronal US planes as an oval structure located in its bony groove (Fig. 14.34). Depending on the incidence of the US beam, substantial anisotropy may be evident in the popliteus tendon (De Maeseneer et al. 2002). The US examination of the lateral aspect of the knee should be completed with an evaluation of the superior tibiofibular joint. Transverse and coronal US scans obtained over the anterior aspect of the fibular head are adequate for this purpose.

14.4.4 Posterior Knee

To examine the posterior region of the knee, the patient is asked to lie prone with the knee extended. Additional images can be obtained at different

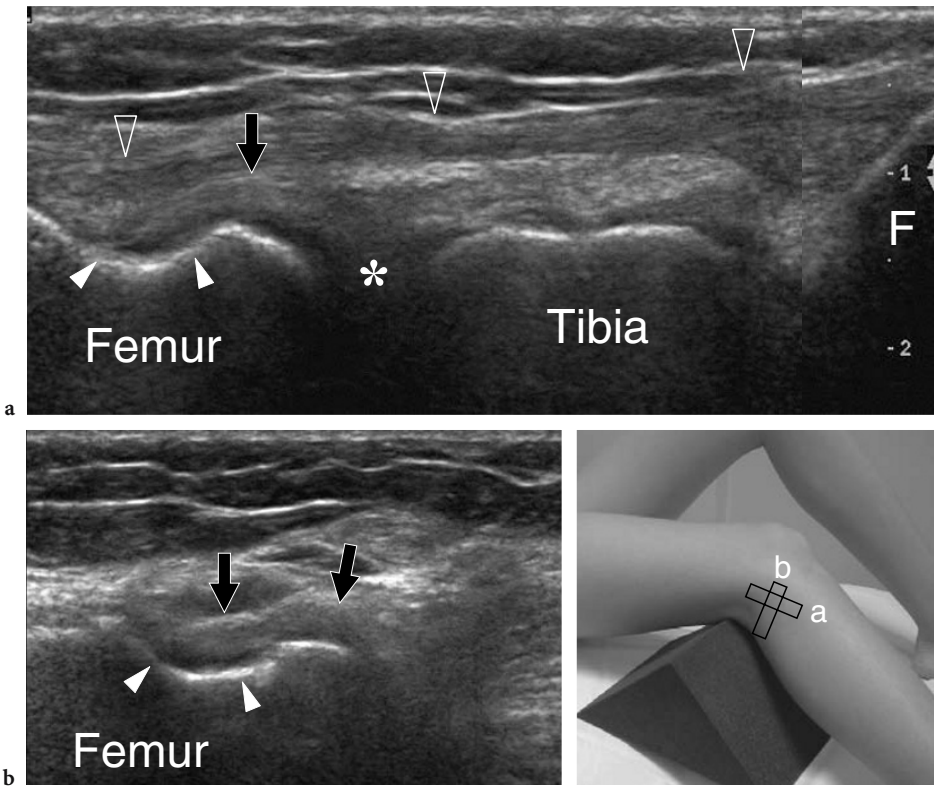

Fig. 14.34a,b. Lateral collateral ligament and popliteus tendon. **a** Coronal oblique and **b** transverse 12–5 MHz US images demonstrate the cord-like lateral collateral ligament (*open arrowheads*) joining the lateral femoral condyle with the fibular head (*F*). Deep to the proximal insertion of the ligament, the popliteus tendon (*arrow*) is seen inserting into a small fossa (*white arrowheads*) located at the lateral aspect of the lateral condyle. Note the close relationship of this tendon with the lateral meniscus (*asterisk*). The photograph at the bottom right of the figure indicates probe positioning

degrees of knee flexion if a better distension of the popliteal veins or opening of the pedicle of a Baker cyst is required. From both technical and anatomic standpoints, the posterior aspect of the knee includes three zones: internal, central and external.

In the posterior internal zone, the main soft-tissue structures that can be examined with US are: the proximal portion of the long tendons forming the pes anserinus complex, the semimembranosus tendon and the semimembranosus-gastrocnemius bursa (Fig. 14.35). As regards the pes anserinus tendons, the sartorius is the most medial and has an oval hypoechoic appearance because, at this level, it is mainly composed of muscle fibers. The gracilis tendon lies just posterior to the sartorius; as its name suggests ("gracilis" means "weak" in Latin), it is the thinnest. The semitendinosus tendon is found posterior to the semimembranosus muscle and then located behind the semimembranosus tendon. More distally, these three tendons join together to form the pes anserinus complex. The largest of the posterior internal tendons of the knee is the semimembranosus, which courses more laterally to insert on the posteromedial aspect of the tibial epiphysis through a direct tendon (Fig. 14.35). It also has an indirect tendon which cannot be appreciated with US. Between the tendon of the semimembranosus and the medial head of the gastrocnemius there is the semimembranosus-gastrocnemius synovial bursa, which is barely depicted with US in normal individuals (Fig. 14.35b). In young healthy subjects, this bursa does not communicate with the knee joint, while in adults it is connected by a short pedicle to the posterior articular cavity. The bursa has two components: deep and superficial. The smaller deep component is located between the medial head and the posterior aspect of the knee and may communicate with the joint cavity through a break in the capsule, whereas the larger superficial component is located in the fatty tissue planes superficial to the medial head of the gastrocnemius. Knee flexion opens the communication between the bursa and the joint cavity leading to an easier demonstration of the cystic pedicle. The cartilage of the posterior

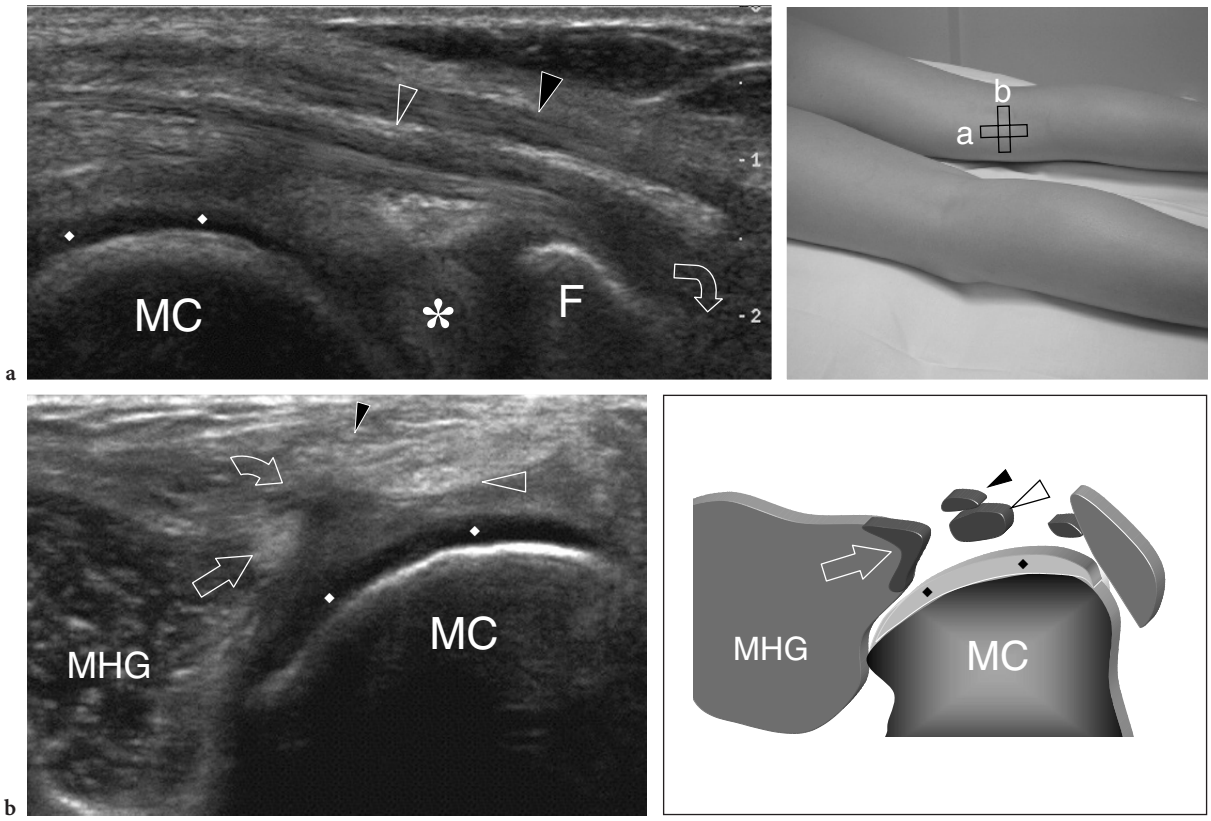

Fig. 14.35a–c. Posteromedial tendons. **a** Longitudinal and **b** transverse 12–5 MHz US images with **c** transverse schematic drawing correlation illustrate the main structures of the posterior internal zone that are amenable to US demonstration. Superficial to the medial condyle (*MC*), which is covered by a hypoechoic band of cartilage (*rhombi*), the large semimembranosus tendon (*open arrowhead*) lies just anterior to the small semitendinosus tendon (*black arrowhead*). The posterior horn of the medial meniscus (*asterisk*) can be appreciated between the medial condyle and the tibia (*T*). Curved arrow indicates the distal insertion of the semimembranosus tendon. In **b**, the tendon (*arrow*) of the medial head of the gastrocnemius (*MHG*) is depicted as a comma-shaped structure. Between it and the semimembranosus tendon (*open arrowhead*), the semimembranosus-gastrocnemius medial head synovial bursa (*curved arrow*) can be seen. The bursa appears as a hypoechoic area due to the apposition of synovial walls and, in normal states, lacks internal fluid. The photograph at the upper right of the figure indicates probe positioning

aspect of the medial femoral condyle is also well recognized with US (Fig. 14.35a,b). However, the weight-bearing area located at the junction between the middle and posterior thirds of the condyle and frequently involved by degenerative disorders, cannot be accurately assessed.

In the posterior central zone, the medial head of the gastrocnemius, the popliteal artery and vein, the tibial nerve and the intercondylar space are the structures to be examined with US. The medial head of the gastrocnemius has a triangular shape when assessed on transverse planes (Fig. 14.35b,c). Its tendon is located at the medial aspect of the muscle and can be demonstrated as a comma-shaped hyperechoic structure with internal convexity. It should not be confused with the more cranial myotendinous junction of the semimembranosus, which also assumes a comma-shaped appearance. As regards the popliteal neurovascular bundle, the popliteal artery is the deepest structure and can be found lateral to the medial head; the popliteal vein lies more superficially and slightly lateral to the artery, whereas the tibial nerve is the most superficial structure and courses lateral to the vein. On transverse US images, the artery, the vein and the nerve are aligned on a sagittal oblique plane (Fig. 14.36a,b). The pulsatile lumen and the characteristics of the wall of the popliteal artery can be easily appreciated with US. Because the patient is prone, the popliteal vein tends to collapse and, therefore, is not well depicted with US. A small elevation of the leg from the examination table, which is obtained while flexing the knee, causes filling of the popliteal vein and enhances its detection. When the examiner has to distinguish partial from complete thrombosis of the vein and to assess the overall size of the thrombus, the patient

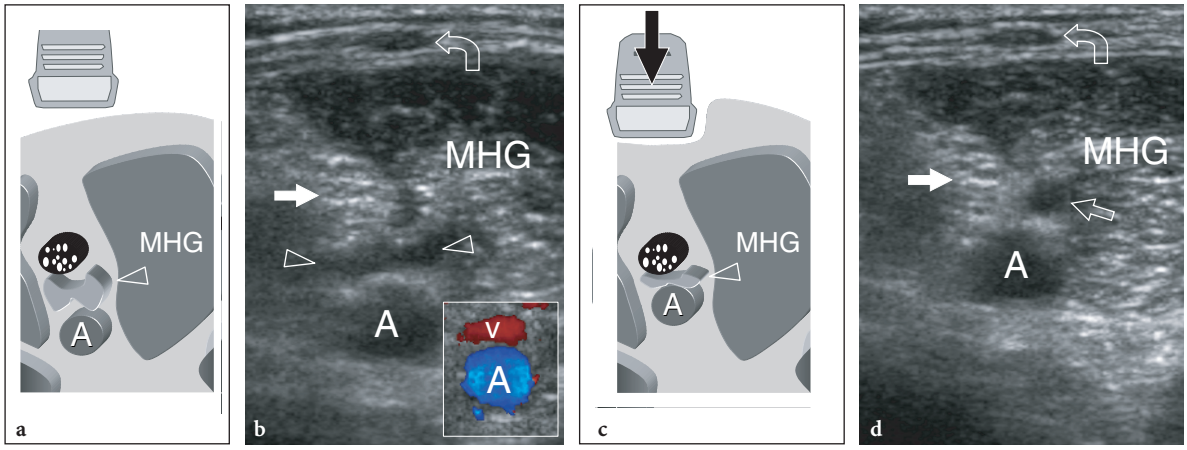

Fig. 14.36a–d. Popliteal neurovascular bundle. **a,c** Schematic drawings and **b,d** corresponding transverse 12–5 MHz US images obtained over the mid-popliteal space **a,b** without and **c,d** with probe compression (*black arrow*) demonstrate, from anterior to posterior, the typical alignment of the popliteal artery (*A*), the popliteal vein (*arrowhead, V*) and the tibial nerve (*white arrow*) in a sagittal oblique plane. In the subcutaneous tissue, superficial to the medial head of the gastrocnemius (*MHG*), the small saphenous vein (*curved arrow*) can also be identified. In **c,d** note that the popliteal vein completely disappears while compressed. This is a sign of venous patency. Color Doppler imaging (see *insert* in **b**) can also be helpful for ruling out vessel thrombosis. *Open arrow*, inferior medial genicular artery

can also be examined standing to obtain full venous distension. The collapse of the popliteal vein by local compression with the probe is a simple and reliable means to exclude venous thrombosis (Fig. 14.36c,d) (Cronan et al. 1987). When vascular pathology is suspected, however, both artery and vein should be evaluated with color Doppler imaging. At the apex of the popliteal space the sciatic nerve splits into the tibial and the common peroneal nerves. On transverse planes, US can identify these nerves by detecting their typical echotexture, which consists of a honeycomb-like appearance with several hypoechoic spots reflecting the fascicles, embedded in a hyperechoic background (Silvestri et al. 1995; Martinoli et al. 1999). The tibial nerve has a larger size than the common peroneal nerve and can be followed straight downward from its origin through the ankle on transverse planes. The peroneal nerve reaches the lateral region of the popliteal space soon after its emergence from the sciatic. In the intercondylar fossa, the intermediate and distal portion of the posterior cruciate ligament can be demonstrated with US as a deep thick hypoechoic band (Wang et al. 1999b). The proximal portion of this ligament and its insertion into the femur cannot be assessed with US. The posterior cruciate ligament is best depicted in its long axis by means of oblique sagittal planes, with the proximal end of the probe rotated slightly medially in the direction of the medial femoral condyle (Fig. 14.37). Careful scanning is needed to avoid misinterpreting the posterior hyperechoic fat plane as the ligament itself (Cho et al. 2001). Due to its deep location and oblique orientation, the anterior cruciate ligament is barely visible with US. Some authors suggest an anterior approach with the knee in maximal flexion to directly image this ligament (Grobbelaar and Bouffard 2000). They place the probe in a sagittal plane over the patellar tendon to use the Hoffa fat pad as an acoustic window. The distal insertion of the ligament is recognized deep to it. The anterior cruciate ligament appears as an obliquely oriented taut hypoechoic band (Fig. 14.38a). Then, the proximal end of the probe is rotated laterally in the direction of the lateral femoral condyle to visualize the distal portion of the ligament. In this latter position, the normal ligament becomes hyperechoic and exhibits a fibrillar structure (Fig. 14.38b). Using this technique, the distal two thirds of the ligament can be visualized (Grobbelaar and Bouffard 2000). However, in our view this technique works well in only a minority of subjects, strongly depends on the technology used and is not reliable to avoid further imaging when a ligament tear is suspected at US. Some authors have suggested assessing the integrity of the cruciate ligaments by measuring the grade of tibial subluxation during stress maneuvers, including the drawer test (Gebhard et al. 1999).

In the posterior external zone, the structures that are amenable to US examination include the muscles and tendons of the biceps femoris and the lateral head of the gastrocnemius, the common peroneal nerve

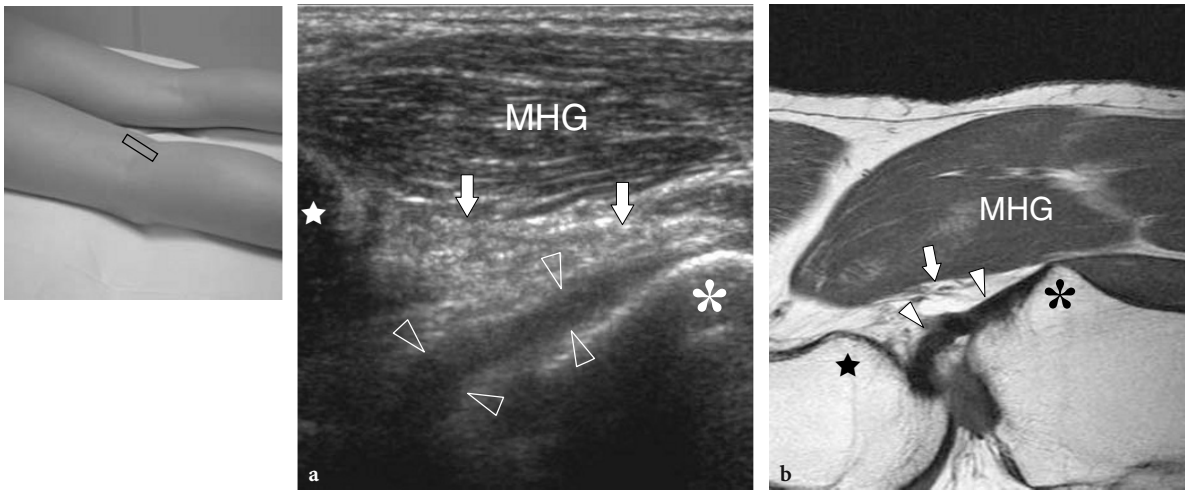

Fig. 14.37a,b. Posterior cruciate ligament. **a** Sagittal oblique 12–5 MHz US image of the posterior fossa with **b** T1-weighted MR imaging correlation demonstrates the posterior cruciate ligament as a thick hypoechoic cord-like structure (*arrowheads*) with a bucket-handled appearance. Only the distal two thirds of the ligament can be appreciated due to problems of access. Note the distal insertion of the ligament into the posterior aspect of the tibial epiphysis (*asterisk*). Posterior to the ligament, a triangular fat pad (*arrows*) and the medial head of the gastrocnemius (*MHG*) can be appreciated. *Star*, femur. The photograph at the upper left of the figure indicates probe positioning

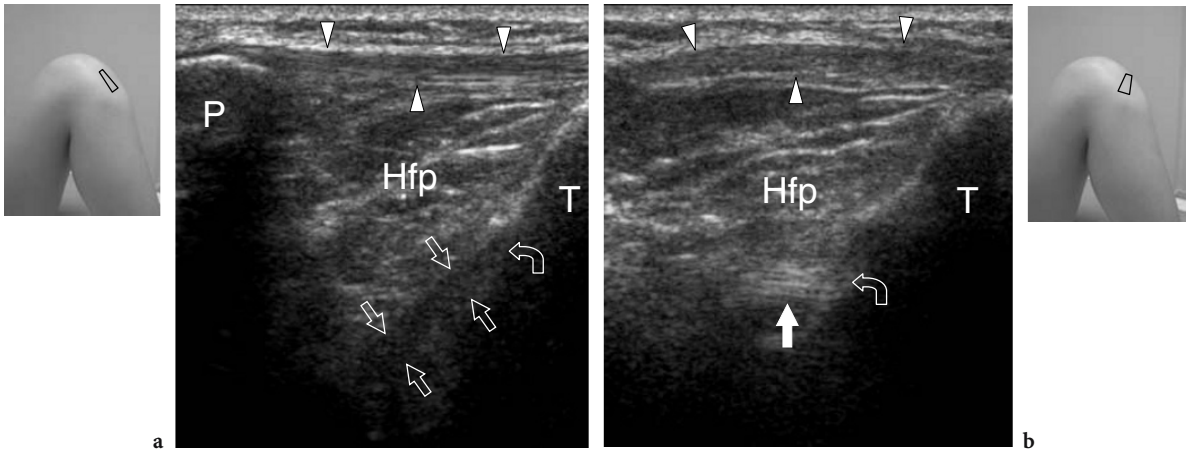

Fig. 14.38a,b. Anterior cruciate ligament. **a** Longitudinal 12–5 MHz US image over the patellar tendon (*arrowheads*) with the knee maximally flexed depicts the anterior cruciate ligament (*arrows*) in its long axis, just deep to the Hoffa fat pad (*Hfp*). The ligament appears as a cord-like hypoechoic structure due to its oblique orientation relative to the US beam. Its distal insertion (*curved arrow*) on the tibia (*T*) can be appreciated. *P*, patella. **b** Rotating the proximal end of the probe laterally, toward the lateral femoral condyle, the more distal portion of the ligament becomes hyperechoic and shows a fibrillar structure. The photographs at the upper left and right of the figure indicate respective probe positioning

with its divisional branches and the posterior aspect of the lateral femoral condyle covered by cartilage. The two heads of the biceps femoris muscle join together distal to the upper limit of the popliteal space to form a strong tendon that inserts into the fibular head. The biceps muscle and tendon are easily demonstrated with US by means of long- and short-axis images (Fig. 14.39). Proximal images must always include a careful evaluation of the myotendinous junction because this is a common site of sport-related tears. Transverse US planes are able to distinguish the lateral collateral ligament from the biceps tendon. The common peroneal nerve arises from the lateral aspect of the sciatic nerve and, soon after its origin, joins the posteromedial border of the biceps muscle to descend toward the fibula. This small nerve is composed of only a few fascicles and, due to its oblique course, can preferentially be imaged on transverse planes

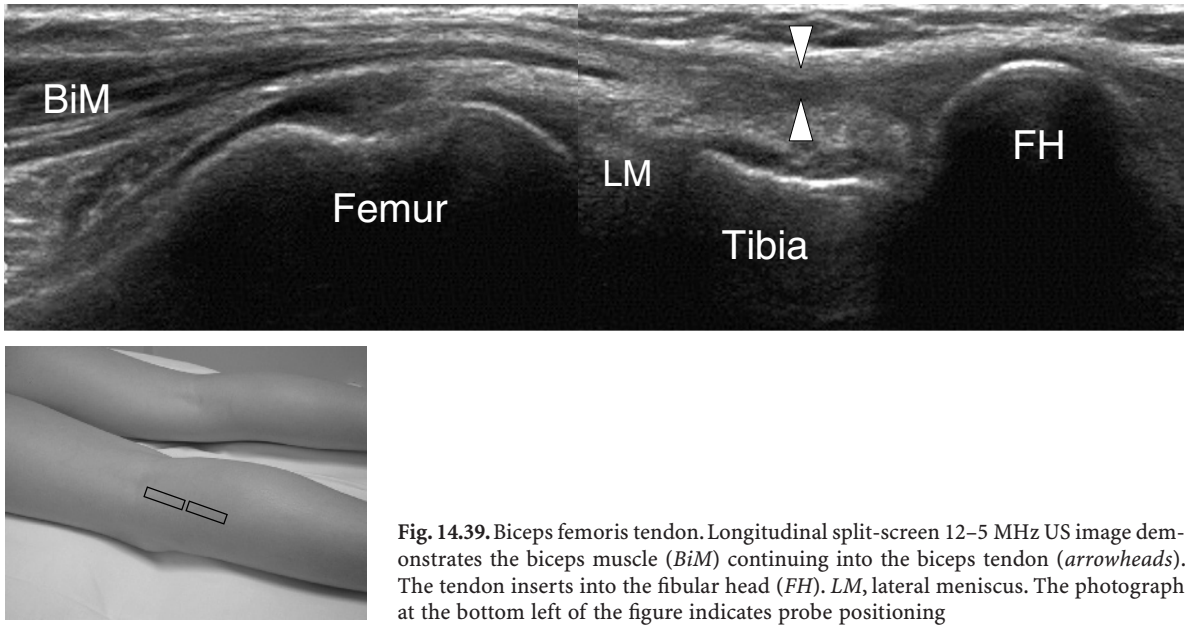

Fig. 14.39. Biceps femoris tendon. Longitudinal split-screen 12–5 MHz US image demonstrates the biceps muscle (*BiM*) continuing into the biceps tendon (*arrowheads*). The tendon inserts into the fibular head (*FH*). *LM*, lateral meniscus. The photograph at the bottom left of the figure indicates probe positioning

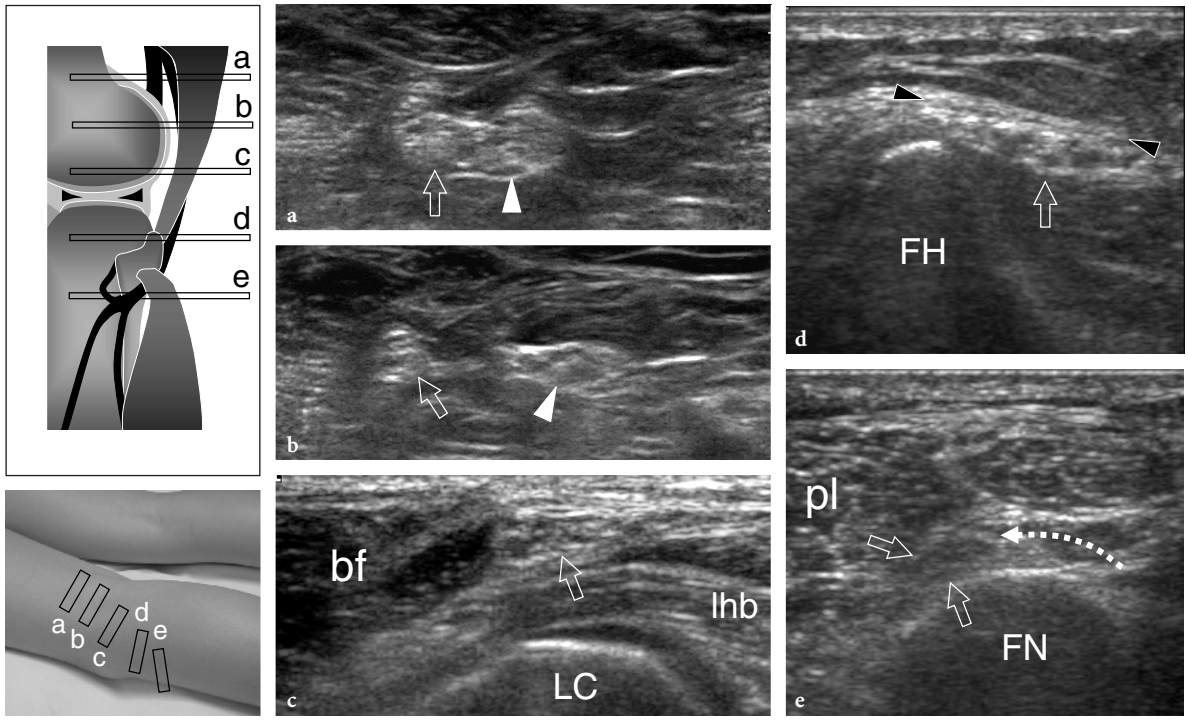

Fig. 14.40a–e. Common peroneal nerve. Series of transverse 12–5 MHz (**a–c**) and 15–7 MHz (**d,e**) US images obtained over the common peroneal nerve according to the levels shown in the diagram at the upper left of the figure. **a** Just proximal to the bifurcation, the sciatic nerve is composed of two paired bundles of fascicles for the tibial (*arrowhead*) and common peroneal (*arrow*) nerves. **b** These nerves assume a diverging course in the middle of the popliteal fossa. **c** Then, the common peroneal nerve (*arrow*) descend the popliteal fossa along the posteromedial aspect of the biceps femoris muscle (*bf*), superficial to the lateral head of the gastrocnemius (*lhg*) and the lateral condyle (*LC*). **d,e** More distally, the common peroneal nerve (*arrows*) reaches the fibular head (*FH*) passing in a restricted space between the bone and the fascia (*arrowheads*) and winds (*dotted arrow*) around the fibular neck (*FN*) deep to the attachment of the peroneus longus (*pl*). The photograph at the bottom left of the figure indicates respective probe positioning

by sweeping the probe up and down along its major axis (Fig. 14.40). At the peroneal head, the common poroneal nerve is located in the subcutaneous tissue between the skin and the bone cortex and splits into the superficial and deep peroneal nerves (Martinoli et al. 2000a). These divisional branches can be appreciated as individual structures with very high frequency probes (15 MHz). The peroneal head region should be accurately assessed because it represents the usual location at which the nerve can be injured by local trauma (Fig. 14.40d,e). The lateral head of the gastrocnemius is smaller than the medial head. Its tendon may contain the fabella ("little bean"), a sesamoid bone that appears as a curvilinear hyperechoic structure showing well-defined posterior acoustic shadowing (Fig. 14.41). The examiner should be careful not to confuse the fabella with an intra-articular loose body, an osteophyte or a capsular calcification (Duncan and Dahm 2003). The intratendinous location of the fabella and its fixed position during dynamic scanning can exclude an intra-articular fragment. Diagnosis of capsular calcifications basically relies on a sharper and more irregular appearance of the borders of the fragment.

14.5 Knee Pathology

A variety of disorders can involve the soft tissues around the knee joint. They are here reviewed by location according to the four compartments of the joint – anterior, medial, lateral and posterior – because multiple disorders related to specific anatomic sites may share similar characteristics.

14.5.1 Anterior Knee Pathology

In terms of clinical relevance, disorders related to the extensor mechanism are the leading pathology of the anterior knee. Other conditions in which US plays a diagnostic role include prepatellar and infrapatellar bursitis, some bone and positional abnormalities of the patella and the so-called mediopatellar plica syndrome.

14.5.1.1 Quadriceps Tendinopathy

Quadriceps tendinopathy is far less common than patellar tendinopathy and usually relates to sporting activities or strenuous exercise. Clinically, this condition is characterized by focal pain over the distal portion of the tendon, exacerbated by resisted extension of the knee or firm pressure over it. The skin is normal and there is no evidence of intra-articular effusion at physical examination. Similar to other tendinopathies, the involvement of the quadriceps tendon mainly relates to degeneration and fibromyxoid changes. In this setting, the main value of

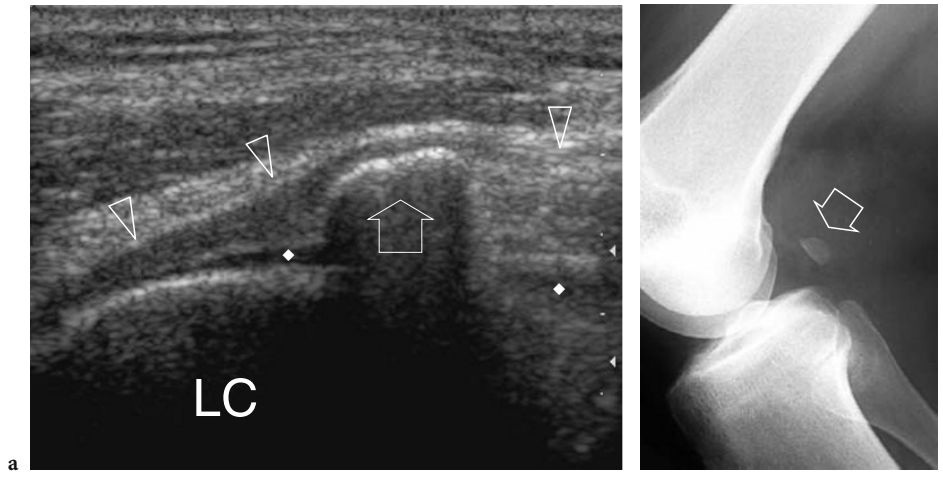

Fig. 14.41a,b. Fabella. **a** Longitudinal 12–5 MHz US image with **b** lateral radiographic correlation demonstrates the fabella (*arrow*) as an oval hyperechoic image with posterior acoustic shadowing included in the tendon (*arrowheads*) of the lateral head of the gastrocnemius. Note the close relationship of this accessory bone with the underlying articular cartilage (*rhombi*) of the lateral femoral condyle (*LC*)

US is to confirm the clinical diagnosis and assess the severity of tendon involvement. In mild abnormalities, pathologic changes usually affect a single layer of the tendon and appear as oval, ill-defined hypoechoic areas located either in the middle or on the sides of the quadriceps tendon (Fig. 14.42). Short-axis US images must always be obtained because focal involvement of the lateral or medial tendon edges can easily be missed on midsagittal images (Fig. 14.42b). Color Doppler imaging often reveals a hypervascular pattern in relation to the intratendinous focal hypoechoic areas (Fig. 14.42c). Less commonly, this condition affects the full thickness of the distal tendon, which appears diffusely swollen and heterogeneous. In these cases, the fibrillar echotexture and the multilayered appearance of the tendon become more indistinct (Fig. 14.43). If surgical treatment is warranted, as is the case in elite sportsmen after 6–12 months of unsuccessful medical therapy, an accurate assessment of the size of the hypoechoic degenerative nodule is a prerequisite for its successful removal.

Calcifying enthesopathy refers to calcified deposits in the more distal portion of the quadriceps tendon. It usually derives from local chronic stresses (excessive loading due to overweight or professional activities) or peripheral involvement in diffuse idiopathic skeletal hyperostosis (DISH) syndrome. Clinically, the enthesopathy at the quadriceps tendon insertion may be completely asymptomatic or may cause a highly localized pain over the upper pole of the patella. Standard radiographs, with special reference to the laterolateral view, are sensitive for detecting insertional calcifications. US recognizes them as multiple, irregularly hyperechoic images with posterior acoustic shadowing, usually located within the distal portion of the superficial or intermediate tendinous layers (Fig. 14.44) (Wakefield et al. 2004; Kamel et al. 2004). In the symptomatic patient, local palpation with the probe can be painful. Irregularities of the quadriceps enthesis can also be part of the peripheral involvement of seronegative spondyloarthropathies. In these cases, US is able to reveal quadriceps enthesopathy based on detection of bony erosions, local soft-tissue edema and calcifications. Occasionally, fine abnormalities of the tendon echotexture can be encountered in healthy patients (Frediani et al. 2002).

14.5.1.2 Quadriceps Tendon Tear

Compared with Achilles tendon and rotator cuff tears, rupture of the quadriceps tendon is a rare condition which mostly occurs in association with systemic disorders such as gout, rheumatoid arthritis, systemic lupus erythematosus, hyperparathyroidism, diabetes mellitus and chronic renal fail-

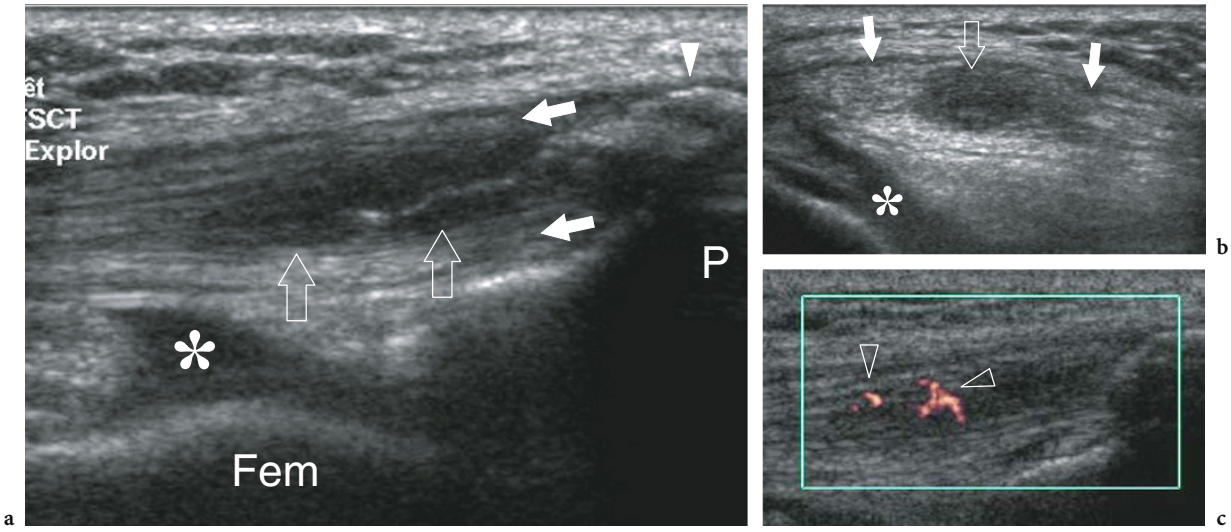

Fig. 14.42a–c. Focal tendinopathy of the quadriceps tendon. **a** Long- and **b** short-axis 12–5 MHz US images reveal an ill-defined fusiform hypoechoic area (*open arrows*) which affects the intermediate layer of the tendon reflecting a degenerative intratendinous nodule. Note **a** the superficial and deep layers (*white arrows*), and **b** the lateral and medial thirds of the tendon which remain unaffected. In **a**, a preinsertional calcification (*arrowhead*) is also observed within the tendon substance. Note a mild intra-articular effusion (*asterisk*) inside the suprapatellar recess. **c** Longitudinal power Doppler US image shows signs of intratendinous hyperemia (*arrowheads*). *P*, patella; *Fem*, femur

ure (Levy et al. 1971; Lotem et al. 1974; Peiro et al. 1975; Potasman and Bassan 1984; Barash et al. 1989). Unlike patellar tendon tears, which are more common in young sportsmen, quadriceps tendon tears usually affect middle-aged or elderly subjects. The pathomechanism is essentially related to a sudden and powerful contraction of the quadriceps muscle with concomitant tendon stretching, such as in the setting of a slip and fall. Clinically, patients present with swelling and tenderness in the suprapatellar region and pain located at the level of the quadriceps tendon. Physical findings are different in complete and partial tendon tears. While in partial tears, active extension of the leg can be obtained because of the residual integrity of one or two tendon layers, this is nearly impossible in full-thickness ruptures. It must be stressed, however, that clinical findings can be misleading, because extension of the leg against gravity can still be achieved as a result of the integrity of the lateral expansions of the tendon (Ramsey and Mueller 1970; Smillie 1971). In these patients, a delayed diagnosis will lead to weakness of the extensor mechanism, secondary joint instability and prolonged disability.

Because partial and complete tears of the quadriceps tendon are managed with different treatment strategies (conservative vs. open tenorrhaphy), diagnostic imaging has a role in differentiating these conditions and orienting the most appropriate therapy. US is able to detect quadriceps tendon tears and to differentiate incomplete from complete lesions (Bianchi et al. 1994; La et al. 2003). In partial-thickness tears, the superficial layer (from rectus femoris) is the most commonly affected, followed by the intermediate one (from the vastus medialis and lateralis) (Fig. 14.45a). From a pathomechanical standpoint, this can be explained by the fact that the most anterior fibers are more eccentric in location relative to the lever of the knee flexion and, therefore, are subjected to a higher vector force. The deep tendinous layer (from vastus intermedius) is the last to rupture. At US, a partial-thickness tear appears as a focal discontinuity of one or two layers located at approximately 1–2 cm from the patellar insertion. The proximal tendon end is retracted, swollen and hypoechoic and lacks a normal fibrillar pattern (Fig. 14.46). Because the layers are separated by thin strips of loose connective tissue, the torn ones may retract proximally for a considerable extent. Detection of a tear and evaluation of tendon retraction is easier when a hypoechoic hematoma fills the gap. In the rare instances in which the peritenon is unaffected, the hematoma remains contained

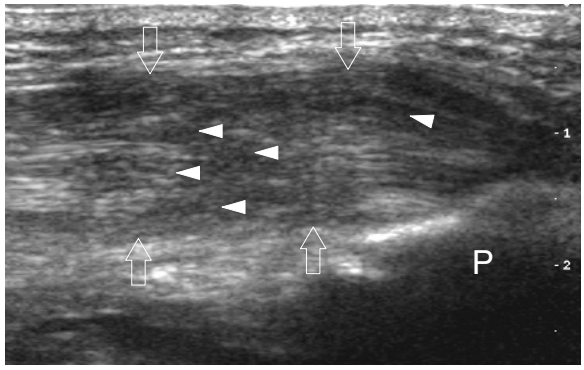

Fig. 14.43. Severe quadriceps tendinopathy. Longitudinal 12–5 MHz US image shows a markedly swollen and heterogeneous quadriceps tendon (*arrows*). Note that the echotextural abnormalities affect all tendinous layers with ill-defined hypoechoic areas (*arrowheads*). The most damaged area seems located at approximately 10–15 mm from the distal tendon insertion into the upper pole of the patella (*P*), the critical area of the quadriceps tendon

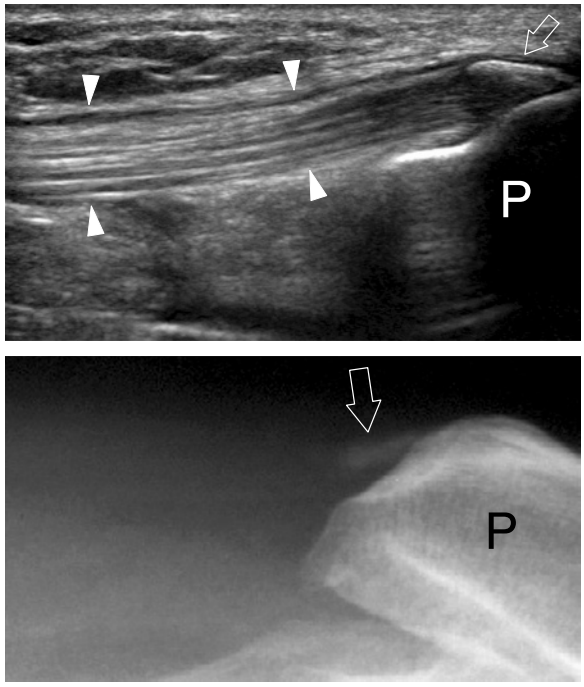

Fig. 14.44a,b. Calcific enthesopathy. **a** Longitudinal 12–5 MHz US image reveals a calcific deposit (*arrow*) at the insertion of the superficial layer of the quadriceps tendon (*arrowheads*) into the upper pole of the patella (*P*). **b** Corresponding lateral radiograph confirms the presence of calcific enthesopathy (*open arrow*) of the quadriceps tendon

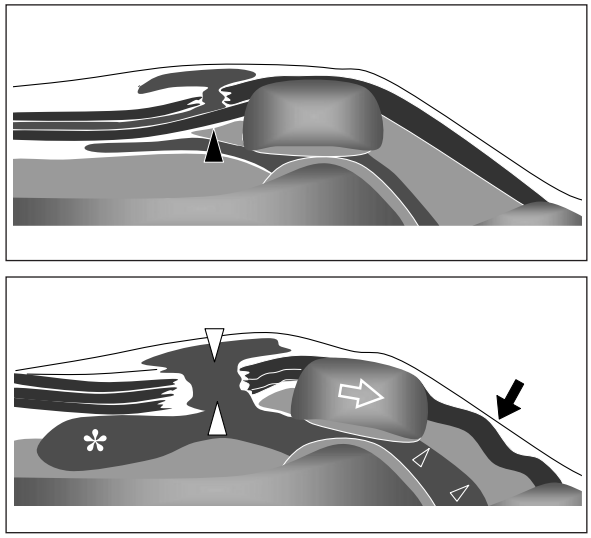

Fig. 14.45a,b. Partial-thickness and full-thickness tear of the quadriceps tendon. **a** Schematic drawing shows a partial-thickness tear of the quadriceps tendon affecting the superficial and intermediate layers of the tendon, while the deep layer (*black arrowhead*) remains unaffected and can be seen inserting regularly into the dorsal aspect of the patella. **b** Schematic drawing illustrates a full-thickness tear of the quadriceps affecting all three tendon layers. The peritendon is torn and the hematoma can spread within the subcutaneous tissue. In complete tears, the rupture is followed by caudal displacement of the patella (*open arrow*) and a crumpled appearance (*black arrow*) of the patellar tendon. Note that the intra-articular effusion (*asterisk*) communicates with the subcutaneous collection through the tendon tear (*white arrowheads*) and displaces the Hoffa fat pad anteriorly (*open arrowheads*)

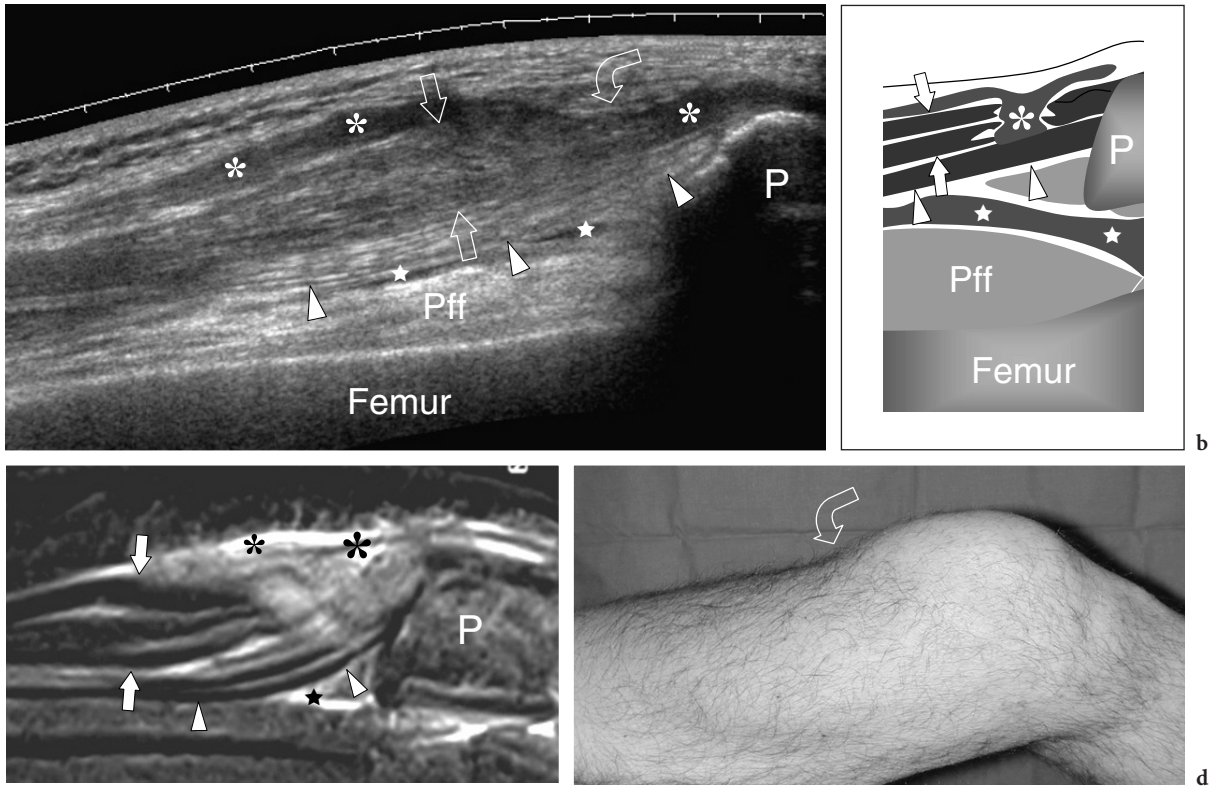

Fig. 14.46a–d. Partial-thickness tear of the quadriceps tendon. **a** Longitudinal extended field-of-view 12–5 MHz US image with **b** corresponding schematic drawing and **c** STIR MR imaging correlation reveal a combined tear of the superficial and intermediate tendon layers (*open straight arrows*), whereas the deep layer is undamaged (*arrowheads*). The hematoma (*asterisks*) fills the gap between the two tendon ends. Note the occurrence of mild intra-articular effusion (*stars*) separated from the hematoma. *Pff*, prefemoral fat pad; *P*, patella. **d** Photograph shows a skin depression (*curved arrow*) in the suprapatellar area reflecting the underlying tendon tear

within the tendinous bed and skin bruise may be absent. If there is disruption of the peritenon, the hematoma spreads in the subcutaneous tissue and becomes clinically manifest as a local ecchymosis. The integrity of the deep tendon layer should be carefully assessed when a partial-thickness tear is suspected at US. Gentle passive flexion of the knee with placement of small pillows below the popliteal fossa to increase the tendon tension may be tolerated by the patient and help to delineate the tendon gap. An intra-articular effusion can be demonstrated if the tear extends laterally or medially to involve the tendon expansions and the joint capsule. Finally, the report should indicate which layer is torn, the percentage thickness of the intact portion relative to the full thickness of the tendonas well as the width of the tear (incomplete vs. complete rupture).

Full-thickness tears of the quadriceps tendon present with complete discontinuity of all tendon layers (Fig. 14.45b). The location of these tears is nearly the same as that of partial tears. Occasionally, bony avulsion from the upper pole of the patella occurs (La et al. 2003). In complete intrasubstance tears, US detects two swollen hypoechoic tendon stumps separated by hypoechoic hematoma (Fig. 14.47). The proximal tendon end can be retracted for a variable distance depending on the strength of the muscle; in general, the distal stump measures 1–2 cm in length (Fig. 14.47). In full-thickness tears of the quadriceps tendon, an intra-articular effusion is almost always seen reflecting a break in the suprapatellar recess. The medial and lateral retinacula should also be carefully evaluated because they commonly tear in association with the tendon. In patients with knee ache who deny flexing the knee, a complete tear can be difficult to distinguish from a partial tear. In these cases, some tricks of the trade can be useful in confirming a complete rupture, such as applying a gentle distal traction on the patella to widen the tendon gap or evaluating the morphology of the patellar tendon. In complete ruptures, the patellar tendon assumes a crumpled appearance due to the caudal displacement of the patella that is no longer retained by the quadriceps tendon (Fig. 14.48). This finding is similar to that described at MR imaging and has value only in traumatized patients (Berlin et al. 1991). In fact, it may also be observed in patients with palsy of the quadriceps muscle, in which the lack of tonicity of the muscle may result in caudal displacement of the bone. Although other modalities, including plain films (Newberg and Wales 1977), arthrography (Aprin and Broukhim 1985; Jelaso and Moris 1975), CT and MR imaging (Barash et al. 1989; Berlin et al. 1991), have been proposed to assess quadriceps tendon tear, we believe US is a readily available, cheap and dynamic tool for its diagnosis (Bianchi et al. 1994). In the postsurgical setting, the operated tendon appears swollen and hypoechoic with irregular margins and contains bright linear echoes corresponding to intratendinous stitches and wires (Fig. 14.49). Dynamic examination during flexion and extension movements can be helpful to assess the continuity of the tendon and to detect peritendinous adhesions.

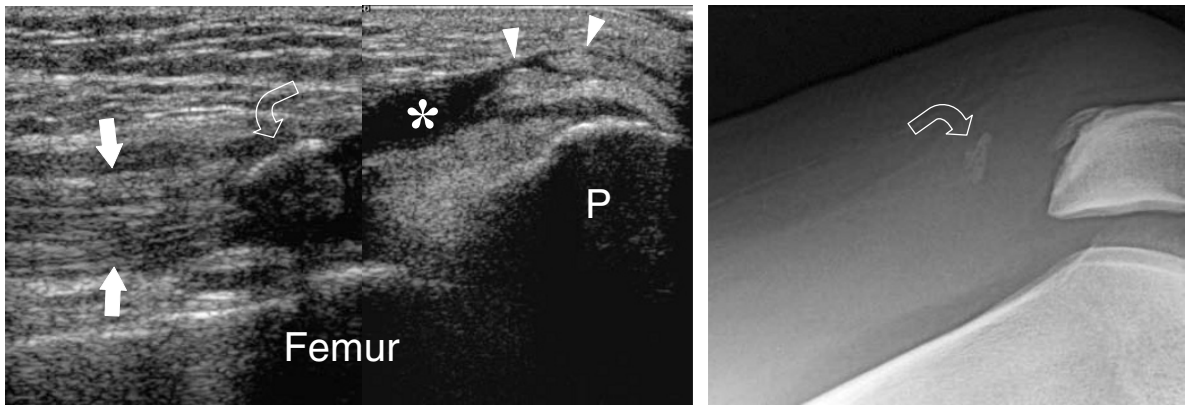

Fig. 14.47a,b. Complete tear of the quadriceps tendon. **a** Longitudinal 12–5 MHz US image of the suprapatellar region with **b** lateral radiographic correlation reveals discontinuity and retraction of all three quadriceps tendon layers (*straight arrows*) reflecting a complete tear. Note the distal ends (*arrowheads*) of these layers which remain attached to the patella (*P*) and the avulsion of a calcification (*curved arrow*) from the tendinous insertion

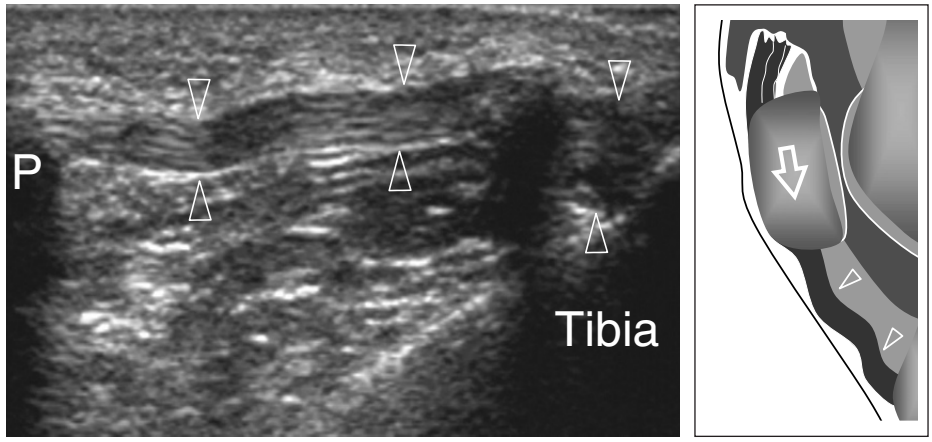

Fig. 14.48a,b. Complete tear of the quadriceps tendon. **a** Longitudinal 10–5 MHz US image of the infrapatellar region with **b** schematic drawing correlation demonstrates a reduced distance between the lower pole of the patella (P) and the tibial epiphysis and a wavy patellar tendon (*arrowheads*)

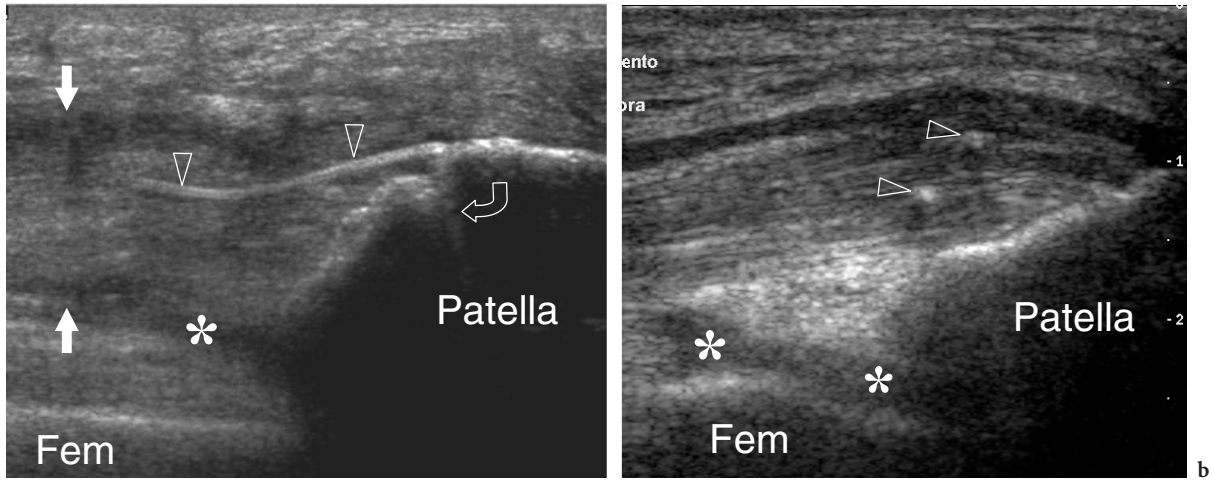

Fig. 14.49a,b. Quadriceps tendon: postsurgical US findings in two different cases previously operated on for complete tendon tear. **a,b** Longitudinal 12–5 MHz US images over a thickened distal quadriceps tendon (*straigh arrows*) demonstrate a heterogeneous echotexture with bright hyperechoic dots and lines (*arrowheads*) corresponding to intratendinous metallic wires. In **a**, note the anchoring point (*curved arrow*) of the wire on the patella. In both cases, a mild intra-articular effusion (*asterisks*) is present in the suprapatellar recess. *Fem*, femur

14.5.1.3 Medial Plica Syndrome

The mediopatellar plica is a synovial fold located between the medial articular facet of the patella and the trochlea. Similar to the suprapatellar plica, the mediopatellar plica is an embryonic remnant. In patients involved in athletic activity requiring repetitive flexion-extension movements, the medial plica can undergo inflammation and fibrosis leading to the so-called medial plica syndrome (Boles and Martin 2001). This condition presents with medial patellar pain, usually exacerbated during flexion-extension of the knee joint, and possibly effusion. At US, the normal mediopatellar plica appears as a triangular hyperechoic structure with a superficial base and the apex pointing toward depth, which is better delineated whether an intra-articular effusion is present (Derks et al. 1986). Medial displacement of joint fluid by pressure applied on the lateral knee during scanning may be helpful to detect it. Medial tilting of the patella while examining its internal aspect can also increase the visibility of the plica. Dynamic US examination obtained during progressive flexion of the knee can show the plica moving into the patellofemoral space during flexion (Derks et al. 1986). Considering arthroscopy as the gold standard, the sensitivity, specificity and accuracy of US in assess-

ing the mediopatellar plica are 92%, 73% and 85%, respectively (Derks et al. 1986). A pathologic plica appears thickened and stiff and may result in dysfunction of the medial patellofemoral joint and cartilage erosions. In our opinion, however, the examiner should be cautious in diagnosing a pathologic mediopatellar plica because a normal thin plica can be encountered in a high percentage (20%) of asymptomatic knees. Although US can image the plica and reveal even its size and elasticity, the US diagnosis of a pathologic plica is challenging and can be suggested only in an appropriate clinical context. In addition, US detection of cartilage erosions at the level of the mediopatellar joint is difficult and basically relies on MR imaging or CT-arthrography.

14.5.1.4 Prepatellar Bursitis

The prepatellar bursa is a synovium-lined structure located in the subcutaneous tissue over the lower half of the patella and the upper third of the patellar tendon. Its main function is to reduce friction between these structures and the skin during joint motion. In normal states, the prepatellar bursa contains a minimal amount of fluid and cannot be detected with US even when the examination is performed with high-frequency transducers. Pathologic conditions affecting this bursa may be acute or chronic. An acute prepatellar bursitis may derive from a direct blow, a fall on the flexed knees, metabolic (gout) or infectious conditions. While the diagnosis of post-traumatic bursitis is essentially based on the patient's history, differentiation between metabolic and infectious bursitis is more problematic because clinical findings are similar and fever can also occur in gout. On the other hand, chronic bursitis is essentially post-traumatic in nature as it follows repetitive local microtrauma, such as in the case of patients working on their knees (housemaid's knee, carpet-layer's knee) (Myllymaki et al. 1993).

US findings of acute prepatellar bursitis reflect the underlying pathology. In an acute gout attack, US detects an anechoic intrabursal effusion, whereas in post-traumatic bursitis the blood filling the bursa

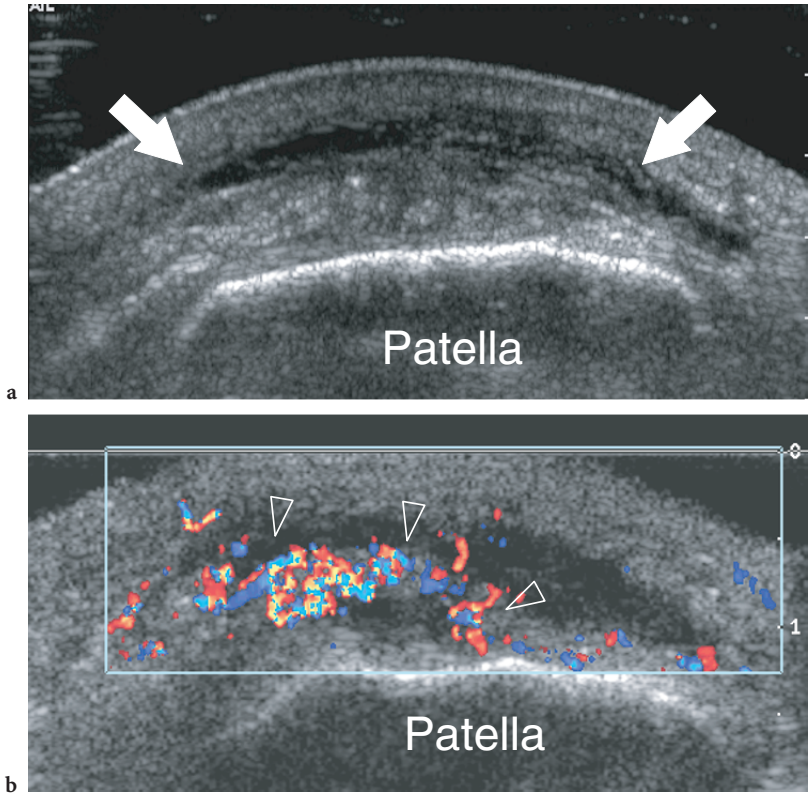

Fig. 14.50a,b. Acute prepatellar bursitis. Transverse **a** gray-scale and **b** color Doppler 12–5 MHz US images over the anterior aspect of the patella demonstrate marked thickening of the prepatellar soft-tissues (*white arrows*) within which a small fluid collection can be seen. Color Doppler imaging reveals an increased vasculature (*arrowheads*) within the thickened bursal walls reflecting inflammatory hyperemia

may appear echogenic (Fig. 14.50a). The bursal walls are only slightly thickened and have no septations. Color Doppler imaging can reveal increased flow signals within the inflamed walls (Fig. 14.50b). In chronic bursitis, thickened walls and internal septations are typically observed (Fig. 14.51). Intrabursal effusion can be negligible and the bursal cavity can be almost completely filled with hypertrophied synovium. Although the diagnosis of prepatellar bursitis is based on clinical findings, US can help to evaluate the bursal content (fluid vs. synovium) before needle aspiration, a procedure required to distinguish gout from local infection. In addition, it can successfully guide the needle puncture by directing the needle tip within the fluid component of the bursal cavity, thus avoiding areas filled with synovial pannus. When bursitis is secondary to local trauma, US can also help to inject steroids into the bursa.

14.5.1.5 Abnormalities of the Patella

Patellar fractures derive from a sudden forceful tension on the extensor mechanism or, more commonly, from a fall on the flexed knees. The diagnosis is based on clinical findings and confirmed by standard radiographs to visualize the fracture line, the number of fragments and their position. In some patients, however, the paucity of clinical signs can erroneously suggest patellar tendinopathy rather than a fracture. In our experience, we have observed more than one patient who was unaware of the patellar fracture and submitted to US examination with a presumptive diagnosis of jumper's knee. In these cases, US reveals a normal patellar tendon and a cleft in the hyperechoic patellar cortex (Fig. 14.52a) (Ditchfield et al. 2000). Once the fracture is suspected, standard radiographs and eventually CT should be obtained to confirm the diagnosis and assess the number, size and position of the fragments (Fig. 14.52b). CT is particularly effective to estimate the involvement of the articular surface.

Patellar retinacula link the patella to the medial and lateral aspects of the knee, playing a role as stabilizers during flexion and extension of the joint. These retinacula can tear following patellar instability. Because the patella almost always displaces laterally due to the physiologic valgus of the knee, the medial retinaculum is the most frequently injured. These tears usually results from a twisting motion, with the knee in flexion and the femur rotating internally on a fixed root. Lateral patellar dislocation causes an impaction of its medial aspect on the lateral femoral condyle and injury of the medial retinaculum as a result of distraction. Most often, dislocation is transient and the patella recoils back into the trochlear groove. An injured medial retinacular complex appears as a cleft in a swollen and hypoechoic retinaculum (Trikha et al. 2003;

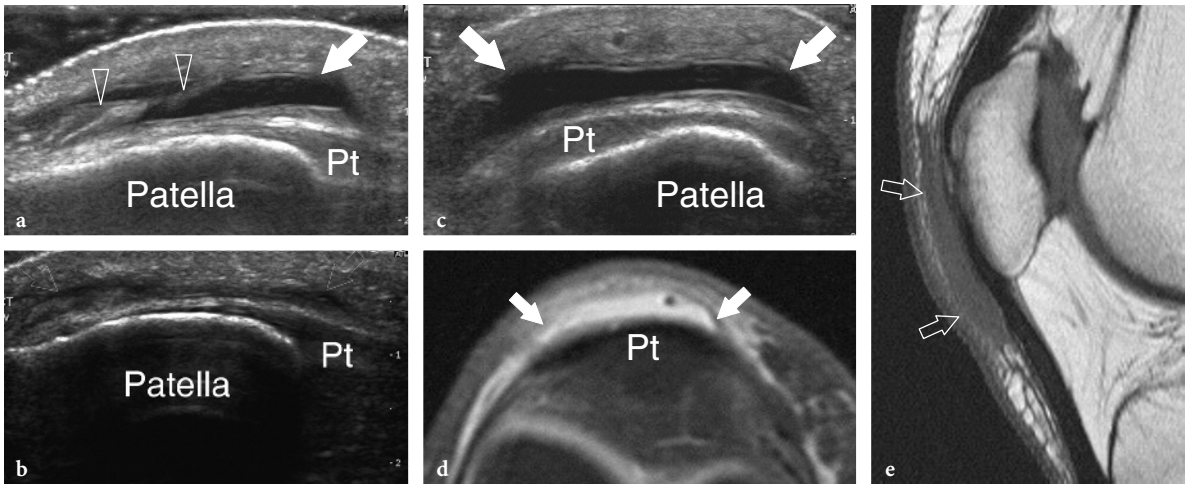

Fig. 14.51a–e. Chronic prepatellar bursitis. **a,b** Longitudinal 12–5 MHz US images obtained over the patella **a** without and **b** with compression with the probe demonstrate diffuse thickening (*arrows*) of the prepatellar bursa walls (*arrowheads*). In **b**, the intrabursal effusion is squeezed away from the field-of-view of the US image by pressure with the probe. **c** Corresponding transverse US image. **d,e** Correlative transverse fat-suppressed proton density (**d**) and sagittal T1-weighted MR (**e**) images reveal abnormal T1-hyperintense and T2-hypointense signal in the prepatellar subcutaneous tissue reflecting prepatellar bursitis. *Pt*, patellar tendon

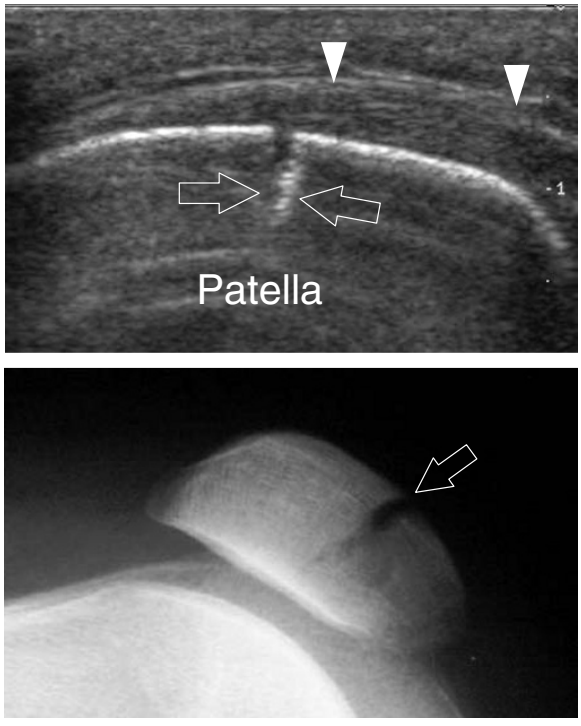

Fig. 14.52a,b. Patella fracture in a patient with persistent anterior knee pain after a traffic accident. **a** Longitudinal 12–5 MHz US image over the anterior aspect of the patella shows an abrupt discontinuity of the anterior cortical line (*arrows*) and a marked thickening of the periosteum (*arrowheads*). **b** Lateral radiograph confirms a clinically undetected patellar fracture

O'Reilly et al. 2003). If the retinaculum appears normal, its medial insertion into the border of the patella should be carefully examined to rule out cortical avulsions (O'Reilly et al. 2003). These have the appearance of subtle hyperechoic foci located in close proximity to the insertion of the retinaculum and are painful when local pressure is applied over them. Differentiation of retinacular tears from a surgical access during arthroscopy is based on demonstration of a more focal discontinuity and on clinical correlation (Fig. 14.53). Tears of the lateral retinaculum are almost always iatrogenic and result from surgical release in patients affected by lateral patellar instability. In these cases, US reveals a sharp discontinuity of both ligament and adjacent tissues.

Patellar cartilage abnormalities can occasionally be detected with US on the medial facet of the patella and may be related to lateral patellar dislocation. US can image an osteochondral fracture as a focal defect of cartilage and irregularity of the hyperechoic line representing the subchondral bone plate (Fig. 14.54). Although US can detect these changes, it should be stressed that a suspected osteochondral injury must be ruled out based on other modalities, such as CT-arthrography, MR imaging and MR-arthrography, which allow visualization of the overall articular surface of the patella.

In patellar osteosynthesis, US reveals the metallic wires and the associated abnormalities in the quadriceps and patellar tendons. In patients who have undergone patellectomy because of a multifragmented fracture, US can assess the healing of tenorraphy between the quadriceps and the patellar tendons as well as local inflammatory changes.

14.5.1.6 Patellar Tendinopathy

Patellar tendinosis most commonly involves the proximal tendon insertion as a result of repetitive microtrauma and overuse. This condition, also refered to as "jumper's knee" affects young active subjects who practice sporting or recreational activities that require powerful contraction of the quadriceps muscle, such as kicking, running or jumping. Soccer and basketball players are particularly vulnerable. Microtrauma between the undersurface of the patellar insertion and a prominent patellar tip has been assumed to be a causative factor for chronic impingement and secondary degenerative changes of the patellar tendon. Histopathologically, tearing of collagen followed by mucoid degeneration and an ongoing repair process are the main findings in the

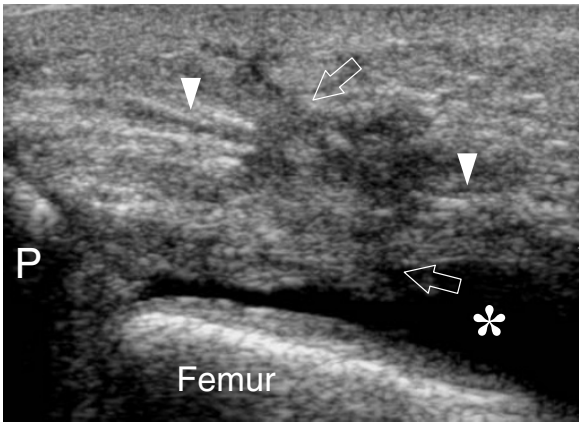

Fig. 14.53. Release of the medial patellar retinaculum. Transverse 12–5 MHz US image obtained at the level of the parapatellar region in a patient operated on for medial release demonstrates a sharply demarcated break of the retinaculum (*arrowheads*) filled by an irregular area of fibrosis (*arrows*). Note the intra-articular effusion (*asterisk*) in the parapatellar recess. *P*, patella

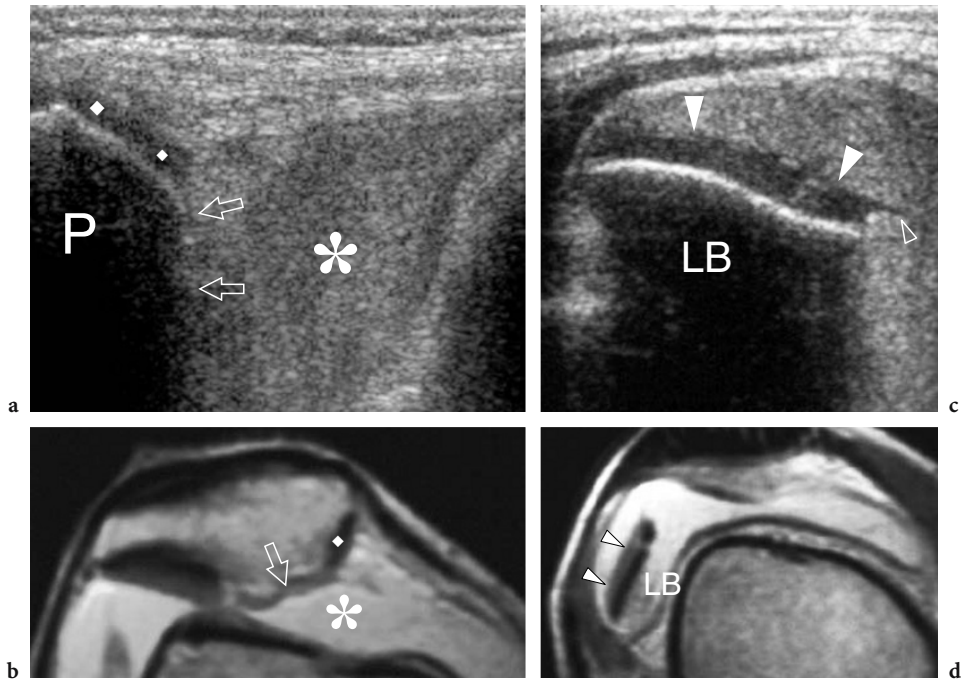

Fig. 14.54a–d. Acute osteochondral fracture of the medial patellar facet. **a** Transverse 12–5 MHz US image over the medial knee at the level of the patella (*P*) with **b** corresponding T2-weighted MR imaging correlation show a hyperechoic bloody effusion within the joint cavity (*asterisk*). The retropatellar cartilage appears normal at the level of its most medial portion (*rhombi*). On the contrary, no hypoechoic band related to the articular cartilage can be appreciated in a more lateral location over the subchondral bone plate (*arrows*). **c** Transverse 12–5 MHz US image of the lateral parapatellar recess with **d** corresponding T2-weighted MR image shows an osteochondral loose body (*LB*) surrounded by bloody effusion. Note the chondral component (*white arrowheads*) of the fragment which shows sharp margins (*open arrowhead*) indicating a fresh detachment

jumper's knee (Khan et al. 1996). Patients complain of a localized sharp pain located just distal to the lower pole of the patella which typically worsens after activity. In more severe cases, pain becomes acute and continuous during sport activities. Physical examination shows a well-circumscribed tenderness over the proximal patellar tendon. Mild forms are treated by rest, local ice and nonsteroidal antiinflammatory drugs, whereas chronic cases can require surgical treatment (Roels et al. 1978).

US examination can be required to confirm the clinical diagnosis and assess the extent and severity of tendinosis. In many cases, a preinsertional fusiform hypoechoic area involving the deep central portion of the tendon can be encountered, possibly associated with focal hyperechoic spots and posterior attenuation of the US beam (Fig. 14.55) (Cook et al. 2000; Carr et al. 2001). On transverse US images, a central posteriori bulging of the tendon is seen due to the presence of a rounded degenerative nodule, whereas the medial and lateral third of the tendon are often unaffected and retain a normal fibrillar appearance (Fig. 14.56a–c). This explains why a midsagittal scan may show a fusiform nodule extending through the proximal tendon portion whereas longitudinal images obtained over the lateral and medial tendon may appear normal. In many cases, the most superficial fibers of the tendon are normal. In chronic longstanding disease, color and power Doppler imaging can show an increased intratendinous vasculature related to prominent angiogenesis (Weinberg et al. 1998; Terslev et al. 2001). Typically, intratendinous vessels can be seen entering the lower aspect of the hypoechoic nodule and branching within it (Fig. 14.56d). It should be pointed out that the extent of the hypoechoic nodule must be accurately measured in three dimensions if the patient is a candidate for a selective surgical approach. As at other sites, distinguishing focal areas of tendinosis from partial tears can be difficult with US. Partial tears may be assumed when discrete anechoic cleavage planes oriented from the bony insertion distally are visible (Fig. 14.57) (Carr et al. 2001).

Patellar tendinopathy involving the tendon diffusely is, for the most part, unrelated to sporting activities and may be observed in patients with

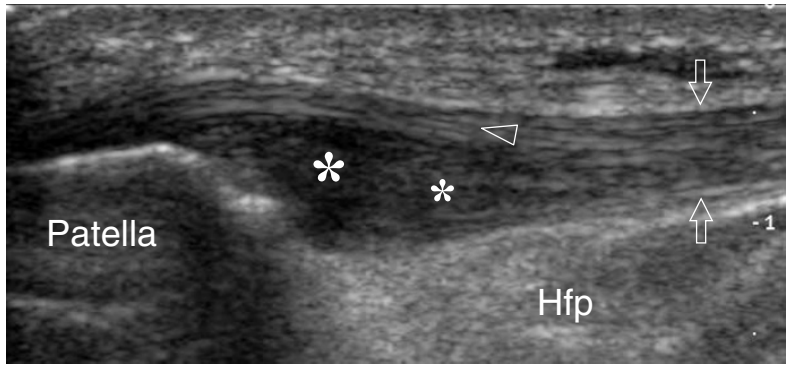

Fig. 14.55. Jumper's knee. Proximal patellar tendinopathy. **a** Long-axis 12–5 MHz US image of the proximal patellar tendon (*arrows*) shows a ill-defined hypoechoic area (*asterisks*) located at the level of the middle and posterior tendon thirds reflecting degenerative tendinopathy. Note the absence of significant tendon thickening and the normal fibrillar appearance of the most superficial fibers (*arrowhead*). *Hfp*, Hoffa fat pad

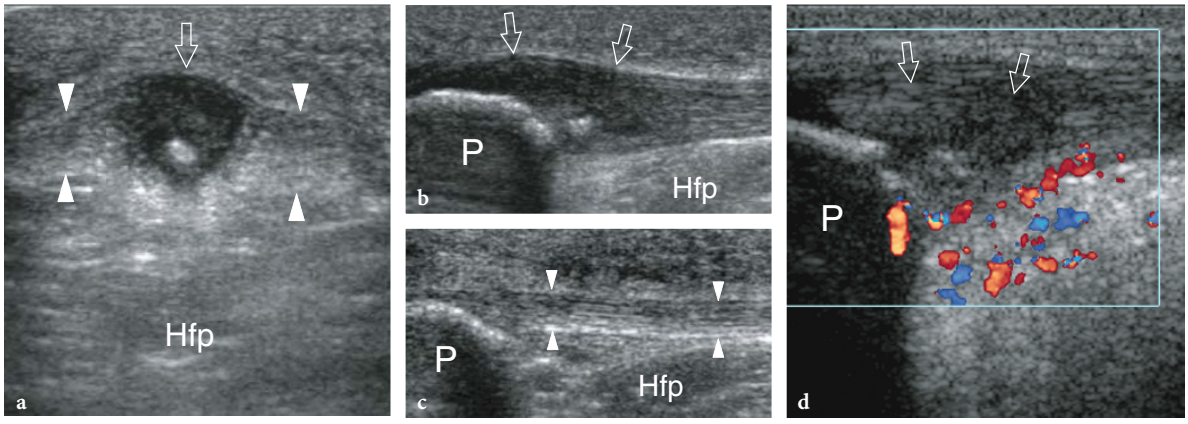

Fig. 14.56a–d. Jumper's knee. Proximal patellar tendinopathy. **a** Transverse 12–5 MHz US image of the proximal patellar tendon and correlative **b,c** longitudinal 12–5 MHz US images obtained **b** in the midline and **c** over the right lateral tendon third. A full-thickness hypoechoic swelling (*arrows*) is seen in the midline of the patellar tendon reflecting central focal tendinopathy whereas the medial and lateral portions (*arrowheads*) retain a normal fibrillar appearance. Note a small intratendinous calcification within the focal hypoechoic area. *Hfp*, Hoffa fat pad; *P*, patella. **d** Color Doppler imaging shows local hyperemia around the deep tendon surface

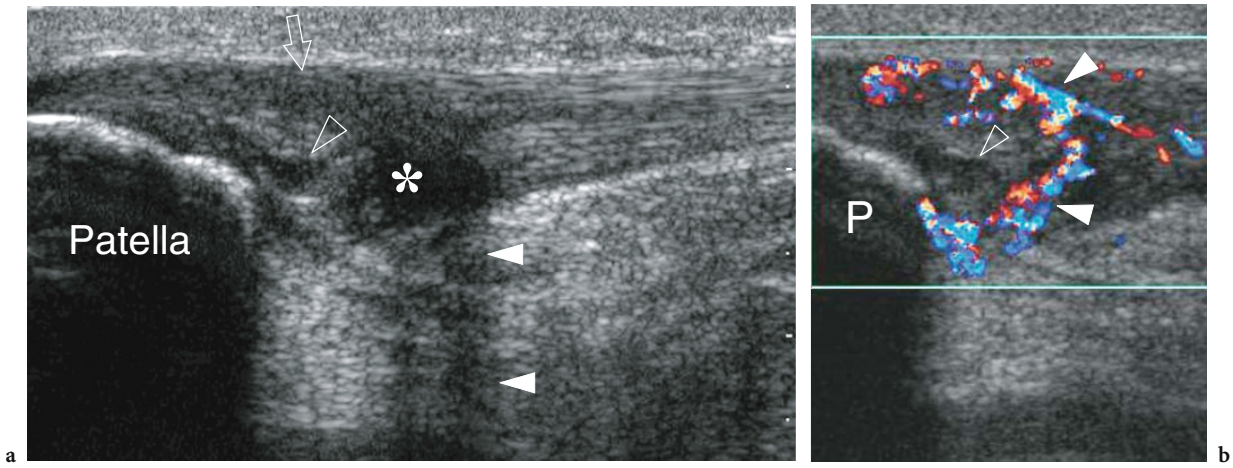

Fig. 14.57a,b. Jumper's knee. Partial thickness tear of the patellar tendon. **a** Longitudinal gray-scale 12–5 MHz US image reveals a longitudinal hypoechoic split (*open arrowhead*) through the substance of the patellar tendon extending from the patella distally. The torn deep fibers (*asterisk*) are retracted just distal to the hypoechoic area and characterized by attenuation of the US beam (*white arrowheads*) due to refraction at the frayed tendon end. Note the integrity of the most superficial tendon fibers (*arrow*). **b** Color Doppler imaging reveals a diffuse intratendinous hyperemia (*white arrowheads*) except for the site of fibers retraction. *P*, patella

metabolic disorder, knee prosthesis or other joint problems in the lower extremity. Gout tendinopathy causes a uniform swelling of the patellar tendon affecting its proximal, middle and distal thirds. Diffuse thickening and a hypoechoic pattern of the affected tendon are readily evident on longitudinal images (Fig. 14.58a). The patient's history may reveal a metabolic disorder and exclude previous local surgery. In fact, tendons previously operated on for jumper's knee may have a similar appearance (Fig. 14.59).

Overall, both MR imaging and US can accurately assess jumper's knee (Davies et al. 1991). US is recommended as the initial diagnostic investigation because of its low cost and availability. In our opinion, MR imaging should be reserved for evaluating doubtful cases. Although follow-up examinations are frequently requested by the clinician in an effort to monitor the evolution of the process and, even more likely, to decide whether the athlete can return to agonistic activity, we believe that US has limited value in this field. Routine practice indicates that many patients get better clinically without any improvement of the US appearance of the tendon. One should also consider that abnormal US findings can occasionally be found in asymptomatic knees (Lian et al. 1996; Cook et al. 2001). On the other hand, US signs of patellar tendinopathy in asymptomatic sportsmen have been associated with a higher risk of developing symptomatic jumper's knee in the future (Fredberg and Bolvig 2002).

Complete tears of the patellar tendon may follow a direct local blow or represent end-stage chronic tendinopathy. In both cases, the tear is usually complete and can easily be diagnosed on physical examination. Patients are young, have a swollen knee, striking infrapatellar pain and tenderness and are unable to extend the joint. There may be associated intra-articular effusion. A standard laterolateral radiograph of the knee can help to confirm the diagnosis by showing a higher position of the patella than normally expected as it is retracted upward by the quadriceps muscle. US reveals an interrupted wavy tendon with separation of the tendon ends (Fig. 14.60) (Carr et al. 2001). Incomplete tears are extremely rare and difficult to recognize clinically (Fig. 14.61).

In patients treated for anterior cruciate ligament reconstruction with thw bone-tendon-bone technique, the patellar tendon appears composed of two tendon cords separated by a central vertical hypoechoic cleft (Fig. 14.62) (Kartus et al. 2000). In these cases, a defect in the anterior surface of the lower

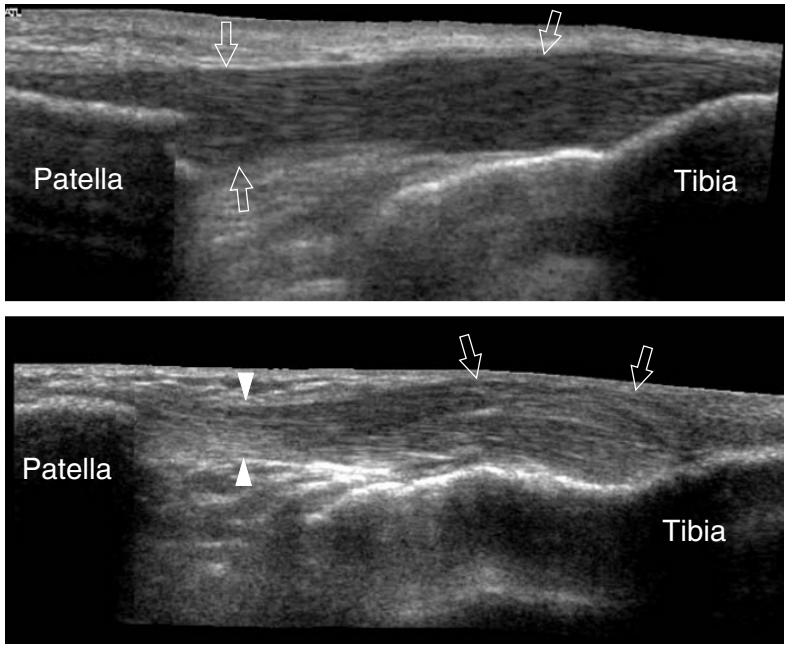

Fig. 14.58a,b. Spectrum of patellar tendinopathies. Two different patients. **a** Longitudinal extended field-of-view 12–5 MHz US image reveals a diffusely thickened and heterogeneous hypoechoic patellar tendon (*arrows*) reflecting diffuse tendinopathy. **b** Longitudinal extended field-of-view 12–5 MHz US image demonstrates selective thickening (*arrows*) of the distal third of the patellar tendon as an expression of distal tendinopathy. The proximal portion of the tendon (*arrowheads*) retains a normal appearance

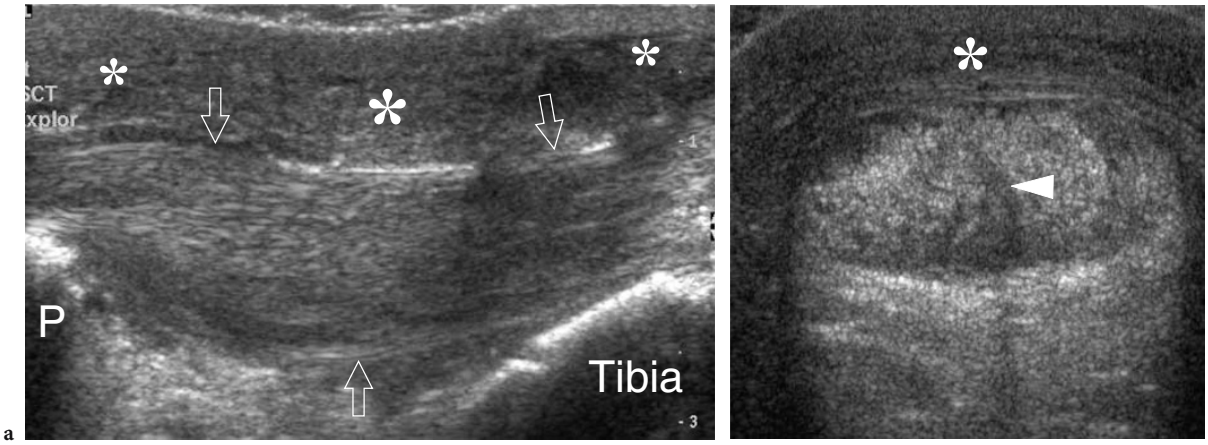

a b

Fig. 14.59a,b. Postsurgical appearance of the patellar tendon. **a** Long- and **b** short-axis 12–5 MHz US images of the patellar tendon in a patient who underwent surgical treatment for jumper's knee reveal an overall tendon appearance similar to that of diffuse patellar tendinopathy (*arrows*). Note the postoperative thickening of the anterior soft-tissues (*asterisks*) and an intrasubstance fissuration (*arrowhead*). *P*, patella

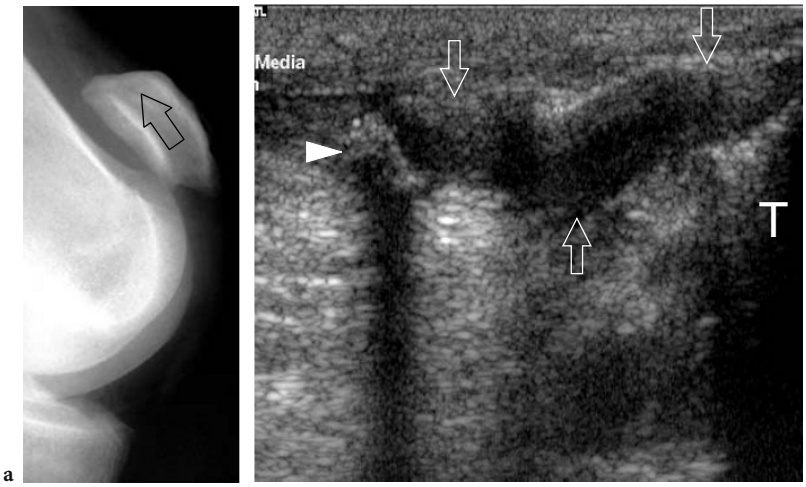

a b

Fig. 14.60a,b. Complete patellar tendon tear. **a** Lateral radiograph of the affected knee demonstrates cranial displacement (*arrow*) of the patella as a result of traction from an intact quadriceps tendon. **b** Longitudinal 12–5 MHz US image of the infrapatellar region confirms the complete rupture of the patellar tendon (*arrows*). The tendon appears wavy and retracted from its patellar insertion. A small fleck of bone (*arrowhead*) is attached at its proximal edge, as a result of an avulsion mechanism. *T*, tibia

third of the patella and a corresponding groove in the tibial tuberosity can be observed (Fig. 14.62c,e). This finding should not be confused with a longitudinal splitting and the osseous abnormalities should not be misinterpreted as erosions or post-traumatic changes (Adriani et al. 1995). In fact, these features relate to the harvesting procedure of central third bone–patellar tendon-bone autograft. Correlation with the patient's history and clinical data may relate this finding to the previous surgery. At long-term follow-up after the harvesting procedure, the patellar tendon remains thickened, without evidence of hyperemia at power Doppler imaging (Jarvela et al. 2004).

14.5.1.7 Deep and Superficial Infrapatellar Bursitis

Distal patellar tendinopathy is often associated with deep infrapatellar bursitis. Bursitis can result from local blunt trauma or may be secondary to micro-trauma. US reveals a swollen and hypoechoic distal tendon associated or not with fluid distension of the infrapatellar bursa, which is a synovial structure located between the posterior tendon surface and the tibial cortex (Fig. 14.63). It must be noted that a minimal amount of bursal fluid can be detected with US in normal states, particularly if high-fre-

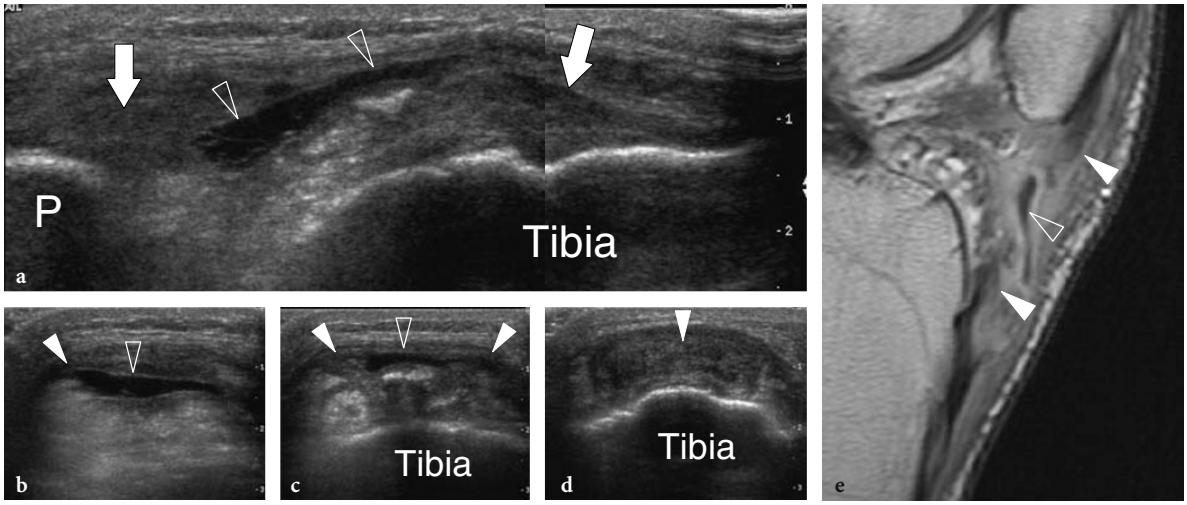

Fig. 14.61a–e. Subtotal patellar tendon tear. **a** Longitudinal split-screen 12–5 MHz US image of the patellar tendon shows two swollen hypoechoic tendon ends (*white arrows*) separated by an anechoic effusion (*arrowheads*). *P*, patella. **b–d** Transverse 12–5 MHz US images obtained over the severed tendon from proximal (**b**) to distal (**d**) show the effusion (*open arrowheads*) and some intact peripheral tendon fibers (*white arrowheads*). **e** Corresponding midsagittal postcontrast T1-weighted MR image confirms the US findings. Note the absence of cranial displacement of the patella confirming a partial tear of the patellar tendon

quency transducers are used. As a consequence, the diagnosis of infrapatellar bursitis is based on detection of more than a minimal amount of fluid and becomes reliable only after bilateral examination and adequate clinical correlation (Fig. 14.64). In patients with small effusions in the deep infrapatellar bursa, the fluid tends to accumulate in the most dependent lateral and medial pouches of the bursa with a typical hourglass appearance on transverse planes. Because of this peculiar destribution, the fluid can go unnoticed on sagittal US images obtained in the midline of the tendon. In these cases, transverse US images are essential for the detection of bursal fluid.

Tendon degeneration, subcutaneous infrapatellar bursitis and soft-tissue inflammatory changes can be seen as a result of prolonged work activity while kneeling in an upright position. This condition is described as "housemaid's knee" or "clergyman's knee", but can also be noted in professional carpet-and floor-layers. US shows a distended hypoechoic subcutaneous bursa located superficially to the distal patellar tendon (Fig. 14.65) (Carr et al. 2001). The bursa can have a thickened wall, internal septations and, in acute cases, a definite hyperemic pattern at color Doppler imaging. In chronic cases, calcifications may develop inside the bursal wall and appear at US as hyperechoic masses with posterior acoustic shadowing. The surrounding soft tissues may be diffusely thickened, hypoechoic and hyperemic (Fig. 14.66).

Pretibial ganglion cysts in patients who have undergone anterior cruciate ligament reconstruction should not be confused with superficial infrapatellar bursitis. These uncommon cysts arise more caudally, in relation to the anterior opening of the tibial tunnel, probably as a result of inflammatory reaction secondary to degraded material from either bioabsorbable screws or Gore-Tex grafts, and may communicate with the knee joint (Martinek and Friederich 1999; Sekiya et al. 2004). US demonstrates a painful mass over the anteromedial proximal tibia filled with gelatinous material (Fig. 14.67). Careful scanning demonstrates a stalk communicating with the opening of the tibial tunnel (Fig. 14.67a). Treatment includes removal en-bloc of the cyst along with its stalk and the irritating suture material.

14.5.2 Medial Knee Pathology

Soft-tissue disorders arising from the medial knee essentially comprise traumatic injuries of the medial collateral ligament and pes anserinus tendinopathy and bursitis.

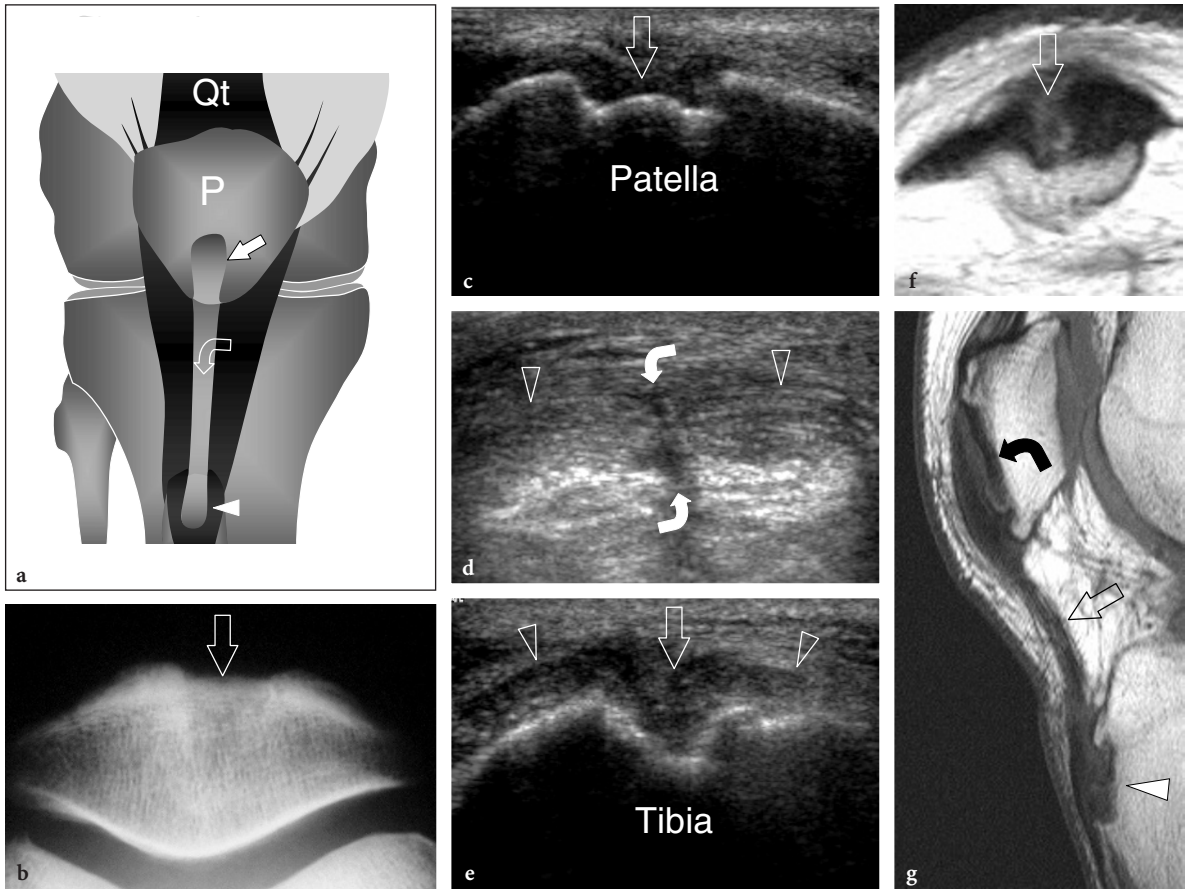

Fig. 14.62a–g. Harvested patellar tendon for anterior cruciate ligament reconstruction. **a** Schematic drawing illustrates the harvesting procedure of central third bone–patellar tendon–bone autograft. A bone-tendon-bone strip composed of the middle third of the patellar tendon (*curved arrow*) attached to two pieces of bone from the lower pole of the patella (*straight arrow*) and the tibial tuberosity (*arrowhead*) are removed to serve as a neoligament, while the external tendon thirds remain on site. **b** Axial radiograph of the femoropatellar joint recognizes postsurgical changes at the anterior aspect of the lower pole of the patella (*open arrow*). **c–e** Transverse 12–5 MHz US images obtained **c** at the level of the proximal patellar insertion, **d** at the mid-tendon level and **e** at the level of the tibial tuberosity demonstrate a defect (*straight arrow*) in the anterior surface of the lower third of the patella and a corresponding groove in the tibial tuberosity. The patellar tendon shows a well-delineated central vertical split (*curved arrows*) separating two tendon cords (*arrowheads*). Distally, it inserts on each side (*arrowheads*) of the tibial groove. **f,g** Corresponding **f** transverse and **g** sagittal T1-weighted MR images depict the harvested central portion (*straight arrow*) of the tendon and the removal of bone at its proximal (*curved arrow*) and distal (*arrowhead*) insertions

14.5.2.1 Medial Collateral Ligament Injury

Owing to the superficial location of the medial collateral ligament, its injuries can readily be diagnosed with US (Lee et al. 1996a; Mathieu et al. 1997). This ligament is most often severed in sport trauma, especially in soccer players and skiers when an excessive force is applied on a flexed, valgus and extrarotated knee. In most cases, tears affect the proximal part of the superficial layer of the collateral ligament and the deep meniscofemoral ligament (Fig. 14.68a,b). Cortical avulsion at the cranial insertion of both layers can be seen with resulting formation of osseous fragments (Fig. 14.68c,d). Patients complain of pain radiating along the internal aspect of the knee associated, in the acute phase, with local soft-tissue swelling. The coexistence of an intra-articular effusion would indicate associated severe intra-articular lesions, including meniscal or anterior cruciate ligament ruptures. Based on the severity of ligamentous injuries, a three-grade scale has been proposed. Grade 1 indicates simple ligament stretching with no associated laxity; grade

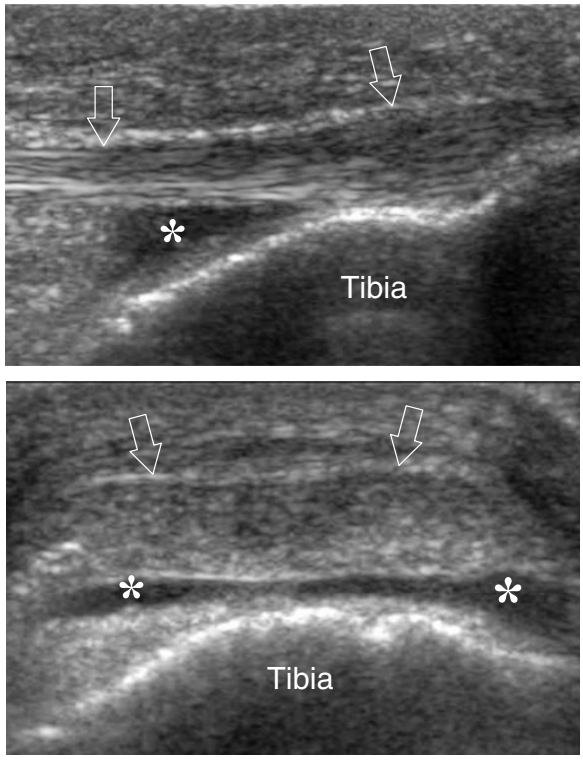

a b

Fig. 14.63a,b. Deep infrapatellar bursa. **a** Longitudinal and **b** transverse 12–5 MHz US images over the distal patellar tendon (*arrows*) demonstrate a small anechoic effusion (*asterisks*) intervening between the deep tendon margin and the tibial epiphysis, reflecting mild distension of the deep infrapatellar bursa

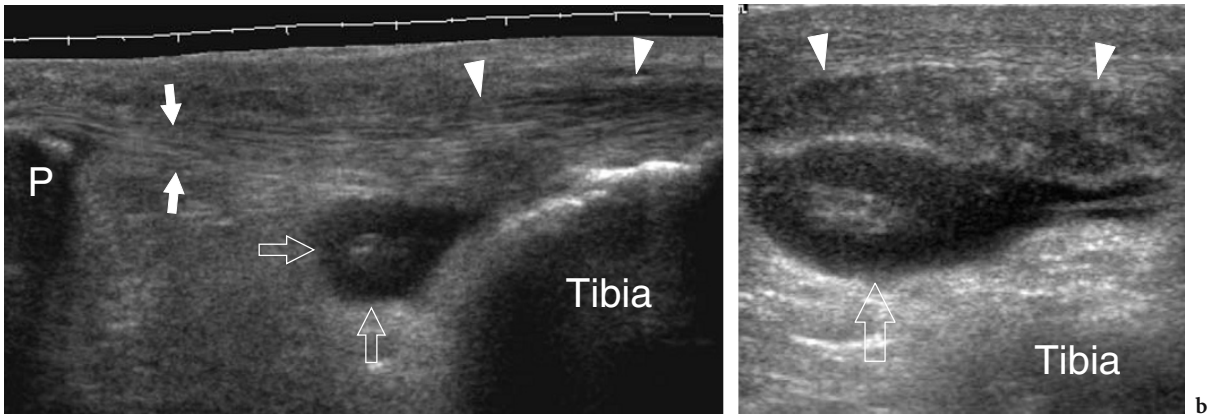

a b

Fig. 14.64a,b. Distal patellar tendinopathy and infrapatellar bursitis. **a** Longitudinal extended field-of-view and **b** transverse 12–5 MHz US images of the infrapatellar region reveal a deep infrapatellar bursa markedly distended by effusion and debris (*open arrows*) associated with a focally enlarged distal patellar tendon (*arrowheads*). The proximal patellar tendon (*white arrows*) is normal. As shown in Figure 14.63a, the bursa has a typical triangular shape on longitudinal scans when distended by small effusions; it assumes an oval convex profile in large effusions. *P*, patella

2 is associated with partial ligament discontinuity and moderate instability; grade 3 consists of a complete ligament tear associated with marked instability. The appropriate treatment for medial collateral ligament ruptures depends on the presence of associated intra-articular lesions. Isolated tears of the ligament are treated conservatively, whereas combined lesions involving the meniscus and the anterior cruciate ligament require arthroscopic surgery.

In medial collateral ligament injuries, US reveals a thickened and heterogeneous ligament (Fig. 14.69). Partial-thickness tears most commonly affect the meniscofemoral ligament and can be difficult to

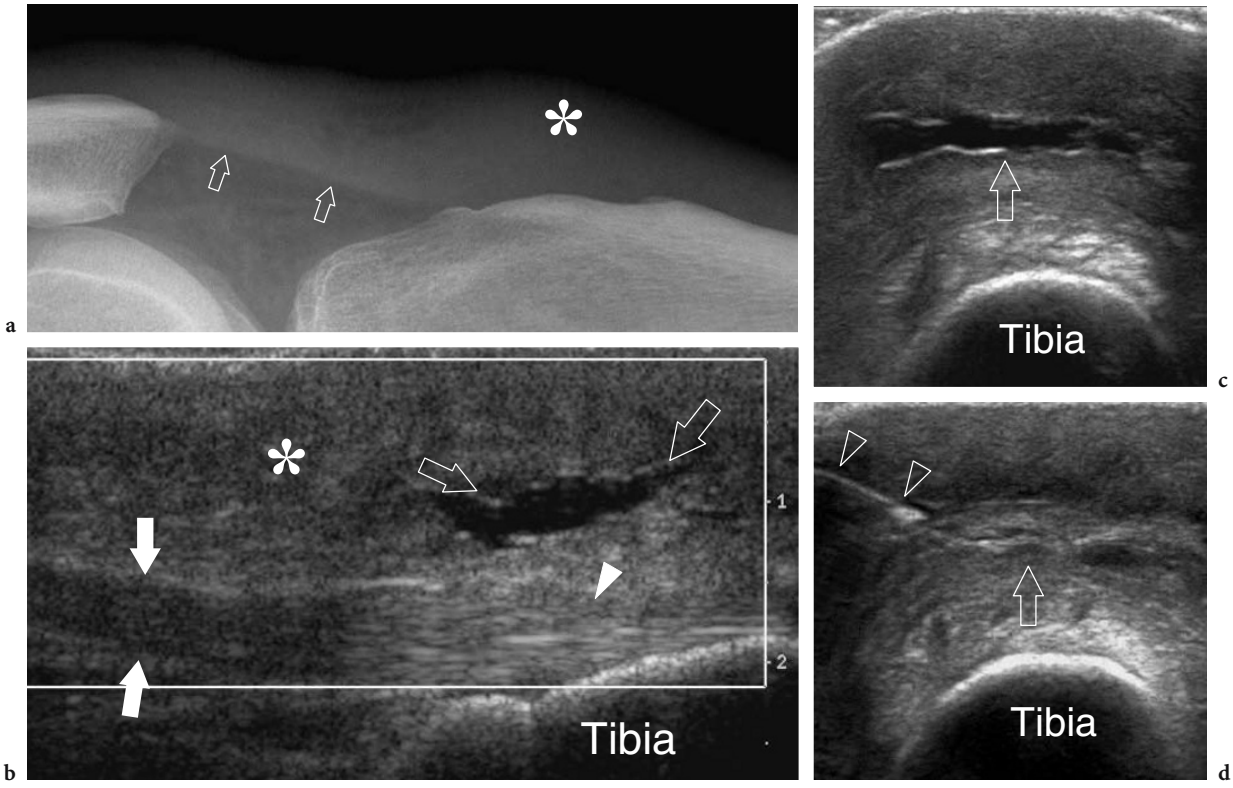

Fig. 14.65a–d. Housemaid's knee, superficial infrapatellar bursitis. **a** Lateral radiograph of the knee shows nonspecific thickening of the soft-tissues (*asterisk*) over the anterior tibial tuberosity. In this area, radiographic examination is not able to distinguish between tendon or soft-tissue involvement. **b** Longitudinal and **c** transverse 12–5 MHz US images obtained over the distal patellar tendon reveal a fluid collection (*open arrows*) within a thickened and heterogeneous subcutaneous tissue (*asterisk*) consistent with subcutaneous bursitis. The underlying distal insertion (*arrowhead*) of the patellar tendon (*white arrows*) is normal. **d** US-guided needle (*arrowheads*) aspiration of bursal fluid revealed absence of local infection

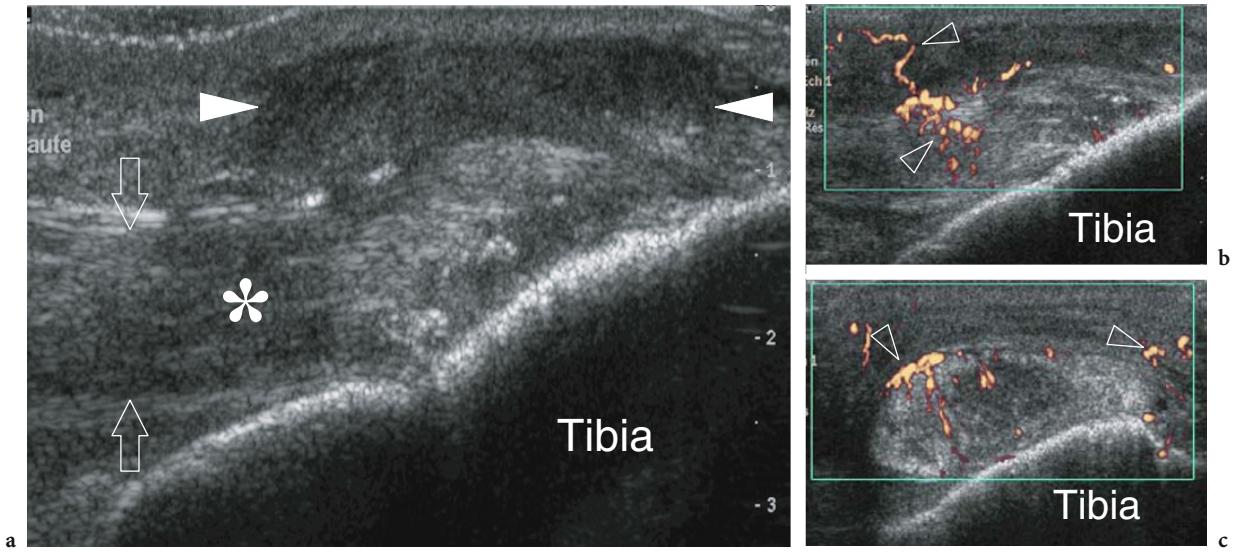

Fig. 14.66a–c. Housemaid's knee. **a** Longitudinal 12–5 MHz gray-scale US image of the anterior aspect of the knee shows a focally enlarged (*arrows*) and diffusely heterogeneous (*asterisk*) patellar tendon. A hypoechoic swelling of the prepatellar soft tissues without detectable effusions (*arrowheads*) is also appreciated. **b** Long- and **c** short-axis power Doppler US images of the distal patellar tendon show marked hyperemia (*arrowheads*) inside the tendon substance and in the surrounding soft tissues

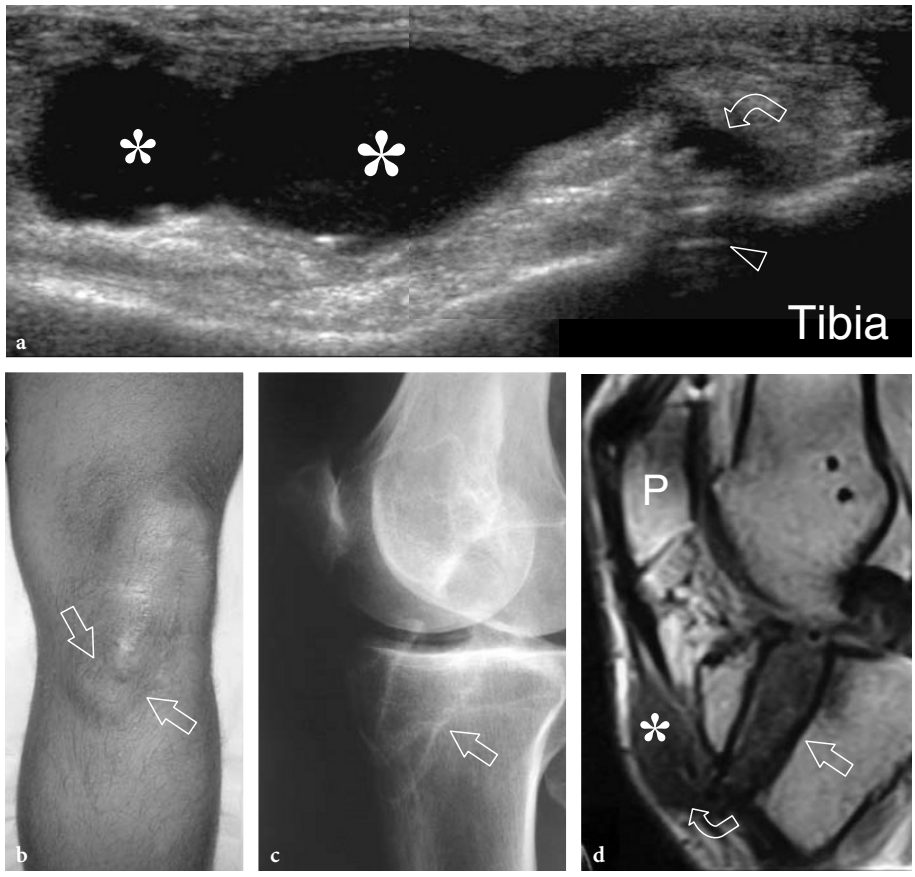

Fig. 14.67a–d. Pretibial ganglion cyst in a patient with previous anterior cruciate ligament reconstruction. **a** Longitudinal 12–5 MHz US image over the anteromedial knee, just distal to the anterior tibial tuberosity, demonstrates a large lobulated cystic structure (*asterisks*) characterized by a thin and tortuous pedicle (*curved arrow*) directed toward the anterior opening of the tibial tunnel (*arrowhead*). **b** Photograph shows the lump (*arrows*) on the anteromedial knee. **c** Oblique lateral radiograph of the patient reveals marked widening of the tibial tunnel (*arrow*) and resorption of the fixation material. **d** Sagittal T1-weighted MR image demonstrates the continuity (*curved arrow*) of the tibial tunnel (*straight arrow*) with the anterior cyst (*asterisk*). *P*, patella

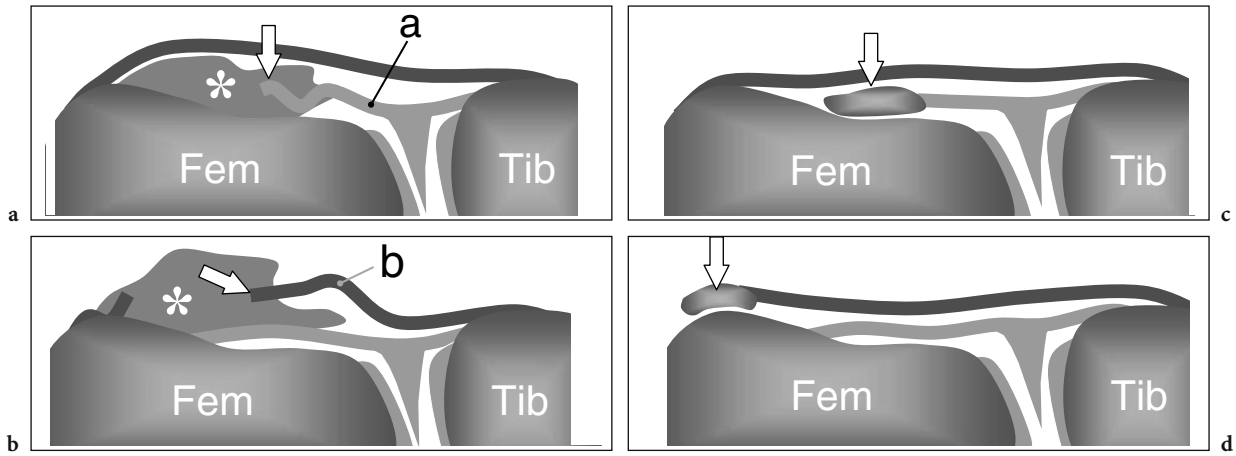

Fig. 14.68a–d. Medial collateral ligament tear. Schematic drawings of a coronal view through the medial knee show the spectrum of abnormalities affecting the medial collateral ligament, including: **a** intrasubstance tear (*arrow*) of the meniscofemoral (*a*) ligament; **b** proximal intrasubstance tear (*arrow*) of the superficial component (*b*) of the ligament; **c** bone avulsion (*arrow*) at the proximal insertion of the meniscofemoral ligament; **d** bone avulsion (*arrow*) at the proximal insertion of the superficial component of the medial collateral ligament. *Asterisks* indicate hematoma. *Fem*, femur; *Tib*, tibia

differentiate from complete ruptures. US diagnosis of a partial tear is based on detection of an irregular hypoechoic component of the ligament with the unaffected one retaining a normal appearance (Fig. 14.70). Detachment of the meniscofemoral ligament from its femoral insertion may result in development of an avulsed bony fragment (Fig. 14.71). Injuries of the meniscotibial component are infrequent and difficult to assess with US. Healing of the femoral insertion of the superficial ligament can result in formation of a calcification, which is commonly referred to as the Pellegrini-Stieda lesion. This condition can be painful and may limit sport activity. In these cases, US demonstrates the calcification located at the proximal insertion of the ligament (Fig. 14.72).

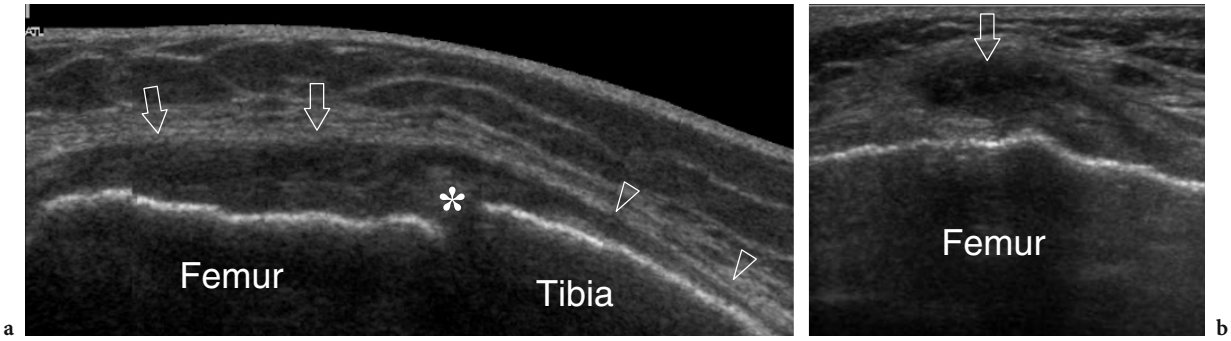

a b

Fig. 14.69a,b. Intrasubstance tear of the medial collateral ligament. **a** Long-axis extended field-of-view and **b** short-axis 12–5 MHz US images obtained over a severed medial collateral ligament. The proximal portion of the ligament (*arrows*) appears diffusely swollen and hypoechoic. Note the normal appearance of the distal ligament (*arrowheads*). *Asterisk*, medial meniscus

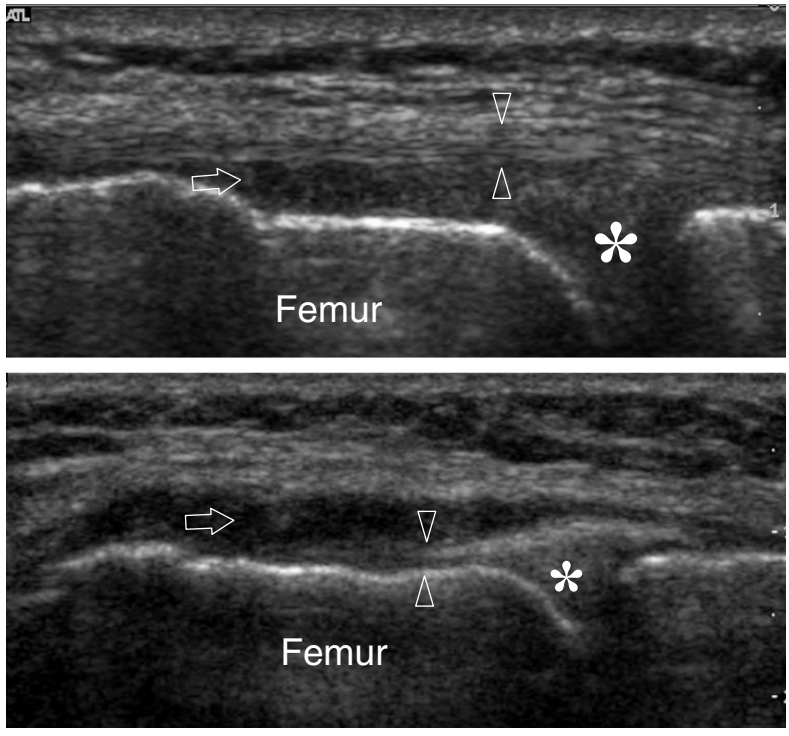

a b

Fig. 14.70a,b. Partial-thickness tears of the medial collateral ligament. Two different patients. **a** Long-axis 12–5 MHz US image of the proximal medial collateral ligament reveals hypoechoic effusion (*arrow*) at the deep meniscofemoral insertion reflecting its detachment. Note the integrity of the superficial component (*arrowheads*) of the ligament. **b** Long-axis 12–5 MHz US image of the proximal medial collateral ligament demonstrates rupture of the superficial component (*arrow*), whereas the deep meniscofemoral component (*arrowheads*) is unaffected. *Asterisk*, medial meniscus

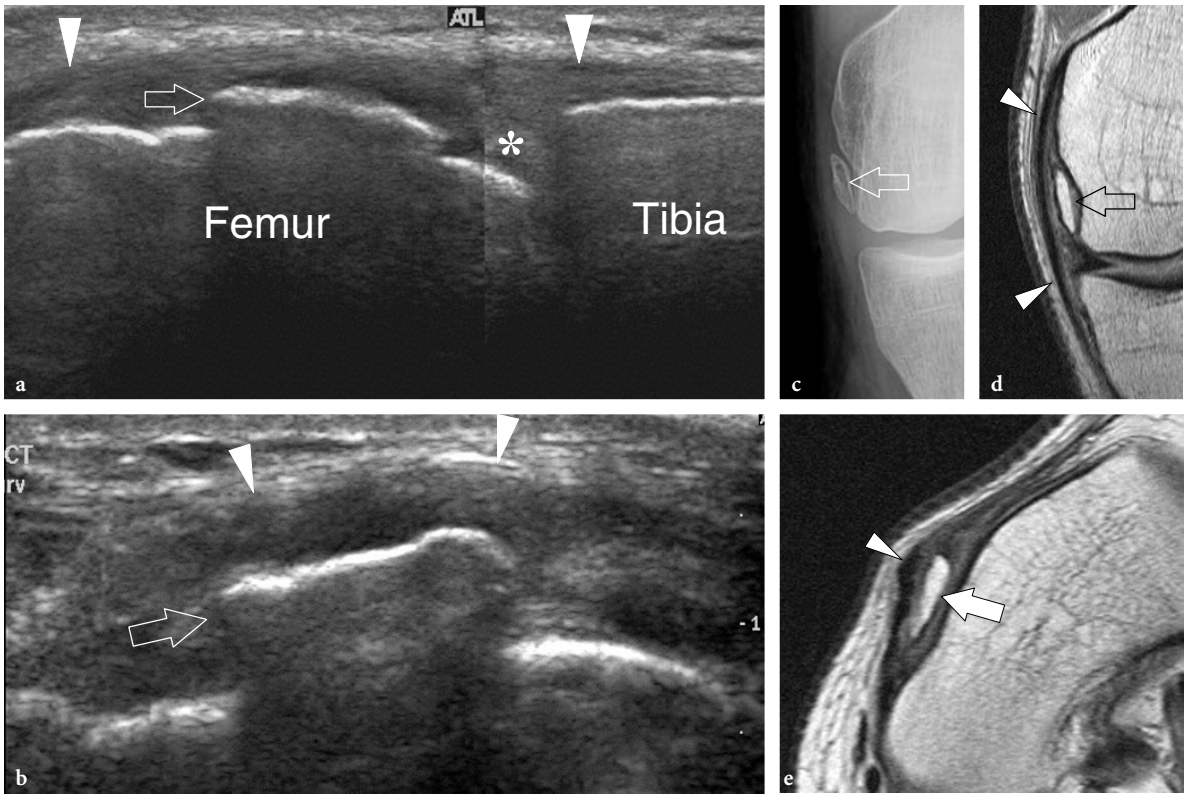

Fig. 14.71a–e. Medial collateral ligament calcification. **a,b** Coronal **a** low-magnification and **b** high-magnification 12–5 MHz US images over the medial aspect of the knee with **c** radiographic correlation reveal a large calcified image (*arrow*) with posterior acoustic shadowing at the proximal insertion of the meniscofemoral ligament, between the intact superficial component of the ligament (*arrowheads*) and the femur. *Asterisk*, medial meniscus. **d** Coronal and **e** transverse T1-weighted MR images confirm the presence of a flat fragment of bone (*arrow*) between the superficial collateral ligament (*arrowheads*) and the femur

14.5.2.2 Pes Anserinus Bursitis

Bursitis and ganglion cysts can develop at the level of the pes anserinus complex and present clinically as local soft-tissue masses. Ganglia are usually painless and firm at palpation because of their mucoid viscid content, while bursitis can be painful and may be softer at palpation. Bursitis is commonly observed in patients affected by rheumatoid arthritis and type II diabetes mellitus (Unlu et al. 2003). At US examination, anserine bursitis appears as an anechoic mass located in close proximity to the synovial bursae interspersed among the pes anserinus tendons (Fig. 14.73) (Voorneveld et al. 1989). Pressure with the probe can reveal shape changes of the bursa secondary to fluid displacement. Intramural flow signals are detected in acute inflammation. US can guide needle puncture of the bursa for diagnostic (analysis of crystals and bacteria) and therapeutic (steroid injection) purposes. Ganglion cysts are more rounded in shape and may have internal thick septations and a tortuous pedicle (Fig. 14.74a). Pressure with the probe over these cysts does not affect their shape significantly. Needle aspiration should be performed with a large-bore needle to evacuate the thick intrabursal fluid. Signs of tendinopathy are infrequently associated with bursitis (Fig. 14.74b).

14.5.3 Lateral Knee Pathology

Lateral knee pain is a common clinical challenge that may be secondary to a variety of soft-tissue and intra-articular disorders. US is able to provide clinically useful information to identify injuries of the lateral collateral ligament and the iliotibial band as well as meniscal cysts. In addition, it can give a full depiction of ganglion cysts arising from the

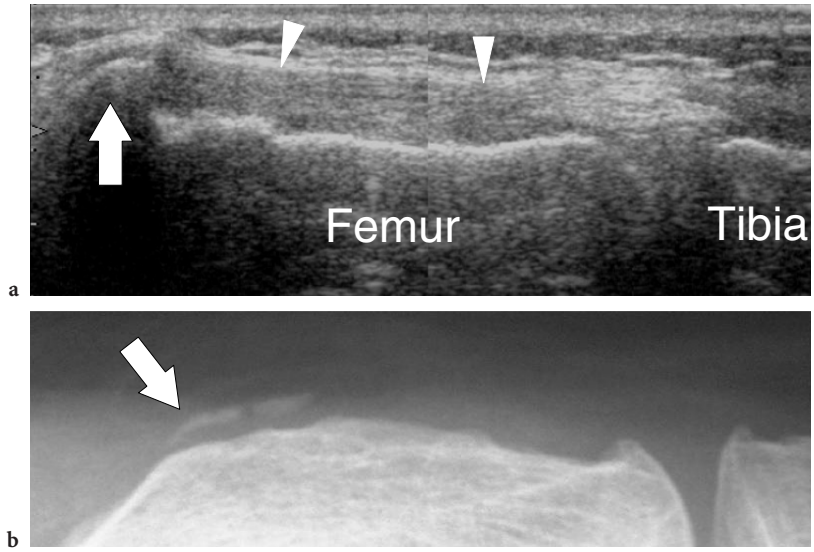

Fig. 14.72a,b. Pellegrini-Stieda lesion. **a** Coronal 12–5 MHz US image over the medial aspect of the knee with **b** radiographic correlation shows a calcification (*arrow*) at the proximal insertion of the superficial band of the medial collateral ligament (*arrowheads*). The US appearance of this calcification is typical of the Pellegrini-Stieda lesion and can be considered the result of a localized ligament tear

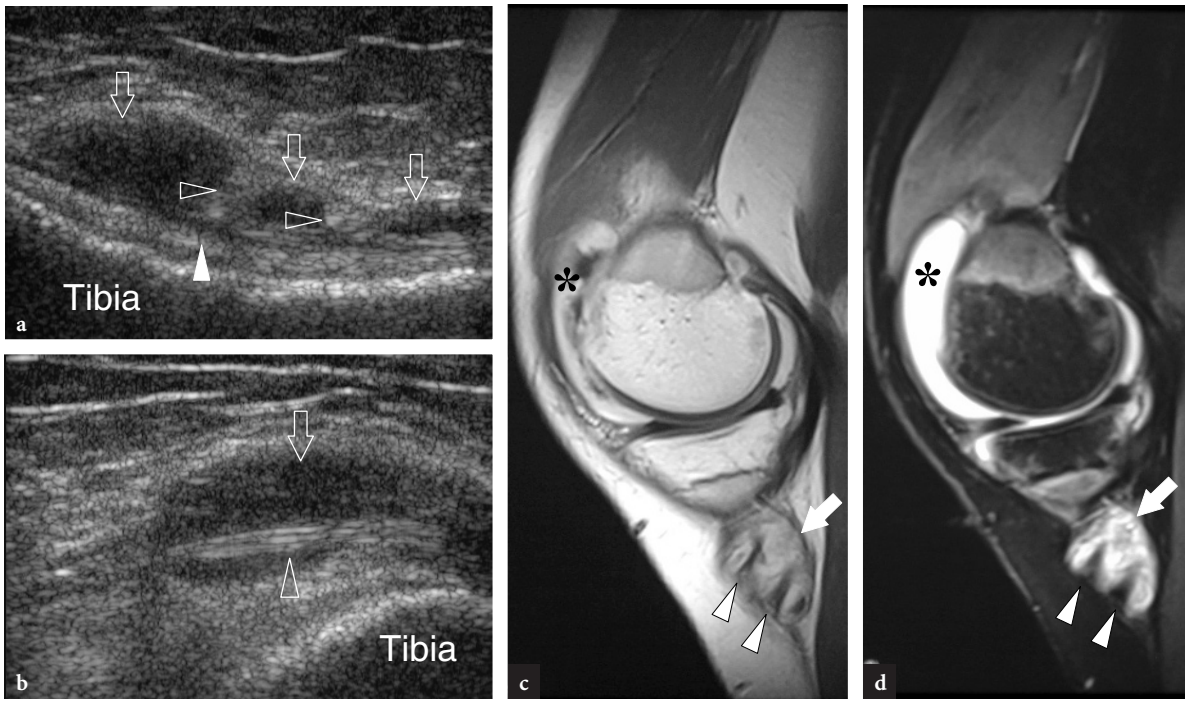

Fig. 14.73a–d. Pes anserinus bursitis in a child with active juvenile idiopathic arthritis. **a** Longitudinal oblique and **b** transverse oblique 12–5 MHz US images over the tibial insertion of the pes anserinus complex demonstrate distension of the anserine bursa (*arrows*) by effusion and synovial pannus. Note the irregular shape of the bursa which separates the pes anserinus tendons (*open arrowheads*) from the distal insertion of the medial collateral ligament (*white arrowhead*). **c** Sagittal gadolinium-enhanced fast T1-weighted and **d** STIR MR imaging correlation confirm the distension of the bursa (*arrow*) filled with hyperintense synovial pannus. Observe that the bursa is located deep to the pes anserinus tendons (*arrowheads*). Discrete intra-articular effusion (*asterisk*) is associated

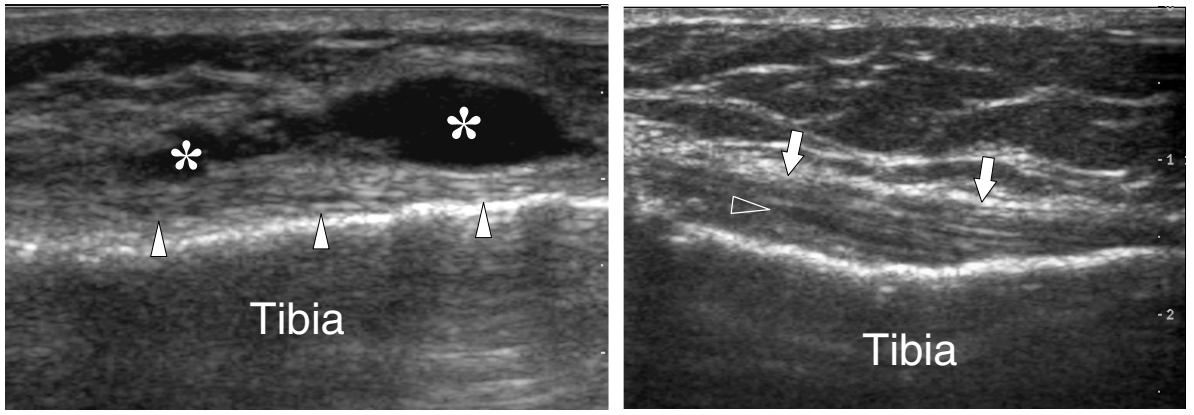

a b

Fig. 14.74a,b. Pes anserinus abnormalities. **a** Longitudinal 12–5 MHz US image obtained over the pes anserinus complex demonstrates the normal tendons (*arrowhead*) overlaid by an irregularly shaped lobulated cystic mass (*asterisk*) consistent with a ganglion. The mass was noncompressible. **b** Long-axis 12–5 MHz US image over the pes anserinus complex reveals a thickened tendon insertion (*arrows*). Note the small amount of fluid (*arrowhead*) between these tendons and the distal insertion of the medial collateral ligament

superior tibiofibular joint, possibly leading to the involvement of the peroneal nerve.

14.5.3.1 Lateral Collateral Ligament Injury

The lateral collateral ligament is more rarely injured than the medial collateral ligament. Sprains and tears of this ligament follow varus stresses and are usually associated with rupture of the anterior cruciate ligament and injury to other intra-articular structures. Due to a possible association with severe intra-articular lesions, MR imaging is usually obtained as it allows an accurate assessment of the intraarticular strucutres requested. At US examination, the torn ligament appears as a thickened structure (Fig. 14.75). Clinical correlation is important to distinguish partial from complete lesions: in fact, this differentiation can be difficult on the basis of US findings alone.

14.5.3.2 Iliotibial Band Friction Syndrome

At the level of its distal third, the iliotibial band contacts the lateral aspect of the lateral femoral condyle, moving forward in extension and backward in flexion. At this site, a synovial bursa intervening between these structures helps to decrease local attrition during movements of the knee joint. During sporting activities, and particularly after forceful training or strenuous physical activity, such as occurs in long-distance runners, cyclists, soccer players and weightlifters, chronic local impingement of the iliotibial band against the lateral condyle may lead to local inflammation and pain that lessens knee function and sporting performance, the so-called "runner's knee". When inflamed, the bursa between the iliotibial band and the lateral condyle appears distended by fluid and can be associated with iliotibial band thickening. Clinically, the diagnosis is suspected in sportsmen who show local pain and tenderness on palpation of the external aspect of the lateral condyle. With increasing tension of the iliotibial band, lateral knee pain typically worsens during flexion and extension of the knee. MR imaging can help to confirm the clinical data by showing changes in the bursal shape and, in more severe cases, marrow edema on the lateral condyle (Muhle et al. 1999). US can detect soft-tissue changes suggestive of chronic iliotibial band friction syndrome by showing thickening and hypoechoic changes in the area of the iliotibial band adjacent to the lateral femoral condyle (Bonaldi et al. 1998). A hypoechoic area located between the inflamed band and the superior aspect of the lateral condyle can be an associated finding reflecting bursitis or loose connective tissue inflammation (Fig. 14.76). US-guided palpation is painful and may help to enhance the diagnostic confidence of the examiner. Other lesions mimicking iliotibial band friction syndrome, such as tendinopathies or tears of the biceps, hamstrings or popliteal tendons, can be ruled out while performing the US examination (Bonaldi et al. 1998).

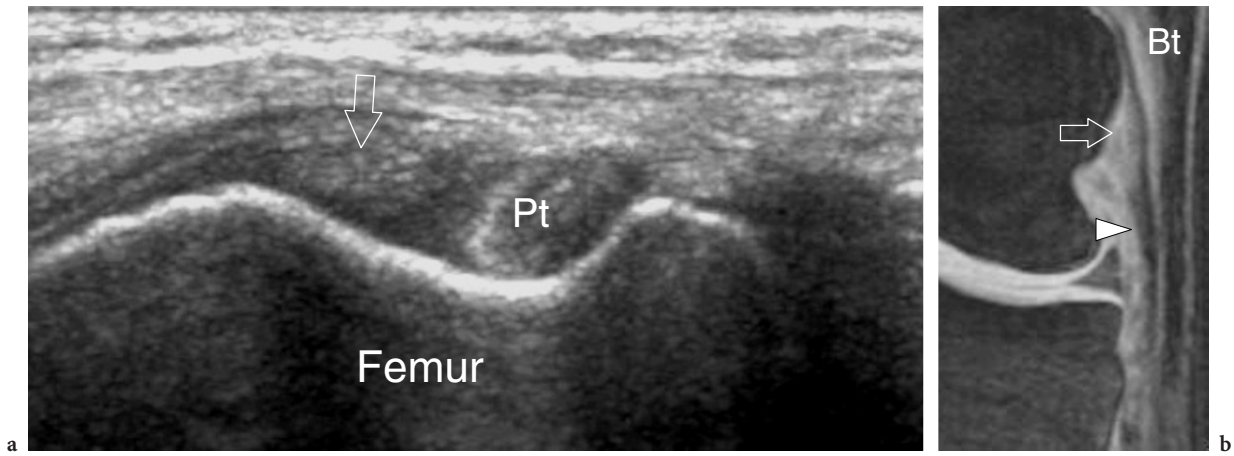

Fig. 14.75a,b. Partial tear of the lateral collateral ligament. **a** Coronal 12–5 MHz US image obtained over the popliteal groove of the femur shows a swollen proximal insertion (*arrow*) of the lateral collateral ligament. The popliteal tendon (*Pt*) appears normal. **b** Corresponding coronal fat-suppressed T2-weighted MR image confirms high signal intensity (*arrow*) within the proximal ligament, whereas its distal portion (*arrowhead*) appears normal. *Bt*, biceps tendon

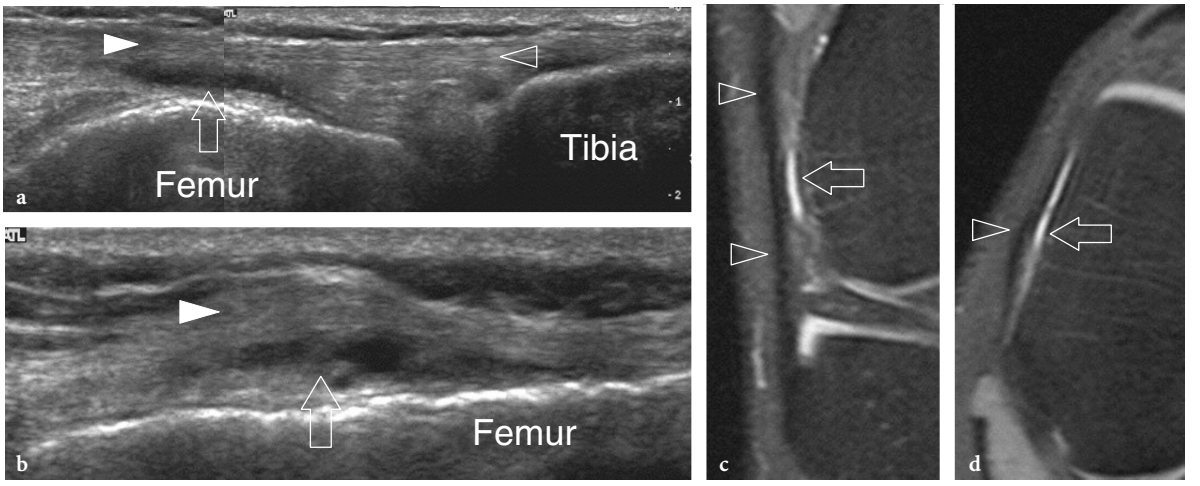

Fig. 14.76a–d. Iliotibial band friction syndrome. **a** Coronal split-screen and **b** transverse 12–5 MHz US images over the lateral knee with correlative **c** coronal and **d** transverse fat-suppressed T2-weighted MR images demonstrate fusiform hypoechoic swelling of the distal iliotibial band (*white arrowhead*) as it courses over the lateral femoral condyle as a result of impingement. Note that the distal part of the band has a normal echotexture (*open arrowhead*). A hypoanechoic area (*arrow*) located between the band and the condyle reflects a fluid collection within the synovial bursa

14.5.3.3 Distal Iliotibial Band Tendinopathy

Patients with distal iliotibial band tendinopathy present with local pain and tenderness over the preinsertional portion of the band, in a more distal location than the site of iliotibial band friction syndrome. These lesions usually occur in middle-aged subjects who have undergone previous placement of a knee prosthesis or are affected by knee osteoarthritis. In the former case, the deep boundary of the iliotibial band may impinge over the sharp metallic edge of the tibial prosthetic component. In patients with osteoarthritis, pathologic changes are probably secondary to increased stress forces on the band during walking as a result of an altered weight related to varus-valgus deformity. The clinical findings in distal iliotibial band tendinopathy can be misleading. Local pain over the distal band can be misinterpreted as pain over the lateral aspect of the distal patellar tendon. In addition, some patients may report a radiating pain along the lateral aspect

of the thigh, possibly leading to confusion with symptoms of lumbar hernia. Due to the straight appearance and superficial location of the distal band, US can easily assess its pathologic changes. Coronal US images are best suited to investigate the middle and distal portions of the band in the same image for comparison. Transverse scanning planes may also be helpful to estimate any increase in the cross-sectional area of the band. US signs of distal iliotibial band tendinopathy include a swollen band characterized by echotextural abnormalities, including hypoechoic changes and loss of the fibrillar pattern (Fig. 14.77). As the preinsertional portion of the band is normally thick and may have a slight hypoechoic appearance, the diagnosis of distal tendinopathy should be made by comparison with the contralateral side and adequate correlation with clinical findings. US-guided palpation may help to confirm the diagnosis.

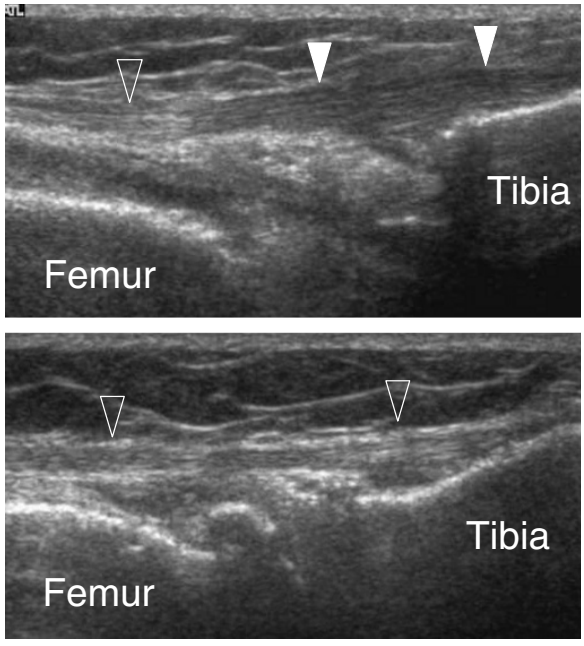

Fig. 14.77a,b. Distal iliotibial band tendinitis in a patient with knee osteoarthritis. **a** Coronal 12–5 MHz US image obtained over the lateral knee reveals a swollen and hypoechoic preinsertional portion (*white arrowheads*) of the iliotibial band. The proximal part of the band retains a normal echotexture (*open arrowhead*). **b** Contralateral side showing a normal-appearing band (*open arrowheads*)

14.5.3.4 Superior Tibiofibular Joint Ganglia

In terms of prevalence, the most common cysts around the knee are Baker and meniscal cysts. Ganglia arising from the superior tibiofibular joint are less recognized entities although they can compress the tibial and peroneal nerves by their proximity and size (Fig. 14.78). These ganglia are large cystic masses that may cause swelling on the external aspect of the peroneal neck and may rarely be associated with local pain radiating down in the leg. Similar to peroneal intraneural ganglia (see next paragraph), they are in connection with the superior tibiofibular joint by means of a thin and tortuous pedicle (Wadstein 1931; Ellis, 1936; Clark 1961; Parkes 1961). The superior tibiofibular joint from which these ganglia arise is a small synovial joint absorbing torsional stresses that is vulnerable to repeated microtrauma, ankle injuries and altered knee biomechanics. Superior tibiofibular ganglia are believed to arise at sites of capsular stress and can be associated with osteoarthritis of the joint. As the joint pumps out fluid, the cyst expands within the compartmental spaces, the regional muscles (the tibialis anterior and the peroneus longus being most commonly involved) or even within the fibular bone, possibly causing secondary compression on the neighboring structures (Brooks 1952; Stener 1969; Muckart 1976). Diagnostic imaging is essential for detecting intramuscular ganglia. When large, such ganglia can cause scalloping and cortical bone erosions on the adjacent proximal tibia and fibula that can mimic a more aggressive lesion. At US examination, superior tibiofibular ganglia have a pear-shaped appearance with the proximal pointed portion near to the superior tibiofibular joint and a distal rounded portion expanding within or among the muscles (Fig. 14.79) (Bianchi et al. 1995a). A peculiar feature of these cysts is the presence of a thick and irregular echogenic wall. Septations arising from the internal side of the fibrous wall are usually manifest in the largest cysts. Differential diagnosis of intramuscular ganglia essentially includes meniscal cysts. These cysts arise from the outer aspect of the lateral meniscus and are almost always located in the subcutaneous tissue. Intramuscular myxomas have the same US features of intramuscular ganglia. However, they usually affect the muscles around the buttock, the thigh and the shoulder (Abdelwahab et al. 1992). Demonstration of a stalk connecting the ganglion with the superior tibiofibular joint is critical to draw a definitive diagnosis.

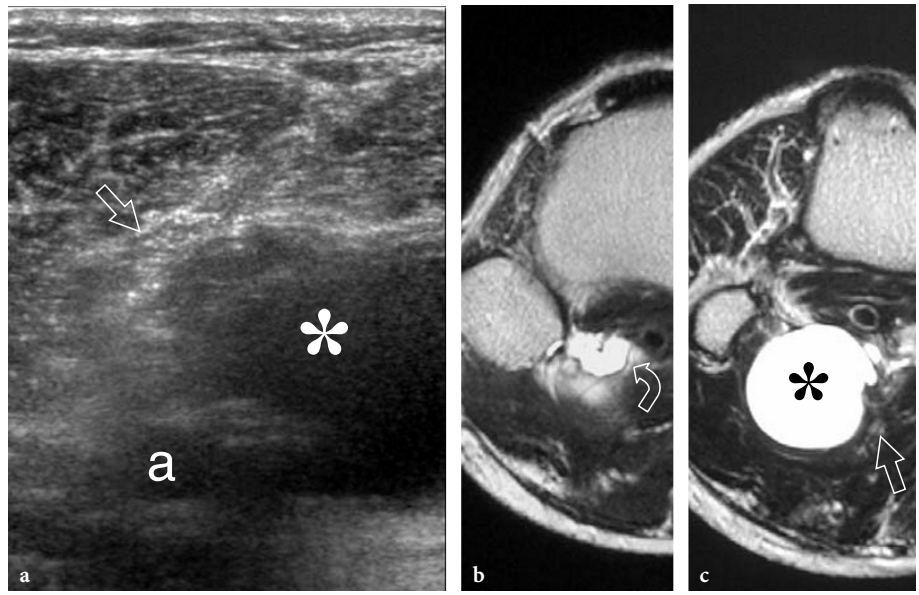

Fig. 14.78a–c. Superior tibiofibular joint ganglion and tibial neuropathy. **a** Transverse 12–5 MHz US image of the lateral popliteal fossa in a patient with sensory disturbances in the territory of innervation of the tibial nerve demonstrates a large cystic structure (*asterisk*) which causes compression on the tibial nerve (*straight arrow*). A certain displacement of the nerve relative to the popliteal artery (*a*) can be appreciated as a result of the compression effect of the ganglion. **b,c** Correlative transverse T2-weighted MR images demonstrate the ganglion cyst (*asterisk*) connected with the superior tibiofibular joint by a thin and tortuous pedicle (*curved arrow*)

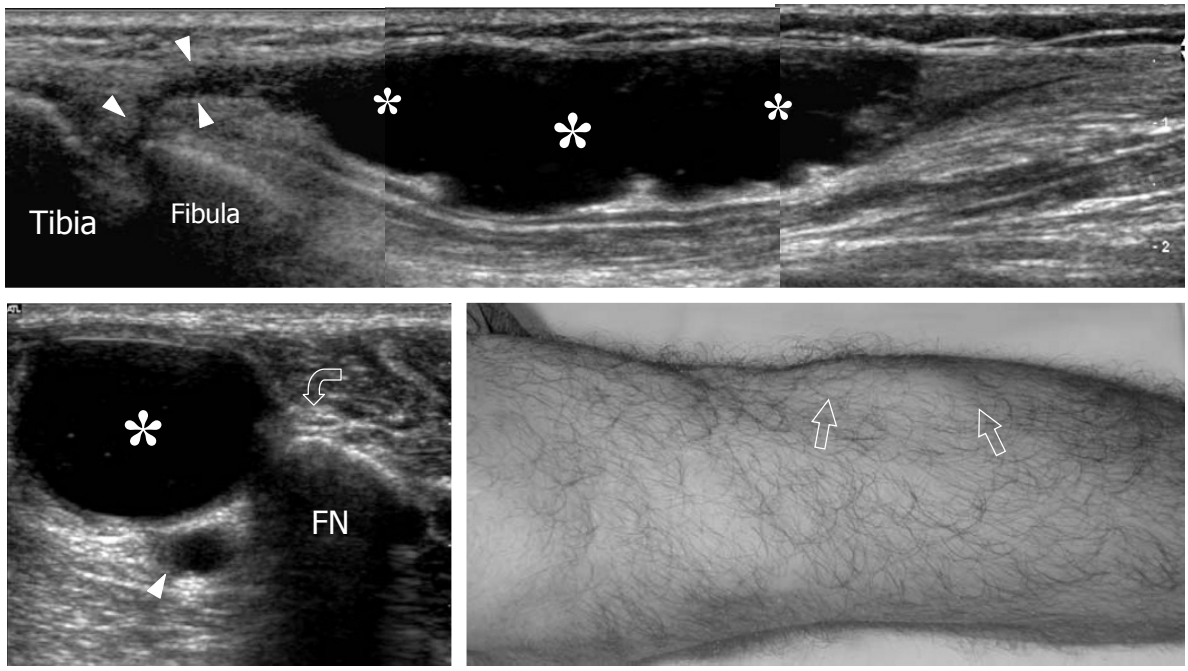

a

b

c

Fig. 14.79a–c. Superior tibiofibular joint intramuscular ganglion. **a** Longitudinal split-screen and **b** transverse 12–5 MHz US images obtained over the proximal portion of the anterolateral compartment of the leg and at the level of the fibular neck, respectively, demonstrate an elongated anechoic ganglion cyst (*asterisks*) originating from the superior tibiofibular joint by means of a thin pedicle (*arrowheads*). No internal septa are evident within the cyst. In **b**, note the close proximity of the cyst with the peroneal nerve (*curved arrow*). In this case, the patient had no symptoms indicating dysfunction of this nerve. **c** Photograph of the patient's leg shows the lump (*arrows*) produced by the ganglion on the skin

14.5.3.5 Peroneal Neuropathy

Although relatively rare, the entrapment of the common peroneal nerve typically occurs in the restricted space between the bone and the fascia as the nerve winds around the back of the fibular neck. In this area, the nerve passes through the lateral intermuscular septum and into the fibular tunnel, which is made up of the aponeurosis of the soleus and superficially, laterally and medially by an extended fibrous arch formed by the aponeurosis of the peroneus longus muscle. Nerve lesions may derive from either a pathologic cause, such as a thick arch which fits tightly around the nerve inducing a state of chronic irritation, or may have a postural, dynamic or idiopathic origin, such as pressure on the nerve exerted at the fibular neck during sleep or habitual leg-crossing. Other causes of nerve compression include space-occupying lesions, fractures, osteophytes and bony deformities at the level of the fibular head, and tight casts or bandages around the knee. Direct trauma to the posterolateral aspect of the knee may also be implicated (Trappeniers et al. 2003). In most cases, the nerve dysfunction (foot drop, sensory disturbance) recovers with conservative management. When spontaneous recovery does not occur at electrophysiologic testing within 6 months, surgical exploration is indicated. At US, the compressive agent can produce the usual changes in nerve shape observed at other sites, including flattening of the nerve at the compression point and fusiform swelling at a more proximal level (Martinoli et al. 2000a). However, one should be aware that mild peroneal neuropathies with spontaneous recovery may not show any abnormal US finding. In this regard, US examination would also have a prognostic role in separating patients with a normal-appearing nerve, who will probably benefit from conservative management, from those with an abnormal nerve, in which surgery can be indicated.

Ganglion cysts are one of the leading causes of peroneal nerve compression at this site. These ganglia may be divided into extraneural ganglia, which develop outside the nerve and intraneural ganglia, developing within the nerve. Extrinsic ganglia have been described in the previous paragraph. These ganglia compress the nerve and its branches as they pass in the restricted space of the fibular tunnel (Figs. 14.80, 14.81). In these cases, US is a useful means of acquiring a full depiction of the cystic mass and its relationships with the nerve (Fig. 14.80). Demonstration of an increased echogenicity of the innervated muscles (most often obseved in the tibialis anterior and the extensors) reflecting fatty infiltration and atrophy, may enhance confidence in the diagnosis (Fig. 14.80c). In cases of nerve dysfunction, percutaneous aspiration of the cyst can be attempted under US guidance. The procedure is easy to perform with a free-hand technique and using large-bore needles ($\geq$18 gauge) due to the mucoid viscous nature of the fluid contained in the cyst. With time after the procedure there may be recurrence of the cyst, but the patient's symptoms may regress as a result of a decreased intracystic pressure and such functional improvement is lasting in most cases. In our opinion, percutaneous needle aspiration of the ganglion should be recommended, not to treat the cyst itself but as a means of obtaining its decompression and a temporary improvement in nerve function when surgical intervention cannot be planned immediately after the onset of symptoms.

Intraneural ganglia are similar to common ganglia but are located within the nerve substance, between the nerve sheath and the fascicles (Yamazaki et al. 1999). The peroneal nerve is typically involved. Peroneal intraneural ganglia share a common clinical presentation with a predominant involvement of the deep peroneal component and have a high rate of postoperative recurrence. At US examination, intraneural ganglia have a stereotypical appearance. They appear as intraneural cystic masses causing peripheral displacement of the fascicles and fusiform thickening of the nerve (Figs. 14.82, 14.83) (Leijten et al. 1992; Masciocchi et al. 1992; Martinoli et al. 2000a; Pedrazzini et al. 2002). The pathogenesis of intraneural ganglia is debated. The "degenerative theory" assumes that the cyst would arise from myxoid metaplasia of the epineurium or perineurium, from intraneural hemorrhage or from embryonic remnants of ectopic synovium. On the other hand, the "synovial theory" hypothesizes that the ganglion arises as an extension of the neighboring proximal tibiofibular joint, tracking along a small nerve branch and reaching backward to its final position within the peroneal nerve (Fig. 14.84). Based on recent studies on large series of patients, this second theory seems more likely (Spinner et al. 2003a,b). As previously stated, distal to the division of the main trunk of the nerve into the deep and superficial peroneal nerves, the deep peroneal nerve gives off a third branch, the articular branch, which approximates the size of the others

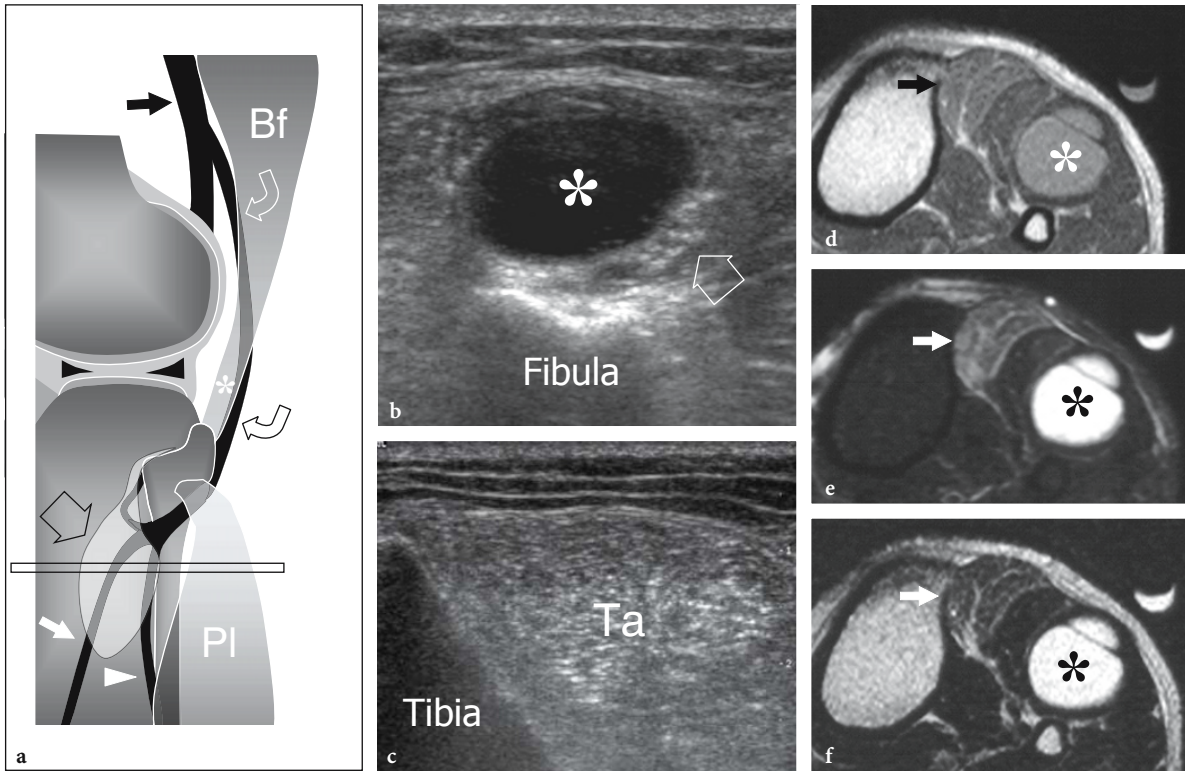

Fig. 14.80a–f. Peroneal neuropathy secondary to extrinsic compression by a superior tibiofibular joint ganglion. **a** Schematic drawing illustrates the course of the sciatic (*black arrow*) and the common peroneal nerve (*curved arrows*) with its terminal branches, the superficial (*arrowhead*) and deep (*white arrow*) peroneal nerves, relative to the biceps muscle (*Bf*) and tendon (*asterisk*), the fibular head and the peroneus longus muscle (*Pl*). The typical site of extrinsic nerve compression by ganglion cysts (*open large arrow*) arising from the superior tibiofibular joint is illustrated. **b** Transverse 12–5 MHz US image over the fibular neck region reveals an intramuscular ganglion (*asterisk*) causing displacement of the common peroneal nerve (*arrow*). **c** More anterior transverse 12–5 MHz US image demonstrates diffuse hyperechoic changes in the tibialis anterior muscle (*Ta*) reflecting denervation atrophy. **d–f** Transverse **d** proton density, **e** STIR and **f** fat-suppressed T2-weighted MR images reveal the ganglion (*asterisk*) containing thin septa and abnormal signal in the tibialis anterior muscle (*arrow*) indicating denervation edema

and assumes a J- or U-shaped recurrent course around the fibula to supply the superior tibiofibular joint and even part of the femorotibial joint. In normal conditions, this branch can be recognized on longitudinal planes over the anterior aspect of the fibula as a small hypoechoic rounded structure embedded in the hyperechoic fat deep to the peroneus longus (Fig. 14.85a). According to recent clinical series, this branch seems to play a central role in the pathogenesis of peroneal intraneural cysts (Spinner et al. 2003a,b). Spinner et al. found that these lesions derive from the superior tibiofibular joint and communicate with it via a "one-way valve" mechanism. Given access to the articular branch (stage I) (Fig. 14.84a), the cyst dissects proximally by the path of least resistance within the epineurium to join the deep peroneal nerve (stage II), the deep peroneal nerve component of the common peroneal nerve (stage III) (Fig. 14.84b) and, more proximally, even the sciatic nerve (stage IV) (Fig. 14.84c). In the early stages, the fibers of the superficial peroneal nerve may remain unaffected. Therefore, patients with peroneal intraneural ganglia usually have selective deficit of the deep peroneal nerve with the peroneal muscles spared. Typically, US identifies the bulk of the ganglion on the anterolateral aspect of the superior tibiofibular joint, located remotely from the position of the peroneal nerve (Fig. 14.86a,b). The ganglion has a long tubular process reflecting the articular branch, which joins the peroneal nerve on the posterolateral aspect of the fibula and infolds within it (Fig. 14.86c,d). The articular branch appears markedly enlarged and assumes a cystic appearance

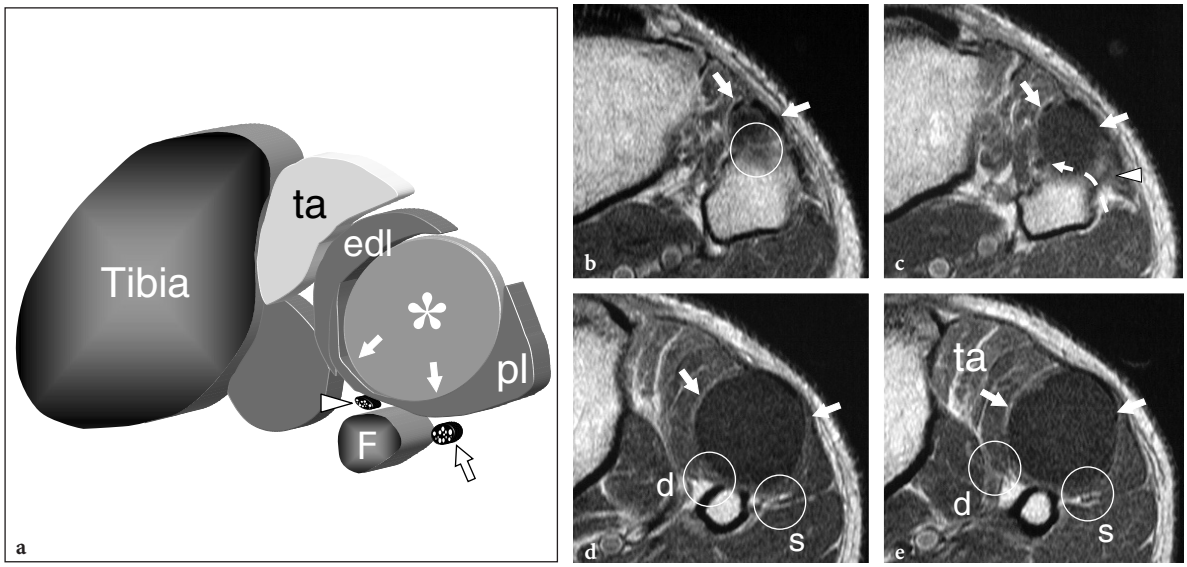

Fig. 14.81a–e. Pathoanatomy of peroneal neuropathy caused by an intramuscular ganglion. **a** Schematic drawing illustrates the relationship of the ganglion (*asterisk*) with the adjacent muscles of the anterolateral compartment of the leg (tibialis anterior, *ta*; extensor digitorum longus, *edl*; peroneus longus, *pl*), the fibula (*F*) and the superficial (*arrow*) and deep (*arrowhead*) peroneal nerves. **b–e** Series of transverse T1-weighted MR images obtained from **b** cranial to **e** caudal over the fibular head and neck region reveal the ganglion (*white arrows*) developing within the peroneus longus. **b** The common peroneal nerve (*circled structure*) passes between the bone and the most cranial portion of the ganglion. **c** The deep branch of the peroneal nerve (*dashed arrow*) is seen crossing the fibula deep to the ganglion. Note the superficial peroneal nerve (*arrowhead*). **d,e** More caudal scans demonstrate the diverging course of the superficial (*circled structure* indicated by ***s***) and deep (*circled structure* indicated by ***d***) peroneal nerves relative to the ganglion as well as denervation changes in the tibialis anterior muscle (*ta*)

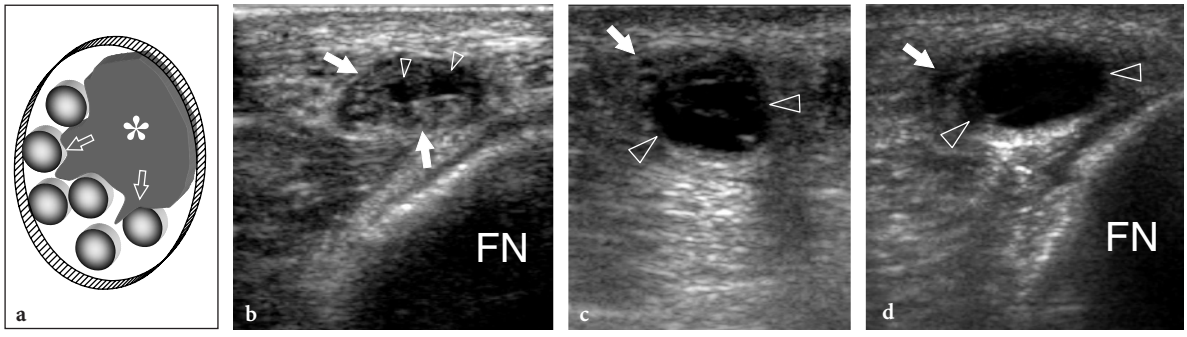

Fig. 14.82a–d. Peroneal intraneural ganglion. **a** Schematic drawing illustrates the ganglion cyst (*asterisk*), which develops within the outer epineurial sheath of the nerve, thus compressing (*arrows*) the fascicles. **b–d** Series of transverse 12–5 MHz US images of the common peroneal nerve in a patient with an intraneural ganglion obtained, respectively, **b** at baseline, at **c** 3 months and **d** 6 months later demonstrate progressive enlargement of the intraneural cyst (*arrowheads*) and subsequent peripheral displacement of the fascicles (*arrows*). During this period, the nerve function progressively worsened. *FN*, fibular neck

without detectable fascicles (Fig. 14.85b–d). More proximally, the fascicles of the deep and common peroneal nerve are displaced eccentrically by the cyst growing within the epineurium and may be thickened as a possible result of intraneural compression. The overall size of the ganglion and the entity of nerve deficit may vary with time, producing fluctuating phases of worsening and recovery of symptoms. In some cases, the cyst can disappear spontaneously. For successful surgery of peroneal intraneural ganglia, combined drainage of the cyst and ligation of the articular branch seems essential to avoid recurrence, whereas intricate dissection of the cyst with internal neurolysis or resection of the

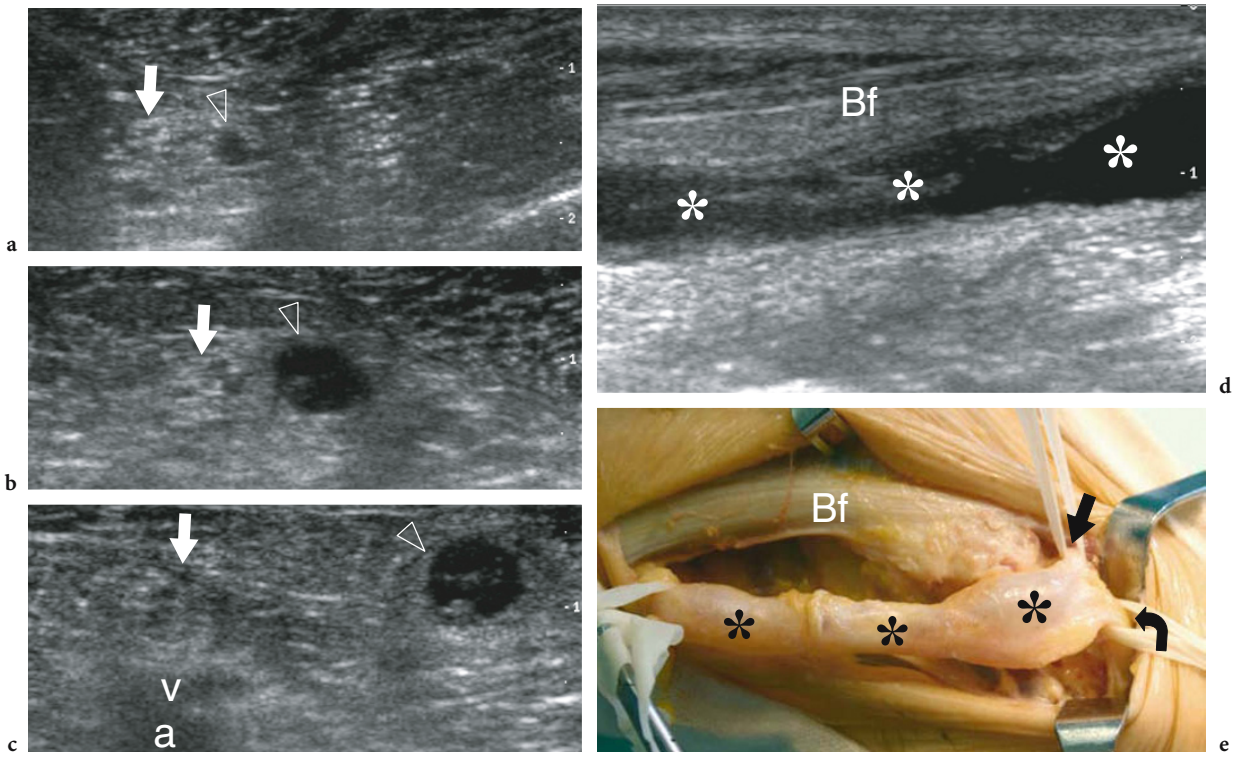

Fig. 14.83a–e. Peroneal intraneural ganglion in a patient with symptoms indicating complete denervation of the peroneal nerve around the fibular area. **a–c** Transverse 12–5 MHz US images obtained from **a** cranial to **c** caudal in the popliteal fossa demonstrate an abnormal peroneal nerve (*arrowhead*) which diverges from a normal-appearing tibial nerve (*arrow*). The peroneal nerve is markedly thickened and has a hypoanechoic structure reflecting the cyst which expands from the superior tibiofibular joint proximally, dissecting the fascicles. *a*, popliteal artery; *v*, popliteal vein. **d** Long-axis 12–5 MHz US image of the peroneal nerve shows fluid-filled intraneural channels (*asterisks*) reflecting the ganglion fluid. **e** Gross operative photograph confirms the presence of a large intraneural peroneal ganglion (*asterisks*). Note the superficial peroneal nerve (*straight arrow*) and the articular branch (*curved arrow*). *Bf*, biceps femoris

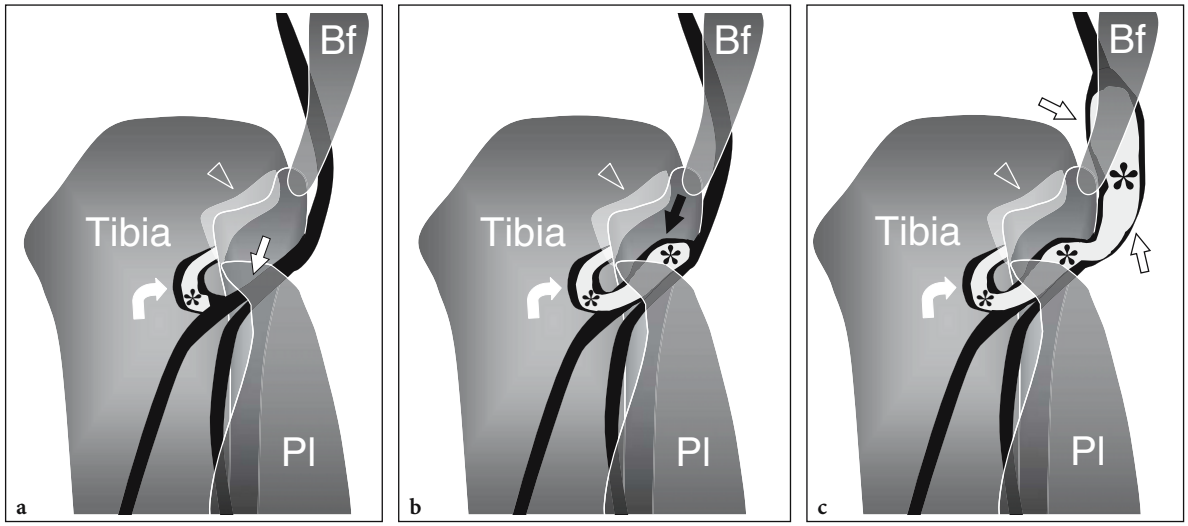

Fig. 14.84a–c. Stages of intraneural peroneal ganglia. The clinical presentation of peroneal intraneural ganglia can be understood in terms of their pathoanatomy. **a–c** The clinical symptoms and findings can be correlated with the extent of cyst propagation. The ganglion (*asterisks*) extends from the superior tibiofibular joint (*open arrowhead*): stage 0, not shown; **a** proximally to the articular branch (*curved arrow*), stage I; **b** to the deep peroneal nerve (*black straight arrow*), stage II; and **c** to the common peroneal nerve (*open straight arrow*), stage III. *Bf*, biceps femoris; *Pl*, peroneus longus

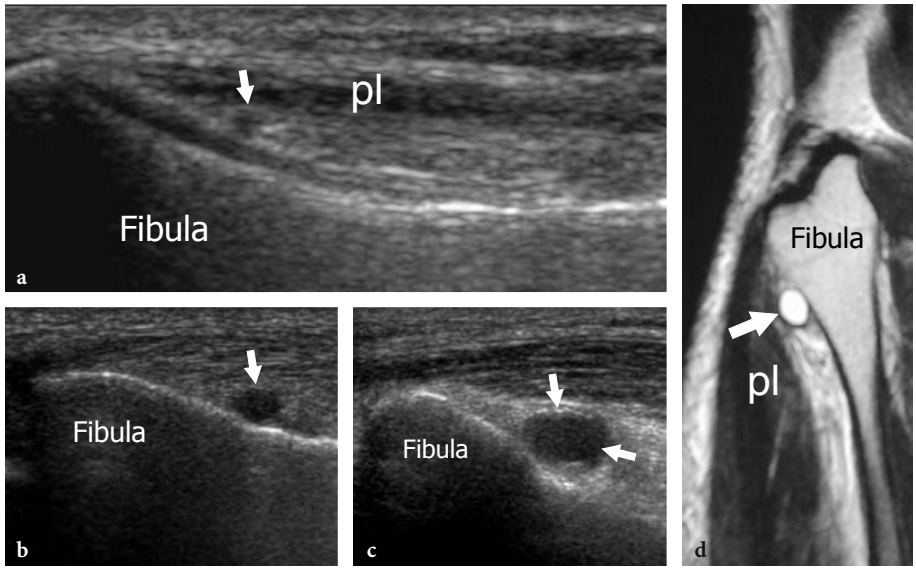

Fig. 14.85a–d. Articular branch of the peroneal nerve. **a** Sagittal 12–5 MHz US image obtained over the anterior aspect of the fibula demonstrates the normal articular branch of the peroneal nerve as a small hypoechoic dot (*arrow*) located deep to the peroneus longus (*pl*) muscle. Note the smooth down-sloping contour of the cortical bone of the fibular neck. **b,c** Sagittal 12–5 MHz US images obtained over the articular branch of the peroneal nerve in two different patients affected by peroneal intraneural ganglion reveal a grossly hypoechoic enlargement of this branch (*arrows*) due to fluid distension. **d** Sagittal T2-weighted MR image of the case shown in **c** confirms the cystic dilatation of the articular branch (*arrow*) of the peroneal nerve

cyst wall may lead to further functional damage to the nerve (Fig. 14.86e). Also, if the articular branch is not ligated during operation, the elevated intra-articular pressure may lead to a conspicuous leakage of fluid in the adjacent soft tissues.

Due to its length and oblique course, the common peroneal nerve is particularly susceptible to stretching injuries in the popliteal fossa. These injuries occur in association with knee dislocation, fractures, repetitive sprain or strain lesions involving the lateral corner of the knee and may typically be encountered in young people as a result of prolonged squatting, crouching or kneeling. In these cases, a long fusiform hypoechoic swelling of the common peroneal nerve with loss of the fascicular echotexture and posterior acoustic attenuation can be appreciated in the popliteal fossa reflecting a spindle neuroma with intraneural fibrosis internal to a nondisrupted nerve trunk (Fig. 14.87). In general, the abnormal segment extends 1–2 cm distal to the nerve origin down to the level of the lateral femoral condyle. When the knee trauma is more significant, laceration of the common peroneal nerve may occur secondary to a traction mechanism. In these cases, US can depict disruption of the fascicles and a wavy course of the severed nerve (Fig. 14.88).

14.5.4 Posterior Knee Pathology

The posterior knee is the predominant site for cystic masses (Tschirch et al. 2003). There is some confusion about the correct terminology of popliteal cysts in the radiological and clinical literature. A popliteal cyst can be defined as a cystic lesion located on the posterior aspect of the knee joint, within the popliteal space. In this location, the most common popliteal cysts are Baker cysts. These cysts result from the distension of the semimembranosus-gastrocnemius bursa and are not synonymous with popliteal cysts (Baker 1877). Posterior extra-articular ganglia are rare and may be located anywhere in the popliteal fossa but not at the level of the semimembranosus-gastrocnemius bursa. Differentiation between these two entities is clinically relevant because they have different characteristics, pathogenesis, imaging features and therapeutic implications.

14.5.4.1 Baker Cyst

Baker cysts can be idiopathic or secondary to joint disorders. The former are almost exclusively seen

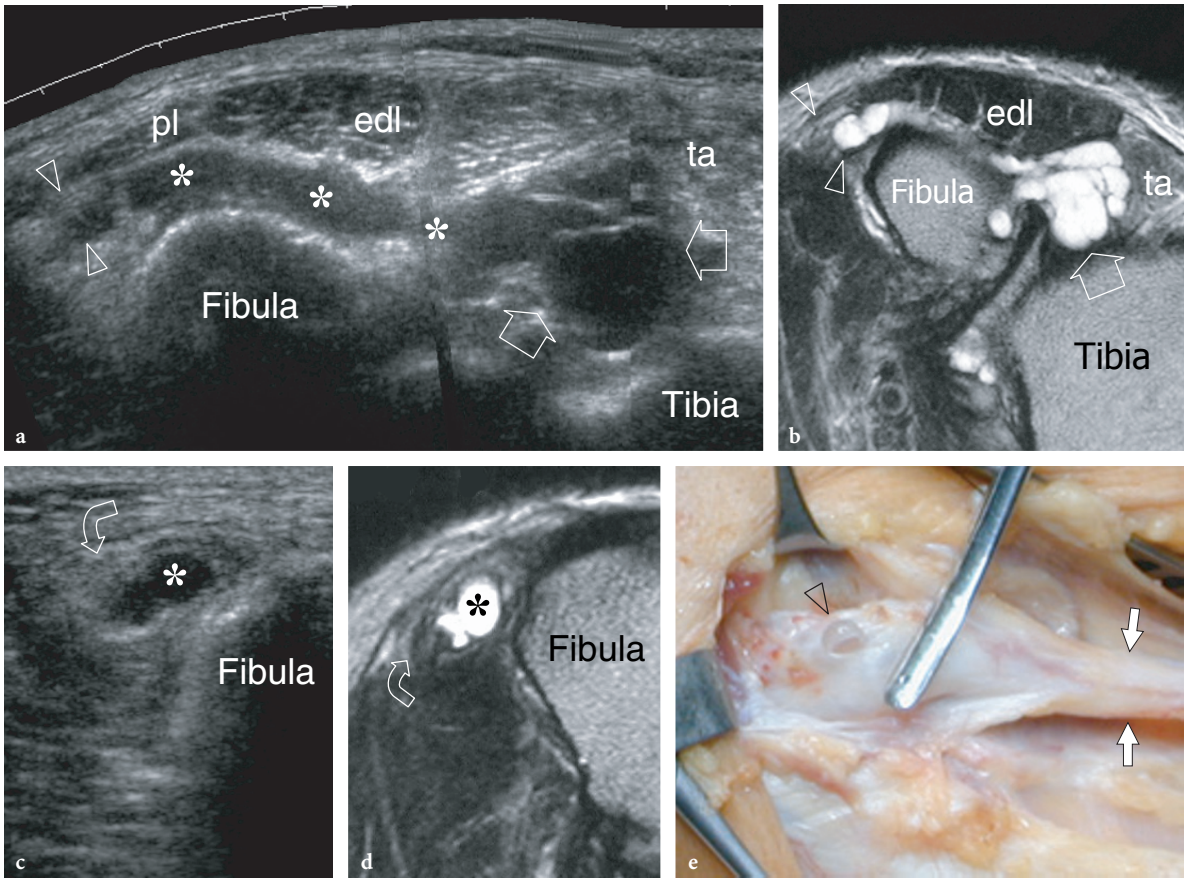

Fig. 14.86a–e. Intraneural peroneal ganglion. **a** Transverse extended field-of-view 12–5 MHz US image with **b** T2-weighted MR imaging correlation demonstrates a large lobulated ganglion (*straight arrows*) with internal septations arising from the anterior aspect of the superior tibiofibular joint. The ganglion expands in the anterolateral compartment of the proximal leg and appears to be in continuity with a long tubular process (*asterisks*) reflecting the articular branch of the peroneal nerve up to reach the main trunk of the nerve (*arrowheads*). Note the course of the articular branch deep to the extensor digitorum longus (*edl*) and peroneus longus (*pl*) muscle. Note the signs of denervation atrophy of the tibialis anterior muscle (*ta*). **c** Transverse 12–5 MHz US image with **d** T2-weighted MR imaging correlation reveals the cyst (*asterisk*) involvement of the common peroneal nerve. *Curved arrow* indicates the fascicles of the superficial peroneal nerve which are spared by the cyst. **e** Gross surgical view confirms the intraneural involvement of the ganglion. Neurolysis shows spilling (*arrowhead*) of ganglion fluid within the substance of the peroneal nerve (*arrows*)

in pediatric patients and will be discussed later (see Chapter 19). Baker cysts related to joint disorders are encountered in adults (Miller et al. 1996). In these cases, a communication with the knee joint space induces a progressive distension of the semimembranosus-gastrocnemius bursa (Fig. 14.89). Once the joint fluid moves within the bursa, it tends to accumulate within it, because the bursal neck acts as a one-way valve mechanism (Lindgern and Rauschning 1979; Rauschning and Lindgern 1979). With knee flexion, the joint fluid is pushed into the bursa by increased intra-articular pressure secondary to the squeezing of the suprapatellar recess by the quadriceps muscle. During knee extension, the apposition of the semimembranosus and gastrocnemius tendons against the medial condyle closes any communication with the joint cavity and prevents retrograde movement of the cystic fluid. Intra-articular loose bodies, joint debris and hypertrophied synovium may also move from the joint into the bursa. The size of a Baker cyst depends on the chronicity of the underlying joint disorder. In chronic arthritis, repeated joint effusions can cause phases of increasing internal pressure leading to slow progressive bursal enlargement. In these cases, even large cysts may be well tolerated by the patient, as the process of enlargement is slow and gradual. This is particularly true in longstanding

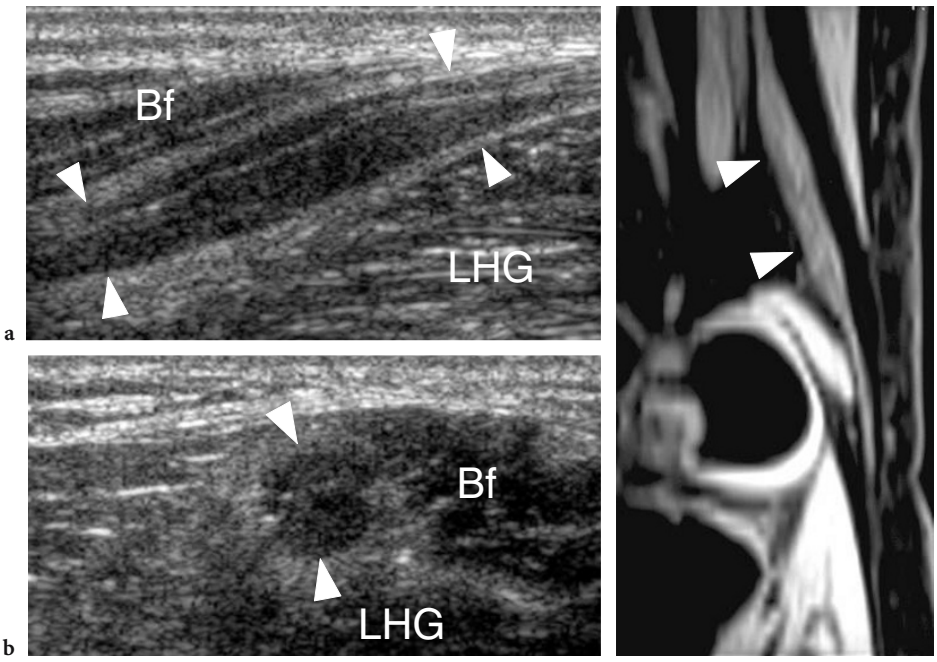

Fig. 14.87a–c. Fusiform neuroma of the common peroneal nerve in the popliteal fossa. The patient reported sudden onset of nerve deficit a knee sprain. **a** Longitudinal and **b** transverse 12–5 MHz US images with **c** fat-suppresse T2*-weighted MR imaging correlation demonstrate a fusiform hypoechoic swelling of the common peroneal nerve (*arrowheads*) as a result of a stretching injury in the popliteal fossa. Observe the position of the nerve between the biceps femoris (*Bf*) and the lateral head of the gastrocnemius (*LHG*)

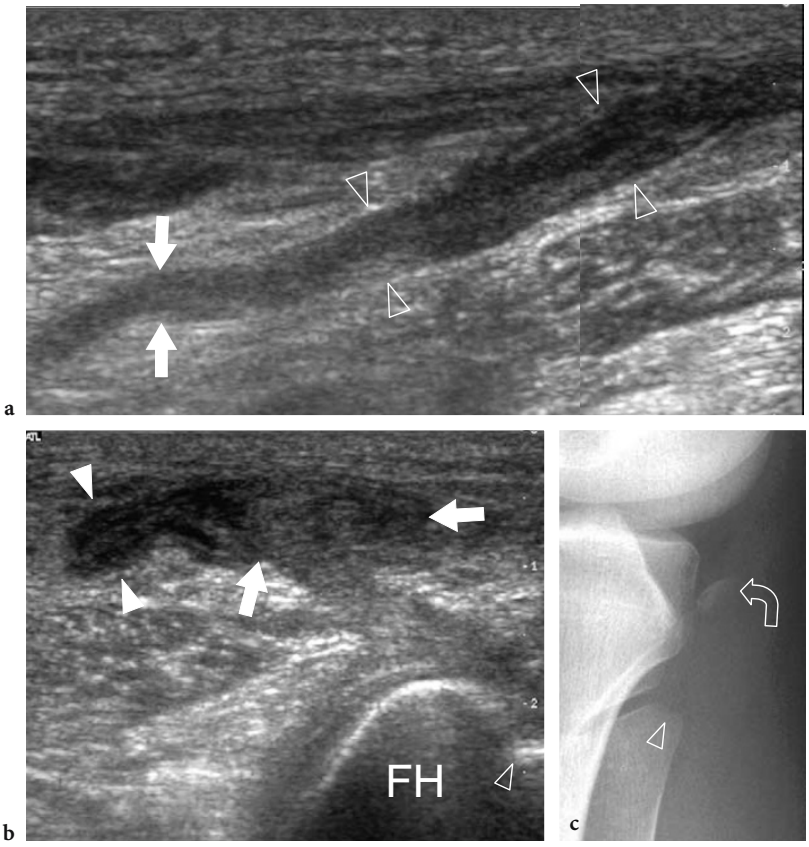

Fig. 14.88a–c. Complete tear of the common peroneal nerve in a patient with previous knee dislocation. **a** Long-axis 12–5 MHz US image over the peroneal nerve in the popliteal fossa. The nerve has a wavy course and is characterized by abnormal thickened (*arrowheads*) and thinned (*arrows*) segments related to the interruption and laceration of the fascicles. **b** Transverse oblique 12–5 MHz US image over the lateral knee with **c** lateral radiographic correlation demonstrates abnormal hypoechoic tissue related to the avulsion of the biceps femoris tendon (*arrows*) from its insertion (*open arrowhead*) into the fibular head (*FH*). Note the close relationship of the ruptured biceps with the torn nerve (*white arrowheads*). On the radiograph, a small fleck of bone (*curved arrow*) appears retracted proximally with the torn biceps tendon

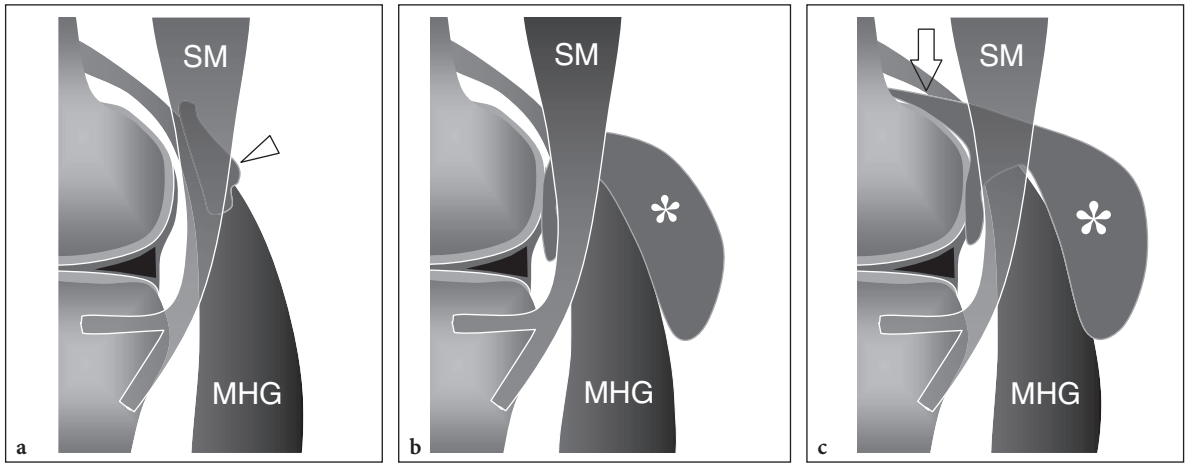

Fig. 14.89a–c. Semimembranosus-gastrocnemius bursa. Schematic drawings of a sagittal view through the posterior medial knee. **a** Normal bursa (*arrowhead*) located between the semimembranosus (*SM*) and the medial head of the gastrocnemius (*MHG*). **b** In children, fluid distention of the bursa results in a Baker cyst (*asterisk*), a cavity not communicating with the knee joint. **c** In adults, chronic friction and microtrauma among the semimembranosus tendon, the tendon of the medial head of gastrocnemius and the posterior capsule induce a localized perforation allowing the bursa (*asterisk*) to communicate with the joint cavity. The communication is almost invariably located at the supracondylar level (*open arrow*)

rheumatoid arthritis, where giant Baker cysts can be seen extending down through the calf even reaching the medial malleolus.

Clinically, Baker cysts can be asymptomatic or may cause mild local tension. The most common disorders associated with Baker cysts mirror the prevalence of knee disorders, meniscal pathology, anterior cruciate ligament and chondral tears being the most common, followed by inflammatory and degenerative arthropathies. In a series based on MR imaging selection, for example, the most commonly related lesions were meniscal tears (83%), particularly those affecting the posterior horn of the medial meniscus (Sansone et al. 1995). At physical examination, a typical Baker cyst appears as a palpable lump over the posteromedial aspect of the knee (Fig. 14.90). The imaging features of Baker cysts have been extensively reported in the literature (Torreggiani et al. 2002). Standard radiographs are obtained to assess the presence of an associated joint disorder or intracystic loose bodies (Fig. 14.91). Arthrography is performed with intra-articular injection of iodinated contrast, air or a mixture of both. This technique remains the best modality to prove the communication of the cyst with the articular cavity (Hermann et al. 1981). Direct injection of the cyst (bursography) seems less useful. Although Baker cysts can be identified on baseline CT scan, the intra-articular injection of contrast material (CT-arthrography) increases the ability to prove a direct communication of the cyst with the joint cavity and to assess its internal structure. When performed with spiral or multislice equipment, reconstructed images in the sagittal and coronal plane allow excellent visualization of the cyst and, most importantly, can detect associated meniscal and chondral lesions (Vande Berg et al. 2002). In this field, MR imaging is superior even to CT, due to its higher soft-tissue contrast capabilities and absence of ionizing radiation exposure (Fig. 14.92).

Baker cyst assessment has been one of the first applications of musculoskeletal US. At US examination, Baker cysts appear as space-occupying masses located at the level of the semimembranous-gastrocnemius bursa and characterized by a wide spectrum of appearances (Fig. 14.93) (Helbich et al. 1998). In most cases, the three components of the cyst can be demonstrated. The base is located among the semimembranosus tendon, the tendon of the medial head of the gastrocnemius and the posterior capsule. The base of cyst is usually smaller than its superficial part. A small stalk connecting the base with the posterior joint is rarely demonstrated. Beginners should be careful not to indicate the neck of the cyst as the stalk, mistaking the cystic base for the joint space. Imaging of the neck is best obtained on transverse planes as they allow simultaneous demonstration of the tendons of the semimembranosus and the medial head of the gastrocnemius. We believe US images obtained at this level are the most important, because a fluid collection between these two tendons is the most reliable

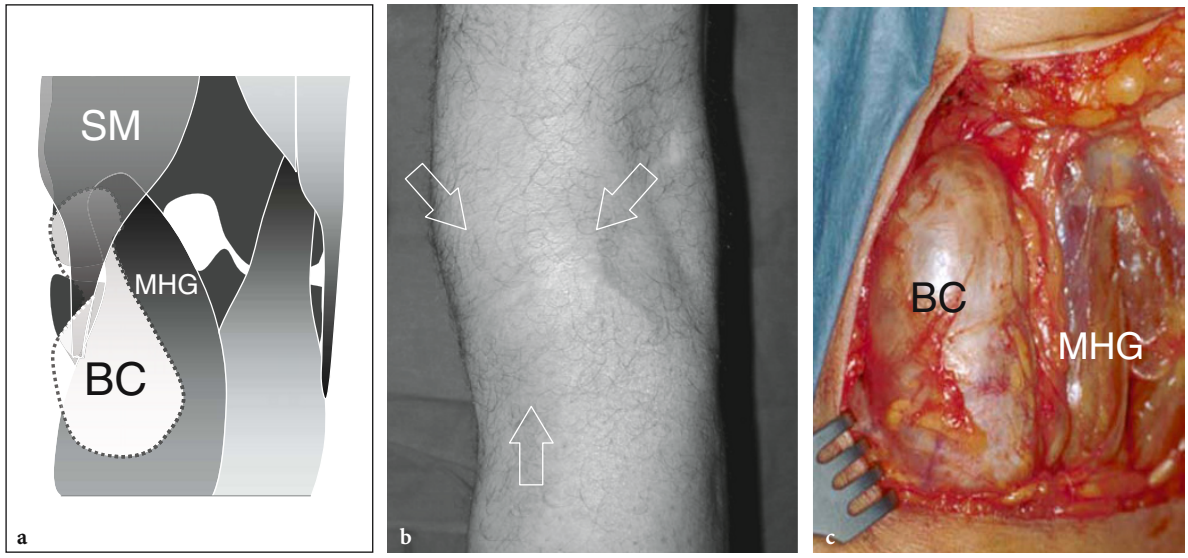

Fig. 14.90a–c. Baker cyst. **a** Schematic drawing of a coronal view of the posterior knee illustrates the anatomic relationships of the Baker cyst (*BC*) with the medial head of the gastrocnemius muscle (*MHG*) and the semimembranosus muscle and tendon (*SM*) in a coronal plane. **b** Photograph of the popliteal space in a patient with a Baker cyst reveals focal soft-tissue swelling at the inferomedial aspect of the posterior knee. **c** Gross surgical view of a Baker cyst (*BC*) depicts its relationship with the medial head of the gastrocnemius (*MHG*). (Courtesy of Prof. Dr. med. C.J. Wirth, Hannover, Germany)

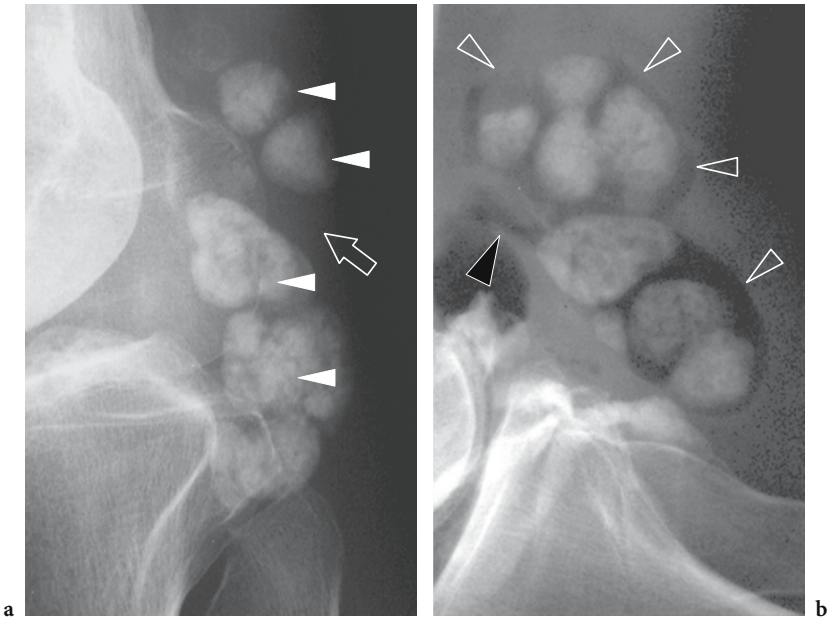

Fig. 14.91a,b. Baker cyst and intra-articular loose bodies. **a** Standard radiograph reveals multiple intracystic loose bodies which appear as rounded calcified structures (*white arrowheads*) located in the popliteal space. The fragments seem to fill the whole bursal cavity. Note the separation among them caused by the intervening tendon of the medial head of the gastrocnemius (*arrow*). **b** After injection of air within the femorotibial joint, laterolateral arthrogram obtained in knee flexion shows the passage of air (*open arrowheads*) within the semimembranosus-gastrocnemius bursa through a thin pedicle (*black arrowhead*). The air contained in the Baker cyst outlines the loose bodies confirming their intracystic location

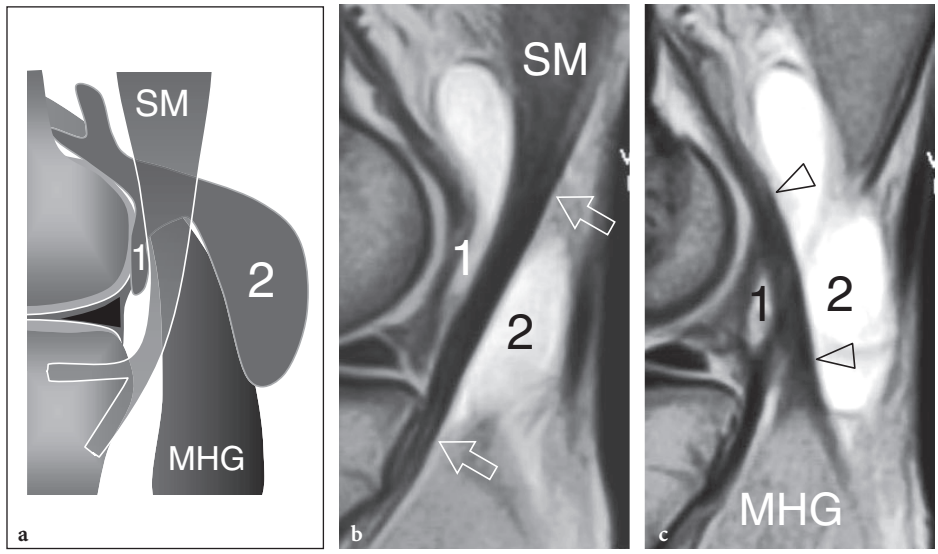

Fig. 14.92a–c Baker cyst: MR imaging appearance. **a** Schematic drawing of a sagittal view through the posterior medial knee and **b,c** corresponding sagittal T2-weighted MR images demonstrate a typical Baker cyst formed by a small base (*1*) and a large body (*2*). The two components of the bursa and their typical relationships with the tendon (*arrows*) of the semimembranosus (*SM*) and the tendon (*arrowheads*) of the medial head of the gastrocnemius (*MHG*) are displayed

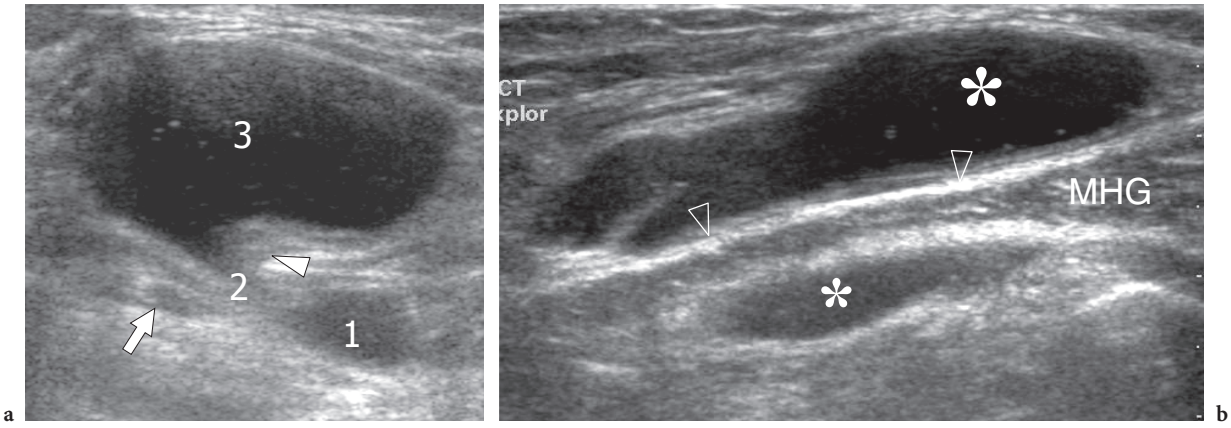

Fig. 14.93a,b. Baker cyst: US appearance. **a** Transverse 12–5 MHz US image shows the different components of a typical Baker cyst: the base (*1*), the neck (*2*), located between the tendon of the semimembranosus (*arrow*) and the tendon (*arrowhead*) of the medial head of the gastrocnemius, and the large body (*3*). **b** Longitudinal 12–5 MHz US image depicts the base and the body of the cyst (*asterisks*) separated by the straight tendon (*arrowheads*) of the medial head of the gastrocnemius (*MHG*)

indicator of a Baker cyst. When US is performed with the knee extended, the two tendons are tightly apposed and almost completely close the neck. In this position, even high pressure applied with the probe over the cyst is not able to empty it. A slight degree of knee flexion obtained by placing a small pillow under the ankle is necessary to open the neck and allow a decrease of the internal pressure. The superficial portion of the cyst – the body – is subcutaneous and ends with a rounded pole. It is directed distally and medially. Variations exist in both the size and location of the different components of a Baker cyst. Namely, the base may dissect inferiorly between the medial head of the gastrocnemius and the soleus muscle (Fig. 14.94). These cysts are difficult to evaluate at physical examination due to their deep position. In rare instances, the cyst may also expand cranially and deeply, to lie posterior to the distal femoral metaphysis (Fig. 14.95). These lesions are difficult to palpate too. Occasionally, large cysts

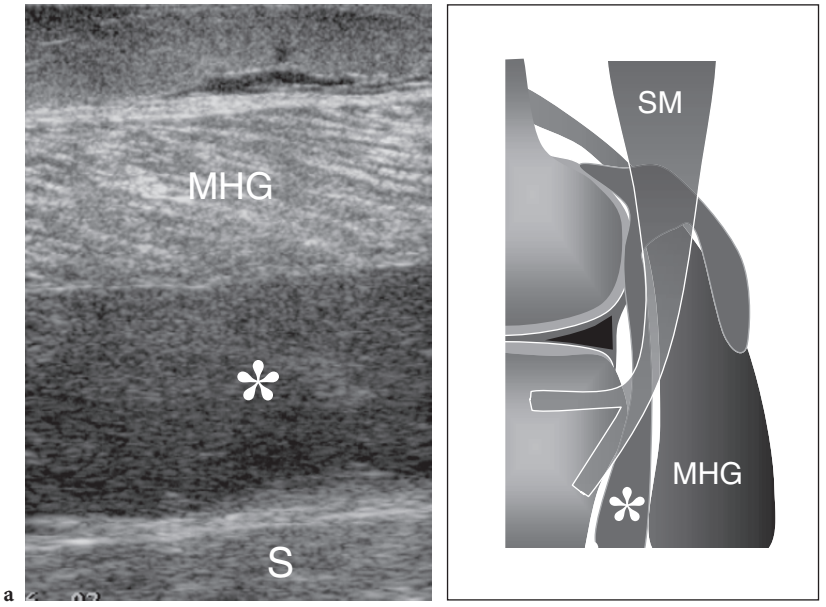

Fig. 14.94a,b. Baker cyst: anomalous caudal extension. Patient with longstanding rheumatoid arthritis. **a** Longitudinal 12–5 MHz US image over the proximal medial leg with **b** schematic drawing correlation reveals a large base of the cyst (*asterisk*) extending distally between the medial head of the gastrocnemius (*MHG*) and the deep soleus muscle (*S*)

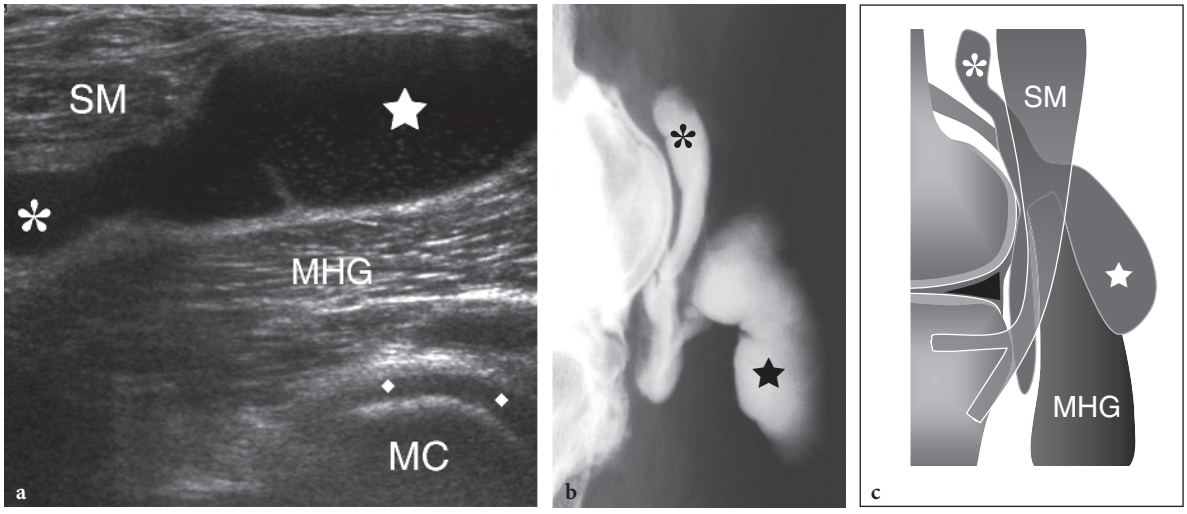

Fig. 14.95a–c. Baker cyst: anomalous cranial extension. **a** Longitudinal 12–5 MHz US image of the posterior medial knee with **b** corresponding arthrogram and **c** schematic drawing correlation show the base (*asterisk*) of a Baker cyst which extends cranially between the semimembranosus (*SM*) and the medial head of the gastrocnemius (*MHG*) as far as the metaphysis of the femur. Note the medial condyle (*MC*) covered by a hypoechoic layer of articular cartilage (*rhombi*). *Star*, body of the cyst

can compress adjacent structures, such as the popliteal vein and its branches, causing venous insufficiency. An accurate gray-scale and color Doppler imaging assessment of the popliteal vein should be part of the routine examination of exceedingly large Baker cysts.

The content of a Baker cyst may assume variable appearances. In cysts deriving from simple posterior extrusion of joint fluid, the content tends to be anechoic reflecting synovial fluid, and the cystic walls appear thin and regular (Fig. 14.93). In rheumatoid arthritis or other conditions associated with synovial hypertrophy, such as seronegative arthritides or pigmented villonodular synovitis, the cystic lumen can be partially or completely filled with synovium (Fig. 14.96). Tuberculous bursitis is very rare and

may appear irregularly hyperechoic reflecting intracystic caseous material (Fig. 14.97). In patients with osteoarthritis, neuropathic joint disease, or synovial abnormalities such as chondromatosis or osteochondromatosis, intra-articular loose bodies can be appreciated within the cyst as a result of migration of the fragments from the joint. As with cysts in other locations, three types of loose bodies may be encountered in a Baker cyst: calcified, osteochondral or purely chondral (Brossmann et al. 1996). Calcified fragments appear as single or multiple hyperechoic foci with posterior acoustic shadowing, like gallstones (Fig. 14.98a,b). Osteochondral fragments are characterized by a hyperechoic bone component that shows posterior shadowing and a definite hypoechoic chondral component (Fig. 14.98c,d). Purely cartilaginous loose bodies are rare and appear as hypoechoic fragments without posterior acoustic attenuation (Fig. 14.99). Fragments may be retained by the valve mechanism within the cyst, where they grow with time to completely fill its lumen. If any doubt exists whether loose bodies or wall calcifications are present, changing the patient's position (alternating standing and prone position) may be helpful to demonstrate mobility of the fragments and confirm their intracystic location (Fig. 14.99).

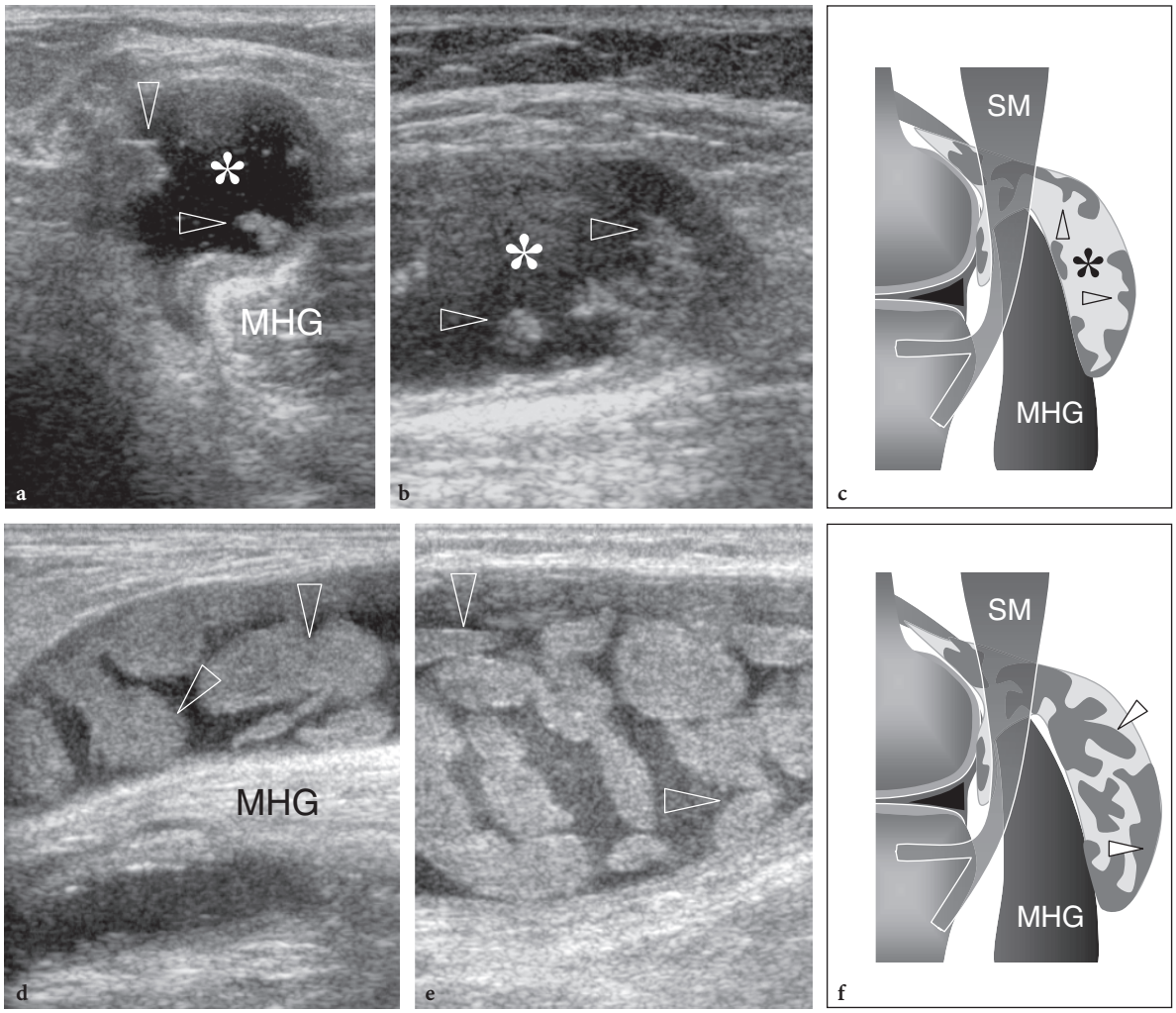

Fig. 14.96a–f. Baker cyst: synovial proliferation. Two different patients affected by rheumatoid arthritis. **a–c** Mild intrabursal synovial proliferation. **a** Transverse and **b** longitudinal 12–5 MHz US images with **c** schematic drawing correlation demonstrate the cyst filled with fluid (*asterisk*) and peripheral synovial projections (*arrowheads*) pointing toward the center of the lumen. **d–f** Severe intrabursal synovial proliferation. **d,e** Longitudinal 12–5 MHz US images with **f** schematic drawing correlation reveal a cyst almost completely filled with synovial fronds (*arrowheads*). *MHG*, medial head of the gastrocnemius muscle; *SM*, semimembranosus muscle

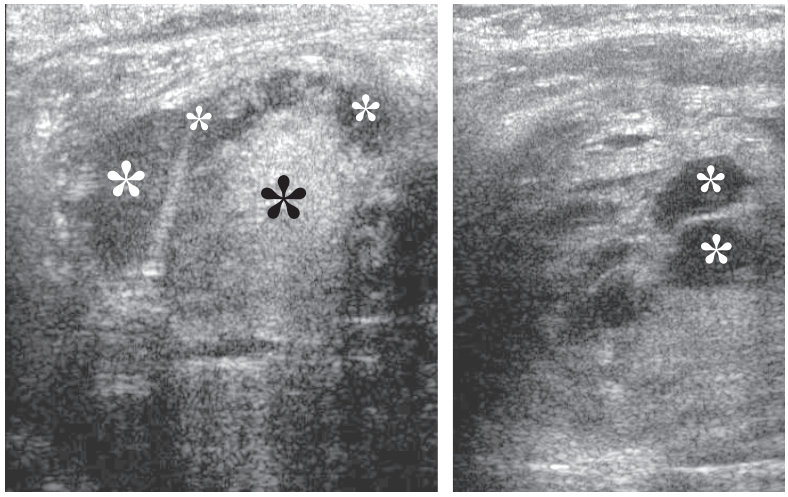

Fig. 14.97a,b. Tuberculous bursitis. Transverse 10–5 MHz US images obtained at different levels in a patient presenting with a popliteal mass show a Baker cyst filled with solid hyperechoic material (*black asterisk*) and anechoic fluid (*white asterisks*). Surgical exploration revealed a caseum-like content of the cyst. Culture was positive for *Mycobacterium tuberculosis*

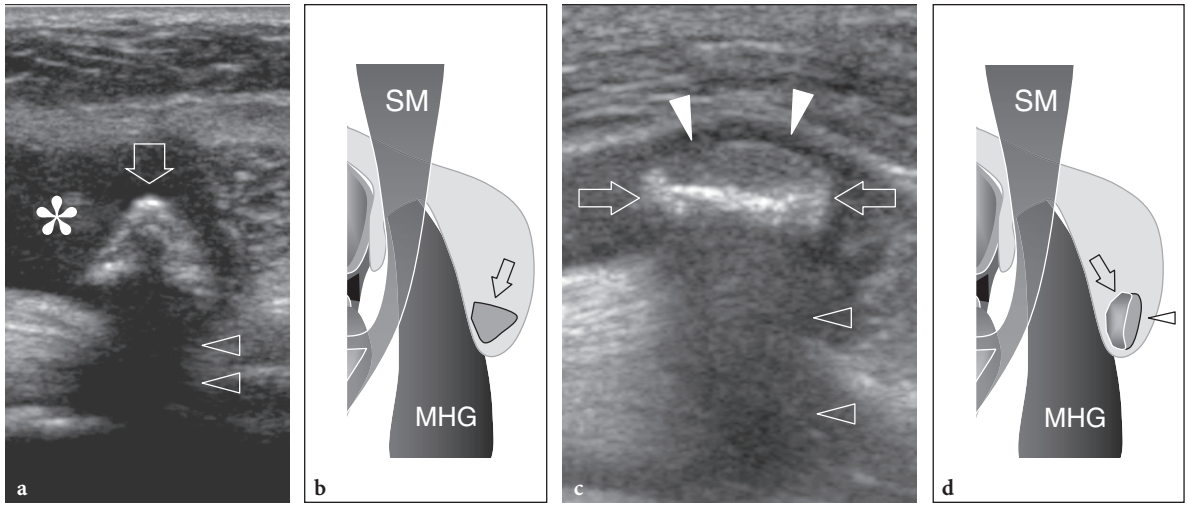

Fig. 14.98a–d. Intrabursal loose bodies: **a,b** Osseous and **c,d** osteochondral fragments in two different patients. **a** Longitudinal 12–5 MHz US image with **b** corresponding schematic drawing demonstrates the dependent portion of a Baker cyst filled with fluid (*asterisk*) and containing a loose body (*arrow*). The fragment is characterized by a hyperechoic structure and well-defined posterior acoustic shadowing (*arrowheads*), reflecting a purely osseous structure. **c** Longitudinal 12–5 MHz US image with **d** corresponding schematic drawing in a patient with previous osteochondral fracture reveals a loose body composed of a deep hyperechoic component (*arrows*) with posterior acoustic shadowing (*open arrowheads*) related to the osseous part of the fragment and a superficial hypoechoic component (*white arrowheads*) corresponding to its chondral part. Note that the fluid filling the cyst aids the detection of the loose body. *MHG*, medial head of the gastrocnemius muscle; *SM*, semimembranosus muscle

The most common complication of a Baker cyst is its rupture. Clinically, this condition is characterized by diffuse painful swelling and tenderness over the calf. This picture closely resembles that of thrombophlebitis (pseudothrombophlebitis syndrome) and can be diagnosed at US by showing partial or complete emptying of the cyst with extravasion of fluid in the distal subcutaneous tissue (Figs. 14.100, 14.101) (Miller et al. 1996). The distal pole of the cyst more commonly ruptures, changing its shape from a rounded to a pointed appearance (Fig. 14.100e). When a rupture is suspected but the cyst is no longer visible because of the extensive leakage of fluid in the surrounding tissues, the examiner should look for any residual fluid between the semimembranosus and medial head tendons as an indicator of its

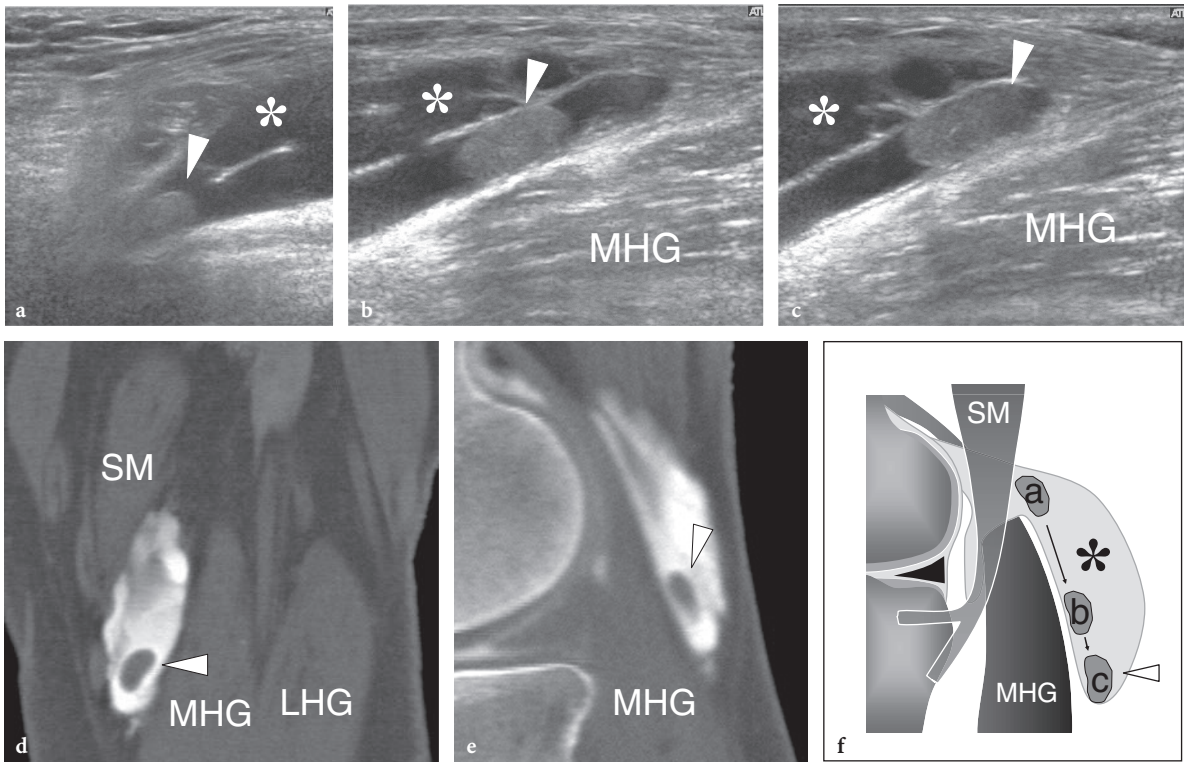

Fig. 14.99a–f. Intrabursal loose bodies: chondral fragment. **a–c** Longitudinal 12–5 MHz US images obtained with the patient **a** prone and **b,c** standing. In a Baker cyst with septations and anechoic content (*asterisk*), a purely chondral loose body (*arrowhead*) appears as a mobile oval hypoechoic fragment without posterior acoustic shadowing. Note the progressive intrabursal motion of the fragment from cranial (**a**) to caudal (**c**) following the change in the patient's position. *MHG*, medial head of the gastrocnemius. **d,e** MR arthrography confirms the presence of a loose body (*arrowhead*) within the Baker cyst. Note the position of the distended bursa relative to the semimembranosus (*SM*) and the medial (*MHG*) and lateral (*LHG*) heads of the gastrocnemius. **f** Corresponding schematic drawing of a sagittal view through the posterior medial knee illustrate the different position of the fragment within the Baker cyst (*asterisk*) when the patient is prone (**a**) and standing (**b,c**)

previous existence. Intracystic hemorrhage may be encountered particularly in patients taking anticoagulant drugs. In these cases, US depicts an irregular cystic content made of mixed hypoanechoic areas reflecting a combination of serum and clots filling the lumen (Fig. 14.102). New bleeding can follow percutaneous needle aspiration of these cysts. Infection is a rare complication of Baker cysts and mostly affects immunocompromised patients. Clinical findings include fever, warmth and local pain. The US appearance of an infected cyst is nonspecific: in general, purulent material appears more echogenic and the cystic walls are markedly thickened and irregular. The examiner should, however, be careful not to exclude an infected Baker cyst on the basis of the US findings alone. If an infection is suspected clinically, needle sampling of fluid, possibly guided by US, must always be carried out for laboratory and cultural analysis.

Needle aspiration of a Baker cyst can also be performed to reduce the high pressure of the fluid within the cyst when it causes pain and popliteal tension. In this latter case, percutaneous evacuation of the cyst may relieve the patient's symptoms. Demonstration of popliteal vessels and nerves can help selection of the most appropriate needle pathway. The differential diagnoses of Baker cysts include popliteal aneurysms, posterior extra-articular ganglia and soft-tissue tumours. It should be pointed out that differentiation of a Baker cyst from a posterior ganglion basically relies on demonstration of fluid between the medial head and the semimembranosus tendons. This is regarded as the most indicative feature for a correct diagnosis (Ward et al. 2001). When multiple internal septations make the diagnosis difficult, demonstration that the epicenter of the lesion is the semimembranosus-gastrocnemius bursa may enhance the examiner's confidence that a Baker cyst

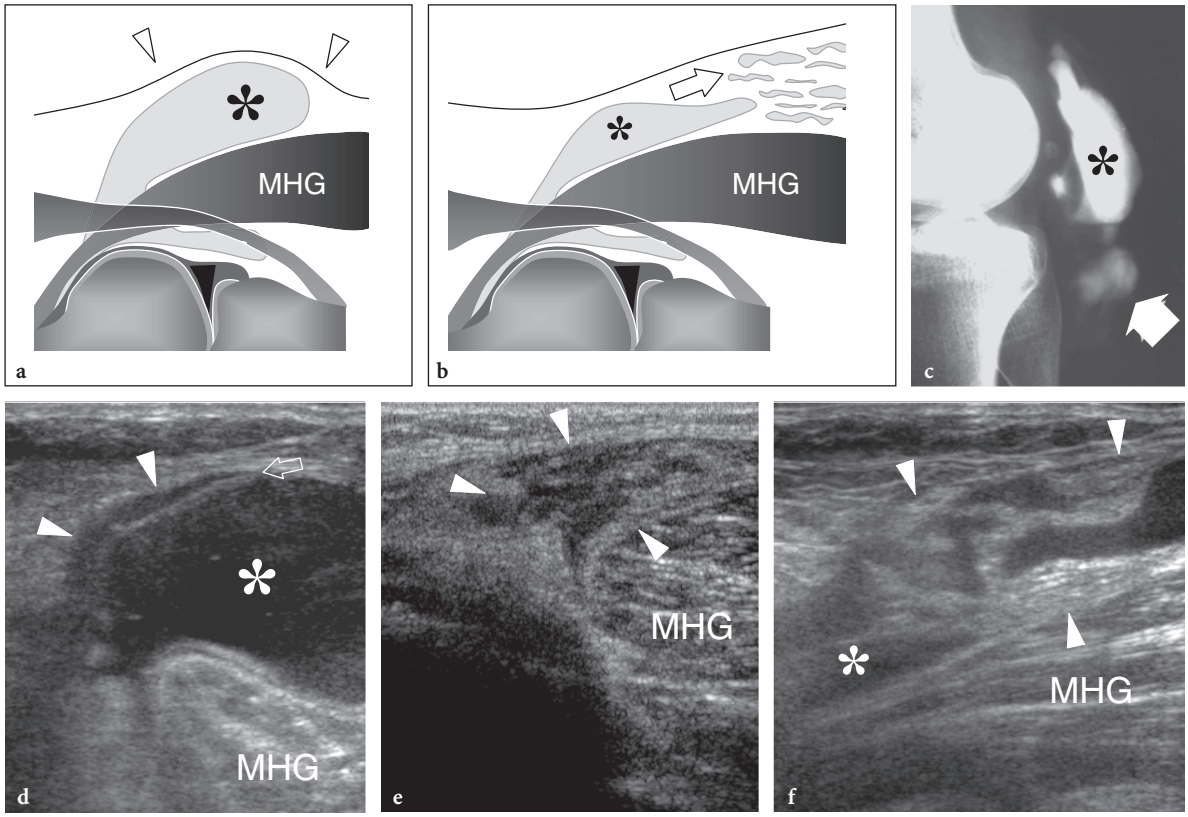

Fig. 14.100a–f. Complicated Baker cyst: rupture. **a,b** Schematic drawings of a sagittal view through the posterior medial knee show the appearance of **a** an uncomplicated and **b** a ruptured Baker cyst. Observe the shape of the distal end of the cyst (*asterisk*), which is normally rounded (**a**) but assumes a pointed appearance (**b**) when the cyst is ruptured as the fluid contained in it leaks into the surrounding distal fatty tissue planes (*arrow*). At physical examination, the local swelling (*arrowheads*) related to the bulk of the cyst is no longer apparent after its rupture. **c** Laterolateral arthrogram demonstrates the Baker cyst (*asterisk*) and the distal leakage of fluid (*arrow*) within the subcutaneous tissue. **d,e** Transverse 12–5 MHz US images of a ruptured Baker cyst (*asterisk*) obtained **d** at the level of the neck and **e** caudal to the distal end of the cyst depict the extravasion of fluid (*arrowheads*) out of the cystic walls (*arrow*). **f** Longitudinal 12–5 MHz US image obtained at the middle third of the calf, caudal to the distal end of the cyst (*asterisk*) demonstrates free fluid spreading into the fatty tissue planes (*arrowheads*). *MHG*, medial head of the gastrocnemius muscle

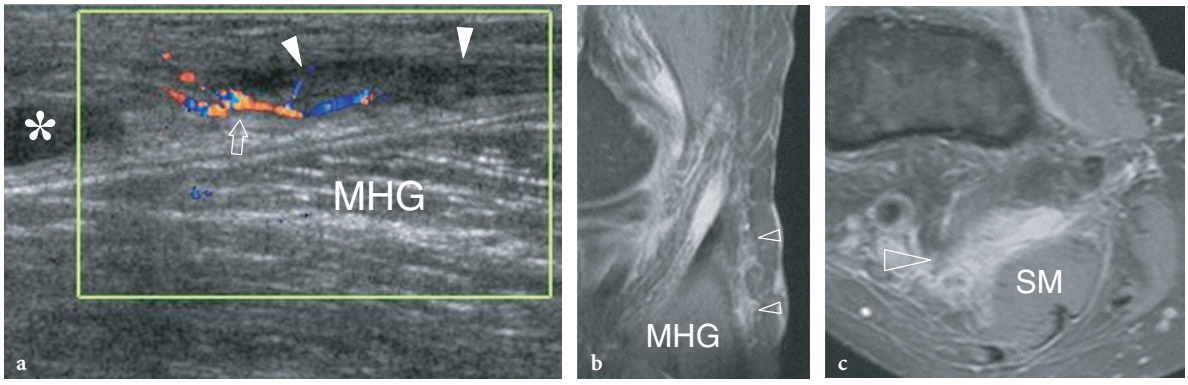

Fig. 14.101a–c. Complicated Baker cyst: recent rupture. **a** Longitudinal color Doppler 12–5 MHz US image with **b** sagittal and **c** transverse fat-suppressed MR imaging correlation shows caudal leakage of fluid (*white arrowheads*) from a ruptured Baker cyst (*asterisk*). The extravasion of fluid is associated with local hyperemic flow (*arrow*) and increased uptake of gadolinium (*open arrowheads*). *MHG*, medial head of the gastrocnemius muscle; *SM*, semimembranosus muscle

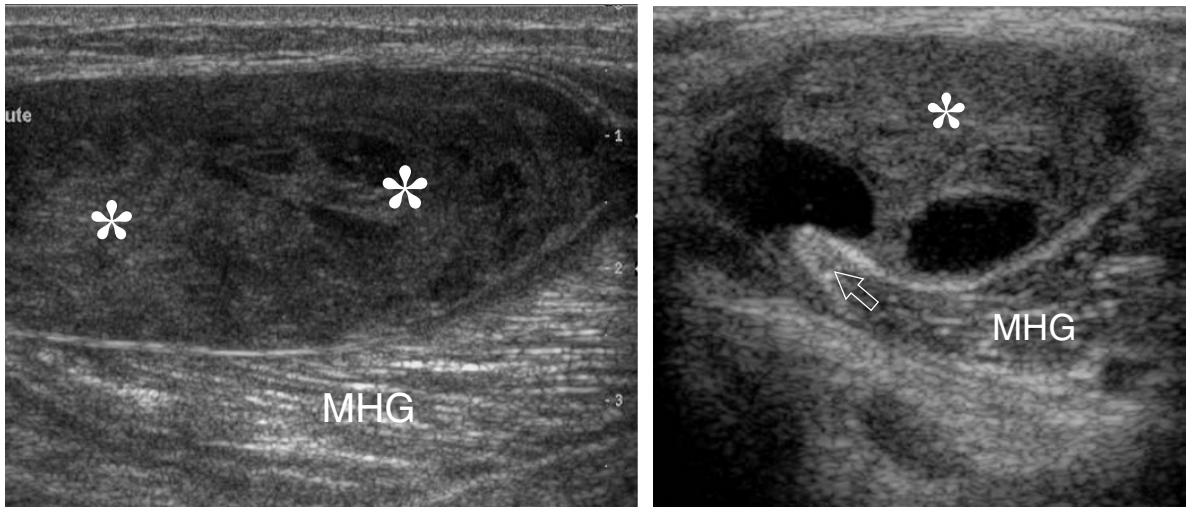

a b

Fig. 14.102a,b. Complicated Baker cyst: intrabursal hemorrhage. **a** Longitudinal and **b** transverse 12–5 MHz US images reveal echogenic material reflecting blood clots (*asterisks*) which almost completely fills the lumen of the bursa. Note the tendon (*arrow*) of the medial head of the gastrocnemius muscle (*MHG*)

is present (Torreggiani et al. 2002). Detection of a link between a mixed or pseudosolid mass with the fluid seen between the semimembranosus and the medial head of the gastrocnemius may help to differentiate complicated echogenic cysts from tumors (Ward et al. 2001).

In conclusion, the role of imaging modalities to diagnose Baker cysts depends on the questions raised by the referring clinicians. If the clinicians want to know whether a Baker cyst exists in a patient with a well-defined intra-articular disorder, such as rheumatoid arthritis, US is the technique of choice. If he or she already knows that a Baker cyst is present, US can be used to detect complications, such as rupture and compression, and can guide diagnostic puncture. MR imaging is, however, necessary to assess the intraarticular structures.

14.5.4.2 Extra-articular Ganglia

Extra-articular ganglion cysts are a common finding around the knee. Unlike synovial cysts, ganglia are characterized by a mucoid content and fibrous wall without a lining of synovial cells. These cysts are usually located deeply, in close proximity with the posterior aspect of the distal femoral metaphysis (36.7%) (Kim et al. 2004). Other locations, in decreasing order of occurrence, include superolateral (23.3%), inferomedial (20%) and inferolateral (13.3%) knee regions (Kim et al. 2004). Ganglion cysts can be totally asymptomatic or may cause nonspecific posterior knee pain and limitation of flexion. US depicts ganglia as well-circumscribed anechoic masses which may have a single- or multichambered appearance (Figs. 14.103, 14.104). Their wall can be either thin or thick, probably reflecting the age of the cyst. Color Doppler imaging does not show intralesional flow signals, even though some ganglia may encircle adjacent vessels thus mimicking an internal vasculature (Fig. 14.103c,d). The tortuous pedicle can be difficult to be visualized with US and may be seen on delayed arthrography (Malghem et al. 1998). The US appearance of popliteal ganglia is relatively specific and US-guided aspiration is obtained for therapeutic rather than diagnostic purposes. Extra-articular ganglia related to the superior tibiofibular joint and intraneural peroneal ganglia have already been addressed (see Sect. 14.5.3.4 and 14.5.3.5). Cystic lesions within the Hoffa fat pad are intra-articular in location, as they usually derive from the anterior cruciate ligament.

14.5.4.3 Semimembranosus Bursitis

Semimembranosus tenosynovitis and bursitis is a condition affecting aged women that should be differentiated from a Baker cyst, as it requires a differ-

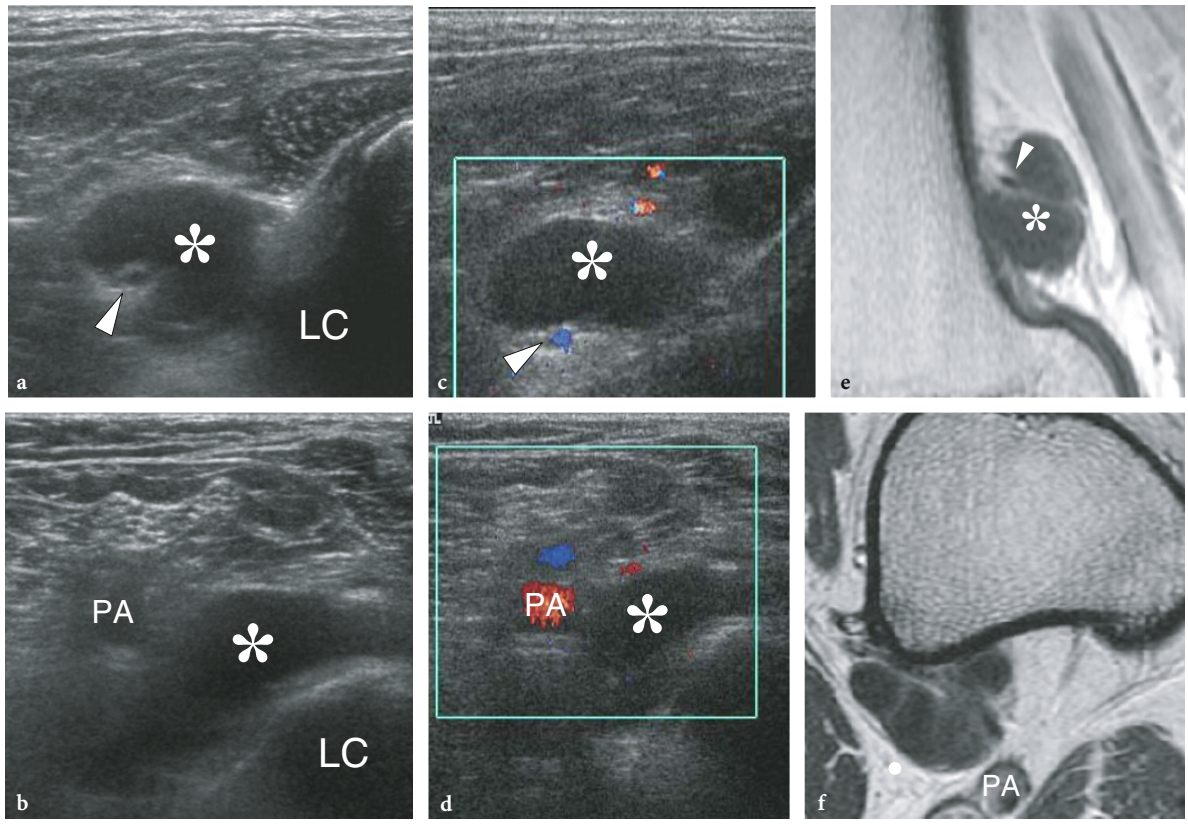

Fig. 14.103a–f. Posterior extra-articular ganglion cyst. **a** Longitudinal and **b** transverse gray-scale 12–5 MHz US images obtained at the posteromedial aspect of the knee demonstrate a well-defined cystic-like mass (*asterisk*) in contact with the lateral condyle (*LC*). Observe the proximity of the mass with the posterosuperior geniculate artery (*arrowhead*) and the popliteal artery (*PA*). **c,d** Corresponding color Doppler US images show absence of internal flow signals within the cyst and confirm the close relationships of the mass with the adjacent vessels. **e,f** Corresponding **e** sagittal and **f** transverse T1-weighted MR images obtained **e** before and **f** after intravenous injection of gadolinium confirm the US findings. Note the weak enhancement of the cystic walls and the internal fluid content of the ganglion

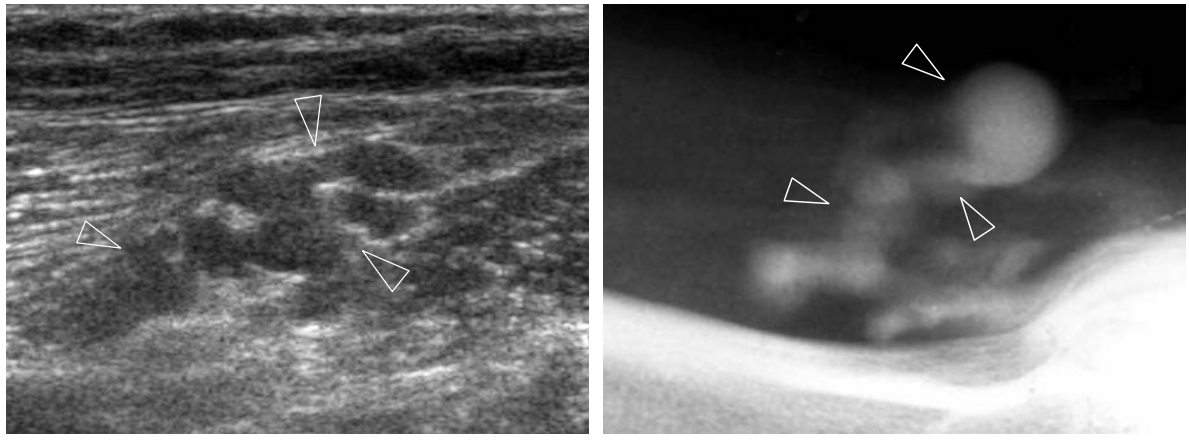

Fig. 14.104a,b. Posterior extra-articular ganglion cyst. **a** Longitudinal 12.5 MHz US image obtained at the posteromedial aspect of the knee shows a well-defined cystic lesion (*arrowheads*) with irregular and lobulated shape. **b** Corresponding delayed arthrogram confirms the presence of a ganglion cyst (*arrowheads*) characterized by a tortuous pedicle reaching the posterior joint space

ent therapy. In these patients, the reflected tendon of the semimembranosus and the adjacent synovial bursa become inflamed as a result of impingement against osteophytes over the medial aspect of the tibial plateau. Conservative treatment includes anti-inflammatory drugs, physical therapy and local steroid injections. In refractory cases, surgical excision of the tendon sheath results in a good outcome (Halperin et al. 1987). On transverse planes, US reveals semimembranosus tenosynovitis as an anechoic fluid collection surrounding the oval tendon associated with fluid distension of the adjacent bursa, located between the tendon and the tibial cortex (Fig. 14.105). US-guided needle injection of the bursa is usually better tolerated than blind puncture and prevents inadvertent steroid injection in the neighboring soft tissues.

14.5.4.4 Cruciate Ligament Ganglia

Ganglion cysts arising in close proximity to the cruciate ligaments may be the cause of intra-articular derangement of the knee. These cysts develop in the femoral synovial notch, a depression in the distal femur which lies between the lateral and medial condyles that contains the posterior and anterior cruciate ligaments. The cruciate ligaments are surrounded by loose connective tissue and fat that reduce friction of the ligaments against the bone surfaces during joint motion. The synovial membrane of the femorotibial joint reflects over the anterior aspect of the anterior cruciate ligament, covers the internal and posterior faces of both condyles to join the posterior capsule and inserts into the bone-cartilage interface. The posterior capsule is tightened between the posterior portions of the condyles. This anatomic arrangement explains why the structures contained inside the notch are intracapsular but extrasynovial (Lee et al. 1996b; De Maeseneer et al. 2004). Two fatty-tissue spaces exist in the intercondylar notch (Lee et al. 1996b). The first, the triangular space of the cruciate, is bounded by the two cruciate ligaments and the tibial plateau; the second has a crescent shape and is delimited by the posterior aspect of the posterior cruciate ligament and the posterior fibrous capsule. Neither space communicates with the joint cavity and every fluid collection or mass located within them should be regarded as extrasynovial (Fig. 14.106).

The pathogenesis of cruciate ligament cysts is still debated. Some authors hypothesize they derive from herniation of intra-articular synovium between the

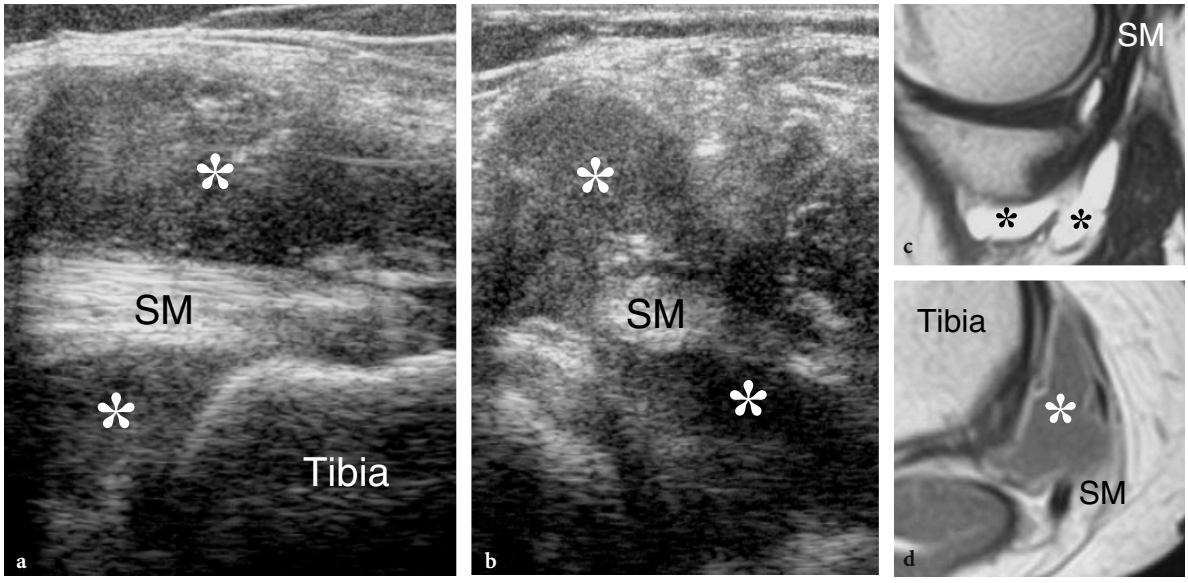

Fig. 14.105a–d. Semimembranosus bursitis. **a** Longitudinal and **b** transverse 12–5 MHz US images obtained at the posteromedial aspect of the knee show the direct tendon of the semimembranosus (*SM*) inserting onto the tibia. The tendon is characterized by a normal size and echotexture. A discrete hypoechoic effusion with hypertrophied synovium (*asterisks*) is seen around the tendon reflecting semimembranosus bursitis. Corresponding **c** sagittal T2-weighted and **d** transverse postcontrast T1-weighted MR images confirm the presence of a bursal effusion (*asterisks*) and the integrity of the direct tendon (*SM*) of the semimembranosus

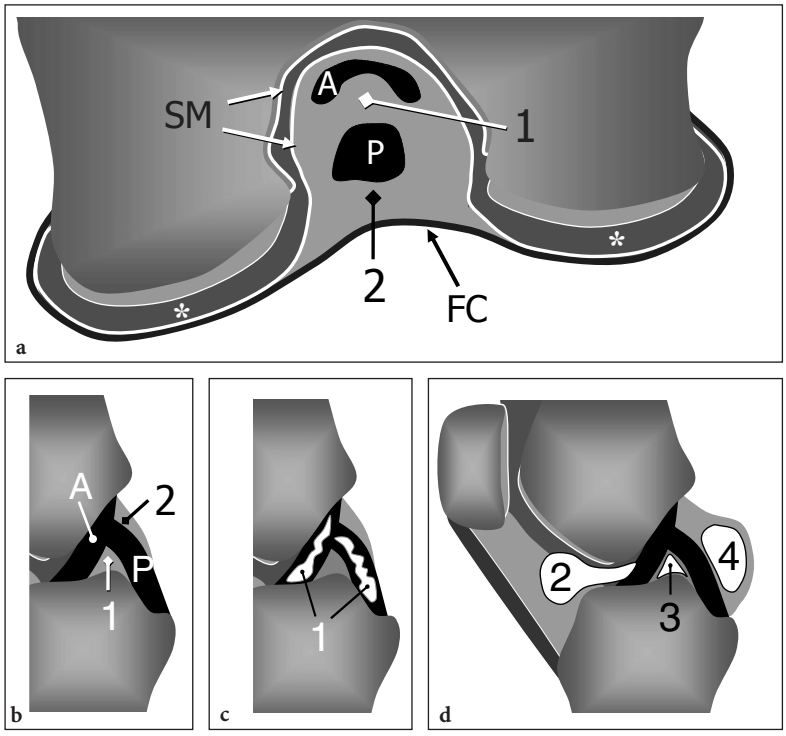

Fig. 14.106a–d. Anatomy of the cruciate ligament area. **a,b** Schematic drawings of a transverse (**a**) and sagittal (**b**) view through the intercondylar fossa illustrate the anatomic spaces of the cruciate ligament area. Note the posterior fibrous capsule of the joint (*FC*) and the synovial space (*asterisks*) delimited by reflections of the synovial membrane (*SM*). The anterior (*A*) and posterior (*P*) cruciate ligaments lie in an intracapsular but extrasynovial fatty tissue space, which includes the triangular space of the cruciate ligaments (*1*) and the area posterior the posterior cruciate ligament (*2*). **c,d** Cruciate ligament cysts. Schematic drawings illustrate the spectrum of intra-articular cruciate ligament ganglia. Based on their location, these include: **c** intraligamentous ganglia (1) and **d** extraligamentous ganglia. The latter (*2-4*) may arise from either the anterior cruciate ligament (*2*), projecting toward the Hoffa fat pad, or the posterior cruciate ligament (*4*), or from both ligaments (*3*), resting in the triangular space

ligaments. Others suppose they result from myxoid degeneration of connective tissue in an area under continuous mechanical stress. The evidence that cruciate ligament cysts do not communicate with the joint cavity and that a fibrous wall is found in association with high viscous internal fluid makes the second theory more likely. Depending on their location, four types of cruciate ligament cysts can be recognized: anterior to the anterior cruciate ligament; between the anterior and posterior cruciate ligaments; inside both ligaments; and posterior to the posterior cruciate ligament (Fig. 14.106c,d). The cysts located anterior to the anterior cruciate ligament expand within the Hoffa fat pad and may reach a large size (Fig. 14.107) (Saddik et al. 2004). On the other hand, cysts deriving from the triangular space of the cruciates tend to extend posteriorly. Intraligamentous cysts have a fusiform shape extending along the long axis of the ligaments and appear smaller in size because their growth is probably constrained by the ligament bundles (Kim et al. 2003). Cysts arising posterior to the posterior cruciate ligament expand dorsally and may reach a considerable volume (Fig. 14.108). Cruciate ligament cysts may be discovered incidentally during imaging examinations obtained for other purposes (Bui-Mansfield and Youngberg 1997). The most frequent finding at physical examination is limitation of extension (anterior cysts) or flexion (posterior cysts) movements. Joint locking may derive from large cysts or from changes in the volume and shape of the ganglion which causes irritation of nerve endings in the synovial membrane during knee movements (Kim et al. 2003; Noda et al. 1999). During its expansion, the ganglion may cause local bony erosion (Choi and Kim 2002). Because of their vague clinical appearance and deep location, imaging studies are required to diagnose cruciate ligament cysts as well as to assess their actual size, exact location and relationship with adjacent structures. Owing to problems of access related to the surrounding bony structures, the value of US in detecting and assessing cruciate

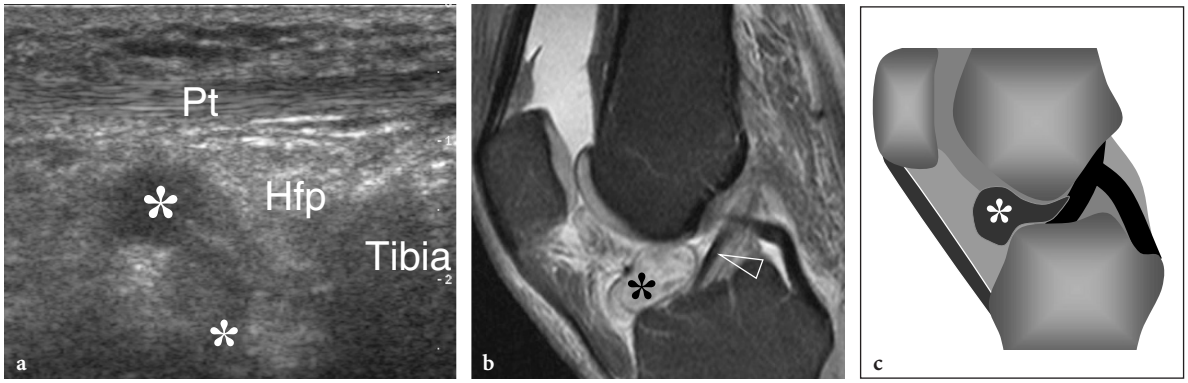

Fig. 14.107a–c. Anterior cruciate ligament ganglion. **a** Longitudinal 12–5 MHz US image obtained over the patellar tendon (*Pt*) reveals an anechoic well-defined cystic lesion (*asterisk*) expanding inside the deep Hoffa fat pad (*Hfp*). **b** Sagittal fat-suppressed proton density MR image with **c** schematic drawing correlation confirms the US findings showing a hyperintense cystic lesion (*asterisk*) located between the anterior border of the anterior cruciate ligament and the Hoffa fat pad. In **b**, note the normal appearance of the anterior cruciate ligament (*arrowhead*)

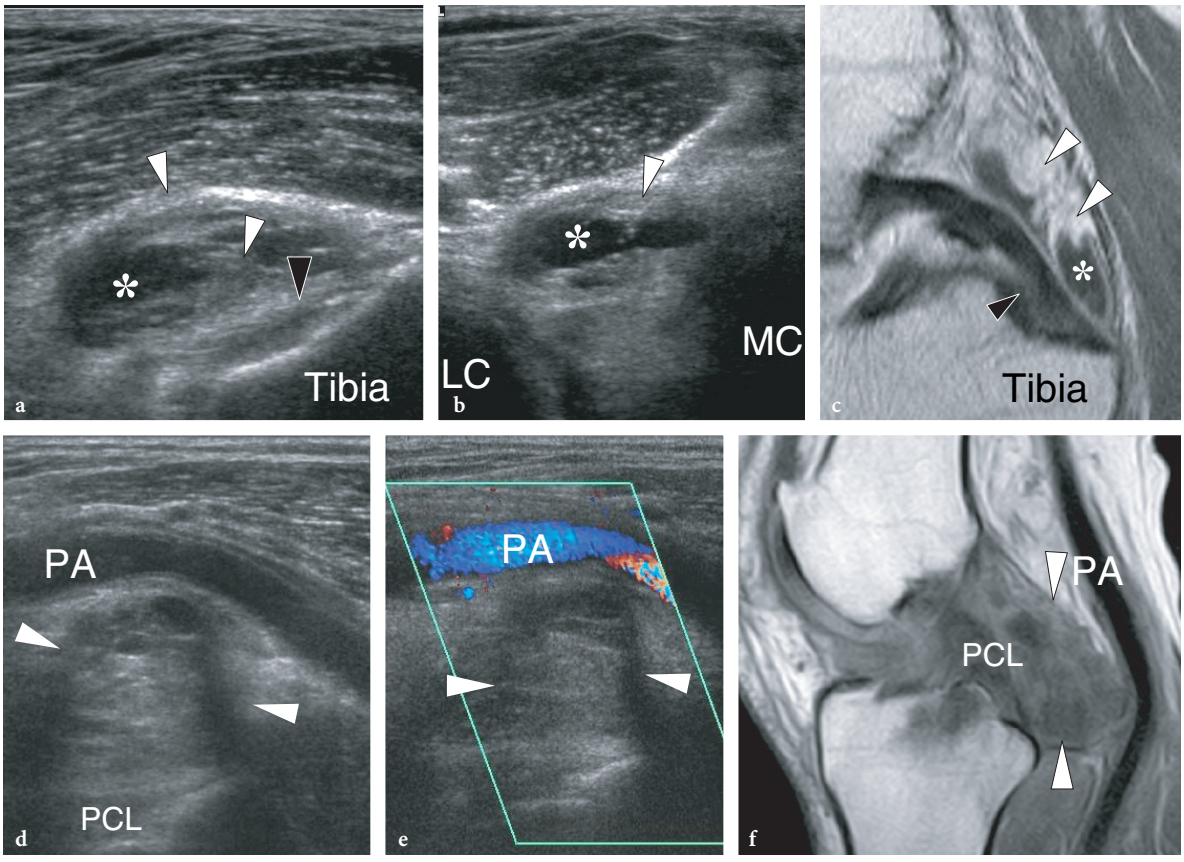

Fig. 14.108a–f. Posterior cruciate ligament ganglia. Two different cases (**a–c** and **d–f**). **a** Longitudinal and **b** transverse 12–5 MHz US images obtained over the intercondylar fossa show a well-defined anechoic cystic lesion (*asterisk*) with thickened walls (*white arrowheads*) in close relationship with the posterior cruciate ligament (*black arrowhead*). Note the location of the ganglion in the midline of the posterior knee, between the lateral (*LC*) and medial (*MC*) condyles. **c** Corresponding postcontrast T1-weighted MR image confirms the presence of a cystic mass in close contact with the ligament. **d,e** Longitudinal **d** gray-scale and **e** color Doppler 12–5 MHz US images obtained at the posterior aspect of the knee show a mixed mass (*white arrowheads*) with predominant solid components displacing the popliteal artery (*PA*) posteriorly. **f** Corresponding T1-weighted MR image shows a ganglion (*white arrowheads*) adherent to the posterior cruciate ligament (*PCL*). Note the posterior displacement of the adjacent popliteal artery (*PA*)

ligament cysts is limited by the fact that this modality can detect large cysts located only anterior to the anterior cruciate ligament and posterior to the posterior cruciate ligament. Intraligamentous and intercruciate cysts cannot be detected with this technique. A low-frequency (5 MHz center frequency) probe may be required for such an assessment. At US examination, cruciate ligament cysts appear as well-defined hypoanechoic masses with sharp margins. The fact that these cysts can show variable internal echogenicity is mainly related to the presence of internal septations: unilocular cysts are usually anechoic, whereas multilocular ganglia exhibit a mixed structure due to a combination of anechoic fluid and echogenic septations. Color and power Doppler imaging do not show internal flow signals.

Cruciate ligament cysts should be differentiated from meniscal cysts (Lektrakul et al. 1999). Careful analysis of the posterior horn of the medial meniscus should be performed when a cyst-like structure is seen adjacent to the posterior cruciate ligament. In addition, synovial proliferations, such as pigmented villonodular synovitis, and some tumors, including synovial hemangioma and synovial sarcoma can mimic a cruciate ligament cyst. In these cases, the differential diagnosis requires gadolinium-enhanced MR imaging. In doubtful cases, arthroscopy is mandatory. Percutaneous aspiration of cruciate ligament cysts has diagnostic and therapeutic implications. In the proper clinical and imaging setting, aspiration of mucoid fluid definitely indicates a cruciate ligament cyst; then, percutaneous evacuation of the cyst may be effective in relieving the patient's symptoms (De Friend et al. 2001). Both CT and US have been proven useful to guide the cystic puncture using a posterior approach (De Friend et al. 2001). Compared with CT, US is less invasive and allows a real-time assessment of needle tip positioning. Large-bore needles (18 gauge) should be used because of the viscous nature of the intracystic material. If the fluid is too thick to be aspirated, multiple transfixions of the cyst with the needle should be performed to allow breaking of the wall with secondary diffusion and resorption of the mucoid content into the surrounding tissues (Fig. 14.109). An intralesional injection of steroids can also be guided by CT and US.

14.5.5.5 Cruciate Ligament Tears

The diagnosis of cruciate ligament tears is essentially based on clinical findings, including a history of "giving way" of the knee and positive clinical tests, such as the anterior drawer sign obtained at 25° knee flexion, the so-called Lachman test and

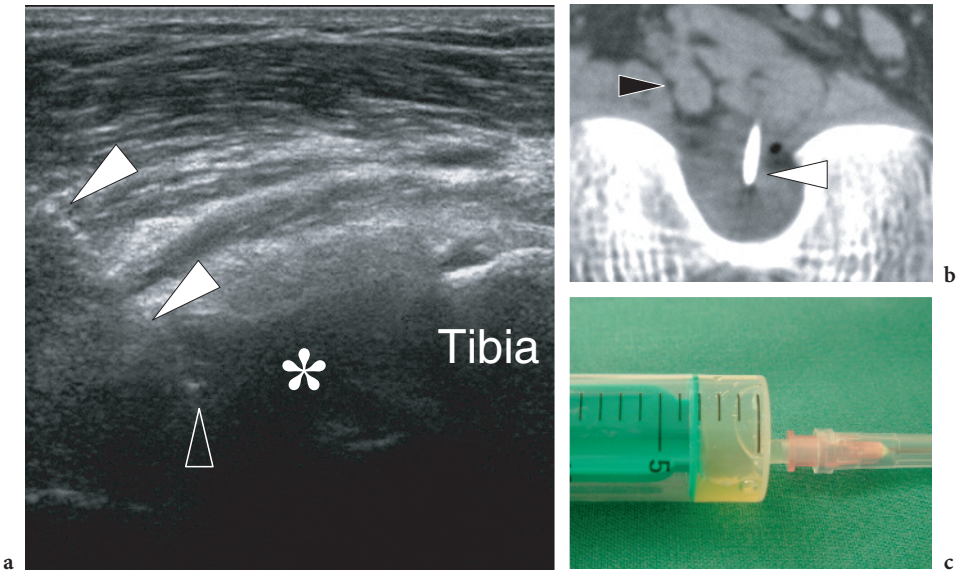

Fig. 14.109a–c. Imaging-guided percutaneous needle aspiration of cruciate ligament ganglia. **a** US-guided procedure. Longitudinal 12–5 MHz US image obtained at the posterior aspect of the knee shows a ganglion cyst (*asterisk*) located posterior to the posterior cruciate ligament. Observe the tip (*open arrowhead*) of the needle (*white arrowheads*) positioned in the cyst under US guidance. **b** CT-guided procedure. The needle tip (*white arrowhead*) is located within a posterior cruciate ligament ganglion. Note the direction of the needle which steers clear of the popliteal artery (*black arrowhead*). **c** Syringe containing the aspirated yellowish mucoid fluid of the ganglion

the jerk test. Nevertheless, diagnostic problems may arise when soft-tissue edema, pain and reflex paraarticular muscle contractions occur. In addition, the clinical diagnosis of partial ruptures may not be so easy. There is no question that MR imaging is the modality of choice for an accurate assessment of the cruciate ligaments. This refers not only to the ability of this technique to depict the tear but also, and more importantly, to demonstrate associated lesions that can be difficult to appreciate at physical examination, including meniscal lesions, bone bruises and small fractures. In recent years some reports have focused on the ability of US to assess the anterior (Fuchs and Chylarecki 2002; Ptasznik et al. 1995; Suzuki et al. 1991; Skovgaard Larsen and Rasmussen 2000) and posterior (Cho et al. 2001; Miller 2002) cruciate ligaments. US detection of a localized fluid collection at the posterocranial portion of the anterior cruciate ligament seems to correlate with acute tears (Ptasznik et al. 1995). Furthermore, US can give an indirect assessment of the integrity of the cruciate ligaments by estimating the degree of tibial subluxation during stress maneuvers (Gebhard et al. 1999).

14.5.4.6 Popliteal Aneurysms

Popliteal aneurysms account for approximately 70% of all peripheral arterial aneurysms and, if untreated, pose a serious threat to the affected limb (Duffy et al. 1998). They predominantly affect men during the sixth and seventh decades of life (the male:female ratio ranges from 10:1 to 30:1) and, in most cases, are undetectable on physical examination, suggesting that US may be appropriate in their recognition among men with severe atherosclerotic disease and abdominal aortic aneurysms. The incidental detection of a popliteal aneurysm during a routine US examination of the knee should be an indication to extend the study to the femoral artery and the abdominal aorta, because a coexistent aortic aneurysm is found in 30–50% patient with a popliteal aneurysm (Wright et al. 2004). In addition, popliteal aneurysms are bilateral in 50–70% of cases. When large, popliteal aneurysms can cause extrinsic compression of the adjacent popliteal vein, possibly leading to leg swelling and deep venous thrombosis. The clinical importance of these lesions, however, is not dependent on their size, as even small aneurysms are associated with a high incidence of thrombosis, clinical symptoms and distal occlusive disease (Asher et al. 2003). US is a reliable means to determine the presence of a popliteal aneurysm and measure its size and extent. Difficulties may arise when the aneurysm is thrombosed. In these instances, the lesion may appear solid and should not be confused with a neurogenic tumor arising from the tibial nerve and other soft-tissue masses of the popliteal space (Fig. 14.110). Color Doppler imaging may help the diagnosis by showing the arterial occlusion and the infrapopliteal run-off. A thrombosed aneurysm requires thrombolitic therapy in patients who can withstand an additional period of ischemia.

The popliteal artery is susceptible to injury due to its proximity to the distal femur and the knee joint. Its occlusion is encountered in 30–50% of patients with knee dislocation (Wright et al. 2004). Occasionally, US can identify popliteal pseudoaneurysms, which may be related to osseous abnormalities such as hereditary multiple exostoses and femoral osteochondromas (Fig. 14.111) (Chamlou et al. 2002; Klebuc et al. 2001). Thrombosis or varicosities of the popliteal vein and its afferent branches can also be diagnosed with US and Doppler techniques (Cronan et al. 1987; Fraser and Anderson 1999).

14.5.4.7 Popliteal Artery Entrapment Syndrome

Popliteal artery entrapment refers to compression of the popliteal artery secondary to the anatomic relationships between the vessel and an abnormal proximal insertion of the medial head of the gastrocnemius or the popliteus. This syndrome is rare and mostly encountered in young healthy males (15:1 male predilection) with symptoms of vascular insufficiency and no evidence of atherosclerotic disease. It may be asymptomatic or may present with progressive calf claudication and absence of arterial pulses on dorsiflexion or plantar flexion of the ankle due to the contraction of the medial head of the gastrocnemius. The phenomenon of popliteal occlusion in response to plantar flexion is, however, highly prevalent in normal asymptomatic population, which makes this test of limited diagnostic value. Chronic arterial compression may lead to vascular microtrauma, stenosis and occlusion of the artery with acute distal ischemia. Therapy involves surgical release of the anomalous band of tissue and, in complicated cases, treatment of vascular occlusion with bypass grafting and thromboarterectomy.

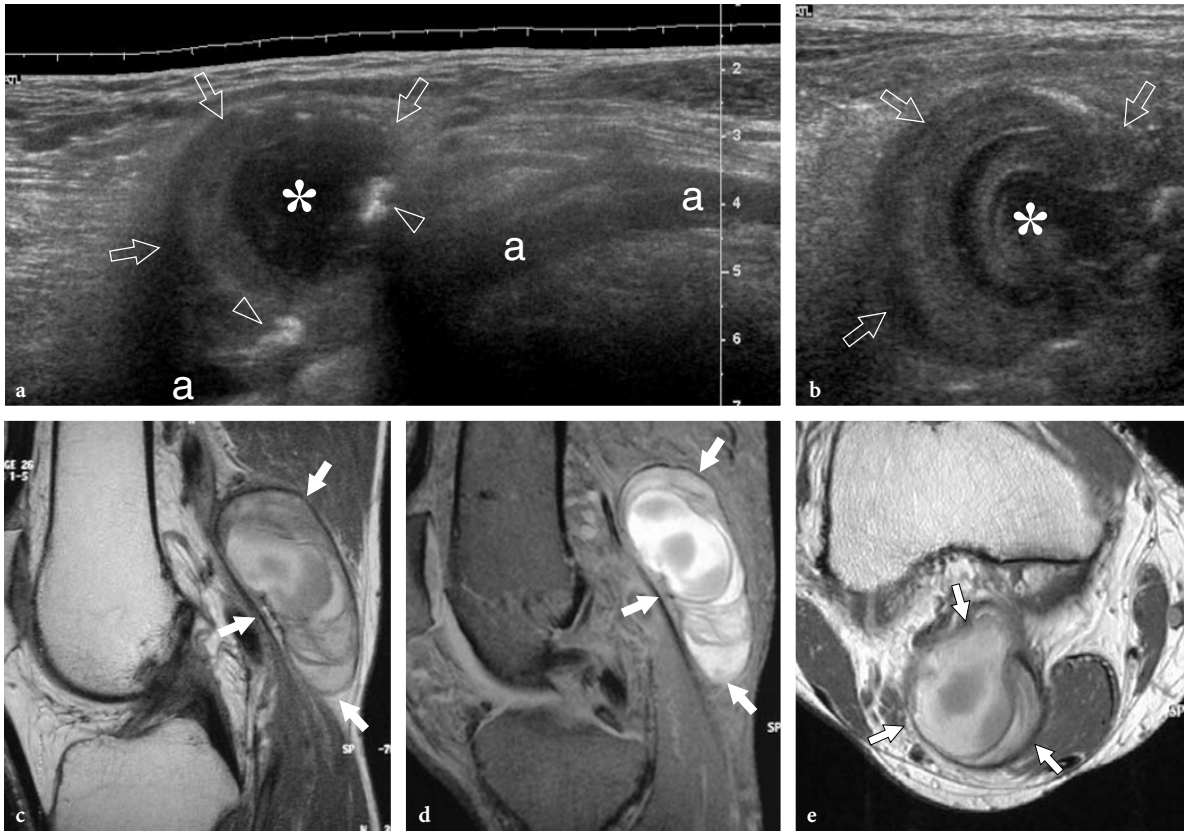

Fig. 14.110a–e. Thrombosed aneurysm of the popliteal artery. **a** Longitudinal extended field-of-view and **b** transverse 12–5 MHz US images over the popliteal fossa in a 68-year-old man who presented with acute ischemia of the left lower extremity demonstrate an occluded aneurysm (*arrows*) of the popliteal artery (*a*). Note the layered appearance of the thrombus (*asterisk*) and some calcified plaques (*arrowheads*) in the walls of the aneurysmal sac. **c** Sagittal T2-weighted, **d** sagittal fat-suppressed T1-weighted and **e** transverse T1-weighted MR images over the popliteal aneurysm (*arrows*) reveal a heterogeneous hyperintense content of the sac reflecting its complete occlusion by thrombus

In normal states, the popliteal artery, the popliteal vein and the tibial nerve lie lateral to the medial head of the gastrocnemius muscle in the popliteal fossa (Fig. 14.113a). In cases of altered embryonic development, five main types of anomalous relationship between the muscle and the artery have been identified as possible cause of extrinsic arterial compression (Rich et al. 1979): in type 1 anomaly, the popliteal artery passes medially around the medial head of the gastrocnemius which arises at its normal site of insertion above the medial femoral condyle (Fig. 14.113b); type 2 anomaly is characterized by an aberrant origin of the medial head of the gastrocnemius which arises from the intercondylar notch and forms a sling around the lateral side of the popliteal artery (Fig. 14.113c); in type 3 anomaly, an accessory medial slip of the medial head of the gastrocnemius arises from the intercondylar notch and forms a sling around the lateral aspect of the popliteal artery (Fig. 14.113d); type 4 anomaly refers to a deep entrapment of the popliteal artery underneath the popliteal muscle or beneath fibrous bands in the popliteal fossa (Fig. 14.113e); type 5 anomaly is somewhat similar to type 1 but refers to also the popliteal vein (Fig. 14.113f). From the practical standpoint, however, this classification system has limited clinical implications, because the identification of the type of anomaly does not affect prognosis and the treatment approach.

On transverse planes, US can identify arterial compression by depicting abrupt narrowing of the vessel lumen within the popliteal fossa, abnormal deviation of the vessel, poststenotic ectasia or aneurysm (Macedo et al. 2003). Changes in the arterial size may be more noticeable during plantar flexion and dorsiflexion of the foot (dynamic stenosis). In some cases, the abnormal sling can be visualized while crossing over the artery, but this sign is inconsistent

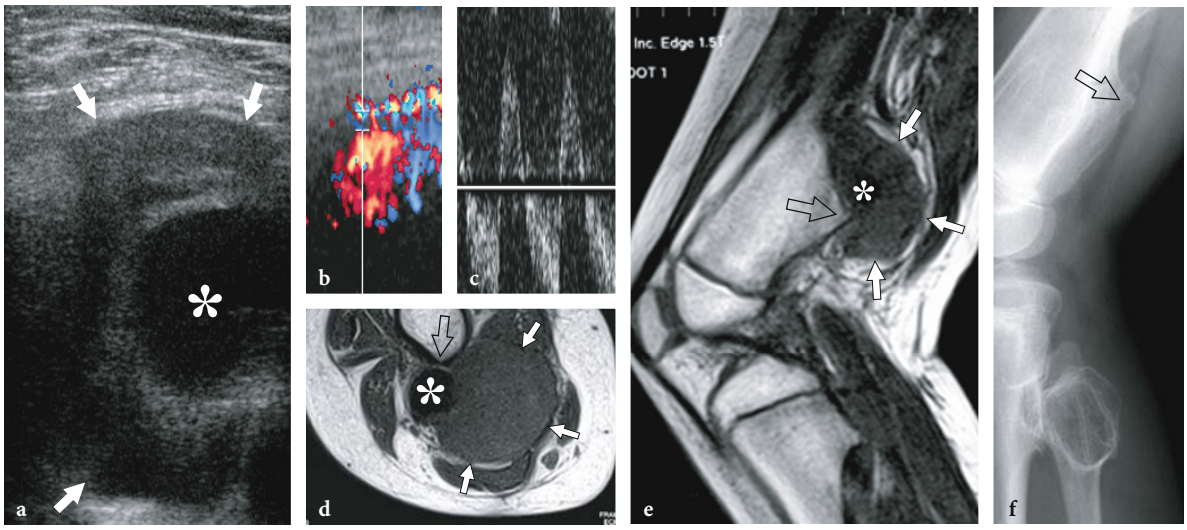

Fig. 14.111a–f. Pseudoaneurysm of the popliteal artery. **a** Transverse 12–5 MHz US image over the cranial part of the popliteal fossa in an 8-year-old girl affected by hereditary multiple exostoses presenting with a rapidly enlarging pulsatile popliteal mass after a fall reveals a large complex mass (*arrows*) with thickened walls and a hypoechoic central cavity (*asterisk*). **b** Longitudinal color Doppler 12-US image and **c** duplex Doppler analysis demonstrate turbulent whirling flow within the cavity and bidirectional velocities as the forward flow in systole is ejected in diastole at the communicating tract of the sac with the popliteal artery reflecting a pseudoaneurysm. **d** Transverse and **e** sagittal T1-weighted MR images confirm a partially thrombosed pseudoaneurysm (*white arrows*) of the popliteal artery in relation with a prominent exostosis (*open arrow*) on the posterior aspect of the femoral shaft. Note the patent portion of the sac indicated by signal void (*asterisk*). **f** Lateral radiograph of the distal thigh demonstrates the exostosis (*arrow*) which led to the traumatic damage of the vessel wall

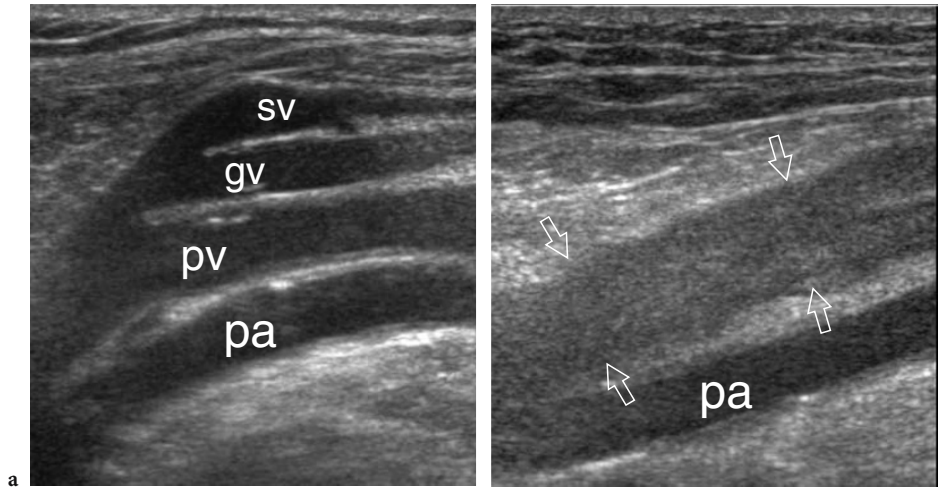

Fig. 14.112a,b. Venous abnormalities in the popliteal fossa. Two different patients. **a** Longitudinal 12–5 MHz US image obtained in the midline of the popliteal fossa of a patient with common femoral vein thrombosis at the groin reveals a multilayered arrangement of vessels reflecting, from depth to surface, the popliteal artery (*pa*) and a series of ectatic veins including the popliteal vein (*pv*), tributaries of the genicular veins (*gv*), and the small saphenous vein (*sv*). **b** Longitudinal 12–5 MHz US image over the popliteal vessels demonstrates complete thrombosis of the popliteal vein (*arrows*). Observe the distended lumen of the vein which contains echogenic material compared with the underlying patent popliteal artery (*pa*)

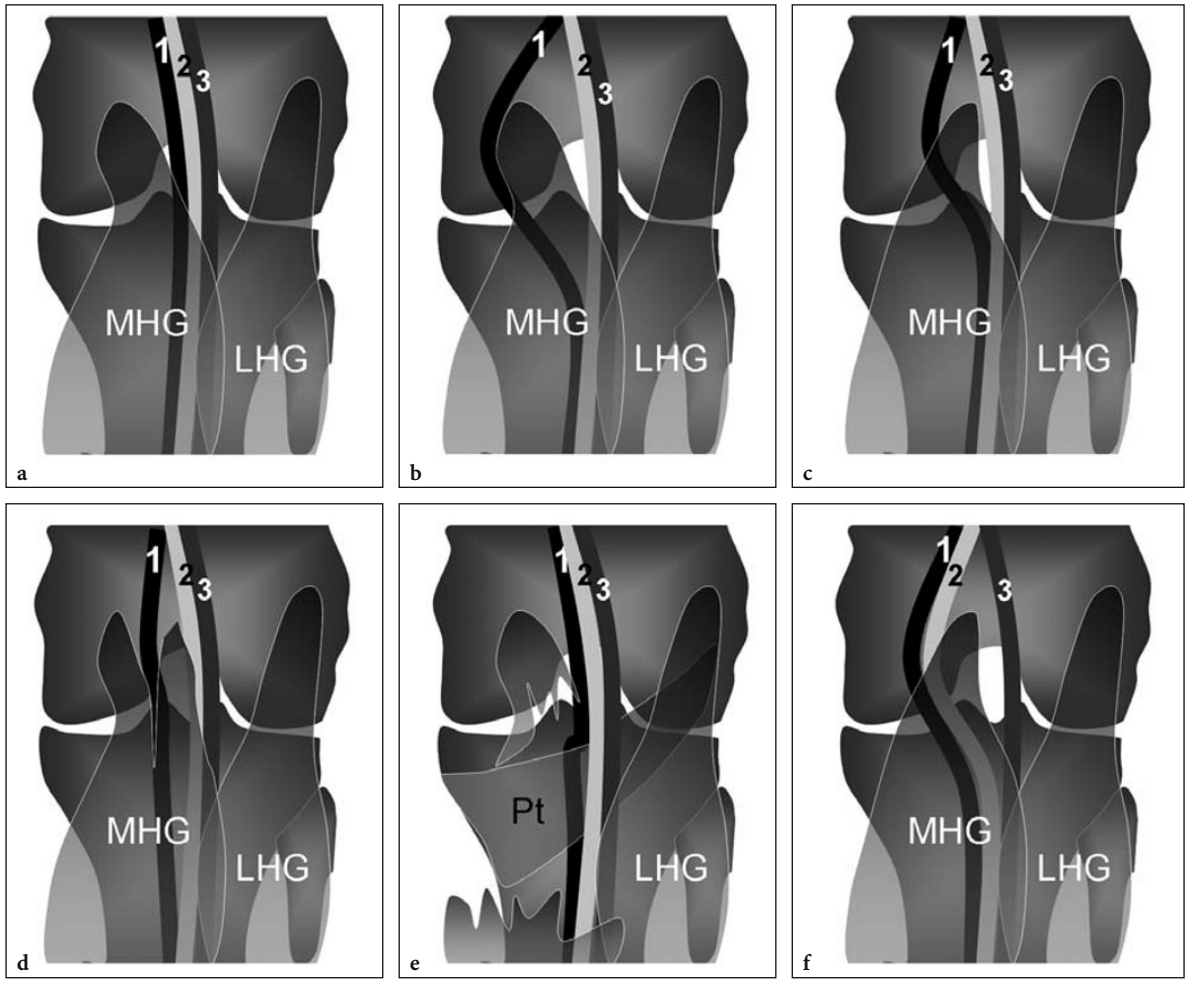

Fig. 14.113a–f. Popliteal artery entrapment syndrome. **a–f** Schematic drawings illustrate the classification system for popliteal artery entrapment syndrome. **a** Normal anatomy of the popliteal fossa. Popliteal artery (*1*), popliteal vein (*2*) and tibial nerve (*3*) course lateral to the medial head of the gastrocnemius muscle (*MHG*). **b** In type 1 anomaly, the medial head of the gastrocnemius muscle is normal, and the popliteal artery is displaced medially around and beneath the muscle. **c** In type 2 anomaly, the medial head of the gastrocnemius originates from an abnormal lateral position. The popliteal artery descends normally but passes medial to and beneath the muscle. **d** In type 3 anomaly, the popliteal artery is compressed by an anomalous slip of the gastrocnemius muscle. **e** In type 4 anomaly, the popliteal artery is entrapped by a fibrous band or by the popliteus (*Pt*) muscle. **f** In type 5 anomaly, both popliteal artery and vein are displaced medially around and beneath the gastrocnemius. *LHG*, lateral head of the gastrocnemius muscle

and the different types of anomaly cannot reliably be distinguished with US (Figs. 14.114, 4.35). Duplex and color Doppler imaging should be always obtained to confirm the stenosis by depicting increased peak systolic velocities and a fall in distal blood flow, as well as to rule out vessel thrombosis (Wright et al. 2004). Compared with US, MR imaging is superior in depicting the abnormal muscular anatomy responsible for the entrapment and drawing a vascular map of the lesion using MR-angiographic techniques (Elias et al. 2003; Macedo et al. 2003). This imaging modality should always be used to evaluate the anatomy of the popliteal fossa and vascular compromise. On the other hand, conventional angiography is reserved for acute cases in which arterial occlusion leads to a limb-threatening ischemia and in a preoperative setting.

14.5.5 Joint and Bone Disorders

Differentiation between knee joint disorders from para-articular pathologies is clinically relevant because treatment and prognosis are different. Although the role of US is well-established for assessment of joint effusions and intra-articular

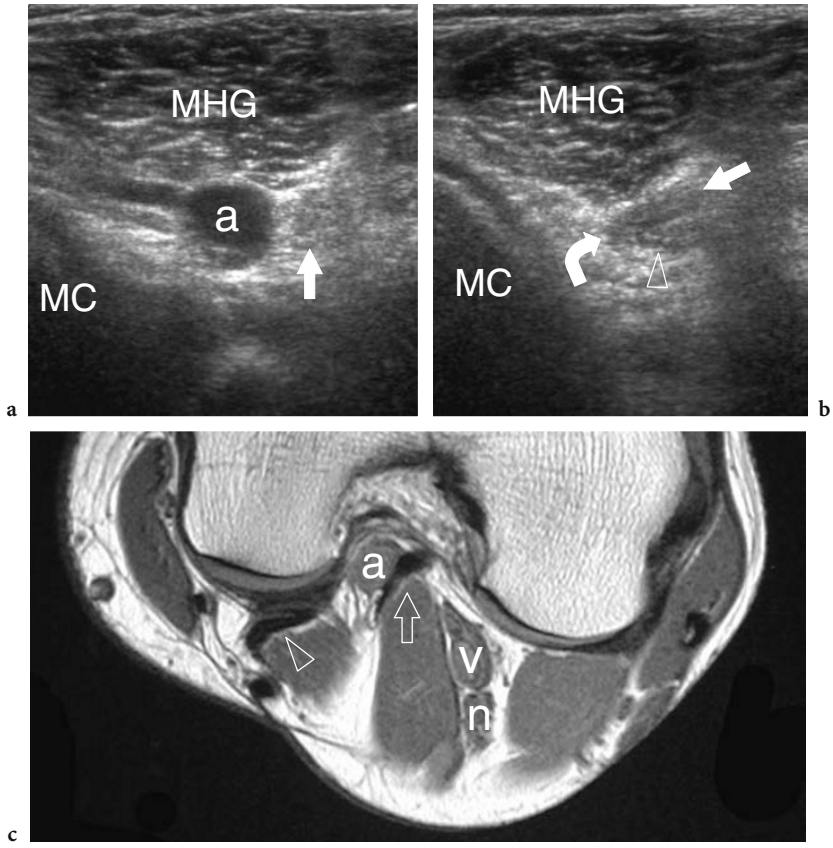

Fig. 14.114a–c. Popliteal artery entrapment syndrome. **a,b** Transverse 12–5 MHz US images obtained over the popliteal fossa in a 25-year-old runner presenting with acute claudication of the right lower extremity. **a** Proximal US image demonstrates a normal-appearing popliteal artery (*a*) located deep to the medial head of the gastrocnemius muscle (*MHG*). Note the abnormal hyperechoic tendinous structure (*straight arrow*) lying on the lateral side of the vessel. **b** At a more distal level, the lumen of the popliteal artery (*arrowhead*) appears compressed by the anomalous tendinous band (*arrows*). This sign suggests a popliteal entrapment. *MC*, medial femoral condyle. **c** Transverse T1-weighted MR image confirms the presence of an accessory slip (*arrow*) of the medial head of the gastrocnemius (*arrowhead*) coursing lateral to the artery (*a*). This slip separates the artery from the popliteal vein (*v*) and the tibial nerve (*n*). MR imaging allowed this muscle abnormality to be categorized as a type 3 anomaly

loose bodies, the information obtained in degenerative conditions and meniscal pathology has intrinsic limitations and should always be substantiated with other imaging modalities.

14.5.5.1 Knee Synovitis

In general, knee intra-articular effusion of less than 6–8 ml cannot be appreciated clinically. Below this threshold, lateral X-ray projections are able to demonstrate intra-articular fluid by demonstrating the "fat pad separation sign", which consists of the presence of a soft-tissue opacity >5 mm between the suprapatellar fat and the prefemoral fat (Fig. 14.115). This sign has been reported positive even for effusions of 2 ml (Hall 1975). MR imaging has proved to be an excellent modality for detecting small amounts of fluid. Based on the intra-articular injection of cadaveric knees, some authors have documented so high a sensitivity of this technique as to detect even a 1 ml effusion (Schweitzer et al. 1992). Such a small quantity of fluid is delineated as a thin rim lying between the condyles and the Hoffa fat pad. With increasing amounts (3 ml), the fluid is consistently detected in the suprapatellar recess. We routinely assess fluid effusions with US in this recess (Fig. 14.116). A careful scanning technique avoiding excessive pressure with the probe on the skin should be used for this purpose because there may be a shift of fluid toward other synovial recesses. The smallest collections can occasionally be demonstrated only at the level of the medial and lateral parapatellar

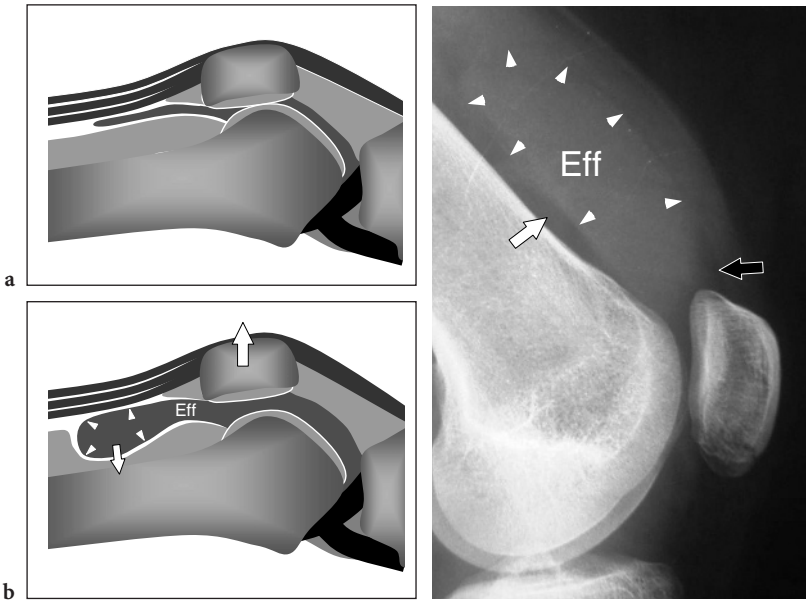

Fig. 14.115a–c. Suprapatellar recess: intra-articular effusion. **a,b** Schematic drawings illustrate **a** the normal suprapatellar recess and **b** the recess distended by an intra-articular effusion (*arrowheads*). In **b**, the fluid contained in the recess (*eff*) squeezes (*arrows*) the prefemoral fat against the femur and displaces the patella anteriorly. **c** Corresponding lateral radiograph reveals the effusion (*Eff*) inside the suprapatellar recess as a mild and homogeneous soft-tissue radiopacity located between the suprapatellar (*black arrow*) and the prefemoral (*white arrow*) fat pads

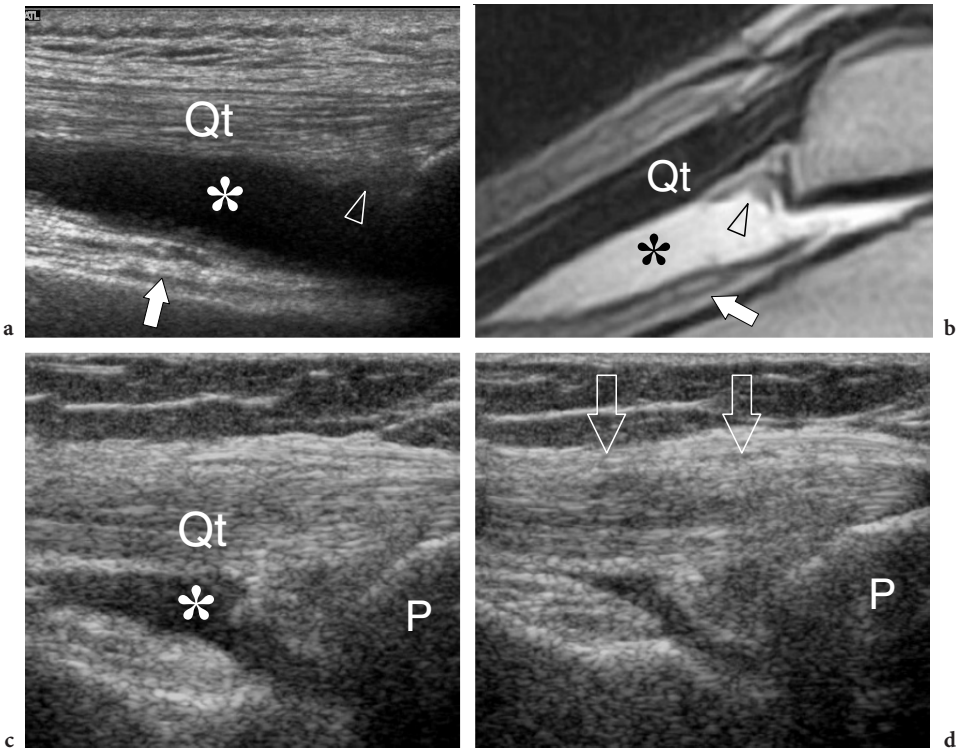

Fig. 14.116a–d. Suprapatellar recess: intra-articular effusion. **a** Longitudinal 12–5 MHz US image obtained over the quadriceps tendon (*Qt*) with **b** sagittal T2-weighted MR imaging correlation reveals a suprapatellar recess distended by intra-articular effusion (*asterisk*). Note that the fluid collects between the suprapatellar (*arrowhead*) and the prefemoral (*arrow*) fat pads. **c,d** Longitudinal 12–5 MHz US images obtained in another patient **c** under normal conditions and **d** while applying pressure (*open arrows*) with the transducer over it. During compression, the fluid contained in the recess (*asterisk*) is displaced away from it. *P*, patella

recesses, as these are the most dependent recesses of the knee while the patient is supine. When looking for a knee effusion, the examiner should be aware that changes in the patient's position can cause a shift of the fluid toward sites not subjected to pressure (Singer 1985). When a discrete effusion is present, US may be helpful to select the best site for puncture as well as to prove the correct intra-articular positioning of the needle. Usually, US-guided arthrocentesis is less painful than blind punctures.

The suprapatellar recess is the preferred site for synovial membrane assessment in knee disorders. Its routine examination is almost always completed using transverse US images obtained over the lateral and medial parapatellar recesses (Backhaus et al. 2001). In normal conditions, the synovial membrane is too thin to be detected at US examination. Following a variety of local or systemic disorders, the synovium can undergo hypertrophy to reach a thickness detectable at US (Fig. 14.117). The appearance of synovial membrane hypertrophy should be considered nonspecific, and it does not allow a precise differentiation among various pathologies (Wang et al. 1999a). The thickened synovium leads to a hypoechoic appearance of the recess walls and may show projections within the joint cavity. Depending on the degree of hypertrophy, the synovial pannus can fill the articular cavity in part or completely. Synovial proliferation is one of the early manifestations of rheumatoid arthritis and its detection has practical importance because it can indicate early aggressive treatment to try to limit extensive erosive changes, tears of para-articular ligaments and tendons as well as functional disabilities.

Somewhat similar to gadolinium-enhanced MR imaging, color and power Doppler techniques have been proved to be useful means of distinguishing active (hypervascular) from fibrous (hypovascular) pannus. Demonstration of a hypervascular pannus has therapeutic implications as it correlates with disease activity (Carotti et al. 2002). Microbubble-based contrast agents seem promising in this field to enhance the sensitivity of US to detect synovial blood flow and assess the response to therapy in patients with rheumatoid arthritis (Doria et al. 2001; Taylor et al. 2004). As for the suprapatellar recess, US can assess similar pathologic changes at the level of the lateral and medial parapatellar pouches (Fig. 14.118).

14.5.5.2 Lipohemarthrosis

Lipohemarthrosis can be defined as the occurrence of blood and fat within an articular cavity. This is a common finding in acutely injured knees with a fracture involving the articular surfaces or a severe

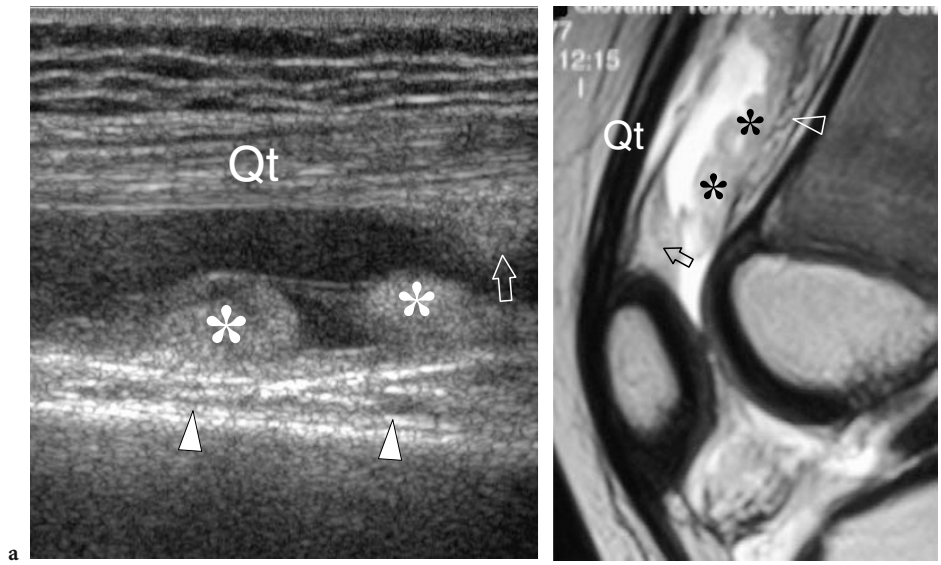

a b

Fig. 14.117a,b. Subquadriceps recess: synovial hypertrophy. **a** Longitudinal 12–5 MHz US image obtained over the quadriceps tendon (*Qt*) in a child with juvenile idiopathic arthritis with **b** sagittal T2-weighted MR imaging correlation demonstrates nodular thickenings (*asterisks*) of the synovial membrane associated with intra-articular effusion (*asterisk*). Synovial hypertrophy must be distinguished from the suprapatellar (*arrow*) and prefemoral (*arrowhead*) fat pads based on its location and echotexture

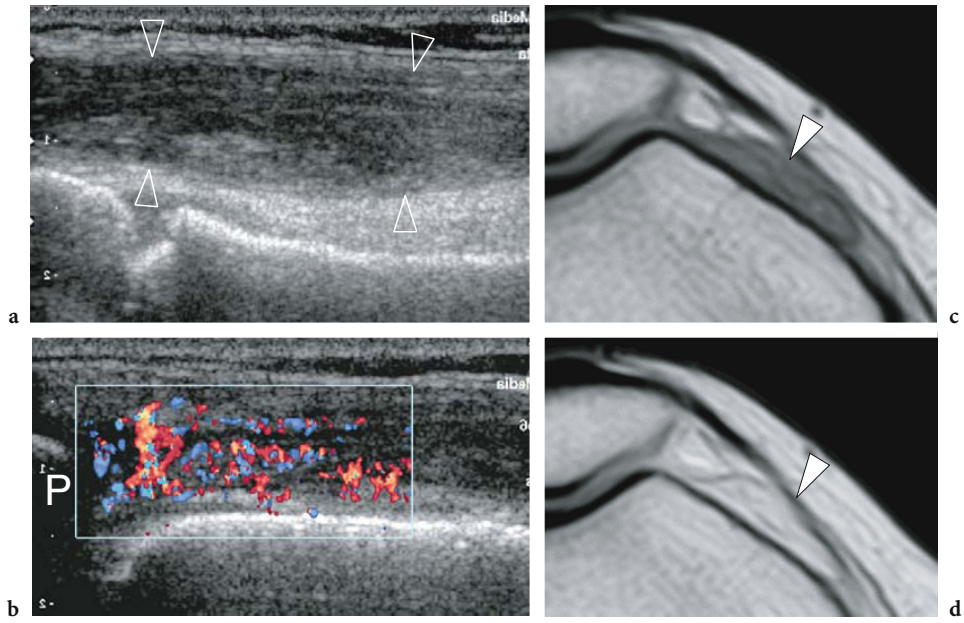

Fig. 14.118a–d. Parapatellar recess: synovial hypertrophy. **a** Transverse gray-scale and **b** color Doppler 12–5 MHz US image obtained over the medial aspect of the knee at the level of the patella in a child with juvenile idiopathic arthritis shows abundant synovial pannus filling the parapatellar recess as a band of hypoechoic tissue (*arrowheads*) intermingled with fluid. *P*, patella. Marked synovial hyperemia is observed at color Doppler examination indicating active pannus. **c,d** Corresponding transverse T1-weighted MR images obtained **c** before and **d** after intravenous contrast material administration confirm thickening of the synovium (*arrowhead*) in the parapatellar recess. In the postcontrast scan, note the marked enhancement of the pannus which parallels the color Doppler image

capsuloligamentous injury. In patients with intra-articular fractures, the fat found inside the joint cavity derives from yellow bone marrow, whereas in capsuloligamentous tears it derives from the synovial membrane or from the intra-articular fat pads. The clinical importance of lipohemarthrosis relies on the fact that its presence in a traumatized patient with negative radiographic studies suggests a nondisplaced fracture or a severe intra-articular lesion which warrants further imaging evaluation. Standard radiographs recognize lipohemarthrosis by demonstrating a fat-fluid level resulting from floating of the fat on the blood (Fig. 14.119a) (Butt et al. 1983). A double fat-fluid level can be seen when a suprapatellar plica or lobulations of the capsule are present (Sandretto and Carrera 1983). Both MR and CT imaging can easily reveal lipohemarthrosis. CT shows a fat-fluid level with the typical negative density of fat overlying the blood (Fig. 14.119b). On the other hand, MR imaging may depict a four-layer effusion which includes, from superficial to deep: fat, chemical shift artifact, serum and red blood cells (Kier and McCarthy 1990). Similar to these techniques, US can identify a layered appearance of the intra-articular effusion (Bianchi et al. 1995b). In a routine posttraumatic study, the incidental detection of lipohemarthrosis with US should alert the examiner to the possibility of an intra-articular fracture. An experimental setting demonstrated that the US appearance of lipohemarthrosis critically depends on the time of examination (Bianchi et al. 1995b). In this study a mixture of cooking oil and fresh blood in a bag was examined at various time intervals. Early US images (obtained at 1 and 5 min) revealed a two-layered appearance consisting of a hyperechoic superior band corresponding to the fat floating inside the bag and an inferior band of intermediate echogenicity related to the blood. Delayed images (obtained at 30 min) displayed a three-layered pattern with an intermediate thin anechoic band corresponding to the serum over the cellular blood component. In practice, patients immobilized for long periods of time (more than 30 min) reveal a three-layered pattern while those mobilized have only a two-layered pattern (Fig. 119c,d). While examining post-traumatic knees, care should be taken not to confuse the normal suprapatellar fat pad with free fat floating on the effusion. In these

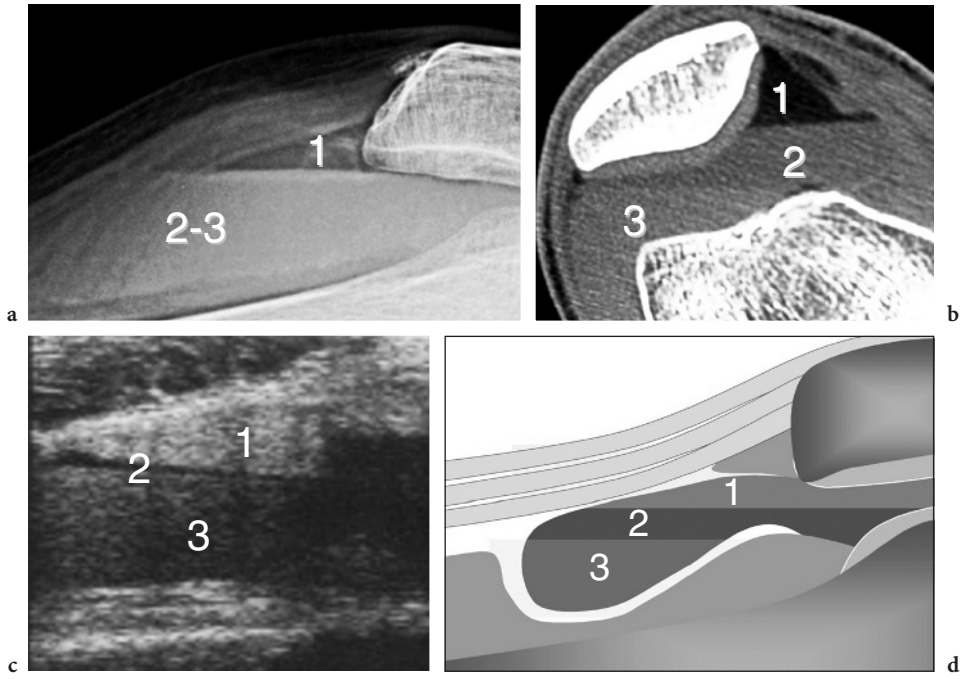

Fig. 14.119a–d. Lipohemarthrosis. **a** Horizontal cross-table radiograph of the suprapatellar recess in a patient with acute knee fracture shows a radiolucent fatty layer (*1*) overlying a more opaque layer reflecting the blood (*2-3*). This radiograph does not allow further differentiation between serum and red blood cells. **b** Transverse CT scan reveals the typical trilaminar appearance of lipohemarthrosis consisting of hypodense fat (*1*), intermediate-density serum (*2*) and hyperdense blood cells (*3*). **c** Longitudinal 12–5 MHz US image of the suprapatellar recess distended by lipohemarthrosis with **d** schematic drawing correlation shows a trilaminar appearance due to sedimentation of fluid-fluid levels: hyperechoic fat (*1*) anechoic serum (*2*) and hypoechoic red blood cells (*3*)

cases, squeezing the suprapatellar recess can be helpful to mix the different components of the effusion and to cause the disappearance of the fat-fluid level. Compared with other imaging modalities, the main advantage of US is its ability to diagnose lipohemarthrosis after only a minute of immobilization. An accurate assessment of the suprapatellar recess to rule out a floating hyperechoic band should be part of the routine US examination in all traumatized knees.

14.5.5.3 Intra-articular Loose Bodies

The knee is the joint most commonly affected by intra-articular loose bodies (Milgram, 1991). Fragments may derive from either traumatic injuries (i.e., transchondral fractures and osteochondritis dissecans) or a variety of joint disorders (i.e., degenerative osteoarthritis, neuropathic joint disease) in which the articular surfaces are severely damaged and fragmented. More rarely, loose bodies can be found in primary and secondary synovial osteochondromatosis, a disease characterized by foci of chondral and osseous metaplasia in the synovium leading to the formation of multiple loose bodies of similar shape and size (Milgram, 1991). Irrespective of their origin, the fate of the fragments depends on their composition: osseous fragments undergo necrosis as they lack of a proper vasculature, whereas mixed (chondral and osteochondral) lesions can increase in size due to the progressive apposition of cartilage on their surface (Milgram et al. 1978). The clinical findings mainly depend on the mobility of the fragments. Fragments that are adherent to the internal joint wall as a result of local inflammation or fibrosis or are embedded within the synovial membrane are usually asymptomatic because they are not trapped between the articular surfaces. On the other hand, even small mobile fragments can be symptomatic when trapped between the articular surfaces and may present intermittent symptoms with joint locking, limitation of motion, pain and joint effusion. In chronic cases, the progressive damage to the joint surfaces leads to cartilage and subchondral erosions

that can ultimately result in secondary osteoarthritis and chronic disability. In a traumatic setting, the sites from which intra-articular loose bodies more commonly arise include the articular surfaces of the patella, the lateral trochlea and the weight-bearing surfaces of the femoral condyles. The main differential diagnosis of intra-articular loose bodies is displaced meniscal fragments, a common cause of intermittent joint locking.

US has proved to be an effective imaging modality for detection and characterization of intra-articular loose bodies (Bianchi and Martinoli. 1999). Because the suprapatellar recess is the widest recess of the knee, it is not surprising that it is the most common location for intra-articular loose bodies (Fig. 14.120). Fragments may appear as hyperechoic structures with posterior acoustic shadowing (osseous and chondral calcified fragments), hypoechoic structures without posterior attenuation of the US beam (purely chondral nature) and hyperechoic images covered by a hypoanechoic rim (osteochondral fragments) (Figs. 14.98, 14.99). The presence of anechoic fluid surrounding the fragments greatly enhances the diagnostic confidence (Fig. 14.121). Consequently, all efforts should be made to shift as large an amount of fluid as possible into the recess to be examined. This can be achieved by asking the patient to contract the quadriceps or simply by pushing the fluid in a cranial direction with the hand. Then, examining the knee in an extended position can avoid squeezing the fluid away from the suprapatellar recess. If a retropatellar fragment is suspected on standard radiographs, examining the knee with different degrees of flexion can move the patella distally from over the fragment (Fig. 14.122). Overall, a conclusive US diagnosis of intra-articular loose bodies basically relies on demonstration of fluid surrounding the fragment or fragment displacement. Flexion and extension movements of the knee and a change in the patient's position (standing vs. supine) can induce mobilization of the fragments. Display of motion excludes synovial and capsular calcifications. If the recess does not contain fluid, intra-articular loose bodies can be found between the prefemoral fat pad and the quadriceps tendon. In this cases, fragments are more difficult to see. Osteophytes of the superior edge of the trochlea can be imaged on longitudinal US images just deep to the patella and should be differentiated from intra-articular loose bodies. Because they are formed by hyperechoic cortical bone covered by a thin layer of cartilage, trochlear osteophytes may mimic a loose body positioned underneath the patella. Correlation of US findings with standard radiographs and examining the trochlea during forced flexion of the knee allow a correct diagnosis.

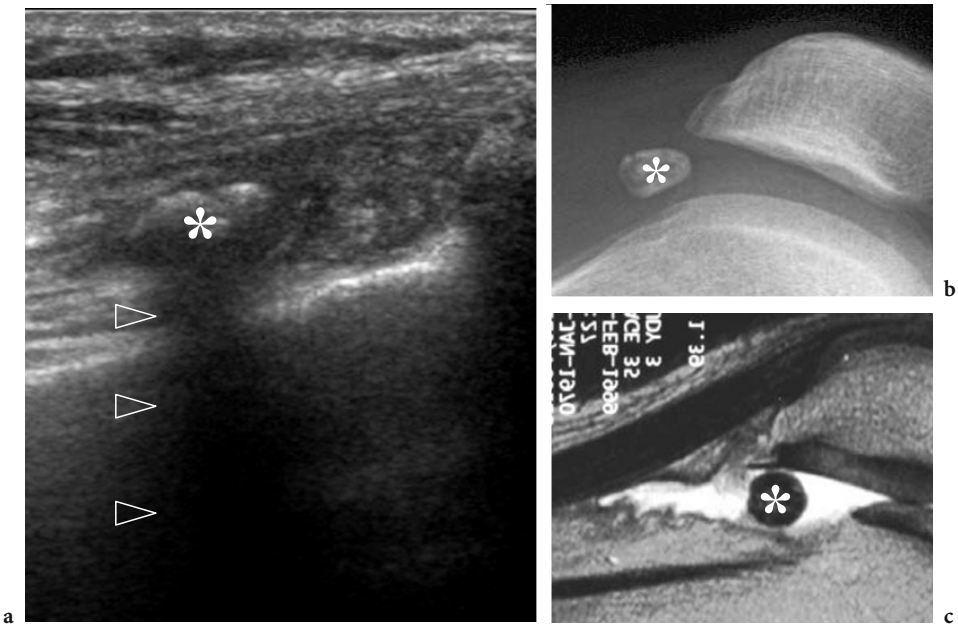

Fig. 14.120a–c. Intra-articular loose body. **a** Longitudinal 12–5 MHz US image of the suprapatellar recess performed with the knee flexed shows a calcified loose body (*asterisk*) as a hyperechoic fragment with posterior acoustic shadowing (*arrowheads*) located within the suprapatellar recess. **b** Corresponding laterolateral radiograph and **c** sagittal T2-weighted MR image obtained with mild knee flexion confirm the presence of a calcified intra-articular fragment (*asterisk*)

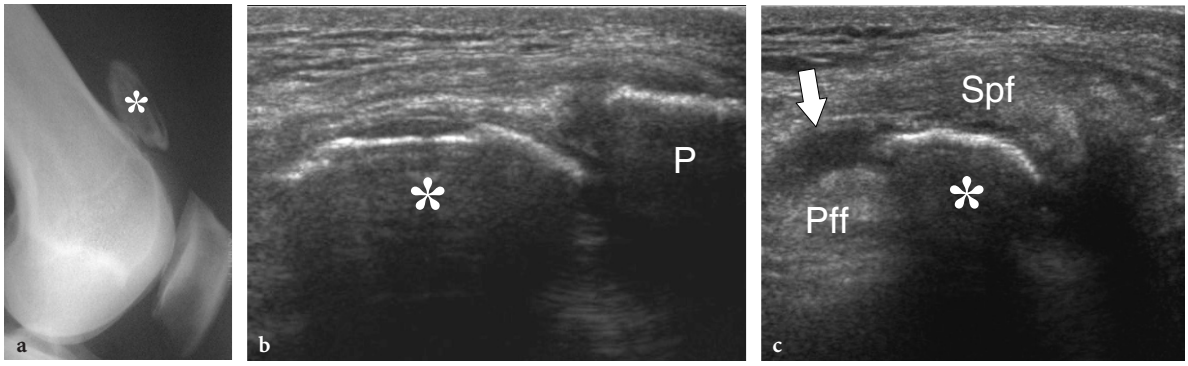

Fig. 14.121a–c. Intra-articular loose body. **a** Laterolateral radiograph of the knee reveals a calcified fragment (*asterisk*) anterior to the metaphysis of the femur. **b** Longitudinal and **c** transverse 12–5 MHz US images of the suprapatellar recess depict the fragment (*asterisk*) as an osseous structure with posterior acoustic shadowing, very similar to the patella (*P*). In the absence of significant intra-articular effusion, the US diagnosis of a loose body is essentially based on demonstration of its location within the suprapatellar recess, between the suprapatellar (*Spf*) and the prefemoral (*Pff*) fat pads

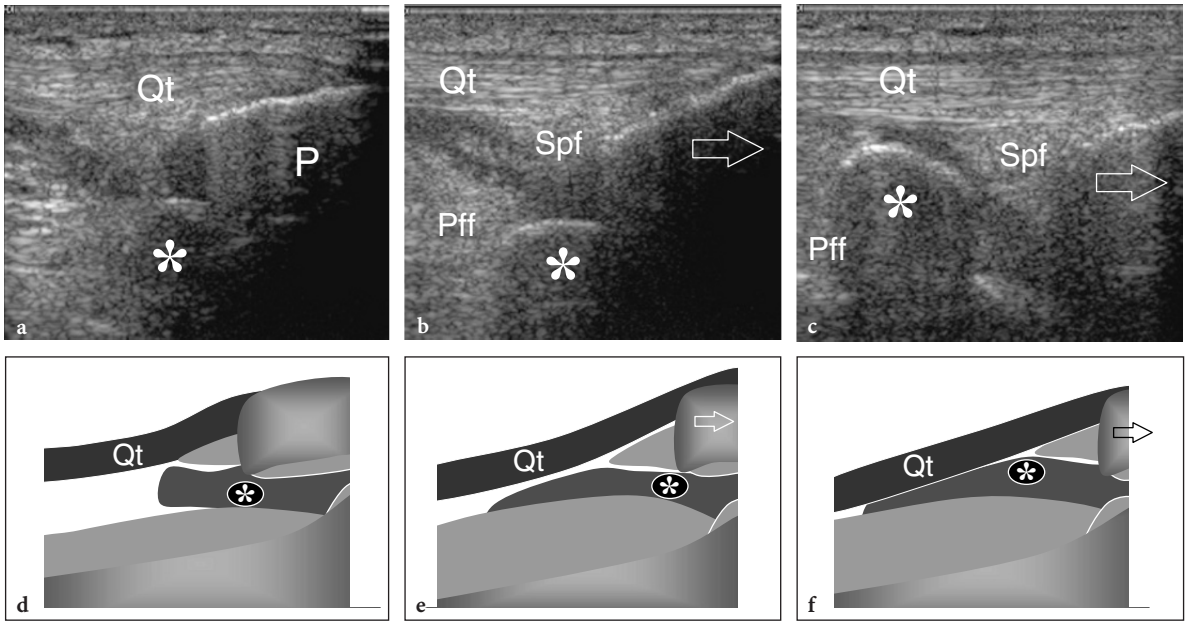

Fig. 14.122a–f. Intra-articular loose bodies: technique of examination. **a–c** Longitudinal 12–5 MHz US images of the suprapatellar recess obtained during progressive degrees of knee flexion with **d–f** corresponding schematic drawings. In **a**, the loose fragment (*asterisk*) is barely visible as it is masked by the overlying posterior acoustic shadowing of the patella (*P*). *Qt*, quadriceps tendon. **b,c** During progressive degrees of knee flexion, the patella moves distally (*open arrow*) relative to the femoral trochlea. This gradually improves the US visualization of the calcified loose body (*asterisk*) and makes it manifest between the suprapatellar (*Spf*) and prefemoral (*Pff*) fat pads

14.5.5.4 Cartilage Abnormalities and Osteoarthritis

With 20°–30° of knee flexion, the patella overlies the trochlea and prevents its US evaluation. Full knee flexion is needed to displace the patella distally, allowing a good evaluation of the trochlear cartilage (Aisen et al. 1984). Although some conditions, such as joint effusion and degenerative pathology, may restrict knee flexion movements, an adequate assessment of the femoral trochlea can be obtained with US in most patients. In large joint effusions, arthrocentesis has been suggested as a preliminary step to permit maximal flexion of the knee (Iagnocco et al. 1992). Elementary changes of the trochlear cartilage have been investigated with

US in degenerative and inflammatory conditions (McCune et al. 1990; Iagnocco et al. 1992; Sureda et al. 1994). They include abnormalities of the cartilage thickness and of the cartilage-subchondral bone or cartilage-joint fluid interfaces (Figs. 14.123, 14.124). Thinning of the cartilage is observed in both degenerative and inflammatory conditions, although the degree of decreased thickness tends to be less pronounced in rheumatoid arthritis. This parameter can, however, be difficult to measure in pathologic knees due to indistinct cartilage boundaries. The acoustic interfaces between cartilage and joint space or cartilage and subchondral bone can be more reliably assessed with US. In pathologic states, both may appear indistinct and less defined than in normal joints. In a study comparing US images and operative findings in a series of osteoarthritic patients who underwent total knee replacement, the loss of hypoechoic appearance of the cartilage and the reduced sharpness of the superficial cartilage interface were found to be the most reliable predictors of cartilage abnormalities, while quantification of cartilage thickness was less useful (McCune et al. 1990). Alterations of the deep cartilage interface can also be appreciated as an increased echogenicity between cartilage and subchondral bone reflecting bone sclerosis. Overall, the trochlear cartilage can effectively be evaluated with US if a proper scanning technique based on transverse planes over the suprapatellar region is used in a maximally flexed knee. One should be aware that qualitative changes are more reliable indicators of the cartilage status than quantitative assessment of cartilage thickness. In patellofemoral osteoarthritis, focal thinning and loss of sharpness of the cartilage at the level of the lateral facet of the trochlea are common findings. Calcifications of the trochlear cartilage can be related to calcium pyrophosphate dehydrate crystals deposition disease (chondrocalcinosis, pseudogout). US is able to detect crystals deposits within the cartilage as a series of bright dots usually located within the middle third of the cartilage thickness (Fig. 14.125) (Sofka et al. 2002).

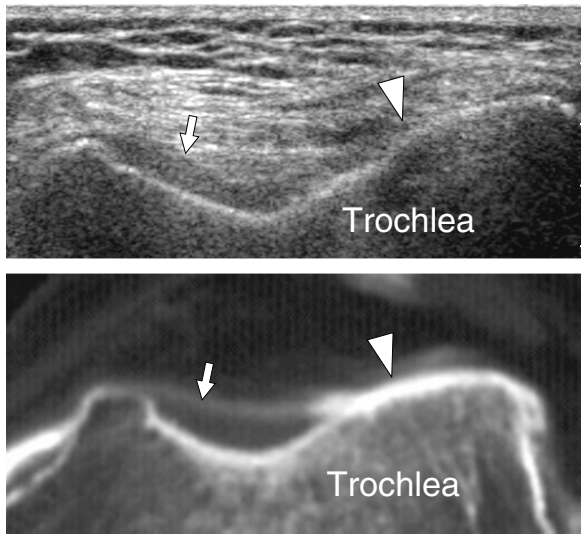

a

b

Fig. 14.123a,b. Trochlear cartilage abnormalities. **a** Transverse 12–5 MHz US of the anterior aspect of the knee obtained during full flexion in a patient with osteoarthritis shows marked thinning of the cartilage of the lateral facet (*arrowhead*) compared with the normal cartilage (*arrow*) which invests the medial facet of the trochlea. **b** Corresponding transverse CT-arthrographic image confirms the absence of the lateral cartilage (*arrowhead*) and a normal medial cartilage (*arrow*)

An accurate evaluation of the depth of the trochlear sulcus is important in the assessment of patellar instability. In fact, a relatively flat sulcus can be an insufficient restraint on the patella during knee flexion. While examining the trochlea, one should consider that the bone sulcus angle (measured at the hyperechoic profile of the subchondral bone) can be different from that of the cartilaginous sulcus (measured at the surface of the hypoechoic cartilage). The evaluation of the sulcus can be obtained by means of radiographic (tangential view of the patellofemoral joint) or CT examinations. Both modalities, however, allow evaluation of the bony sulcus but not the cartilaginous one. Compared with CT, US has proved to be equally effective in the measurement of the bony sulcus (mean value of sulcus angle, 132°) (Martino et al. 1998). More recently, the bone and the cartilaginous sulcus have been evaluated with US in a pediatric series comparing patients with patellar dislocation and normal adolescents (Nietosvaara and Aalto 1997). In this series, the cartilaginous sulcus angle was significantly wider in the patient group than the controls (154°–195° vs. 134°–153°). In addition, patients with patellar instability had a wider cartilaginous sulcus than osseous sulcus. Since the osseous and cartilaginous sulci may have different angles and the latter seems to be functionally more important, imaging techniques able to study the cartilaginous angle, such as US, should be intrinsically more adequate for this assessment.

Standard posteroanterior radiographs obtained with the patient standing and keeping the knee at 20° of flexion are necessary for an accurate examination of the femorotibial space. US can be useful to evaluate the medial and lateral joint spaces by means of coronal planes with the patient standing. US scanning with the patient supine can be effective

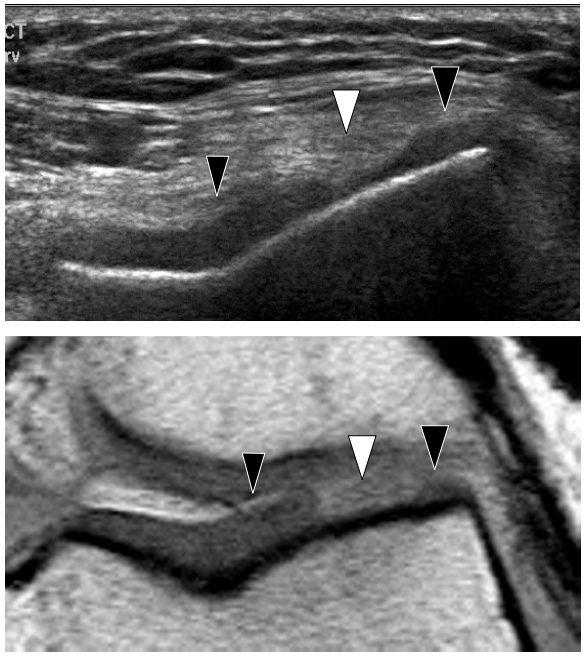

Fig. 14.124a,b. Trochlear cartilage abnormalities. **a** Transverse 12–5 MHz US image of the anterior aspect of the knee obtained during full joint flexion reveals marked thinning of the cartilage of the middle third of the lateral facet (*white arrowhead*). The cartilage of the medial and lateral third (*black arrowheads*) of the lateral facet retains a normal thickness. **b** Transverse proton density MR imaging correlation confirms the US finding

if a varus-valgus stress is applied during the examination (Fig. 14.126). Changes in the joint space with different degrees of knee flexion can reflect the involvement of different parts of the condylar and tibial surface. Severe narrowing of the medial joint space may lead to medial meniscus extrusion and stretching of the superficial layer of the medial collateral ligament. The meniscus is considered "extruded" when it extends superficial to the tibial margin as a result of disruption of collagen fibers within the meniscus that provide hoop strength (Fig. 14.127). When this condition is identified, a high likelihood exists that a meniscal tear is present resulting in disruption of meniscal stability (Costa et al. 2004).

14.5.5.5 Meniscal Cysts

Meniscal cysts are parameniscal lesions filled with thick mucoid fluid that are usually secondary to degenerative meniscal tears. They affect more commonly the lateral meniscus and the right knee and are associated with horizontal or oblique cleavage meniscal tears. From the pathomechanical standpoint, the synovial fluid enters the meniscal body and produces a small intrameniscal cyst. Fluid

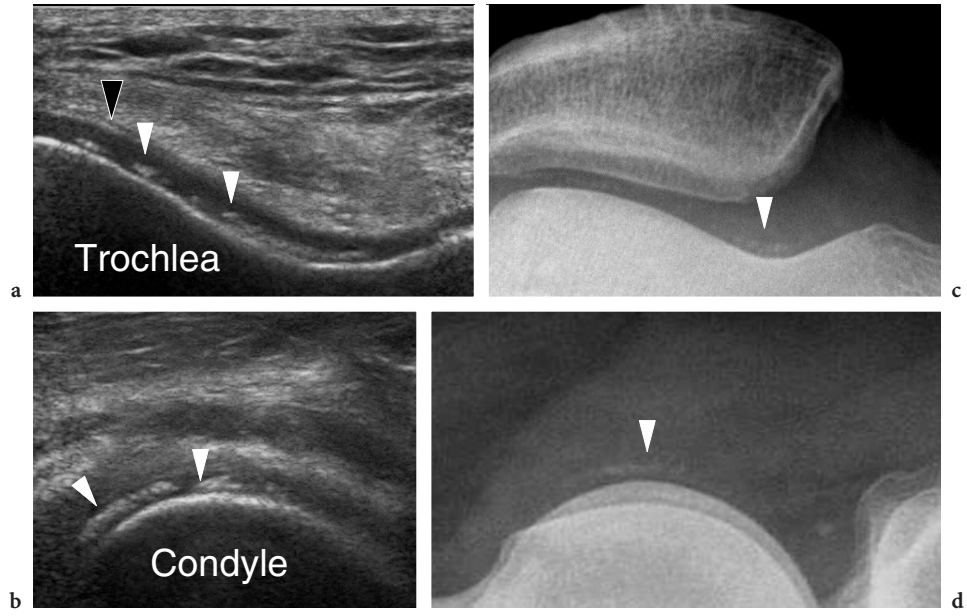

Fig. 14.125a–d. Chondrocalcinosis. **a** Transverse and **b** longitudinal 12–-5MHz US images obtained over the trochlea (**a**) and the medial femoral condyle (**b**) with **c**,**d** radiographic correlation demonstrate fine hyperechoic spots (*white arrowheads*) located in series within the hyaline cartilage, reflecting calcium pyrophosphate dehydrate crystal deposition disease. Note the smooth cartilage outline (*black arrowhead*)

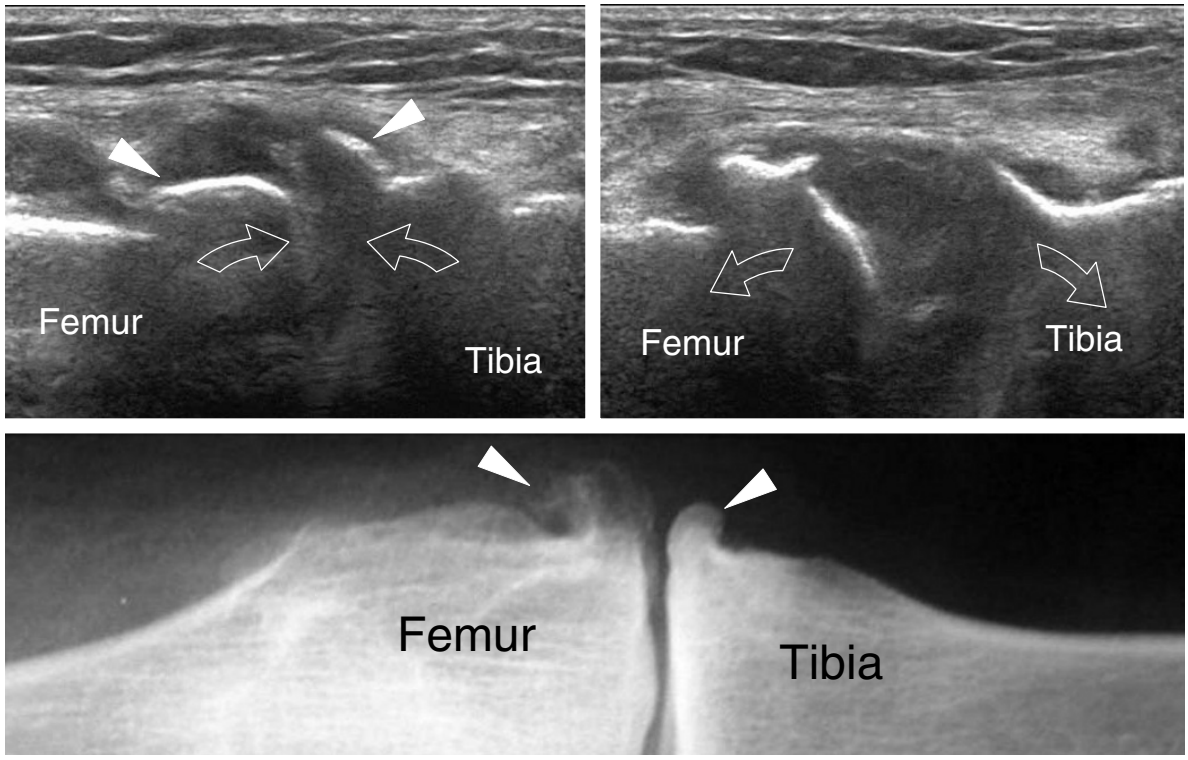

a b c

Fig. 14.126a–c. Osteoarthritis of the medial compartment. **a,b** Longitudinal 12–5 MHz US images obtained over the medial joint line during **a** varus and **b** valgus stress test. **a** The medial joint space is narrowed (*curved arrow*) due to cartilage thinning. Note marginal bone spurs (*white arrowheads*) related to osteophytes. **b** During valgus stress, the joint space opens due to ligament instability. **c** Anteroposterior radiograph shows typical findings of medial knee osteoarthritis, including joint space narrowing, marginal osteophytes (*white arrowheads*) and subchondral sclerosis

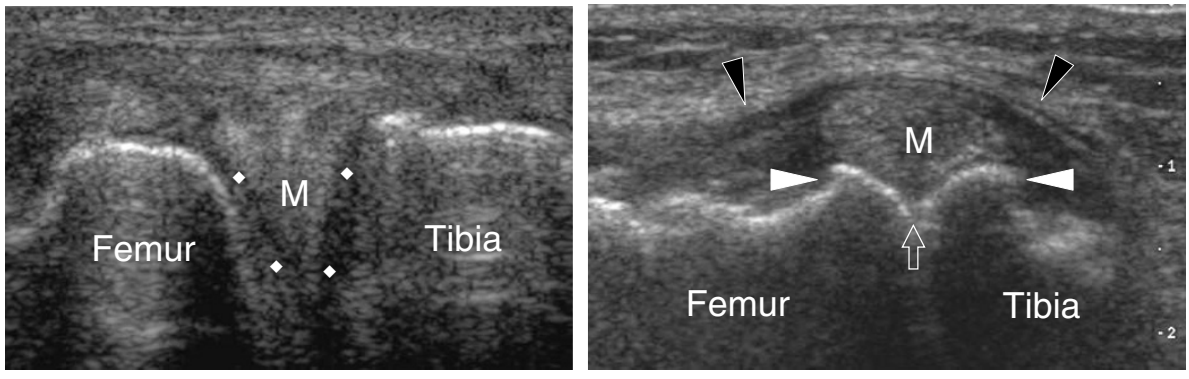

a b

Fig. 14.127a,b. Meniscal extrusion. **a** Coronal 12–5 MHz US image over the medial joint line demonstrates the normal appearance of the meniscus (*M*), a triangular-shaped hyperechoic fibrocartilaginous structure located between the articular surfaces of the femur and tibia which are covered by a layer of hypoechoic hyaline cartilage (*rhombi*). **b** Coronal 12–5 MHz US image of meniscal extrusion in severe medial femorotibial joint space narrowing. Note the severe narrowing of the medial joint space (*arrow*) due to cartilage thinning and the presence of marginal osteophytes (*white arrowheads*). The medial meniscus (*M*) is extruded and stretches the overlying superficial layer of the medial collateral ligament (*black arrowheads*)

accumulates within the meniscus via a one-way mechanism and progressively condenses due to water resorption and production of mucopolysaccharides. With time, the cyst increases in size and expands within the parameniscal soft tissues, even reaching the subcutaneous tissue. Because of the small size of the lateral collateral ligament, cysts arising from the lateral meniscus develop anterior or posterior to it, in close proximity with the tear. In contrast, medial lesions may have a long pedicle and may grow at a considerable distance from the site of meniscal rupture. Clinically, meniscal cysts present with local pain and a palpable, firm, painless or tender soft-tissue swelling. These cysts can show intermittent size changes or a progressive increase in volume and may possibly cause compression on adjacent structures, such as the peroneal nerve, and erosion of the bone.

Although the diagnosis of meniscal cysts is usually based on clinical findings, US can be helpful to confirm it. Depending on the position of the cyst, sagittal or coronal US images are the most useful for their assessment. US demonstrates meniscal cysts as space-occupying lesions located close to the outer meniscal surface (Peetrons et al. 1990; Rutten et al. 1998). The spectrum of their appearance ranges from a unilobulated hypoechoic mass to multilobulated lesions presenting with internal mixed echogenicity (Figs. 14.128, 14.129) (Seymour and Lloyd 1998). This variable appearance of meniscal cysts may depend on the different kinds of fluid they contains, including clear synovium-like fluid, gelatinous or bloody material, up to solid inflammatory tissue (Seymour and Lloyd 1998). In general, the external boundaries of the cyst are always well defined. Color Doppler imaging shows

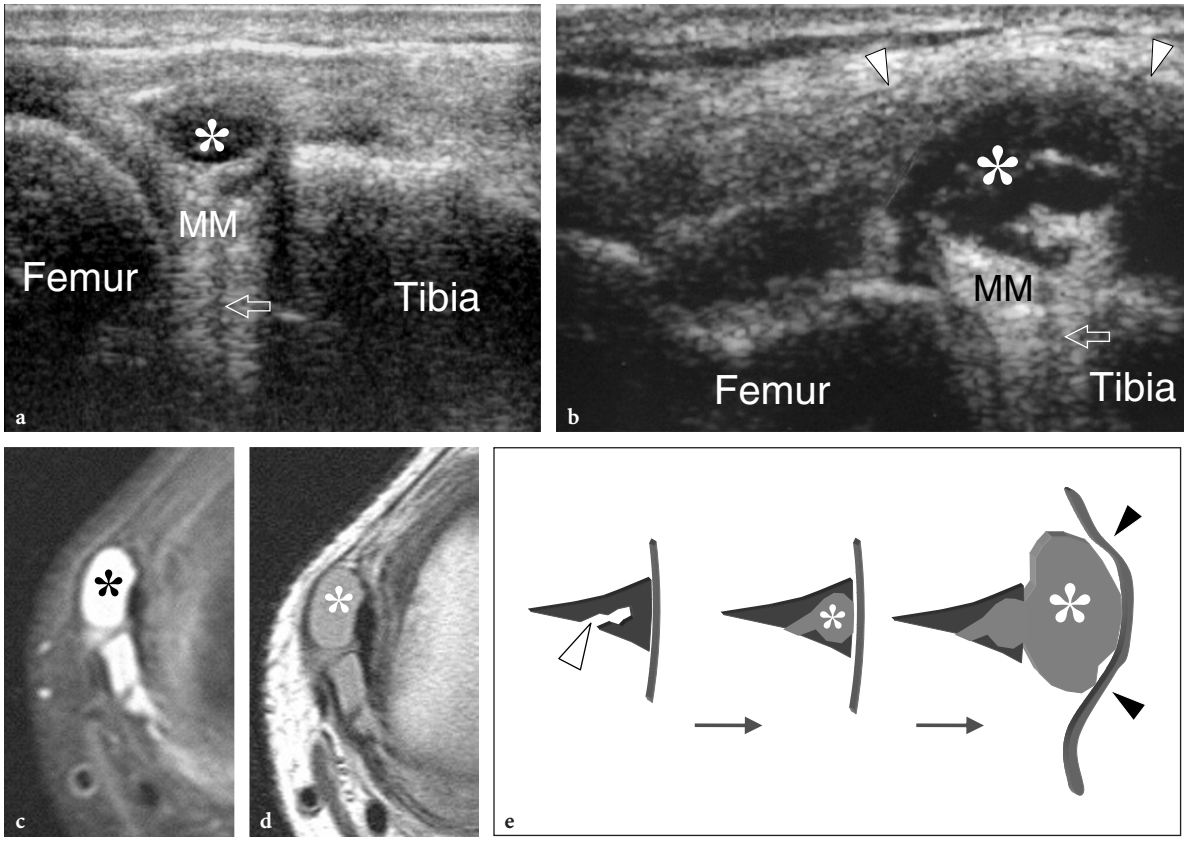

Fig. 14.128a–e. Meniscal cyst. **a,b** Coronal 12–5 MHz US images obtained in two different patients show **a** a small intrameniscal cyst (*asterisk*) and **b** a larger lobulated meniscal cyst (*asterisk*) displacing the medial collateral ligament (*white arrowheads*). In both cases, a horizontal degenerative meniscal tear is present. It appears as a straight hypoechoic band (*arrow*) within the hyperechoic meniscus (*MM*). **c,d** Corresponding transverse **c** fat-suppressed T2-weighted and **d** proton density MR images of the same case shown in **b**. **e** Schematic drawings illustrate the pathomechanism of meniscal cyst formation. Cysts (*asterisk*) arise from oblique or horizontal (*open arrowhead*) meniscal tears; they first lie within the meniscus but, with increasing size, tend to expand in the parameniscal tissues displacing the collateral ligaments (*black arrowhead*)

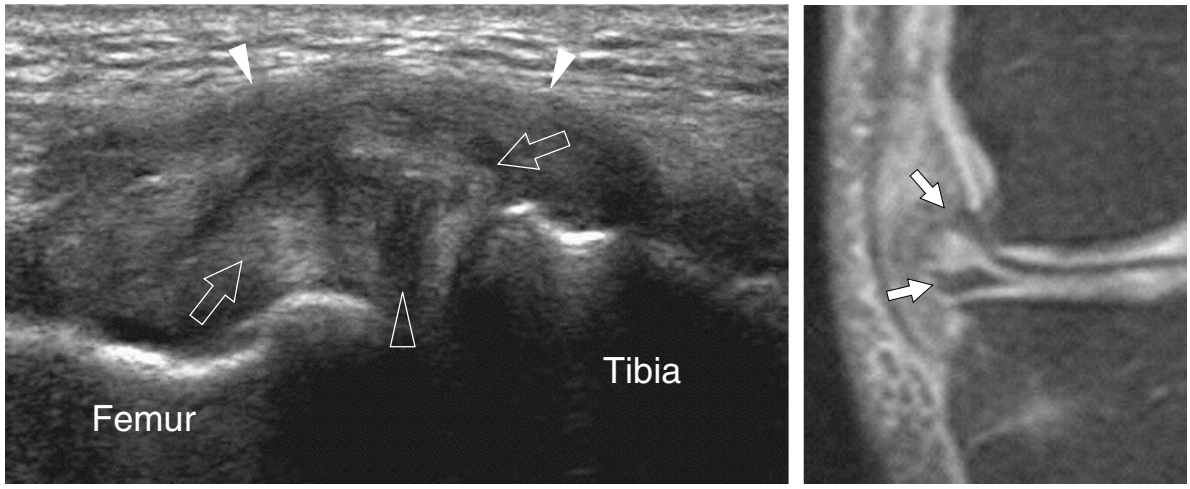

Fig. 14.129a,b. Lateral meniscal extrusion with precystic appearance. **a** Coronal 12–5 MHz US image over the lateral aspect of the joint with **b** coronal fat-suppressed T2-weighted MR imaging correlation reveals an extruded and degenerated lateral meniscus (*arrows*) presenting with a hypoechoic precystic central area (*open arrowhead*). Note the overlying thickened lateral collateral ligament (*white arrowheads*)

no internal blood flow signal. The relationship of the cyst with the surrounding anatomic structures can be easily depicted with US. Pes anserinus ganglia and superior tibiofibular joint ganglia can be easily differentiated from meniscal cysts on the basis of their different location. Because meniscal cysts are always associated with a degenerative tear of the meniscus, arthroscopic treatment is warranted once the cyst is demonstrated with US, without the need to further investigate the knee with MR imaging.

14.5.5.6 Meniscal Degeneration and Tears

The US appearance of early meniscal degeneration, when fluid-filled cavities are not yet visible, has been reported in the literature (De Flaviis et al. 1990). In these cases, the meniscus is swollen and diffusely hypoechoic with its outer margin protruding beyond the articular space (Fig. 14.130). There is general agreement in the literature that the sensitivity and specificity of US to investigate meniscal tears is low and that meniscal tears do not represent an actual indication for US examination (McDonnell et al. 1992; De Maeseener et al. 1998). Other imaging modalities, and especially MR imaging, offer an exquisite evaluation of meniscal tears and are, therefore, recommended if this condition is suspected on clinical grounds. Although difficult to recognize, the US appearance of some meniscal tears, such as meniscocapsular separations and horizontal tears, should be acknowledged by the examiner as these tears can be incidentally found during a routine US examination of the knee (Fig. 14.131) (Gerngross and Sohn 1992). In a postoperative setting, US can occasionally image meniscal sutures following repair of meniscocapsular tears (Fig. 14.132a–c).

14.5.5.7 Meniscal Calcifications

Chondrocalcinosis relates to the deposition of calcium pyrophosphate dehydrate crystals within articular cartilages, fibrocartilaginous structures, synovium and extra-articular tissues, such as ligaments and tendons. This condition can be associated with a variety of systemic disorders, including hyperparathyroidism, hemochromatosis and hypothyroidism, or may be idiopathic. Local reaction to crystal deposition leads to an inflammatory response which may later cause destructive changes. The US appearance of chondrocalcinosis of knee menisci has been reported in the literature (Coari et al. 1995; Kellner et al. 1990). The calcific deposits appear as hyperechoic spots of different size located within the meniscal substance. Overall, the meniscus appears irregular and heterogeneous but not swollen (Fig. 14.132d–f). The appearance of chondrocalcinosis must be acknowledged by the examiner if the

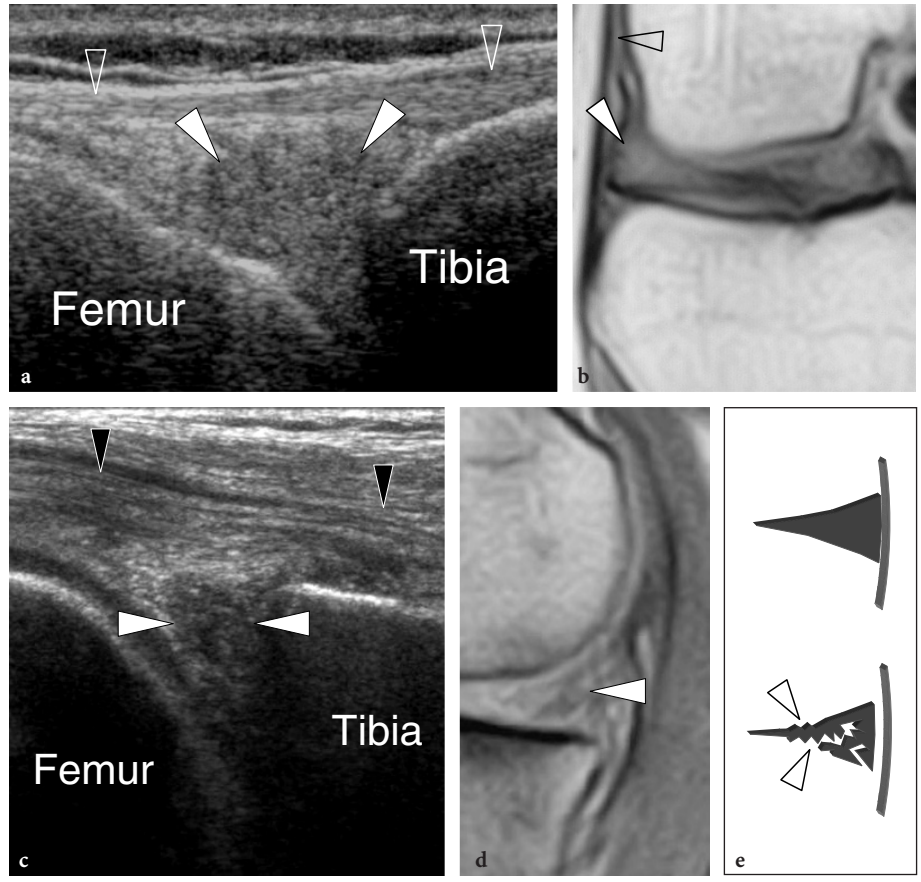

Fig. 14.130a–e. Meniscal abnormalities: spectrum and appearances. **a,b** Meniscal myxoid degeneration. **a** Coronal 12–5 MHz US image with **b** coronal proton density MR imaging correlation shows homogeneous hypoechoic swelling of the anterior horn (*white arrowheads*) of the lateral meniscus. No cleavage planes indicating meniscal tears are visible. Note the normal-appearing iliopsoas band (*open arrowheads*). **c–e** Complex degenerative meniscal tear. **c** Sagittal 12–5 MHz US image obtained over the posterior horn of the medial meniscus with **d** sagittal proton density MR imaging and **e** schematic drawing correlation demonstrates a diffuse hypoechoic appearance of the meniscus (*white arrowheads*) representing a complex degenerative tear. *Black arrowheads*, normal semimembranosus tendon

US examination is performed before a radiographic study. In these cases, recognition of the US findings of chondrocalcinosis can lead to a definite diagnosis or, at least, suggest it (Kellner et al. 1990). Once meniscal calcifications are suspected on the basis of the US findings, the articular cartilages should be accurately examined to detect additional findings that can corroborate the diagnosis.

14.5.5.8 Meniscal Ossicles

Meniscal ossicles are rounded bodies embedded within a meniscal horn, the posterior horn of the medial meniscus being the most commonly affected. These rare lesions, which consist of a peripheral bony cortex and a central trabecular bone, are mainly described in young men (Liu et al. 1994; Glass et al. 1975). Based on the MR imaging findings, their prevalence has been estimated of approximately 0.15% (Schnarkowski et al. 1995). The origin of meniscal ossicles is unclear. Some authors believe they represent vestigial structures; others hypothesize that they are secondary to meniscal trauma with associated avulsion of the meniscal insertion and secondary heterotopic bone formation. Meniscal ossicles can be completely asymptomatic or may present with nonspecific knee pain. They are usually detected on standard radiographs as rounded calcific lesions projecting over the posterior aspect of the medial femorotibial joint space. Because of their rarity, meniscal ossicles are often confused with loose bodies (Yu and Resnick 1994). Diag-

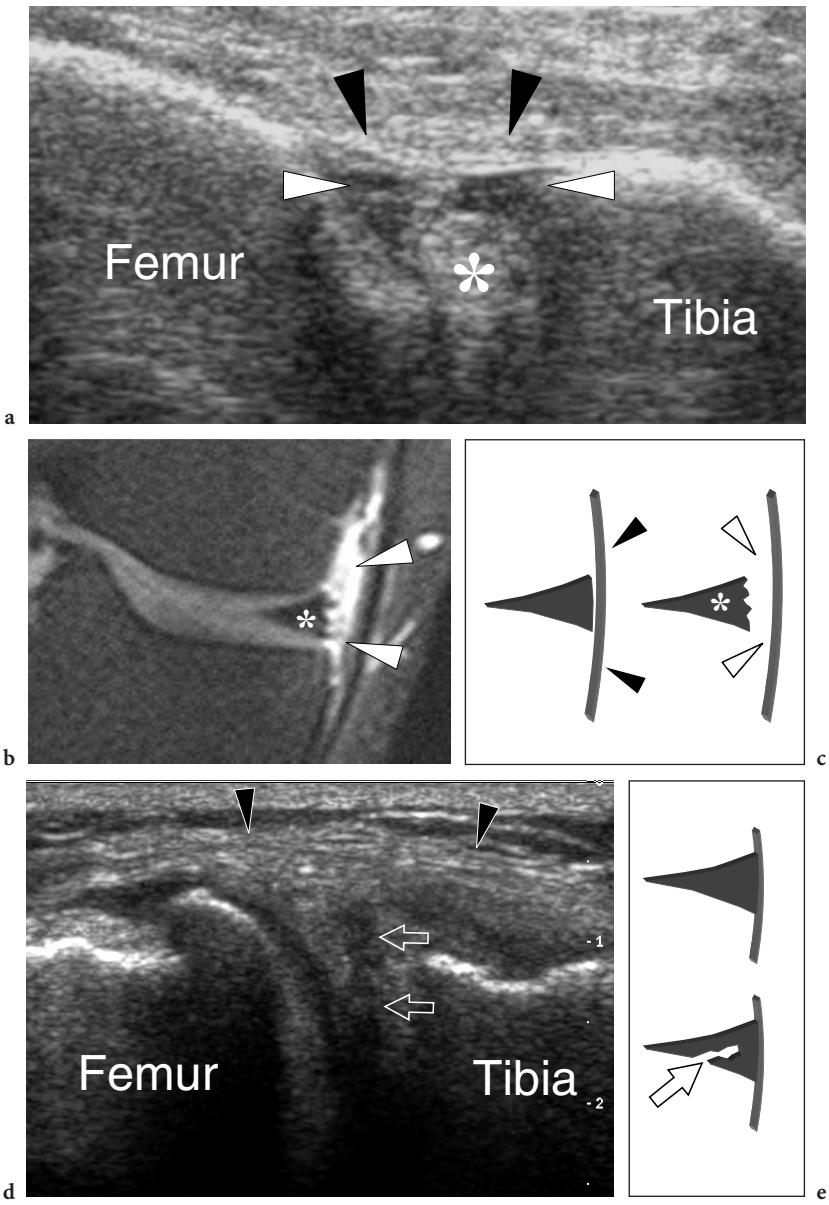

Fig. 14.131a–e Meniscal abnormalities: spectrum of US appearances. **a–c** Meniscocapsular tear **a** Coronal 12–5 MHz US image over the medial joint line with **b** fat-suppressed T2-weighted MR imaging and **c** schematic drawing correlation reveals fluid (*white arrowheads*) between the base of the meniscus (*asterisk*) and its peripheral capsular attachment (*black arrowheads*) indicating a meniscocapsular tear (*asterisk*). **d,e** Degenerative meniscal tear. **d** Coronal 12–5 MHz US image obtained at the level of the meniscal body with **e** schematic drawing correlation shows an intrameniscal hypoechoic linear oblique band (*arrows*) representing a degenerative tear. *Black arrowheads*, normal medial collateral ligament

nostic imaging modalities are generally required to exclude a loose body and avoid an extensive arthroscopic search for phantom loose fragments. MR imaging and CT-arthrography are the preferred modalities to diagnose meniscal ossicles. US can confirm the radiographic findings and may be helpful to differentiate meniscal ossicles from loose bodies (Martinoli et al. 2000b). Meniscal ossicles appear as rounded hyperechoic structures embedded within the posterior meniscal horn (Fig. 14.133). It should be pointed out, however, that only experienced examiners can distinguish between these two conditions based on the intrameniscal location and absence of displacement of meniscal ossicles. We believe the examiner should be aware of the US appearance of meniscal ossicles because they can be

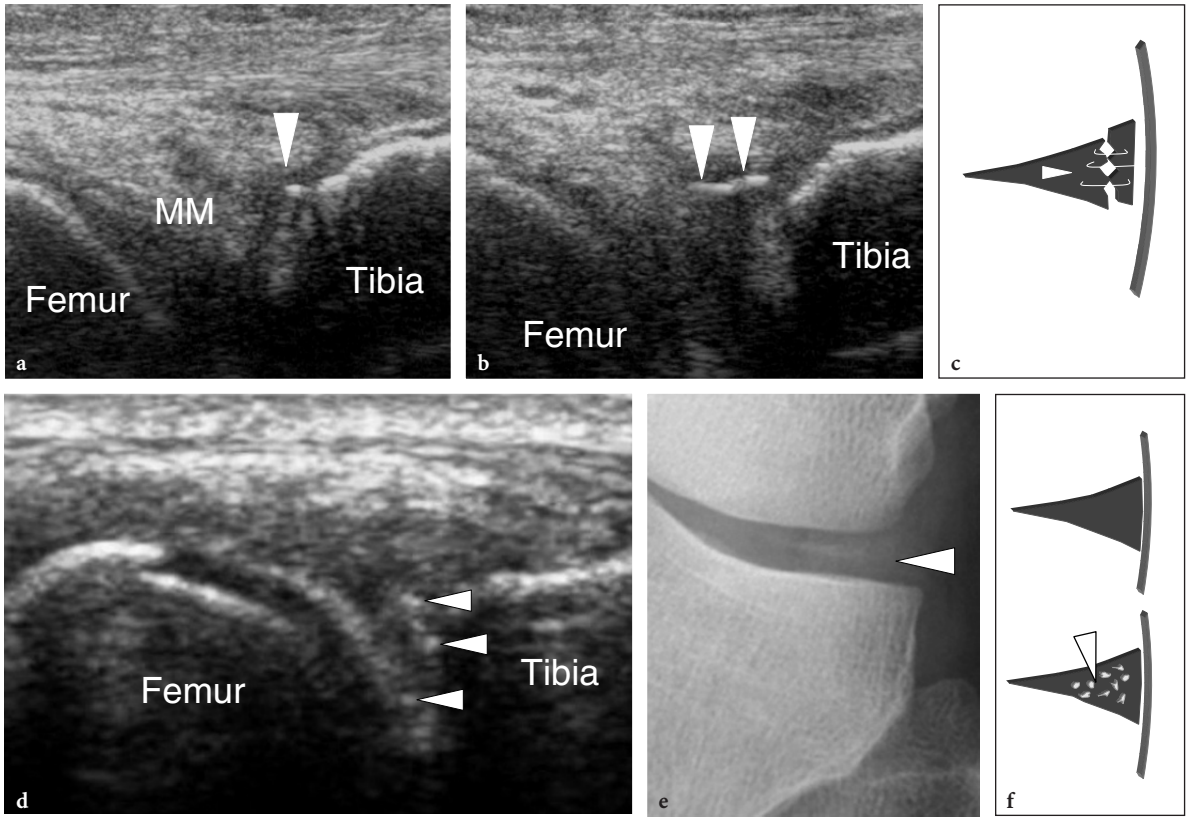

Fig. 14.132a–f. Meniscal abnormalities: spectrum of US appearances. **a–c** Postoperative findings. **a,b** Sagittal 12–5 MHz US images obtained at the middle third of the medial meniscus (*MM*) with **c** schematic drawing correlation demonstrate intrameniscal bright hyperechoic lines (*white arrowheads*) surrounded by a hypoechoic halo. These structures refer to surgical stitches in a patient previously operated on for a peripheral meniscal tear. **d–f** Chondrocalcinosis. **d** Sagittal 12–5 MHz US image obtained at the level of the posterior horn of the medial meniscus with **e** radiographic and **f** schematic drawing correlation shows a diffusely heterogeneous appearance of the meniscus due to the presence of fine hyperechoic spots (*arrowheads*) representing meniscal calcifications

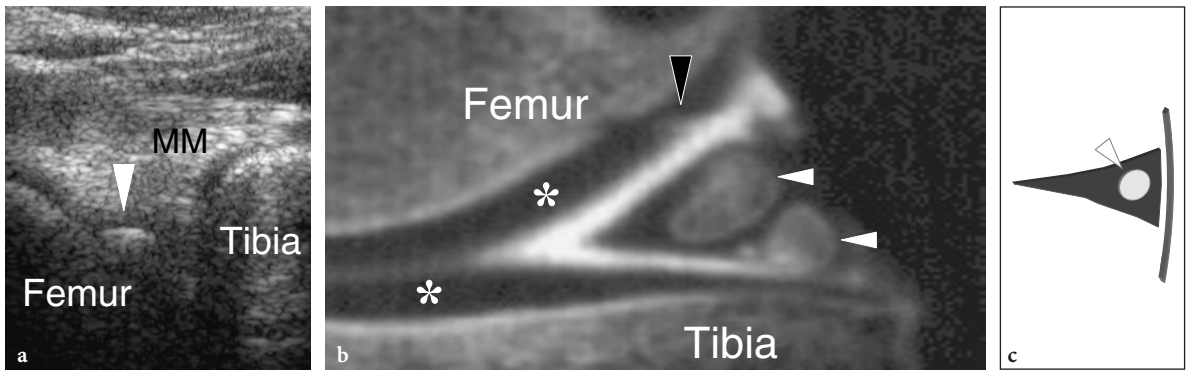

Fig. 14.133a–c. Meniscal ossicle. **a** Sagittal 12–5 MHz US image obtained at the level of the posterior horn of the medial meniscus (*MM*) reveals a well-defined rounded hyperechoic intrameniscal structure (*white arrowhead*). **b** Corresponding sagittal reformatted CT-arthrographic image confirms the presence of two small meniscal ossicles (*white arrowheads*). Note the absence of associated meniscal tears. The articular cartilages (*asterisks*) of the femur and tibia are nicely depicted. A small chondral ulceration probably related to chondral impingement against the ossicles is evident (*black arrowhead*). **c** Schematic drawing correlation

encountered as incidental findings during routine examination of the popliteal space and may cause a diagnostic challenge.

14.5.5.9 Total Knee Replacement

US may also be useful in the assessment of the postoperative knee. In total knee arthroplasty, this technique can be used to assess the polyethylene liners and to measure their thickness with an accuracy comparable to radiographic measurements (Fig. 14.134) (Yashar et al. 1996; Sofka et al. 2003). In this field, US has been proposed as a noninvasive tool to screen patients for potential wear of the polyethylene liner, primarily involving the eccentric portion of the implant (Sofka et al. 2003). Wear and delamination of the polyethylene can cause particulate debris and osteolysis, affecting the overall functionality of the replacement joint. In patients with total knee arthoplasty characterized by functional impairment, stiffness and pain, this technique has also proved able to distinguish arthofibrosis from an uncomplicated postoperative course, based on an increased thickness (cut-off value of 3 mm) and a hypervascular pattern of the synovial membrane in the suprapatellar and parapatellar recesses at gray-scale and color Doppler examination (Boldt et al. 2004). Finally, dynamic US scanning has been shown to detect the impingement of the fabella on the posterior aspect of the polyethylene portion of the tibial component with painful snapping over the prosthesis during flexion (Segal et al. 2004).

14.5.6 Knee Masses

A variety of solid and cystic masses can be encountered around the knee as incidental findings. Most are benign, have an indolent behavior, such as lipomas, synovial and ganglion cysts, bursitis and neurogenic tumors, and can be easily diagnosed with US based on previously described criteria (Fig. 12.135). In the knee, however, there are some specific masses which merit particular attention. These include the lipoma arborescens and pigmented villonodular synovitis. In addition, an accessory muscle, the tensor fasciae suralis, can present as a pseudomass arising on the posterior aspect of the knee and warrants additional brief discussion here.

14.5.6.1 Lipoma Arborescens

Lipoma arborescens (from the word "arbor" meaning "tree" in Latin) is a rare benign intra-articular space-occupying lesion characterized by replacement of the subsynovial tissue by mature fat cells giving rise to a villous proliferation which is almost invariably found inside the suprapatellar recess (Ryu

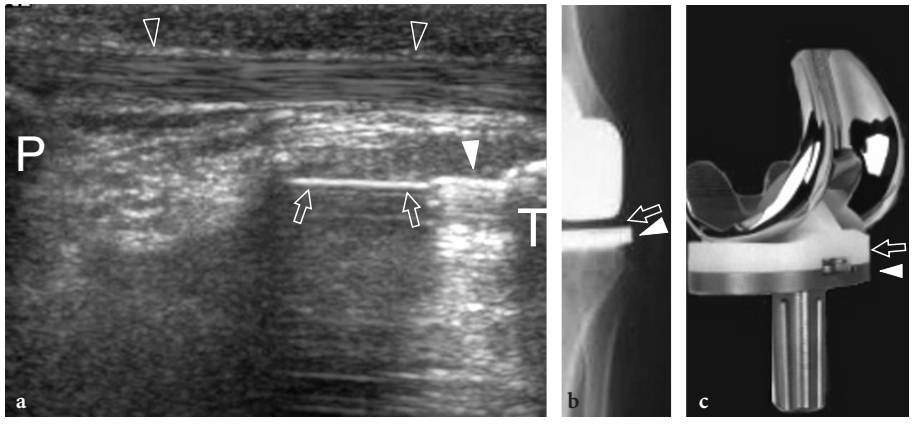

Fig. 14.134a–c. Total knee arthroplasty. **a** Longitudinal 12–5 MHz US image obtained over the patellar tendon (*open arrowheads*) in a 72-year-old man with total knee arthroplasty shows the US appearance of the metal-bone-polyethylene interface. Note the straight echogenic interface (*arrows*) with posterior acoustic shadowing generated by polyethylene. In contrast, the metallic tibial component (*arrowhead*) exhibits posterior reverberation artifact. *P*, patella; *T*, tibia. **b** Correlative anteroposterior radiograph obtained with the patient standing shows the normal radiographic appearance of the tibial metallic component (*arrowhead*) and the radiolucent polyethylene liner (*arrow*) in the implant. **c** Photograph of a knee prosthesis showing the tibial metallic component (*arrowhead*) and the polyethylene liner (*arrow*)

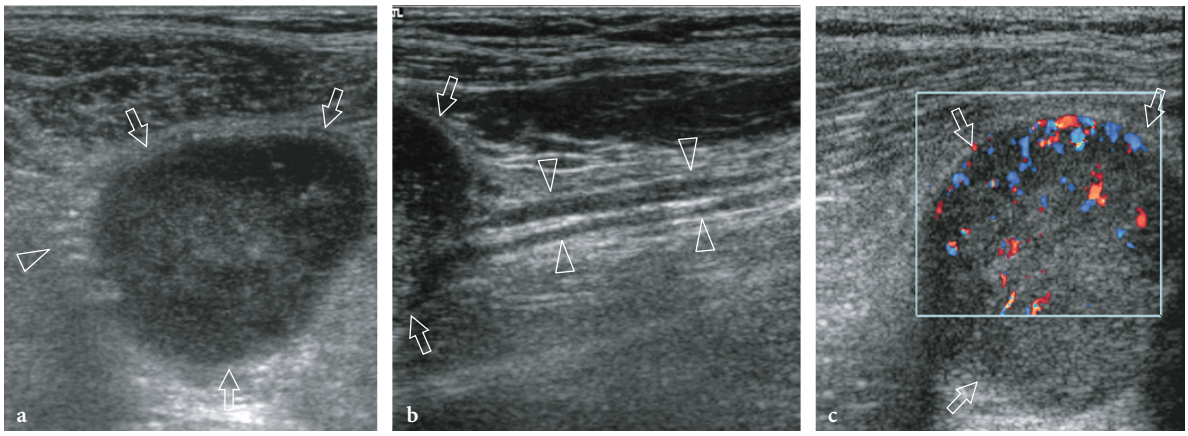

Fig. 14.135a–c. Schwannoma of the tibial nerve. **a** Transverse and **b** longitudinal 12–5 MHz US images over the popliteal fossa reveal a well-defined oval hypoechoic mass (*arrows*) in continuity with the tibial nerve (*arrowheads*). In **a**, note some unaffected fascicles (*arrowhead*) displaced at the periphery of the tumor. **c** Transverse color Doppler US image demonstrates a hypervascular pattern of the tumor (*arrows*) consisting of peripheral and central blood flow signals

et al. 1996). Its origin is undetermined although this mass is believed to represent more a reactive than a neoplastic entity. It can be an isolated condition or can be found in association with chronic arthropathies, such as rheumatoid arthritis or osteoarthritis. In some patients, lipoma arborescens presents clinically as a painless slow-growing mass, whereas in other cases it is painful and can be associated with a decreased range of knee motion and joint effusion. US reveals an intra-articular compressible mass characterized by multiple frond-like projections that allow its differentiation from hypertrophic synovitis (Fig. 14.136) (Learch et al. 2000; Martinez et al. 1992). Correlation with laboratory and clinical data may help to distinguish lipoma arborescens from synovitis. Following the US study, MR imaging allows a conclusive diagnosis so that the adequate treatment, a synovectomy, can be performed (Martin et al. 1998; Vilanova et al. 2003). Differentiation of this condition from the normal superolateral fat pad is based on the typical location, the smaller size and the smooth margins of the fat pad and the larger size and macroscopic villus-like appearance of the lipoma arborescens (Armstrong and Watt 1989).

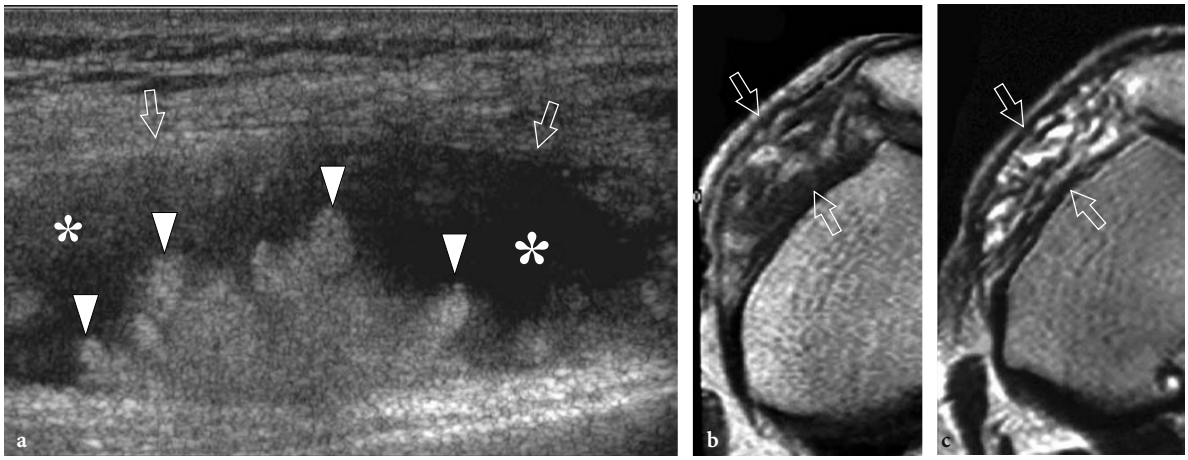

Fig. 14.136a–c. Lipoma arborescens. **a** Transverse 12–5 MHz US image over the lateral parapatellar recess (*arrows*) demonstrates a large effusion (*asterisks*) and villous hyperechoic fatty synovial proliferations (*arrowheads*) with a clearly frond-like morphology inside the pouch, resembling the image of a branched tree. **b,c** Correlative **b** transverse T1-weighted and **c** T2-weighted MR images reveal signal intensity similar to that of subcutaneous fat within the mass (*arrows*)

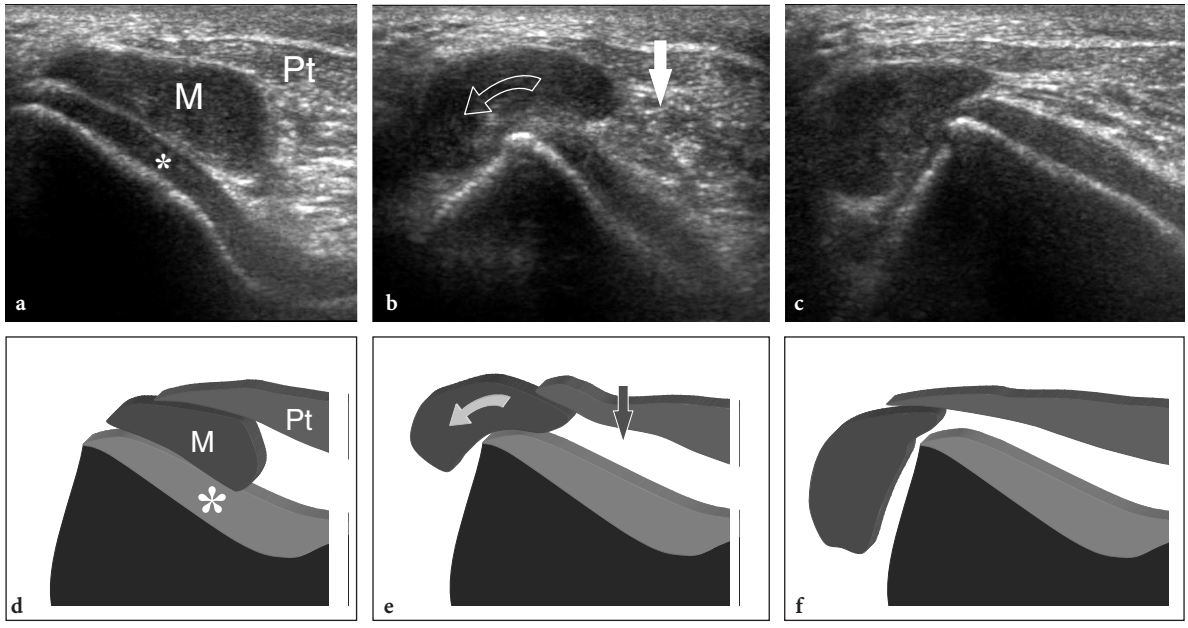

Fig. 14.137a–f. Pigmented villonodular synovitis. **a–c** Transverse 12–5 MHz US images obtained over a palpable anterior soft-tissue mass (*M*) with **a** extended knee and **b,c** during progressive degrees of flexion with **d-f** schematic drawing correlations. With the knee extended, the nodule lies in the Hoffa fat pad between the trochlear cartilage (*asterisk*) and the deep aspect of the patellar tendon (*Pt*). During progressive joint flexion, dynamic US shows **b** lateral subluxation (*curved arrow*) and **c** dislocation of the mass relative to the lateral edge of the trochlea as a result of pressure (*straight arrow*) from the adjacent patellar tendon. Abrupt dislocation of the mass corresponded to the snapping sensation referred by the patient. Surgical removal of the nodule revealed pigmented villonodular synovitis. **d–f** Schematic drawing correlations

14.5.6.2 Pigmented Villonodular Synovitis

Pigmented villonodular synovitis is an uncommon benign proliferative disorder of the synovium which affects joints, bursae or tendons sheaths (Dorwart et al. 1984). Intra-articular pigmented villonodular synovitis of the knee exists in two forms: diffuse and nodular. Histologically, this tumor consists of a fibrous stroma covered by hyperplastic lining cells, histiocytes containing fat or hemosiderin and multinucleated giant cells. Hemosiderin, a breakdown product of hemoglobin, can be found either in the macrophages as a result of phagocytosis or in the fibrous stroma. On gross examination, diffuse pigmented villonodular synovitis appears as a widespread proliferation of synovium that shows finger-like villous projections. Clinically, the patient's symptoms may reflect monoarticular arthritis often associated with a large serous or bloody effusion. The nodular form appears as a firm, well-circumscribed solid nodule often located at the level of the infrapatellar fat pad. It can be detected as an incidental finding during MR imaging performed for unrelated purposes. Depending on its relationships with the posterior tendons and the trochlea, the nodule can produce an anterior snapping sensation during knee flexion as a result of impingement between these structures (Fig. 14.137). US can detect nodular pigmented villonodular synovitis as a well-delineated hypoechoic mass usually located inside the Hoffa fat pad (Bianchi et al. 1998). The diffuse type is most often detected with US at the level of the posterior aspect of the joint, between the posterior tendons and the femoral bone (Fig. 14.138) or developing insde the subquadriceps recess. Color Doppler imaging reveals internal flow signals reflecting a proper vasculature. Based on detection of hemosiderin deposits which exhibit low signal on both T1- and T2-weighted sequences, MR imaging is superior to US in the characterization of this mass (Sheppard et al. 1998). Differential diagnosis of a space-occupying lesion developing over the anterior aspect of the knee joint includes the rare intra-articular chondroma, synovial hemangioma (see Chap. 5), synovial sarcoma and the more common meniscal and cruciate ligaments cysts extending within the Hoffa pad.

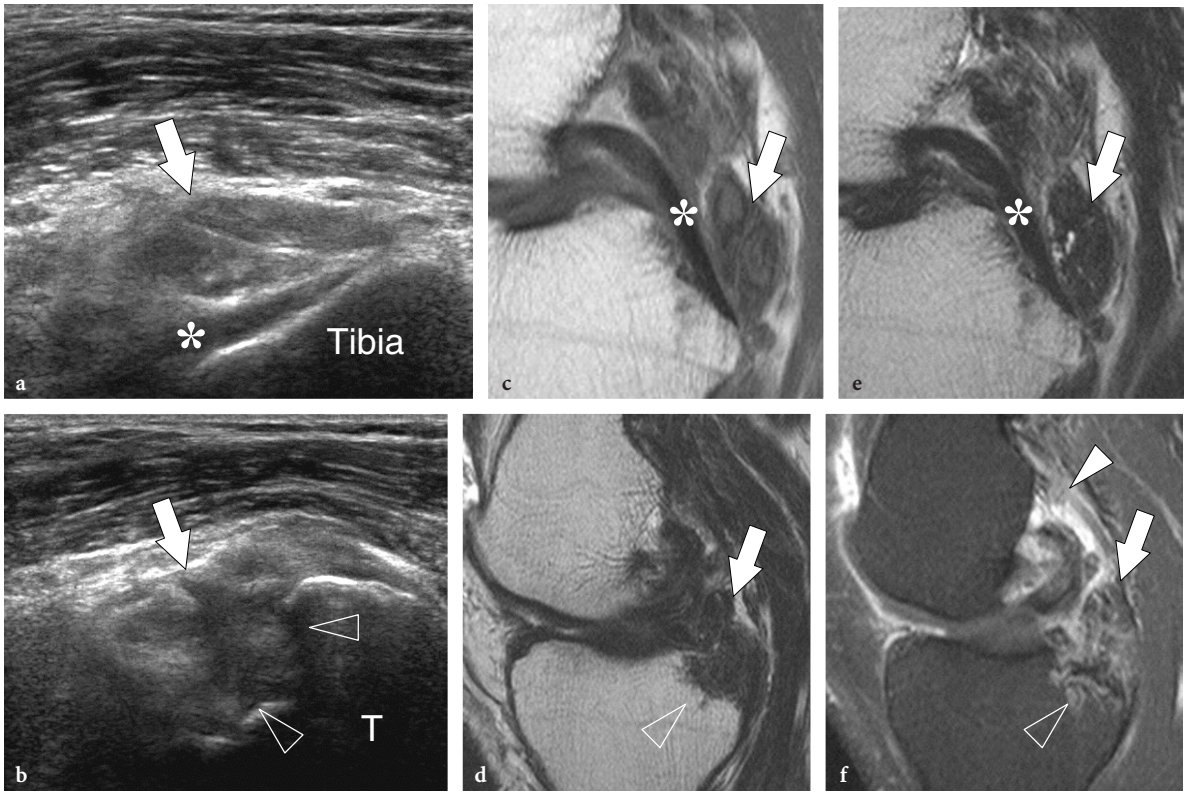

Fig. 14.138a–f. Pigmented villonodular synovitis. **a,b** Sagittal 12–5 MHz US images obtained over the popliteal fossa with **c,d** sagittal T1-weighted, **e** T2-weighted and **f** fat-suppressed T2-weighted MR imaging correlation demonstrate an intra-articular ill-defined solid hypoechoic mass (*arrow*) growing in proximity to the posterior cruciate ligament (*asterisk*) which extends away from the joint space and causes bone erosion (*arrowheads*) on the posterior tibial plateau. On the MR images, note the typical hypointense appearance of the mass on both T1- and T2-weighted sequences, related to hemosiderin deposits

14.5.6.3 Tensor Fasciae Suralis Muscle

The tensor fasciae suralis is a rare anomalous muscle located in the popliteal region (Somayaji et al. 1998; Bergman et al. 1988). This muscle arises from the semitendinosus, courses superficial to the medial head of the gastrocnemius and continues down into a thin long tendon that reaches the calcaneus (Chason et al. 1995; Somayaji et al. 1998; Bergman et al. 1988). Clinically, it appears as a soft mass which becomes more apparent when the patient is prone. During muscle contraction, such as during resisted flexion of the knee, the tensor fasciae suralis becomes firm and more prominent on the skin. Although it can be suspected on physical findings, in most cases an imaging modality is required for its evaluation. The MR imaging and US appearances of this muscle have been reported in the literature (Chason et al. 1995; Montet et al. 2002). US diagnosis is based on demonstration of the typical internal echotexture of the muscle made up of hyperechoic fibroadipose septa and hypoechoic muscle fibers (Fig. 14.139). With high-frequency probes, the thin distal tendon can be demonstrated with US. Transverse US images are the most useful to demonstrate the location of the aberrant muscle and its relationship with the adjacent anatomic structures, whereas longitudinal planes reveal its internal architecture in detail. While evaluating a popliteal mass, it is important to be aware of the possibility that a tensor fasciae suralis is present.

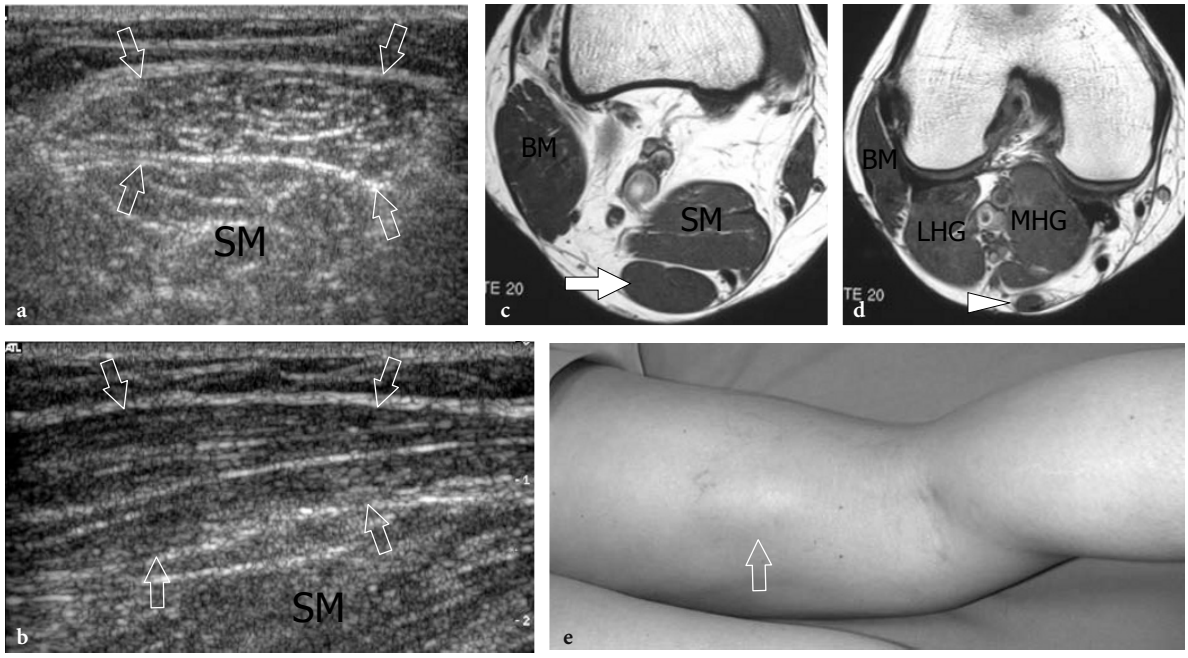

Fig. 14.139a–e. Tensor fasciae suralis muscle. **a** Transverse and **b** longitudinal 12–5 MHz US images obtained over the popliteal space show the accessory belly of the tensor fasciae suralis (*arrows*) which lies superficial to the semimembranosus muscle (*SM*). Note the characteristic internal structure of the muscle made up of hypoechoic bundles and hyperechoic fibroadipose septa. **c** Cranial and **d** caudal transverse T1-weighted MR images confirms the US finding. Note the distal tendon of the tensor fasciae suralis (*arrowhead*) located superficial to the medial head of the gastrocnemius (*MHG*). *BM*, biceps femoris muscle; *LHG*, lateral head of the gastrocnemius. **e** Photograph of the posterior thigh obtained during resisted flexion of the knee shows an anomalous lump (*arrow*) produced by the contracted muscle

References

Abdelwahab IF, Kenan S, Hermann G et al (1992) Intramuscular myxoma, magnetic resonance features. Br J Radiol 65: 485–490

Adriani E, Mariani PP, Maresca G, et al (1995) Healing of the patellar tendon after harvesting of its mid-third for anterior cruciate ligament reconstruction and evolution of the unclosed donor site defect. Knee Surg Sports Traumatol Arthrosc 3: 138–143

Aisen AM, McCune WJ, MacGuire A et al (1984) Sonographic evaluation of the cartilage of the knee. Radiology 153: 781–784

Aprin H, Broukhim B (1985) Early diagnosis of acute rupture of the quadriceps tendon by arthrography. Clin Orthop 195: 185–190

Armstrong SJ, Watt I (1989) Lipoma arborescens of the knee. Br J Radiol 62: 178–180

Asher E, Markevich N, Schutzer RW et al (2003) Small popliteal artery aneurysms: are they clinically significant? J Vasc Surg 37: 755–760

Backhaus M, Burmester GR, Gerber T et al (2001) Guidelines for musculoskeletal ultrasound in rheumatology. Ann Rheum Dis 60: 641–649

Baker WM (1877) The formation of synovial cysts in the leg in connection with diseases of the knee joint. St Bart Hosp Res 15: 245–261

Barasch E, Lombardi L, Arena L et al (1989) MR imaging evaluation of bilateral quadriceps tendon rupture in a patient with secondary hyperparathyroidism: implication for diagnosis and therapy. Comput Med Imaging Graph 5: 407–410

Basso O, Johnson DP, Amis AA (2001) The anatomy of the patellar tendon. Knee Surg Sports Traumatol Arthrosc 9: 2–5

Bergman RA, Thompson SA, Afifi A et al (1988) Compendium of human anatomic variation. Urban and Schwartzenberg, Baltimore, p 23

Berlin RC, Levinsohn EM, Chrisman H (1991) The wrinkled patellar tendon: an indication of abnormality in the extensor mechanism of the knee. Skeletal Radiol 20: 181–185

Bianchi S, Martinoli C (1999) Detection of loose bodies in joints. Radiol Clin North Am 37: 679–690

Bianchi S, Zwass A, Abdelwahab IF et al (1994) Diagnosis of tears of the quadriceps tendon of the knee: value of sonography. AJR Am J Roentgenol 162: 1137–1140

Bianchi S, Zwass A, Abdelwahab IF et al (1995) Sonographic evaluation of intramuscular ganglia. Clin Radiol 50: 235–236

Bianchi S, Zwass A, Abdelwahab IF et al (1995) Sonographic evaluation of lipohemarthrosis: clinical and in vitro study. J Ultrasound Med 14: 279–282

Bianchi S, Mazzola CG, Martinoli C et al (1998) Localized pigmented villonodular synovitis of the knee. Quiz case of the month. Eur Radiol 8: 1275–1276

Blankstein A, Cohen I, Salai M et al (2001) Ultrasonography: an imaging modality enabling the diagnosis of bipartite patella. Knee Surg Sports Traumatol Arthrosc 9: 221–224
Boldt JG, Munzinger UK, Zanetti M et al (2004) Arthrofibrosis associated with total knee arthroplasty: gray-scale and power Doppler sonographic findings. AJR Am J Roentgenol. 182: 337–340
Boles CA, Martin DF (2001) Synovial plicae in the knee. AJR Am J Roentgenol. 177: 221–227
Bonaldi VM, Chhem RK, Drolet R et al (1998) Iliotibial band friction syndrome: sonographic findings. J Ultrasound Med 17: 257–260
Brooks DM (1952) Nerve compression by simple ganglia. J Bone Joint Surg Br 34: 391–400
Brossmann J, Preidler KW, Daenen B et al (1996) Imaging of osseous and cartilaginous intraarticular bodies in the knee: comparison of MR imaging and MR arthrography with CT and CT arthrography in cadavers. Radiology 200: 509–517
Bui-Mansfield LT, Youngberg RA (1997) Intraarticular ganglia of the knee: prevalence, presentation, etiology, and management. AJR Am J Roentgenol. 168: 123–127
Butt WP, Lederman H, Chuang S (1983) Radiology of the suprapatellar region. Clin Radiol 34: 511–522
Carotti M, Salaffi F, Manganelli P et al (2002) Power Doppler sonography in the assessment of synovial tissue of the knee joint in rheumatoid arthritis: a preliminary experience. Ann Rheum Dis 61: 877–882
Carr JC, Hanly S, Griffin J (2001) Sonography of the patellar tendon and adjacent structures in pediatric and adult patients. AJR Am J Roentgenol. 176: 1535–1539
Chamlou R, Stefanidis C, Lambert T et al (2002) Popliteal artery pseudoaneurysm and hereditary multiple exostoses. Acta Chir Belg 102: 467–469
Chason DP, Schultz SM, Fleckenstein JL (1995) Tensor fasciae suralis: depiction on MR images. AJR Am J Roentgenol. 165: 1220–1221
Cho KH, Lee DC, Chhem RK et al (2001) Normal and acutely torn posterior cruciate ligament of the knee at US evaluation: preliminary experience. Radiology 219: 375–380
Choi NH, Kim SJ (2002) A ganglion of the anterior cruciate ligament causing erosion of the lateral femoral condyle. J Bone Joint Surg Am 84: 2274–2276
Clark K (1961) Ganglion of the lateral popliteal nerve. J Bone J Surg Br 43: 460–468
Coari G, Iagnocco A, Zoppini A (1995) Chondrocalcinosis: sonographic study of the knee. Clin Rheumatol 14: 511–514
Cook JL, Khan KM, Harcourt PR et al (1998) Patellar tendon ultrasonography in asymptomatic active athletes reveals hypoechoic regions: a study of 320 tendons. Victorian Institute of Sport Tendon. Clin J Sport Med 8: 73–77
Cook JL, Khan KM, Kiss ZS et al (2000) Patellar tendinopathy in junior basketball players: a controlled clinical and ultrasonographic study of 268 patellar tendons in players aged 14-18 years. Scand J Med Sci Sports 10: 216–220
Cook JL, Khan KM, Kiss ZS et al (2001) Asymptomatic hypoechoic regions on patellar tendon ultrasound: a 4-year clinical and ultrasound follow-up of 46 tendons. Scand J Med Sci Sports 11: 321–327
Costa CR, Morrison WB, Carrino JA (2004) Medial meniscus extrusion on knee MRI: is extent associated with severity of degeneration or type of tear? AJR Am J Roentgenol 183: 17–23
Cronan JJ, Dorfman GS, Scola FH et al (1987) Deep venous thrombosis: US assessment using vein compression. Radiology 162: 191–194
Davies SG, Baudouin CJ, King JB et al (1991) Ultrasound, computed tomography and magnetic resonance imaging in patellar tendinitis. Clin Radiol 43: 52–56
De Flaviis L, Nessi R, Leonardi M et al (1988) Dynamic ultrasonography of capsulo-ligamentous knee joint traumas. J Clin Ultrasound 16: 487-492
De Flaviis L, Scaglione P, Nessi R et al (1990) Ultrasound in degenerative cystic meniscal disease of the knee. Skeletal Radiol 19: 441–445
De Maeseneer M, Lenchnik L, Starok M et al (1998) Normal and abnormal medial meniscocapsular structures: MR imaging and sonography in cadavers. AJR Am J Roentgenol 171: 969–976
De Maeseneer M, Vanderdood K, Marcelis S et al (2002) Sonography of the medial and lateral tendons and ligaments of the knee: the use of bony landmarks as an easy method for identification. AJR Am J Roentgenol 178: 1437–1444
De Maeseneer M, Van Roy P, Shahabpour M et al (2004) Normal anatomy and pathology of the posterior capsular area of the knee: findings in cadaveric specimens and in patients. AJR Am J Roentgenol 182: 955–962
DeFriend DE, Schranz PJ, Silver DA (2001) Ultrasound-guided aspiration of posterior cruciate ligament ganglion cysts. Skeletal Radiol 30: 411-414
Derks WH, de Hooge P, van Linge B (1986) Ultrasonographic detection of the patellar plica of the knee. J Clin Ultrasound 14: 355–360
Ditchfield A, Sampson MA, Taylor GR (2000) Ultrasound diagnosis of sleeve fracture of the patella. Clin Radiol 55: 721–722
Doria AS, Kiss MHB, Lotito APN et al (2001) Juvenile rheumatoid arthritis of the knee: evaluation with contrast-enhanced color Doppler ultrasound. Pediatr Radiol 31: 524–531
Dorwart RH, Genant HK, Johnston WH et al (1984) Pigmented villonodular synovitis of synovial joints: clinical, pathologic, and radiologic features. AJR Am J Roentgenol 143: 877–885
Duc SR, Wentz KU, Käch et al (2004) First report of an accessory popliteal muscle: detection with MRI. Skeletal Radiol 33: 429–431
Duffy ST, Colgan MP, Sultan S et al (1998) Popliteal aneurysms: a 10-year experience. Eur J Vasc Endovasc Surg 16: 218–222
Duncan W, Dahm DL (2003) Clinical anatomy of the fabella. Clin Anat 16: 448–449
Elias DA, White LM, Rubenstein JD et al (2003) Clinical evaluation and MR imaging features of popliteal artery entrapment and cystic adventitial disease. AJR Am J Roentgenol 180: 627–632
Ellis VH (1936) Two cases of ganglia in the sheath of the peroneal nerve. Br J Surg 24: 141–142
Fornage BD (1987) The hypoechoic normal tendon. A pitfall. J Ultrasound Med 6: 19–22
Fraser JD, Anderson DR (1999) Deep venous thrombosis: recent advances and optimal investigation with US. Radiology 211: 9–24
Fredberg U, Bolvig L (2002) Significance of ultrasonographically detected asymptomatic tendinosis in the patellar and Achilles tendons of elite soccer players: a longitudinal study. Am J Sports Med 30: 488–491

Frediani B, Falsetti P, Storri L et al (2002) Ultrasound and clinical evaluation of quadricipital tendon enthesitis in patients with psoriatic arthritis and rheumatoid arthritis. Clin Rheumatol 21: 294–298

Friedman L, Finlay K, Jurriaans E (2001) Ultrasound of the knee. Skeletal Radiol 30: 361–377

Fuchs S, Chylarecki C (2002) Sonographic evaluation of ACL rupture signs compared to arthroscopic findings in acutely injured knees. Ultrasound Med Biol 28: 149–154

Gebhard F, Authenrieth M, Strecker W et al (1999) Ultrasound evaluation of gravity induced anterior drawer following anterior cruciate ligament lesion. Knee Surg Sports Traumatol Arthrosc 7: 166–172

Gerngross H, Sohn C (1992) Ultrasound scanning for the diagnosis of meniscal lesions of the knee joint. Arthroscopy 8: 105–110

Glass RS, Barnes WM, Kells DU et al (1975) Ossicle of the knee menisci. Report of seven cases. Clin Orthop 111: 163–171

Grassi W, Lamanna G, Farina A et al (1999) Sonographic imaging of normal and osteoarthritic cartilage. Semin Arthritis Rheum 28: 398–340

Grobbelaar N, Bouffard JA (2000) Sonography of the knee, a pictorial review. Semin Ultrasound CT MR 21: 231–274

Guerra J Jr, Newell JD, Resnick D, Danzig LA (1981) Pictorial essay: gastrocnemio-semimembranosus bursal region of the knee. AJR Am J Roentgenol 136: 593–596

Hall FM (1975) Radiographic diagnosis and accuracy in knee joint effusions. Radiology 115: 49–54

Halperin N, Oren Y, Hendel D et al (1987) Semimembranosus tenosynovitis: operative results. Arch Orthop Trauma Surg 106: 281–284

Hauzeur JP, Mathy L, De Maertelaer V (1999) Comparison between clinical evaluation and ultrasonography in detecting hydrarthrosis of the knee. J Rheumatol 26: 2681–2683

Helbich TH, Breitenseher M, Trattnig S et al (1998) Sonomorphologic variants of popliteal cysts. J Clin Ultrasound 26: 171–176

Hermann G, Yeh HC, Lehr-Janus C et al (1981) Diagnosis of popliteal cysts: double-contrast arthrography and sonography. AJR Am J Roentgenol 137: 369–372

Hertzbergerten Cate R, Jung I, Bos CF (1992) Septa within the suprapatellar region blocking intraarticular steroid in pauciarticular juvenile chronic arthritis. Clin Exp Rheumatol 10: 93–94

Iagnocco A, Coari G, Zoppini A (1992) Sonographic evaluation of femoral condylar cartilage in osteoarthritis and rheumatoid arthritis. Scand J Rheumatol 21: 201–203

Irizzarry JM, Recht MP (1997) MR imaging of the knee ligaments and the postoperative knee. Radiol Clin North Am 35: 45–76

Jarvela T, Paakkala T, Kannus P et al (2004) Ultrasonographic and power Doppler evaluation of the patellar tendon ten years after harvesting its central third for reconstruction of the anterior cruciate ligament: comparison of patients without or with anterior knee pain. Am J Sports Med 32: 39–46

Jozwiak M, Pietrzak S (1998) Evaluation of patella position based on radiologic and ultrasonographic examination: comparison of the diagnostic value. J Pediatr Orthop 18: 679–682

Kamel M, Eid H, Mansour R (2004) Ultrasound detection of knee patellar enthesitis: a comparison with magnetic resonance imaging. Ann Rheum Dis 63: 213–214

Kartus J, Rostgard-Christensen L, Movin T et al (2000) Evaluation of harvested and normal patellar tendons: a reliability analyses of magnetic resonance imaging and ultrasonography. Knee Surg Sports Traumatol Arthrosc 8: 275–280

Kellner H, Zoller W, Herzer P (1990) Ultrasound findings in chondrocalcinosis Z Rheumatol 49: 147–150

Khan KM, Bonar F, Desmond PM et al (1996) Patellar tendinosis (jumper's knee): findings at histopathologic examination, US and MR imaging. Victorian Institute of Sport Tendon Study Group. Radiology 200: 821–827

Kier R, McCarthy SM (1990) Lipohemarthrosis of the knee: MR imaging. J Comput Assist Tomogr 14: 395–396

Kim RS, Kim KT, Lee JY et al (2003) Ganglion cysts of the posterior cruciate ligament. Arthroscopy 19: E36–E40

Kim JY, Jung SA, Sung MS et al (2004) Extraarticular soft-tissue ganglion cyst around the knee: focus on the associated findings. Eur Radiol 14: 106–111

Klebuc M, Burrow S, Organek A et al (2001) Osteochondroma as a causal agent in popliteal artery pseudoaneurysms: case report and literature review. J Reconstr Microsurg 17: 475–479

La S, Fessell DP, Femino JE et al (2003) Sonography of partial-thickness quadriceps tendon tears with surgical correlation. J Ultrasound Med 22: 1323–1329

Learch TJ, Braaton M (2000) Lipoma arborescens: high-resolution ultrasonographic findings. J Ultrasound Med 19: 385–389

Lee JK, Yao L (1991) Tibial collateral ligament bursa: MR imaging. Radiology 178: 855–857

Lee JK, Song IS, Jung YB et al (1996a) Medial collateral ligament injuries of the knee: ultrasonographic findings. J Ultrasound Med 15: 621–625

Lee SH, Petersilge CA, Trudell DJ et al (1996b) Extrasynovial spaces of the cruciate ligaments: anatomy, MR imaging, and diagnostic implications. AJR Am J Roentgenol 166: 1433–1437

Leijten FS, Arts WF, Puylaert JB (1992) Ultrasound diagnosis of an intraneural ganglion cyst of the peroneal nerve. Case report. J Neurosurg 76: 538–540

Lektrakul N, Skaf A, Yeh L et al (1999) Pericruciate meniscal cysts arising from tears of the posterior horn of the medial meniscus: MR imaging features that simulate posterior cruciate ganglion cysts. AJR Am J Roentgenol 172: 1575–1579

Levy M, Seelefreund M, Maor P et al (1971) Bilateral spontaneous and simultaneous rupture of the quadriceps tendon in gout. J Bone J Surg Br 53: 510–513

Lian O, Holen KJ, Engebretsen L et al (1996) Relationship between symptoms of jumper's knee and the ultrasound characteristics of the patellar tendon among high level male volleyball players. Scand J Med Sci Sports 6: 291–296

Lindgren G, Rauschning W (1979) Clinical and arthrographic studies on the valve mechanism in communicating popliteal cysts. Arch Orthop Trauma Surg 95: 245–250

Lindgren PG, Willen R (1977) Gastrocnemio-semimembranosus bursa and its relation to the knee joint. I. Anatomy and histology. Acta Radiol Diagn 18: 497–512

Liu SH, Osti L, Raskin A et al (1994) Meniscal ossicles: two case reports and a review of the literature. Arthroscopy 10: 296–298

Lotem M, Robson MD, Rosenfeld GD (1974) Spontaneous rupture of the quadriceps tendon in patients on chronic haemodialysis. Ann Rheum Dis 33: 428–429

Macedo TA, Johnson CM, Hallett JW et al (2003) Popliteal artery entrapment syndrome: role of imaging in the diagnosis. AJR Am J Roentgenol 181: 1259–1265
Malghem J, van de Berg BC, Noel H et al (1992) Benign osteochondromas and exostotic chondrosarcomas: evaluation of cartilage cap thickness by ultrasound. Skeletal Radiol 21: 33–37
Malghem J, van be Berg BC, Lebon C et al (1998) Ganglion cysts of the knee: articular communication revealed by delayed radiography and CT after arthrography. AJR Am J Roentgenol 170: 1579–1583
Martinek V, Friederich NF (1999) Tibial and pretibial cyst formation after anterior cruciate ligament reconstruction with bioabsorbable interference screw fixation. Arthroscopy 15: 317–320
Martinez D, Millner PA, Coral A et al (1992) Case report 745: synovial lipoma arborescens. Skeletal Radiol 21: 393–395
Martin S, Hernandez L, Romero J et al (1998) Diagnostic imaging of lipoma arborescens. Skeletal Radiol 27: 325–329
Martino F, De Serio A, Macarini L et al (1998) Ultrasonography versus computed tomography in evaluation of the femoral trochlear groove morphology: a pilot study on healthy, young volunteers. Eur Radiol 8: 244–247
Martinoli C, Bianchi S, Derchi LE (1999) Ultrasound of tendon and nerves. Radiol Clin North Am 37: 691–711
Martinoli C, Bianchi S, Gandolfo N et al (2000a) US of nerve entrapments in osteofibrous tunnels of the upper and lower limbs. RadioGraphics 20: 199–217
Martinoli C, Bianchi S, Spadola L et al (2000b) Multimodality imaging assessment of meniscal ossicle. Skeletal Radiol 29: 481–484
Masciocchi C, Innacoli M, Cisternino S et al (1992) Myxoid intraneural cysts of external popliteal ischiatic nerve. Report of 2 cases studied with ultrasound, computed tomography and magnetic resonance imaging. Eur J Radiol 14: 52–55
Mathieu P, Wybier M, Busson J et al (1997) The medial collateral ligament of the knee. Ann Radiol 40: 176–181
McCarthy CL, McNally EG (2004) The MRI appearance of cystic lesions around the knee. Skeletal Radiol 33: 187–209
McCune WJ, Dedrick DK, Aisen AM et al (1990) Sonographic evaluation of osteoarthritic femoral condylar cartilage. Correlation with operative findings. Clin Orthop 254: 230–235
McDonnell CH 3rd, Jeffrey RB Jr, Bjorkengren AG et al (1992) Intraarticular sonography for imaging the knee menisci: evaluation in cadaveric specimens AJR Am J Roentgenol 159: 573–574
Milgram JW, Rogers LF, Miller JW (1978) Osteochondral fractures: mechanisms of injury and fate of fragments. AJR Am J Roentgenol 130: 651–658
Milgram JW: Osteochondral loose bodies. In: Taveras JM, Ferrucci JT (eds) Radiology: diagnosis, imaging, intervention. JB Lippincott, Philadelphia, pp 1–17
Miller TT, Staron RB, Koenigsberg T et al (1996) MR imaging of Baker cysts: association with internal derangement, effusion, and degenerative arthropathy. Radiology 201: 247–250
Miller TT (2002) Sonography of injury of the posterior cruciate ligament of the knee. Skeletal Radiol 31: 149–154
Montet X, Mauget D, Martinoli C et al (2002) Tensor fasciae suralis: US and MR imaging. Skeletal Radiol 31: 536–538
Muckart RD (1976) Compression of the common peroneal nerve by intramuscular ganglion from the superior tibiofibular joint. J Bone Joint Surg Br 58: 241–244
Muhle C, Ahn JM, Yeh LR et al (1999) Iliotibial band friction syndrome: MR imaging findings in 16 patients and MR arthrographic study of six cadaveric knees. Radiology 212: 103–110
Myllymaki T, Tikkakoski T, Typpo T et al (1993) Carpet-layer's knee. an ultrasonographic study. Acta Radiol 34: 496–499
Newberg A, Wales L (1977) Radiographic diagnosis of the quadriceps tendon rupture. Radiology 125: 367–371
Nietosvaara Y, Aalto K (1997) The cartilaginous femoral sulcus in children with patellar dislocation: an ultrasonographic study. J Pediatr Orthop 17: 50–53
Noda M, Kurosaka M, Maeno K et al (1999) Case report ganglion cysts of the bilateral cruciate ligaments. Arthroscopy 15: 867–870
O'Reilly MAR, O'Reilly PMR, Bell J (2003) Sonographic appearances of medial retinacular complex injury in transient patellar dislocation. Clin Radiol 58: 636–641
Parkes A (1961) Intraneural ganglion of the lateral popliteal nerve. J Bone Joint Surg Br 43:784–790
Pedrazzini M, Pogliacomi F, Cusmano F et al (2002) Bilateral ganglion cyst of the common peroneal nerve. Eur Radiol 12: 2802–2806
Peetrons P, Allaer D, Jeanmart L (1990) Cysts of the semilunar cartilages of the knee: a new approach by ultrasound imaging. A study of six cases and review of the literature. J Ultrasound Med 9: 333–337
Peiro A, Ferrandis R, Garcia L et al (1975) Simultaneous and spontaneous bilateral rupture of the patellar tendon in rheumatoid arthritis: a case report. Acta Orthop Scand 46: 700–703
Potasman I, Bassan HN (1984) Multiple tendon rupture in systemic lupus erythematosus: Case report and review of the literature. Ann Rheum Dis 43: 347–349
Ptasznik R, Feller J, Bartlett J et al (1995) The value of sonography in the diagnosis of traumatic rupture of the anterior cruciate ligament of the knee. AJR Am J Roentgenol 164: 1461–1463
Quinlan DJ, Alikhan R, Gishen P et al (2003) Variations in lower limb venous anatomy: implications for US diagnosis of deep vein thrombosis. Radiology 228: 443–448
Ramsey HR, Mueller GE (1970) Quadriceps tendon rupture: a diagnostic trap. Clin Orthop 70: 161–164
Rauschning W, Lindgren PG (1979) The clinical significance of the valve mechanism in communicating popliteal cysts. Arch Orthop Trauma Surg 95: 251–256
Resnick D, Newell JD, Guerra et al (1978) Proximal tibio-femoral: anatomo-pathologic-radiographic correlation. AJR Am J Roentgenol 131: 133–138
Rich NM, Collins GJ, McDonald PT et al (1979) Popliteal vascular entrapment: its increasing interest. Arch Surg 114: 1377–1384
Roels J, Martens M, Mulier JC et al (1978) Patellar tendinitis (jumper's knee). Am J Sports Med 6: 362–368
Rutten MJ, Collins JM, van Kampen A et al (1998) Meniscal cysts: detection with high-resolution sonography. AJR Am J Roentgenol 171: 491–496
Ryu KN, Jaovisidha S, Schweitzer M et al (1996) MR Imaging of lipoma arborescens of the knee. AJR Am J Roentgenol 167: 1229–1232
Saddik D, McNally EG, Richardson M (2004) MRI of Hoffa's fat pad. Skeletal Radiol 33: 433–444

Sandretto MA, Carrera GF (1983) The double fat fluid level: lipohemarthrosis of the knee associated with suprapatellar plica synovialis. Skeletal Radiol 10: 30–33
Sansone V, de Ponti A, Paluello GM et al (1995) Popliteal cysts and associated disorders of the knee. Critical review with MR imaging. Int Orthop 19: 275–279
Schnarkowski P, Tirman PF, Fuchigami KD et al (1995) Meniscal ossicle: radiographic and MR imaging findings. Radiology 196: 47–50
Schweitzer ME, Falk A, Berthoty D et al (1992) Knee effusion: normal distribution of fluid. AJR Am J Roentgenol 159: 361–363
Segal A, Miller TT, Krauss ES (2004) Fabellar snapping as a cause of knee pain after total knee replacement: assessment using dynamic sonography. AJR Am J Roentgenol 183: 352–354
Sekiya JK, Elkousy HA, Freddie HF (2004) Recurrent pretibial ganglion cyst formation over 5 years after anterior cruciate ligament reconstruction. Arthroscopy 20: 317–321
Seymour R, Lloyd DCF (1998) Sonographic appearances of meniscal cysts. J Clin Ultrasound 26: 15–20
Sheppard DG, Kim EE, Yasko AW et al (1998) Giant-cell tumor of the tendon sheath arising from the posterior cruciate ligament of the knee: a case report and review of the literature. Clin Imaging 22: 428–430
Silvestri E, Martinoli C, Derchi LE et al (1995) Echotexture of peripheral nerves: correlation between US and histologic findings and criteria to differentiate tendons. Radiology 197: 291–296
Singer AM, Naimark A, Felson D et al (1985) Comparison of overhead and cross-table lateral views for detection of knee-joint effusion. AJR Am J Roentgenol 144: 973–975
Skovgaard Larsen LP, Rasmussen OS (2000) Diagnosis of acute rupture of the anterior cruciate ligament of the knee by sonography. Eur J Ultrasound 12: 163–167
Smillie IS (1971) Injuries of the knee joint, 4th edn. William and Wilkins, Baltimore, p 184
Sofka CM, Adler RS, Cordasco FA (2002) Ultrasound diagnosis of chondrocalcinosis in the knee. Skeletal Radiol 31: 43–45
Sofka CM, Adler RS, Laskin R (2003) Sonography of polyethylene liners used in total knee arthroplasty. AJR Am J Roentgenol 180: 1437–1441
Somayaji SN, Vincent R, Bairy KL (1998) An anomalous muscle in the region of the popliteal fossa: case report. J Anat 192: 307–308
Spinner RJ, Atkinson JLD, Scheithauer BW et al (2003a) Peroneal intraneural ganglia: the importance of the articular branch. Clinical series. J Neurosurg 99: 319–329
Spinner RJ, Atkinson JLD, Tiel RL (2003b) Peroneal intraneural ganglia: the importance of the articular branch. A unifying theory. J Neurosurg 99: 330–343
Starok M, Lenchik L, Trudell D et al (1997) Normal patellar retinaculum: MR and sonographic imaging with cadaveric correlation. AJR Am J Roentgenol 168: 1493–1499
Stener B (1969) Unusual ganglion cysts in the neighborhood of the knee joint. Acta Orthop Scand 40: 392–401
Sureda D, Quiroga S, Arnal C et al (1994) Juvenile rheumatoid arthritis of the knee: evaluation with US. Radiology 190: 403–406
Suzuki S, Kasahara K, Futami T et al (1991) Ultrasound diagnosis of pathology of the anterior and posterior cruciate ligaments of the knee joint. Arch Orthop Trauma Surg 110: 200–203
Taylor PC, Steuer A, Gruber J et al (2004) Comparison of ultrasonographic assessment of synovitis and joint vascularity with radiographic evaluation in a randomized, placebo-controlled study of infliximab therapy in early rheumatoid arthritis. Arthitis Rheum 50: 1107–1116
Terslev L, Qvistgaard E, Torp-Pedersen S et al (2001) Ultrasound and power Doppler findings in jumper's knee: preliminary observations. Eur J Ultrasound 13: 183–189
Torreggiani WC, Al-Ismail K, Munk PL et al (2002) The imaging spectrum of Baker's (Popliteal) cysts. Clin Radiol 57: 681–691
Trappeniers L, De Maeseneer M, van Roy P et al (2003) Peroneal nerve injury in three patients with knee trauma: MR imaging and correlation with anatomic findings in volunteers and anatomic specimens. Eur Radiol 13: 1722–1727
Trikha SP, Acton D, O'Reilly M et al (2003) Acute lateral dislocation of the patella: correlation of ultrasound scanning with operative findings. Injury 34: 568–571
Tschirch FTC, Schmid MR, Pfirmann CWA et al (2003) Prevalence and size of meniscal cysts, ganglionic cysts, synovial cysts of the popliteal space, fluid-filled bursae, and other fluid collections in asymptomatic knees on MR imaging. AJR Am J Roentgenol 180: 1431–1436
Unlu Z, Ozmen B, Tarhan S et al (2003) Ultrasonographic evaluation of pes anserinus tendino-bursitis in patients with type 2 diabetes mellitus. J Rheumatol 30: 352–354
Vande Berg BC, Lecouvet FE, Poilvache P et al (2002) Spiral CT arthrography of the knee: technique and value in the assessment of internal derangement of the knee. Eur Radiol 12: 1800–1810
Vilanova JC, Barcelò J, Villalon M et al (2003) MR imaging of lipoma arborescens and the associated lesions. Skeletal Radiol 32: 504–509
Voorneveld C, Arenson AM, Fam AG (1989) Anserine bursal distension: diagnosis by ultrasonography and computed tomography. Arthritis Rheum 32: 1335–1338
Wadstein T (1931) Two cases of ganglia in the sheath of the peroneal nerve. Acta Othop Scand 2: 221–231
Wakefield RJ, McGonagle D, Tan AL et al (2004) Ultrasound detection of knee patellar enthesitis. Ann Rheum Dis 63: 213–214
Wang SC, Chhem RK, Cardinal E et al (1999a) Joint sonography. Radiol Clin North Am 37: 653–668
Wang TG, Wang CL, Hsu TC et al (1999b) Sonographic evaluation of the posterior cruciate ligament in amputated specimens and normal subjects. J Ultrasound Med 18: 647–653
Ward EE, Jacobson JA, Fessell DP et al (2001) Sonographic detection of Baker's cysts: comparison with MR imaging. AJR Am J Roentgenol 176: 373–380
Weinberg EP, Adams MJ, Hollenberg GM (1998) Color Doppler sonography of patellar tendinosis. AJR Am J Roentgenol 171: 743–744
Wright LB, Matchett WJ, Cruz CP et al (2004) Popliteal artery disease: diagnosis and treatment. RadioGraphics 24: 467–469
Yamazaki H, Saitoh S, Seki H et al (1999) Peroneal nerve palsy caused by intraneural ganglion. Skeletal Radiol 28: 52–56
Yashar AA, Adler RS, Grady-Benson JC et al (1996) An ultrasound method to evaluate polyethylene component wear in the knee replacement arthroplasty. Am J Orthop 25: 702–704
Yu JS, Resnick D (1994) Meniscal ossicle: MR imaging appearance in three patients. Skeletal Radiol 23: 637–639